resources

Analysis of Extreme Hydrometeorological Events

Edited by
Brunella Bonaccorso and David J. Peres

Printed Edition of the Special Issue Published in *Resources*

www.mdpi.com/journal/resources

MDPI

Analysis of Extreme Hydrometeorological Events

Analysis of Extreme Hydrometeorological Events

Editors

Brunella Bonaccorso
David J. Peres

MDPI • Basel • Beijing • Wuhan • Barcelona • Belgrade • Manchester • Tokyo • Cluj • Tianjin

Editors
Brunella Bonaccorso
University of Messina
Italy

David J. Peres
University of Catania
Italy

Editorial Office
MDPI
St. Alban-Anlage 66
4052 Basel, Switzerland

This is a reprint of articles from the Special Issue published online in the open access journal *Resources* (ISSN 2079-9276) (available at: https://www.mdpi.com/journal/resources/special_issues/extreme_hydrometeorological_events).

For citation purposes, cite each article independently as indicated on the article page online and as indicated below:

LastName, A.A.; LastName, B.B.; LastName, C.C. Article Title. *Journal Name* **Year**, *Volume Number*, Page Range.

ISBN 978-3-0365-4923-1 (Hbk)
ISBN 978-3-0365-4924-8 (PDF)

Contents

About the Editors . . . . . **vii**

Brunella Bonaccorso and David J. Peres
Analysis of Extreme Hydrometeorological Events
Reprinted from: *Resources* **2022**, *11*, 55, doi:10.3390/resources11060055 . . . . . **1**

Joanna Nowak Da Costa, Beata Calka and Elzbieta Bielecka
Urban Population Flood Impact Applied to a Warsaw Scenario
Reprinted from: *Resources* **2021**, *10*, 62, doi:10.3390/resources10060062 . . . . . **5**

Paola Nanni, David J. Peres, Rosaria E. Musumeci and Antonino Cancelliere
Worry about Climate Change and Urban Flooding Risk Preparedness in Southern Italy: A Survey in the Simeto River Valley (Sicily, Italy)
Reprinted from: *Resources* **2021**, *10*, 25, doi:10.3390/resources10030025 . . . . . **23**

Bogusława Baran-Zgłobicka, Dominika Godziszewska and Wojciech Zgłobicki
The Flash Floods Risk in the Local Spatial Planning (Case Study: Lublin Upland, E Poland)
Reprinted from: *Resources* **2021**, *10*, 14, doi:10.3390/resources10020014 . . . . . **49**

Waldemar Kociuba, Grzegorz Gajek and Łukasz Franczak
A Short-Time Repeat TLS Survey to Estimate Rates of Glacier Retreat and Patterns of Forefield Development (Case Study: Scottbreen, SW Svalbard)
Reprinted from: *Resources* **2021**, *10*, 2, doi:10.3390/resources10010002 . . . . . **69**

Rubens Junqueira, Marcelo R. Viola, Jhones da S. Amorim and Carlos R. de Mello
Hydrological Response to Drought Occurrences in a Brazilian Savanna Basin
Reprinted from: *Resources* **2020**, *9*, 123, doi:10.3390/resources9100123 . . . . . **89**

Małgorzata Biniak-Pieróg, Mieczysław Chalfen, Andrzej Żyromski, Andrzej Doroszewski and Tomasz Jóźwicki
The Soil Moisture during Dry Spells Model and Its Verification
Reprinted from: *Resources* **2020**, *9*, 85, doi:10.3390/resources9070085 . . . . . **101**

About the Editors

Brunella Bonaccorso

Brunella Bonaccorso is an Associate Professor of Hydrology and Water Resources Management at the Dept. of Engineering of the University of Messina (Italy), teaching courses and carrying out research activities in the field of stochastic hydrology and analysis of extreme hydrometeorological events. She has collaborated with several national and European research projects focusing on drought analysis and management, such as SEDEMED (INTERREG IIIb-MEDOCC) and MEDROPLAN (MEDA Water). She has authored/co-authored 90 publications, including peer-reviewed journal articles, book chapters, and contributions to conferences proceedings, and was co-editor of the book *Methods and Tools for Drought Analysis and Management* (Springer). She is the Associate Editor of *Natural Hazard and Earth System Sciences* (Copernicus), *Hydrological Sciences Journal* (Taylor & Francis), and *Hydrology* (MDPI). https://orcid.org/0000-0002-6973-6425.

David J. Peres

David J. Peres is Assistant Professor of Hydrology at the Department of Civil Engineering and Architecture, University of Catania, Italy. He held research grants and scholarships in the period 2013–2021. He obtained his PhD in 2013 with a thesis about hydrological control on shallow landslides. He carried out research abroad as a visiting researcher at Colorado State University in the U.S.A. (2012) and TU Delft in the Netherlands (2017). His main research interests are the hydrological modeling of the initiation of landslides, the identification of rainfall thresholds useful for the development of early-warning systems, the analysis of climate projections for the assessment of the impacts of climate change on management of water resources and hydrological extremes, statistical analysis of droughts, and the active involvement of the population in risk prevention. He also conducted various national and European research projects. His scientific activity is evidenced by more than 90 works published in indexed international scientific journals (h-index: 10), book chapters, and national and international conference proceedings. He collaborates with numerous journals in the field of hydrology and natural disasters as a reviewer, and he is the Associate Editor for the journal *Natural Hazards and Earth System Sciences*.

resources

Editorial

Analysis of Extreme Hydrometeorological Events

Brunella Bonaccorso [1] and David J. Peres [2,*]

[1] Department of Engineering, University of Messina, Villaggio S. Agata, 98166 Messina, Italy; brunella.bonaccorso@unime.it
[2] Department of Civil Engineering and Architecture, University of Catania, Via S. Sofia 64, 95125 Catania, Italy
* Correspondence: djperes@dica.unict.it

Extreme hydrometeorological events (e.g., storms, pluvial, fluvial, and coastal floods, droughts and landslides), with severe consequences in terms of injuries, casualties, and socioeconomic losses, are becoming increasingly frequent worldwide [1]. These events frequently have cascading effects [2], ranging from slope instability, causing infrastructure and service disruptions, to ecological disasters, from water scarcity to yield losses and rises in food prices. Climate variability and anthropogenic changes (e.g., population growth, urbanization, and environmental degradation) both play a role in amplifying the these events' effects on an increasing number of people [3,4]. Understanding the dynamics of these phenomena, improving early warning systems, and developing more coordinated disaster risk reduction strategies are, therefore, critical to properly managing the associated risk, reducing vulnerabilities, and increasing societal resilience to natural disasters. The purpose of this Special Issue was to highlight studies that address challenges in monitoring, modeling, forecasting, and assessing the effects of hydrometeorological hazards.

This Special Issue received six contributions. Three of the papers focus on floods, two on droughts, and one on glacier retreat (related to extreme temperature). Three contributions focus on areas in Poland, the other three studied areas in Italy, Brazil and Norway (Svalbard Islands).

A first contribution focuses on the prediction of the potential impacts of fluvial floods on urban population safety. The impact was estimated by combining the likelihood of a flood and the expected floodwater inundation level with a damage function, considering the purpose of the building, and the number of permanent inhabitants. After the application of the model to the Vistula River, the authors found that 500-year flooding could affect 2.35 percent of buildings and over 122,000 people in Warsaw. In contrast, the expected magnitude of flood impact on human health was estimated to be moderate, i.e., ten people per residential building in 80 percent of flood risk zones, mainly due to the shallow inundation depth of less than 1 m in many parts of the studied area. These models are of key importance for urban planning, and to raise public awareness of flood risks [5].

The issue of flood risk awareness in urban areas is also tackled in [6]. Specifically, they presented the findings of a 10-question survey on climate change and risk perception conducted in 11 municipalities of the Simeto River Valley. The survey, conducted within the activities of the LIFE project SimetoRES, collected 1143 responses from residents. The survey looked at: (a) citizens' level of concern about climate change in relation to extreme storms, (b) risk preparedness, and (c) citizens' willingness to implement sustainable drainage actions for climate change adaptation. According to the findings, more than 52 percent of citizens have insufficient knowledge of proper behavior during flooding events, and only 30 percent believe that they are responsible for reducing flooding risk. The population shows a modest willingness to support the construction of sustainable urban drainage infrastructure. Another interesting finding, derived from a statistical cross-analysis of the responses to the various questions, revealed that increased concern about climate change does not have a significant impact on either people's behavior in dangerous situations during flooding events or their willingness to support financially sustainable solutions.

Citation: Bonaccorso, B.; Peres, D.J. Analysis of Extreme Hydrometeorological Events. *Resources* **2022**, *11*, 55. https://doi.org/10.3390/resources11060055

Received: 2 May 2022
Accepted: 25 May 2022
Published: 5 June 2022

These findings suggest that increasing concern about climate change and related urban flooding risks is insufficient to improve preparedness.

The last contribution concerning floods analyzes whether the threat of flash floods is considered in municipal spatial planning. Using GIS, a preliminary assessment of 369 small catchments' susceptibility to flash floods was conducted through multicriteria analysis. Then, they examined the existing planning documents, flood hazard and risk maps, and flood risk maps for municipalities located in the most susceptible catchments. They found that, even when the risk is significant, flash floods are frequently overlooked at the local government level [7].

Looking at contributions on droughts, the first concerns the Brazilian savanna, one of the world's 25 biodiversity hotspots [8]. The authors examined meteorological and hydrological droughts and their effects on hydrological behavior in the savanna. They computed the Standardized Precipitation Index (SPI) and Standardized Streamflow Index (SSI) at different aggregation scales and analyzed the correlation between the two indices to investigate the propagation of meteorological to hydrological drought. They found no significant difference in the coefficients of correlation from 0- to 6-month lags in drought propagation, while a decrease in correlation was identified with lags at 9 and 12 months.

The second study on drought aimed to develop and test a model to simulate decreases in soil moisture during dry spells [9]. The analyses were based on diurnal data regarding the occurrence of atmospheric precipitation and diurnal values of soil moisture under a bare soil surface from May to October. During dry spells, the moisture rate decreased in six layers of the soil profile, described using a decreasing exponential trend. The least squares method was used to calculate the exponent value, which described the rate of soil moisture decrease, for each dry spell and soil depth. The exponential form of the trend of soil moisture changes over time used for the analysis also allowed for the calculation of the duration of a hypothetical dry spell, a result that can be related to land use.

Finally, the paper on glacier retreat is based on a comparative analysis of high-resolution differential digital elevation models (DEM of Difference (DoD)) based on terrestrial laser scanning (TLS) surveys conducted in the Svalbard Islands [10]. The comparison of DEMs at three-week intervals allowed for the identification of erosion and depositional areas, as well as the volume of the glacier's terminus melting. They found that the retreat of the glacier's snout ranged from 3 to 9 m (mean of 5 m) over a 3-week period, accompanied by an average lowering of the surface of up to 0.86 m (0.03 m) and a decrease in ice volume of 53,475 m^3 (1761 m^3). The deglaciated area increased by 4549 m^2 (5%), resulting in an extensive reshaping of the recently deglaciated area. The DEM of Difference (DoD) analyses offered important insights into the melting dynamics as related to air temperature, humidity, pressure and wind speed.

Overall, the contributions to this Special Issue provide some insights on the possible analyses that can be carried out to obtain a better understanding and management of natural hazards related to extreme hydrometeorological events, as well as highlighting how a greater dialogue between research, decision makers and laymen is desirable to increase community resilience to climate change.

Author Contributions: Writing—original draft preparation, D.J.P.; writing—review and editing, B.B. and D.J.P. All authors have read and agreed to the published version of the manuscript.

Funding: This research received no external funding.

Data Availability Statement: Not applicable.

Acknowledgments: The guest editors are grateful to all the authors and reviewers that contributed to this Special Issue.

Conflicts of Interest: The Gest Editors declare no conflict of interest.

References

1. IPCC. *Climate Change 2014: Synthesis Report. Contribution of Working Groups I, II and III to the Fifth Assessment Report of the Intergovernmental Panel on Climate Change*; Core Writing Team, Pachauri, R.K., Meyer, L.A., Eds.; IPCC: Geneva, Switzerland, 2014; p. 151.
2. Kruse, P.M.; Schmitt, H.C.; Greiving, S. Systemic criticality-a new assessment concept improving the evidence basis for CI protection. *Clim. Chang.* **2021**, *165*, 2. [CrossRef] [PubMed]
3. Raymond, C.; Horton, R.M.; Zscheischler, J.; Martius, O.; AghaKouchak, A.; Balch, J.; Bowen, S.G.; Camargo, S.J.; Hess, J.; Kornhuber, K.; et al. Understanding and managing connected extreme events. *Nat. Clim. Chang.* **2020**, *10*, 611–621. [CrossRef]
4. van der Wiel, K.; Bintanja, R. Contribution of climatic changes in mean and variability to monthly temperature and precipitation extremes. *Commun. Earth Environ.* **2021**, *2*, 1. [CrossRef]
5. Da Costa Nowak, J.; Calka, B.; Bielecka, E. Urban Population Flood Impact Applied to a Warsaw Scenario. *Resources* **2021**, *10*, 62. [CrossRef]
6. Nanni, P.; Peres, D.J.; Musumeci, R.E.; Cancelliere, A. Worry about Climate Change and Urban Flooding Risk Preparedness in Southern Italy: A Survey in the Simeto River Valley (Sicily, Italy). *Resources* **2021**, *10*, 25. [CrossRef]
7. Baran-Zgłobicka, B.; Godziszewska, D.; Zgłobicki, W. The Flash Floods Risk in the Local Spatial Planning (Case Study: Lublin Upland, E Poland). *Resources* **2021**, *10*, 14. [CrossRef]
8. Junqueira, R.; Viola, M.R.; Amorim, J.D.S.; De Mello, C.R. Hydrological Response to Drought Occurrences in a Brazilian Savanna Basin. *Resources* **2020**, *9*, 123. [CrossRef]
9. Biniak-Pieróg, M.; Chalfen, M.; Żyromski, A.; Doroszewski, A.; Jóźwicki, T. The Soil Moisture during Dry Spells Model and Its Verification. *Resources* **2020**, *9*, 85. [CrossRef]
10. Kociuba, W.; Gajek, G.; Franczak, Ł. A Short-Time Repeat TLS Survey to Estimate Rates of Glacier Retreat and Patterns of Forefield Development (Case Study: Scottbreen, SW Svalbard). *Resources* **2021**, *10*, 2. [CrossRef]

resources

MDPI

Article

Urban Population Flood Impact Applied to a Warsaw Scenario

Joanna Nowak Da Costa *, Beata Calka and Elzbieta Bielecka

Institute of Geospatial Engineering and Geodesy, Faculty of Civil Engineering and Geodesy, Military University of Technology, 00-908 Warsaw, Poland; beata.calka@wat.edu.pl (B.C.); elzbieta.bielecka@wat.edu.pl (E.B.)
* Correspondence: joanna.nowakdc@wat.edu.pl

Abstract: The provision of detailed information on the impact of potential fluvial floods on urban population health, quantifying the impact magnitude and supplying the location of areas of the highest risk to human health, is an important step towards (a) improvement of sustainable measures to minimise the impact of floods, e.g., by including flood risk as a design parameter for urban planning, and (b) increase public awareness of flood risks. The three new measures of the impact of floods on the urban population have been proposed, considering both deterministic and stochastic aspects. The impact was determined in relation to the building's function, the number of residents, the probability of flood occurrence and the likely floodwater inundation level. The building capacity concept was introduced to model population data at the building level. Its proposed estimation method, an offshoot of the volumetric method, has proved to be successful in the challenging study area, characterised by a high diversity of buildings in terms of their function, size and density. The results show that 2.35% of buildings and over 122,000 people may be affected by 500-year flooding. However, the foreseen magnitude of flood impact on human health is moderate, i.e., on average ten persons per residential building over the 80% of flood risk zones. Such results are attributed to the low inundation depth, i.e., below 1 m.

Keywords: urban population estimation; building capacity; flood impact; GIS modelling; flood mitigation

Citation: Nowak Da Costa, J.; Calka, B.; Bielecka, E. Urban Population Flood Impact Applied to a Warsaw Scenario. *Resources* **2021**, *10*, 62. https://doi.org/10.3390/resources10060062

Academic Editors: Brunella Bonaccorso and David J. Peres

Received: 26 April 2021
Accepted: 10 June 2021
Published: 14 June 2021

1. Introduction

Flooding is one of the most disruptive natural hazards in the world [1–3]. According to the World Health Organization [4], flooding has affected more than 2.3 billion people worldwide in the last twenty years (1998–2017) and is responsible for 47% of weather-related disasters. Devastation caused by floods can lead to loss of life, damage to property, public infrastructure and nature. Between 1900 and 2014, floods have had the second highest death rate (30%) of all natural disasters [5]. Losses are particularly severe in densely populated and intensely developed urban areas. Roudier et al. [6] established that if global warming reaches +2 °C, the floods' magnitudes will increase in almost all European countries, with a significant upsurge in Northwest Europe. Furthermore, they noticed that the increase in 100-year floods would be much greater than that in 10-year floods. The possible upsurge in the severity of floods was also noticed by Rojas et al. [7]. Blöschl et al. [8] observed a distinct shift in the timing of floods in Europe over the past five decades. Moreover, Blöschl et al. [9] showed that the escalation of floods events in northwestern Europe resulted from higher fall and winter rainfall, while decreasing precipitation and increasing evaporation led to a reduction of floods in southern Europe. Eastern Europe, due to warmer spring temperatures and decreasing snow cover, felt the effects of floods less frequently. Tanoue et al. [10] found that the flood risk forecast is influenced by different scenarios of population growth and population spatial distribution. Furthermore, the availability of detailed and reliable spatial and socio-economic data plays a significant role in estimating flood risk zones and developing flood risk management and

mitigation [11]. The uncertainty of forecasts resulting from the use of different scenarios and different models of climate change were also reported by Roudier et al. [6].

Urbanisation, climate change, topography and the hydrological regime are the main factors determining the probability of inundations [10,12,13] while economic growth results in higher costs of removing the effects of flooding [14]. Due to the concentration of population, dense built-up and other infrastructure necessary for the economic and social well-being of societies and the amount of losses caused by floods, urban areas are of concern to both scientists and practitioners. World literature extensively covers the problem of buildings and populations prone to flooding at all levels, from local to global [15,16]. Knowing the exposure to flooding is one of the elements of flood risk assessment for buildings and people, and thus essential for the preparation of appropriate risk management plans [17]. However, as found by Papilloud et al. [15] the concepts of flood exposure and flood vulnerability are understood differently, which results mainly from the disciplinary backgrounds as well as research aims and questions. As shown in the literature, flood exposure is not only defined ambiguously but also analysed with various approaches and methods [15,18,19]. The most common approaches are based on geographic information system (GIS) technology and methods, in particular the spatial overlap, intersection or spatial joint of flood hazard zones and buildings.

The use of GIS methods in flood exposure assessment can be found in global [10], national [20], regional [21] and local studies [18,19,22]. Nevertheless, this type of flood exposure analysis requires geographic data on building locations, gridded population data and the geographical extent of flood risk zones [22]. Furthermore, Jongman et al. [16] noted that the results of global exposure analyses, in particular the differences in estimates and geographic distribution, are strongly dependent on the methods used. This was also confirmed by Hirabayashi et al. [23] and Tanoue. et al. [10] who applied different scenarios to predict the global threat to the population caused by floods triggered by climate change. Tanoue et al. [10] found that the characteristics of the population exposed to floods are influenced by historical changes in population distribution, with changes in vulnerability to floods reaching 48.9%. The number of people affected by flooding was calculated by the spatial overlaying of the flooded area with the global gridded population. Röthlisberger et al. [20] focused on the problem of data analysis in various risk-based strategies and noted that the analysis of exposure is highly dependent on the availability, spatial resolution and quality of data, namely data on assets (e.g., affected people, buildings and infrastructure) and on the nature of the hazards (i.e., the extent and magnitude of the flood). Bhola et al. [19], inspired by Kolen et al. [24], presented an approach based on a combination of multiple models by considering several exceedance probability scenarios to better support decision making in crisis management. Finally, they proposed a building hazard map, in which flood-affected buildings are marked with varying probabilities of exceeding the flood inundation extent depending on the building use.

Analysing the exposure of the population to urban floods, many studies focus on estimating the people counts at a micro-scale, particularly at the building level. Zhu S. et al. [25] mapped the building-scale population by calculating the correlation coefficient between the POI (point of interest) type and WorldPop population grid to establish the relationship between building function and population distribution in Lishui City, China. Darabi et al. [26] applied machine learning algorithms to predict flood hazard probabilities; they created a vulnerability map and assessed risk as a product of hazard and vulnerability. The factors influencing flood hazard the most were distance to channel, land use, and runoff generation, while population density and building density were the most important factors determining vulnerability. Hossain and Meng [18] aimed to assess the potential risk of damage caused by the exposure of buildings and populations to flooding in urban areas (Birmingham City, AL, USA). The developed GIS-based risk assessment model showed the level of flood risk, quantified and simultaneously mapped commercial buildings, residential buildings and populations at risk of flooding. The findings of Hossain and Meng [18] revealed that approximately 44% of the total population of the Birmingham floodplain area

lived in high and very high flood risk zones. Calka et al. [22] estimated the people counts in buildings based on the regression between a building's footprint area, the building's type (single-family, twin, multi-family), and the average number of people living in one household. The study found that about 30% of residents of villages located on the Bug River floodplain (eastern part of Poland) lived in high flood risk areas.

Several factors vitally influence the extent of flood damage, i.e., water depth, flow speed, geographical extent and duration [27]. However, the factor most commonly applied in studies is water depth, e.g., [15,18,25,27–29]. Flood risk also depends on the types of assets exposed, therefore many studies focused on buildings and road infrastructure, as examples of structural flood damage. Some academics evaluated buildings damaged using the appraisal value [28], while others used the building characteristics [30,31]. There is a broad consensus, however, that as a priority loss of life must be prevented by all means possible [13]. Disaster mitigation efforts increasingly focus on the exposure and vulnerability of human populations [32]. For example, the perception of flood risk among the population is being studied, constating that it is underestimated, and steps are being taken to change this [33–35]. This consequently translates into increasing the awareness of potential flood risks, the preparedness for an emergency case and the willingness to cooperate [35,36].

Poland, the central-eastern European country, suffers few natural hazards except for seasonal flooding, with a prevalence of early spring floods [1,29]. During the last 25 years, several countrywide initiatives have come into existence, amongst which the IT system of the Country's Protection Against Extreme Hazards (ISOK) is one of the major ones [37]. Pursuant to the Directive 2007/60/EC (the so-called Floods Directive) [38] the Polish flood protection ISOK provides all flood risk-management elements, i.e., prevention, protection, proper preparation and floods effects' removal. The potential flood effects relate to human life and health, the environment, cultural heritage, economic activity infrastructure and land cover [38–40]. The loss and damage assessment focuses on post-disaster losses, whereas the loss and damage risk refers to 'assessing the possibility and probability that some people in a community or nation will face severe loss and damage' and is a pre-disaster perspective [41]. Our approach is oriented toward the latter assessment. The common practice of expressing the impacts of flood events in monetary terms [42] can however distract from intangible impacts, the most important being the loss of life.

Our study focuses on the impact of floods on health of urban populations specifically those living in residential buildings in areas exposed to potential fluvial flooding. The aim of this study was to produce flood impact indicators to provide information on the conditions of residents, quantifying the magnitude of the flood impact on human health and to help identify areas of the highest risk to human health. Furthermore, this information can be used to increase public awareness of flood risks and to improve sustainable measures to minimise the impact of floods, for example by including flood risk as a design parameter for urban planning. The presented fluvial flood scenarios were developed by the State Water Holding 'Polish Waters', the national authority responsible for water management. In our approach, a residential building was adopted as the smallest spatial reference area unit. The urban population flood impact on building residents was defined and determined in relation to the following four factors: building capacity, building function, flood probability and flood depth. Our presented approach introduces the novel concept of building capacity and proposes its estimation method, an offshoot of the volumetric method. The remainder of the paper is structured as follows: Section 2 describes the study area, data and methods, Sections 3 and 4 describe and discuss the obtained results, respectively; Section 5 provides conclusions related to the developed research results.

2. Materials and Methods

2.1. Study Area and Data Used Description

The study area covers 27.11 km^2 and encompasses the Vistula River valley from ki-lometre 494.0 to 528.5 (Figure 1).

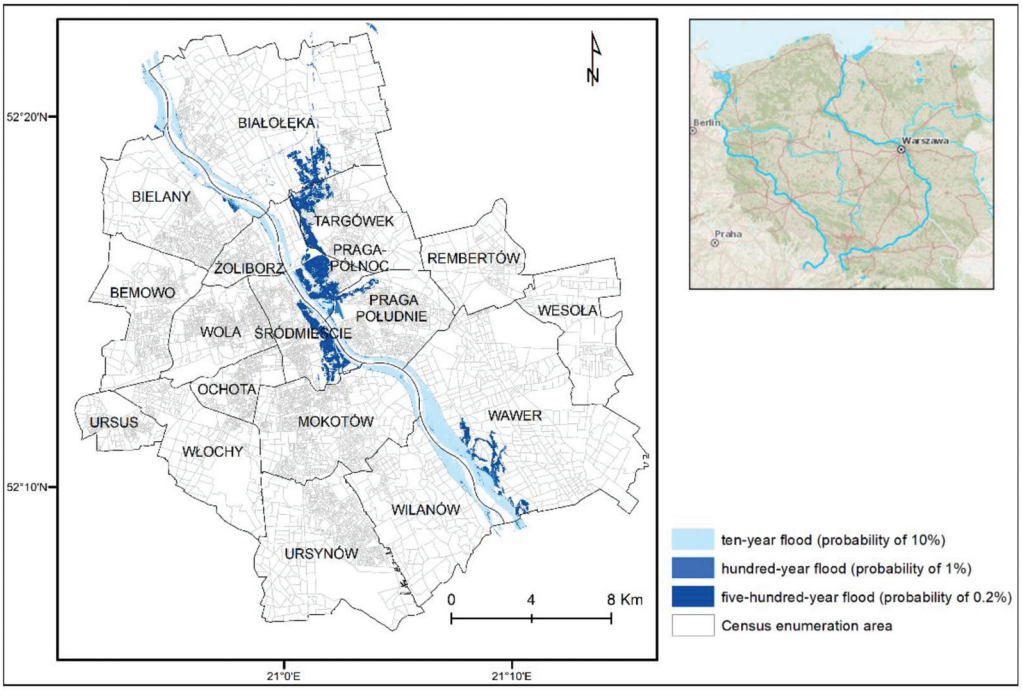

Figure 1. Warsaw, Poland, the flood risk zones.

The natural narrowing of the Vistula valley due to geological conditions was further limited by flood embankments created at the end of the 19th century and in the 1950s. Warsaw has been hit by floods many times. From the nineteenth century, catastrophic floods in the middle course of the Vistula occurred every few or several years (1813, 1838, 1839, 1844, 1845, 1855, 1867, 1884, 1889, 1891, 1903, 1924, 1947, 1960, 1962, 1997, 2010) and seriously affected Warsaw [29,43]. As noticed by [29,43,44] the Vistula River floods have generally been shaped by intensive rainfall in the Carpathian Mountains and rarely by snowmelt. Rainfall-induced floods occur mainly in June–July, while snowmelt—in March–April. Nowadays, 18.5 km left bank and 23 km right bank embankments, located mainly in the north and south part of the river course, protect the city against river inundation. The land cover structure in the Warsaw floodplains is diversified, in parts heavily urbanised and impervious but also covered by urban green areas, such as parks, garden, fruits, forest and bushes [45,46].

The study utilised several data sets listed in Table 1. All data sets are maintained by the public administration therefore they are highly reliable. As an element of the Polish spatial data infrastructure, they are free and publicly available through network services of the Polish Spatial Information Infrastructure Geoportal [47,48]. Flood risk zones with different probabilities of flood occurrence, namely 10-year flood (probability of 10%), 100-year flood (probability of 1%) and 500-year flood (probability of 0.2%), were estimated in the frame of the ISOK project. Flood risk zones were developed on the basis of mathematical-hydraulic MIKE11 models (2D or hybrid 1D/2D) for designing flood waves with different return periods (i.e., 500, 100 and 10 years) [37]. They constitute an indispensable element of flood hazard and flood risk maps, which provide comprehensive information to local authorities and the population, enabling planning of preventive and rescue actions during floods [49]. Flood risk zones were derived in vector format each zone patch is attributed with flooding depth in meters, the area of zone patches is given in square meter. According to the Floods Directive [38] flood risk zones are revised and updated every six years. The 10-year flood

zone covers an area of 14.38 km^2, the 100-year flood spreads over 15.66 km^2, while the 500-year flood—27.11 km^2.

Table 1. Overview of data used.

Data Source Name	Object Type	Data Stakeholder	Spatial Resolution	Temporal
Flood risk zones	Flood risk zones	State Water Holding 'Polish Water'	1:10,000 [m] [1]	2016–2021
Topographic data (BDOT10k)	Buildings	Surveyor General	1:10,000 [m] [2]	2012; 2018–2019
Territorial Division	Census enumeration area	Surveyor General	1:10,000 [m] [1]	2019
Population	Population counts	Central Statistical Office	Census enumeration areas	2011
Housing economy and municipal	Average usable area of dwellings	Central Statistical Office	Warsaw districts	2000–2019
Infrastructure, Housing stocks	Average number of persons dwelling	Central Statistical Office	Warsaw districts	2000–2019

[1,2] The data is available in the vector shapefile format, the accuracy of the horizontal position amounts to 6 m [37], 1 m [48], respectively

Flood risk zones with different probabilities of flood occurrence, namely 10-year flood (probability of 10%), 100-year flood (probability of 1%) and 500-year flood (probability of 0.2%), were estimated in the frame of the ISOK project. Flood risk zones were developed on the basis of mathematical-hydraulic MIKE11 models (2D or hybrid 1D/2D) for designing flood waves with different return periods (e.g., 500, 100, 10 years) [37]. They constitute an indispensable element of flood hazard and flood risk maps, which provide comprehensive information to local authorities and the population, enabling planning of preventive and rescue actions during floods [49]. Flood risk zones were derived in vector format each zone patch is attributed with flooding depth in meters, the area of zone patches is given in square meter. According to the Floods Directive [38] flood risk zones are revised and updated every six years. The 10-year flood zone covers an area of 14.38 km^2, the 100-year flood spreads over 15.66 km^2, while the 500-year flood—27.11 km^2.

The Polish topographic data (BDOT10k), a national vector database with a thematic scope and a level of detail corresponding to civilian topographic maps at a scale of 1:10,000, was the source for the buildings data layer. Buildings' location and characteristics are derived from the cadastre. Buildings' footprint areas expressed in square meters, their function and the number of storeys, are all crucial for this research.

The census enumeration area (also referred to as EA) is the smallest spatial statistical unit defined for censuses and other statistical surveys according to the number of flats and inhabitants, amounting to not more than 500 persons and 200 dwellings. Boundaries of census enumeration areas are adjusted to the administrative division and consistent with the units used in the cadastre. Moreover, census enumeration boundaries are spatially adjacent to the boundaries of towns or settlements [50]. In this case, 532 census enumeration areas covered the studied region, the area of the smallest census unit amounted to 0.11 ha, and the largest to 98.32 ha. In 2011, according to the national census, twelve census EAs were uninhabited, while in five—the number of people exceeded 500. Most, as many as 939 people, lived in an EA unit of 6.46 ha. Statistical data on population, average usable area of a dwelling, and the average number of persons per dwelling was obtained from the Local Data Bank provided by the Central Statistical Office [51].

2.2. Method Applied

Flood risk maps visualise the levels of expected losses i.e., the magnitude and nature of the risk, during a particular time period, as a result of a particular flood event. In contrast to hazard maps, risk maps quantify economic losses, mostly directly expressed as a monetary value. The flood risk maps show the indicative number of persons at risk in an assumed spatial reference area as the population number within this area. Nevertheless, this information is blurred due to the vast informational and thematic scope of the maps and, more importantly, it is not detailed due to the generalised manner of the population distribution portrayal and the spatial incongruity [52]. Consequently, our research goal was

to improve the level of detail and thematic scope of information about the potential risk impact of flooding on the human population. This issue was addressed by estimating the urban population at the building level and redefining the urban population flood impact on building residents.

In order to accomplish this study goal, the basic assumptions were as follows:

1. A flood-occurrence probability (p_{Qi}) amounts to 10%, 1%, 0.2% for high, moderate and low probability floods, correspondingly.
2. A flood scenario is characterised by the floodwater level. This factor also implicates the flood horizontal extent, i.e., area prone to flooding.
3. One building is the smallest spatial reference unit.
4. A building's occupant capacity (hereinafter referred to as building capacity and denoted as b_{cap}) was introduced and defined as the number of permanent residents of any type of residential building or hotel.

The limitation of analysis to residential buildings and hotels is justified in the national [39,40], and EU regulations [38] related to floods and flood hazards. The residential building category (denoted further as b_c) comprises of a single-family building, two-family building, multi-family building (i.e., three or more family building), hotel, monastery as well other houses of permanent residence, i.e., children's home, student dorm, workers' hostel, boarding-school house, homeless shelter. The adopted methodology is based mainly on GIS and cartographic modelling and uses the overlay and spatial relations functions, which are commonly used in flood risk modelling [10,18–20,22].

To analyse the urban population flood impacts based on flood forecasts, flood risk modelling is of great importance. Usually, either a deterministic or stochastic approach is used. Deterministic models identify hazards and exposure outputs in vulnerability analyses, but their limitation is that they do not calculate risk. In contrast, probabilistic models provide information on the amount of risk. Hence, deterministic models used in conjunction with probabilistic models can be used for more detailed threat modelling, which unfortunately is not the standard, in the context of applied practice [53].

Inspired by the above [53], a dual approach was also followed. The expected impact of flooding was defined in the aspect of risk to urban population health and life as the expected value of the cost of flooding, i.e., the sum of the product of the probability of an event p_{Qi} and its cost, expressed by the number of inhabitants (of the building) b_{cap} (Equation (1)). This measure is stochastic in nature.

$$Im_{stoch} = \sum_{i=1}^{n} b_{cap} * p_{Qi}, \quad (1)$$

If the chance of occurrence of the flood event is ignored, it is still possible to identify flood hazard and exposure. Therefore, a measure of the deterministic impact of flooding in terms of risk to human health and life was defined as the product of the building capacity b_{cap} and a damage function $f\left(h,\ b_f\right)$ that depends on two variables, i.e., flood water level h and building function b_f (Equation (2)).

$$Im_{determ} = b_{cap} * f\left(h,\ b_f\right), \quad (2)$$

The term 'function' refers to the purpose of a building, e.g., commercial, office, residential or even farm livestock. The values of the damage function for land use classes and water depth ranges were defined by the National Water Management Authority within the framework of the system for the Country's Protection Against Extreme Hazards. The residential land use takes values as follows (Table 2).

Table 2. The values of the damage function for residential land use (here: b_f is constant and equals 'residential').

Water Level h [m]	Damage Function $f(h, b_f)$ [%]
$h \leq 0.5$	20
$0.5 < h \leq 2$	35
$2 < h \leq 4$	60
$h > 4$	95

Finally, the combined flood impact was defined as the geometric mean of the stochastic and deterministic nature impacts, which we later refer to as Im_{comb} (Equation (3)).

$$Im_{comb} = \sqrt{Im_{stoch} * Im_{determ}}, \tag{3}$$

The impact measures, i.e., Im_{stoch}, Im_{determ} and Im_{comb} express the number of a building's residents whose lives and health would be affected by a flood in a pre-modelled scenario, in the stochastic, deterministic and both aspects, respectively.

Modelling of the building's capacity b_{cap} assumes a relationship between the number of people staying in a residential building and its volumetric characteristic. The proposed approach is a further development of the model defined by [54]. It considers all houses of permanent residence, that is family buildings, children's homes, student dormitories, workers' hostels, boarding-school houses and homeless shelters. Another important factor increasing the accuracy of modelling the number of people in a building is the reduction of the total building footprint area to the total usable space. Hence, the main assumptions were as follows: A single-family house is inhabited by the statistical average number of people (Pd) provided by the Central Statistical Office (the average occupancy rate per household), while in case of a two-family house this number is multiplied by two. To estimate the number of people in multi-family buildings and other houses of permanent residence (see Table 3), the number of dwelling (or rooms, in case of hotel- or hostel-like buildings) are additionally considered, based on the number of storeys (Ns), the building footprint area (Ab) reduced to the total usable space using Ari coefficient and the dwelling (or room) average area. The total building capacity is calculated by multiplying the number of dwellings (or rooms) by the average number of person (Pd). In case of hotels, the occupancy rate (Oh) is also considered. The building capacity was computed using Python scripts according to Equation (4).

$$b_{cap}(f) = \begin{cases} Pd_i, & for\ b_c = 1 \\ 2Pd_i, & for\ b_c = 2 \\ Ns * \left(\frac{Ar_i * Ab}{Da_i}\right) * Pd_i, & for\ b_c = 3 \\ Ns * \left(\frac{Ar_i * Ab}{Da_i}\right) * Pd_i * Oh, & for\ b_c = 4 \\ Ns * \left(\frac{Ar_i * Ab}{Da_i}\right) * Pd_i, & for\ b_c = 5 \\ Ns * \left(\frac{Ar_i * Ab}{Da_i}\right) * Pd_i, & for\ b_c = 6 \end{cases} \tag{4}$$

where: b_c—residential building category, Pd_i—average number of persons per dwelling, Ns—number of storeys, Ab—area of a building's footprint in square meters, Ar_i—coefficient of building footprint area reduction, Da_i—average usable area of dwelling in square meters, Oh—occupancy rate of hotel rooms. The category of a building b_c takes the value: 1—for a single-family building, 2—for a two-family building, 3—for a multi-family building, 4—for a hotel, 5—a monastery and parish house and 6—other houses of permanent residence.

Table 3. The adopted values of coefficients used for building capacity calculation.

Building Function (b_f) Name	b_f Value	Da_i [m^2]	Pd_i	Ar_i	Oh
Single-family building	1		2.3		
Two-family building	2		2.3		
Multi-family building	3	59	2.3	0.75	
Hotel	4	18.5	1.5	0.70	0.75
Monastery and parish house	5	15	1.0	0.50	
Other houses of permanent residence (i.e., children's home, student dorm, workers' hostel, boarding-school house, social care home, homeless shelter)	6	10	2	0.65	

The analysis used 10-year mean values of the Pd_i, Da_i and Oh coefficients (Table 3) calculated from the statistical data for 2010–2019, while Ar_i was adopted on the basis of opinion of experts in the field.

The implemented coefficients for family buildings were verified by summing up the number of inhabitants in those residential building in the year 2012 located within the census enumeration area and comparing the estimated number of inhabitants with the 2011 census data. The accuracy of population estimation was 2%.

3. Results

Out of the total 156,907 buildings located in Warsaw in the year 2019, 3693 (2.35%) are situated within the 500-year flood hazard zone. Slightly more than half (50.8%) of the buildings in the flood hazard zone comprise residential buildings, including, among others, 642 single-family buildings, two semi-detached family houses, 1184 multi-family buildings and 20 hotels (see Table 4). Single-family houses, clustered linearly, are mainly located on the right-bank of Warsaw, in the fringe districts Wawer (on the south) and Białołęka, the norther district. Detached houses are scattered around the northern and southern Warsaw districts, usually in the near vicinity of single-family housing.

Table 4. Buildings and people in the floods risk zone.

Building's Type	Number of Buildings			Total Building's Occupant Capacity		
	500-Year Flood	100-Year Flood	10-Year Flood	500-Year Flood	100-Year Flood	10-Year flood
Single-family building	642	6	0	1478	14	0
Two-family building	2	0	0	9	0	0
Multi-family building	1184	0	0	111,292	0	0
Hotel	20	1	0	4233	57	0
Monastery and parish house	18	0	0	1096	0	0
Other houses of permanent residence	21	3	0	4761	262	0
Other non-residential buildings	1807	98	50	0	0	0
All buildings	3693	108	50	–	—	—
Total number of people	—	—	—	122,869	333	0

Multi-family buildings are concentrated in the city center, namely Śródmieście (20%) and Praga Północ (32.6%), and in Targówek (17.7%). They form housing estates separated by urban greenery and streets; however, several are isolated between buildings of a different type, i.e., office and service premises (see Figure 2). The spatial distribution of people (residents and hotel guests) exposed to the risk of flooding corresponds to the location of residential buildings. In total, 122,869 people may be affected by the 500-year flood and 90.57% of them lived in multi-family houses, i.e., the multifamily building capacity equals 111,292 (see Table 3). Most people at risk of flooding live in Praga Północ (44.6%), Śródmieście (27.1%) and Targówek (20.8%).

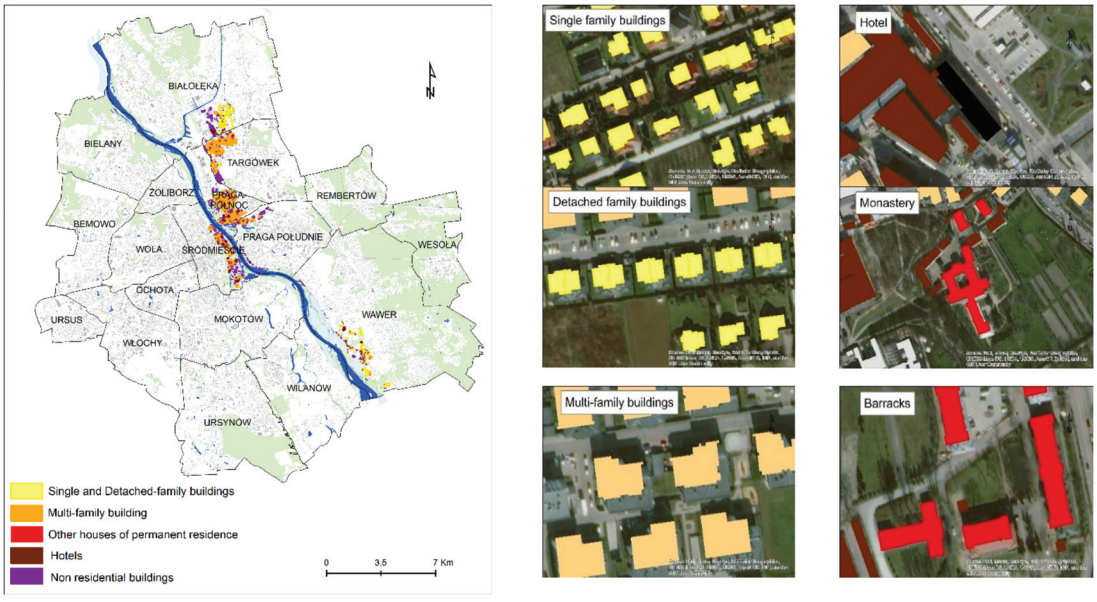

Figure 2. Warsaw, buildings in the 500 flood risk zone.

As shown in Figure 3 (the red color), the percentage of people at risk in the census enumeration areas including multi-family housing may reach even 100% and does not fall below 91%. Among people staying in houses of permanent residence (children's home, student dorm, workers' hostel, boarding-school house, social care home, homeless shelter, barracks) 4761 are exposed to the risk of flooding. On the other hand, the number of hotel guests staying in hotels located within the 500-years flood risk zone can slightly exceed 4200 people. These hotels are mainly located in the central city districts (see Figure 2). Just over a thousand people live permanently in monasteries and parish houses located in the central part of Warsaw, both on the left and right banks of the river.

Only 108 buildings are situated in the 1% risk zone (100-year flood), including six single-family houses, one hotel, three workers' hostels, most of them are located on the right bank of the Vistula, in Wawer (35%), Praga Południe (38%) and Praga Północ (15.7%). Their total capacity amounts to 333 people. The highest building capacity value, as many as 262 residents, is assigned to workers' hostels, while the average building capacity of the Wisełka Hotel equals to 57 people.

The most likely 10-year flood does not affect people staying in residential buildings, because its spatial extent is limited mainly to the Vistula riverbed (see Table 4).

Apart from function, capacity or the number of floors, a building can be characterised by the impact of a flood on its residents, where the higher the value, the more people whose lives and health would be affected by a flood in a pre-modelled scenario. Within the test area, the stochastic, deterministic and combined impacts of the flood on the building's residents range from 0 to 2.8 persons, from 0 to 482.4 persons and from 0 to 36.5 persons, respectively (Table 5).

Buildings located in the flood hazard zone have been classified according to the impact of river flooding, using Natural Break classification method (Table 5, Figure 4). As noted by Jenks [55] Natural Break classification method reduces the variance within classes and maximises the variance between classes. The classes have been assigned colours (Figure 4), which the map reader intuitively associates with the level of risk or flood impact (red—high, yellow—medium, green—low).

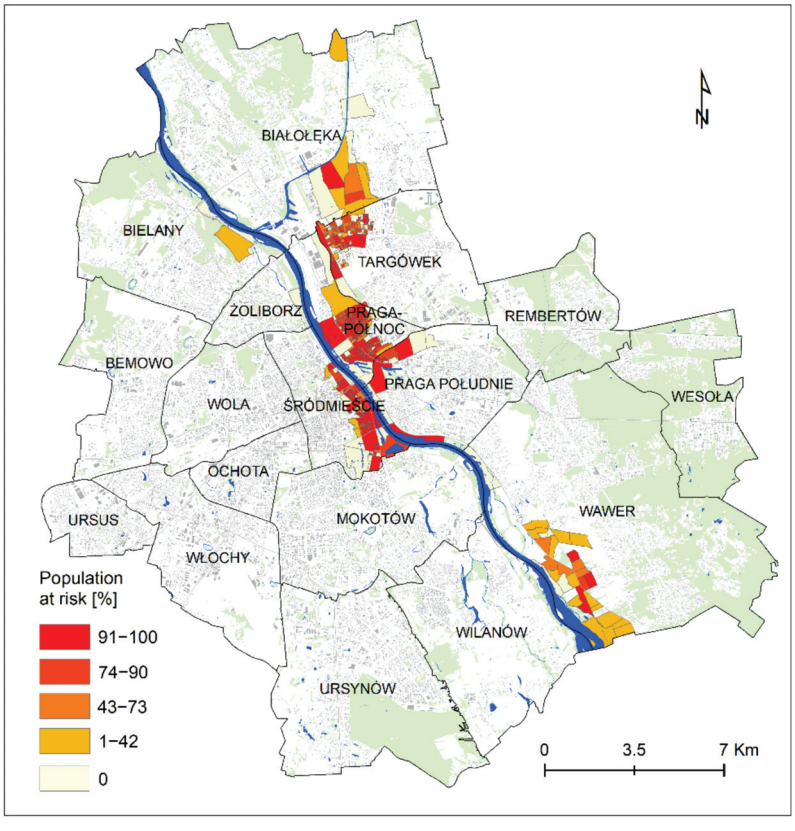

Figure 3. Warsaw population at risk, percentage of people attributed to the census enumeration areas.

Table 5. The percentage of buildings within the classes of the stochastic, deterministic and combined impacts of flooding attributed to buildings.

	Stochastic		Deterministic		Combined	
Flood Impact Class	**Class Range**	**% of Buildings**	**Class Range**	**% of Buildings**	**Class Range**	**% of Buildings**
I (low)	0.0–0.1	89.7	0.0–21.0	82.9	0.0–1.0	77.4
II (medium)	0.2–0.3	6.2	21.1–75.0	13.6	1.1–3.6	15.1
III (high)	0.4–0.7	3.2	75.1–187.0	3.2	3.7–9.1	6.1
IV (very high)	0.8–2.8	0.8	187.1–482.4	0.3	9.2–36.5	1.4
mean	0.07	n/a	11.9	n/a	0.89	n/a

The differences between the three defined impacts values are apparent within a selected sample area where different buildings belong to different flood scenario zones (as in Figure 4). In Warsaw, the number of buildings characterised by a very high flood impact equals 30, 11 or 52 for stochastic, deterministic or total impact, respectively, provided the Natural Breaks classification method is used (Figure 5).

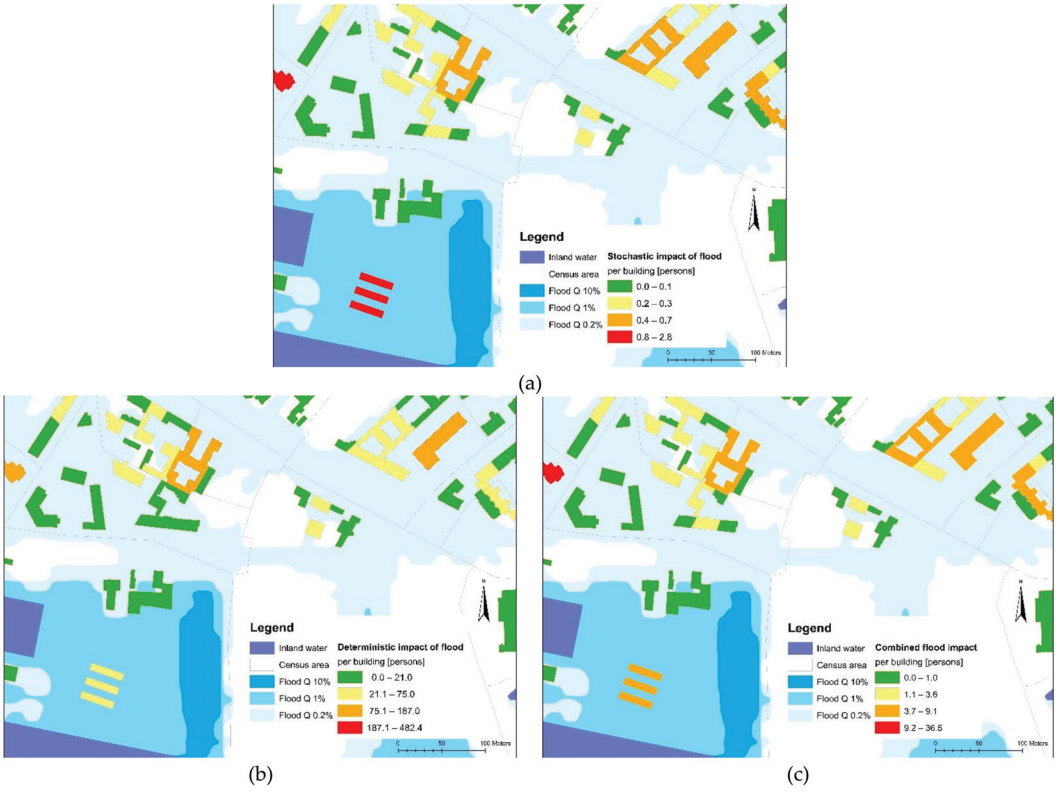

Figure 4. Residents whose lives and health would be affected by a flood in a pre-modelled scenario, in the stochastic (**a**), deterministic (**b**) or both aspects (**c**), attributed to building.

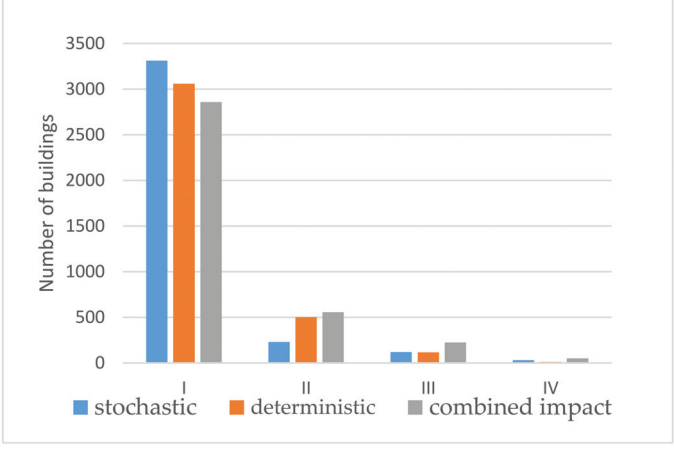

Figure 5. The values of the stochastic, deterministic and combined flood impacts on building residents within classes representing impact levels within Warsaw, Poland. The higher the class number (I, II, III, IV) the higher the impact.

The results show that over 122,000 residents live in the areas that may be affected by 500-year flood. However, the foreseen magnitude of flood impact on human health is moderate, i.e., on average ten persons per residential building over the 80% of flood risk zones. Such results are attributed to the low inundation depth, i.e., below 1 m.

The classes of combined flood impact attributed to a census enumeration area, defined as the mean (building) impact per census area, are presented in Figure 6a. The class with the highest combined impact of flooding attributed to a census area is coloured in red. Figure 6b illustrates the classes of the combined impact of flooding attributed to a building delineated as a point (i.e., building polygon weighted centre). The signatures with variable size, also referred to as quantitative signatures, were chosen to visualise the impact. The red dot applies to the highest combined impact of flooding attributed to the building.

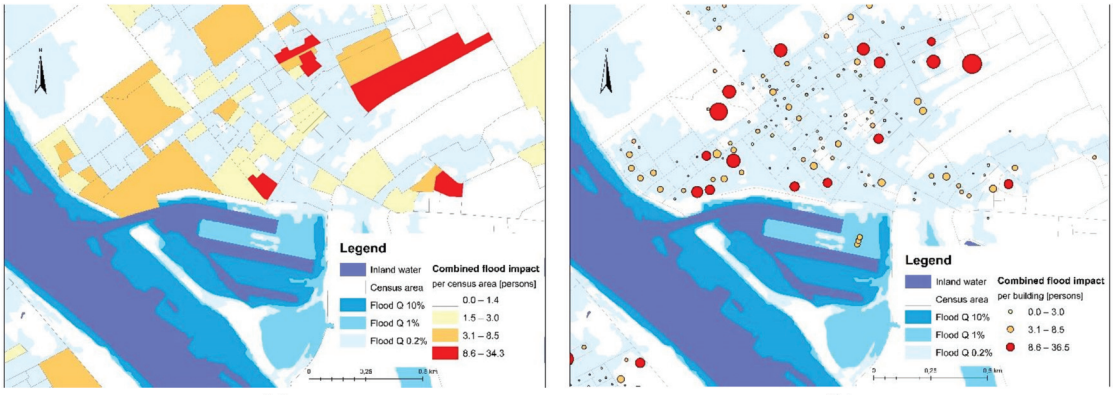

(a) (b)

Figure 6. The combined impacts of flooding attributed to a census enumeration area, selected samples of the Warsaw flood risk zone, visualised by (**a**) quantitative method, (**b**) qualitative method, variable size signatures.

The spatial distribution of the members of classes with the highest combined impact of flooding does not depend on the distance to the river. Instead, it reflects the terrain height and the distribution of the different building classes and their residents' number.

4. Discussion

4.1. Building Capacity

The building-level population represents a very high level of detail of population data, valuable for micro-scale spatial analyses (compare [56]). An example of such an analysis is a study examining the impact of potential flooding on building inhabitants. Due to the detailed population data sensitivity and consequent unavailability, scientists often downscale the global population raster product, available at 30″ resolution, using OpenStreetMap (OSM) or buildings extracted from remotely sensed data (eg, satellite imagery or LIDAR data). Birkmann and Welle [41] exploited the Global Rural-Urban Mapping Project (GRUMP) to assess people affected by natural hazard events, including floods, using a modified WorldRiskIndex. Similarly, the World Risk Index was adopted by [57] to estimate levels of flood exposure, vulnerability and risk in Brazil. To determine the number of people at risk, the authors used LandScan, the global population raster data. Zhu et al. [25] estimated the building-scale population distribution by downscaling Asia WordPop using POIs OSM data and the results obtained were generally consistent with WorldPop data on a macroscopic level (R^2 of 0.86). The global raster population data (GRUMP, LandScan, GHS-POP), however, tends to underestimate people counts in densely populated areas as well as in the transition areas between urban and rural, while overestimation was observed along main roads and in city centres [58–60].

With the advancement of remote sensing technologies, such as LIDAR, aerial and satellite imaging [61–63], it is possible to automatically and remotely measure footprint and height (or volume) of a building, however, obtaining information about the function of a building using this procedure is limited.

In this paper, a quick method to estimate a building capacity, i.e., building-level population in residential buildings and hotels, is proposed and implemented. The method can be classified as an offshoot of the volumetric method for a building population estimation (compare [64], except that it (a) requires detailed information on building types and their number of storeys (available for the whole of Poland), and (b) modifies the building volume based on this information. The effects of tourism (except from hotel occupancy rate), day- and night-time populations were not considered.

4.2. Impact of Flooding on Building's Residents

The EU Floods Directive [38] has left to the Member States, much flexibility on measures. This also applies to the assessment of the potential adverse consequences to human health. Therefore, there is a number of non-mutually exclusive approaches, their results, however, are not harmonised and thus non-comparable.

Flood damage is prevalently shown as total monetary building replacement cost [28,65] or as the number of buildings at risk [18]. Given the significant differences in the buildings considered (e.g., all residential buildings [28]; only single-family residential buildings [65]; buildings of any types [66]; residential and commercial buildings [18,28]) as well as the changes in costs depending on the geographic location of the building and the valuation date, the monetary values described in the literature are incomparable [28,67].

Regarding the defined in this study measures of the impact of flooding on building residents, it is easy to notice that the characterisation of potential losses by the expected value of the cost of flooding results in low numerical values, hence low stochastic impact values. Moreover, irresponsible (i.e., without knowledge of its interpretation) use of such an indicator, which carries information about the rare occurrence of floods, may negatively affect the awareness of flood risks among the public (inhabitants or even members of the local administration). Other worth emphasising features of the stochastic and deterministic flood impacts are their incommensurability and, to some extent, independence. Considering all three of the above-mentioned characteristics, it was somewhat challenging to fairly and correctly include both component influences in the introduced composite flood impact on building residents. To harmonise the two component impacts, their joint impact is described by their geometric mean and expresses the number of people whose health or life would be affected by the flood.

Large variations in the values of the predicted combined impact of flooding on building residents are also readily apparent. This applies both to the large scale, i.e., the level of detail of small administrative units (Warsaw census districts, average area of about 0.25 ha), and to the very large scale, i.e., the level of detail of the building. Similar variation characterises the other measures of flood impact. Such a feature is useful, allowing the classification of buildings based on impact values and consequently also the classification of census enumeration areas.

Regarding the issue of uncertainty of our approach, this is a very complex problem since the total uncertainty is a function of uncertainties of individual factors, such as data sources, data processing methods and error propagation. Models adopted at the different stages of the overall framework, e.g., hydro-modelling method, loss function, contribute to the flood impact uncertainty together with the positional and thematic accuracy of input vector data (e.g., floodplains, buildings). Another bottleneck is these uncertainties accumulations and propagation model. Therefore, the verification of the obtained results, as well as the uncertainty of the assessment of flood losses in buildings and people, was limited to the number of people assigned to the building, i.e., building's capacity.

The developed method slightly overestimated the number of people in the census EAs. The estimates lie 2% above the reference data values. Such a result contributes to the

high reliability of the method. It is a kind of unbiased population estimation approach. Moreover, the building's residents' estimation method performed well despite choosing a study area characterised by a high diversity of buildings, in terms of their function, size, density and rapid change rate.

4.3. Flood Impact Cartographic Visualisation

An adequately selected method of cartographic presentation for a studied phenomenon or indicator positively influences the interpretation of statistical relationships. There are studies (e.g., [68]) that their practical interpretation, in the context of flood risk, is supported by a wider use of qualitative methods. A range of qualitative as well as quantitative methods can be found among the methods of presenting phenomena on maps. Consequently, the cartographic visualisation of the impact of flooding can be an important, valuable and effective tool for risk communication.

The choice of both the method of impact values classification and the method of results presentation, e.g., using the cartographic visualisation, is of great importance as they should facilitate the interpretation of results, and also support the prioritisation of sub-areas within a study area, e.g., according to the magnitude of evacuation demand. Any administrative subdivision (e.g., districts, municipalities) or a special one, e.g., census tracts may serve as a spatial reference unit (sub-areas). In our example (Figure 6), the visualisation of the effects of the large-scale analyses includes the option of taking a building as the smallest spatial reference unit, while the smaller-scale visualisation includes census tracts.

5. Conclusions

As the most valuable resource, people should be targeted for special protection. The proposed new indicators can be used in every phase of the disaster life cycle, whether in investment planning, evacuation planning or educating the public to raise awareness of flood risks and their impact. Detailed information on the distribution of the population and a rapid method of obtaining indicators of the impact of flooding on this population provides a tool to support real-time crisis management in the event of an occurrence of such a hazard. In such a case, the most appropriate indicator is the deterministic flood impact. In contrast, the combined risk, carrying the deterministic and stochastic aspects, contributes to determining the regions with the greatest need for measures to mitigate the potential impacts of flooding on human health (where the higher the indicators, the greater the need) and, subsequently, facilitate to target and prioritise such measures.

The population data estimation at the (residential) building level, i.e., at the virtually highest level of detail, enables GIS analyses at any scale. For flood scenario analyses at the micro-scale is very useful, while for decision support purposes the cartographic visualisations at meso scale (achievable by dedicated generalisation of micro scale results) can be an asset.

Absolute protection against flooding, a natural severe weather phenomenon, is not achievable [69]. The continuous improvement of detailed analyses of different flood scenarios, however, including the use of the flood impact indicators proposed here, as well as their clear cartographic presentation for both decision-makers and inhabitants, contribute to effective mitigation and even protection against the false sense of security.

Our research will continue on this topic through uncertainty quantification analysis and the alternative design of the flood impact cartographic visualisations to help maximise the message comprehension independently of readers abilities or access to technology.

Author Contributions: Conceptualisation, J.N.D.C., B.C. and E.B.; methodology, J.N.D.C. and B.C.; software, B.C.; validation, J.N.D.C., B.C. and E.B.; formal analysis, B.C. and J.N.D.C.; resources, J.N.D.C. and B.C.; data curation, B.C. and J.N.D.C.; writing—original draft preparation, J.N.D.C., E.B. and B.C.; writing—review and editing, J.N.D.C., E.B. and B.C.; visualisation, B.C. and J.N.D.C.; supervision and project administration, J.N.D.C.; funding acquisition, B.C. All authors have read and agreed to the published version of the manuscript.

Funding: This research was funded by Military University of Technology, Faculty of Civil Engineering and Geodesy, grant number 531-4000-22-871/UGB/2021.

Institutional Review Board Statement: Not applicable.

Informed Consent Statement: Not applicable.

Data Availability Statement: Data used in this study were derived from public administration, i.e., buildings and Register of Territorial Division Units—from the national geoportal of Poland https://mapy.geoportal.gov.pl/imap/Imgp_2.html accessed on 5 November 2020; flood risk zones—from the State Water Holding 'Polish Water' 5 November 2020 available by request, while statistical data from Central Statistical Office web page https://stat.gov.pl/en/basic-data/ accessed on 4 January 2021.

Acknowledgments: State Water Holding 'Polish Water' is acknowledged for the flood zones data supply. Thanks to Agata Orych for proofreading the paper.

Conflicts of Interest: Authors declare no conflict of interest. The funders had no role in the design of the study; in the collection, analyses or interpretation of data; in the writing of the manuscript, or in the decision to publish the results.

References

1. Kundzewicz, Z. Adapting flood preparedness tools to changing flood risk conditions: The situation in Poland. *Oceanology* **2014**, *56*, 385–407. [CrossRef]
2. Kron, W.; Eichner, J.; Kundzewicz, Z.W. Reduction of flood risk in Europe—Reflections from a reinsurance perspective. *J. Hydrol.* **2019**, *576*, 197–209. [CrossRef]
3. EEA European Environment Agency. *Economic Losses from Climate-Related Extremes*; European Environment Agency (EEA): Copenhagen, Denmark, 2017; p. 17.
4. Wallemacq, P.; House, R. Economic Losses, Poverty & Disasters (1998–2017). United Nations Office for Disaster Risk Reduction (UNISDR) and Centre for Research on the Epidemiology of Disasters (CRED). Available online: https://www.unisdr.org/files/61119_credeconomiclosses.pdf (accessed on 10 December 2020).
5. Ritchie, H.; Roser, M. Natural Disasters. 2014. Available online: https://ourworldindata.org/natural-disasters (accessed on 10 April 2021).
6. Roudier, P.; Andersson, J.C.M.; Donnelly, C.; Feyen, L.; Greuell, W.; Ludwig, F. Projections of future floods and hydrological droughts in Europe under a +2 °C global warming. *Clim. Chang.* **2016**, *135*, 341–355. [CrossRef]
7. Rojas, R.; Feyen, L.; Bianchi, A.M.; Dosio, A. Assessment of future flood hazard in Europe using a large ensemble of bias-corrected regional climate simulations. *J. Geophys. Res. Space Phys.* **2012**, *117*. [CrossRef]
8. Blöschl, G.; Hall, J.; Parajka, J.; Perdigão, R.A.P.; Merz, B.; Arheimer, B.; Aronica, G.T.; Bilibashi, A.; Bonacci, O.; Borga, M.; et al. Changing climate shifts timing of European floods. *Science* **2017**, *357*, 588–590. [CrossRef] [PubMed]
9. Blöschl, G.; Hall, J.; Viglione, A.; Perdigão, R.A.P.; Parajka, J.; Merz, B.; Lun, D.; Arheimer, B.; Aronica, G.T.; Bilibashi, A.; et al. Changing climate both increases and decreases European river floods. *Nature* **2019**, *573*, 108–111. [CrossRef]
10. Tanoue, M.; Hirabayashi, Y.; Ikeuchi, H. Global-scale river flood vulnerability in the last 50 years. *Sci. Rep.* **2016**, *6*, 36021. [CrossRef]
11. Alfieri, L.; Dottori, F.; Betts, R.; Salamon, P.; Feyen, L. Multi-Model Projections of River Flood Risk in Europe under Global Warming. *Climate* **2018**, *6*, 6. [CrossRef]
12. Schultz, B. Flood management under rapid urbanisation and industrialisation in flood-prone areas: A need for serious consideration. *Irrig. Drain.* **2006**, *55*, S3–S8. [CrossRef]
13. Kron, W.; Löw, P.; Kundzewicz, Z.W. Changes in risk of extreme weather events in Europe. *Environ. Sci. Policy* **2019**, *100*, 74–83. [CrossRef]
14. Bouwer, L.M.; Bubeck, P.; Aerts, J.C.J.H. Changes in future flood risk due to climate and development in a Dutch polder area. *Glob. Environ. Chang.* **2010**, *20*, 463–471. [CrossRef]
15. Papilloud, T.; Röthlisberger, V.; Loreti, S.; Keiler, M. Flood exposure analysis of road infrastructure—Comparison of different methods at national level. *Int. J. Disaster Risk Reduct.* **2020**, *47*, 101548. [CrossRef]
16. Jongman, B.; Ward, P.J.; Aerts, J.C.J.H. Global exposure to river and coastal flooding: Long term trends and changes. *Glob. Environ. Chang.* **2012**, *22*, 823–835. [CrossRef]
17. Jenelius, E.; Mattsson, L.-G. Road network vulnerability analysis: Conceptualization, implementation and application. *Comput. Environ. Urban. Syst.* **2015**, *49*, 136–147. [CrossRef]
18. Hossain, M.K.; Meng, Q. A fine-scale spatial analytics of the assessment and mapping of buildings and population at different risk levels of urban flood. *Land Use Policy* **2020**, *99*, 104829. [CrossRef]
19. Bhola, P.K.; Leandro, J.; Disse, M. Building hazard maps with differentiated risk perception for flood impact assessment. *Nat. Hazards Earth Syst. Sci.* **2020**, *20*, 2647–2663. [CrossRef]

20. Röthlisberger, V.; Zischg, A.P.; Keiler, M. Identifying spatial clusters of flood exposure to support decision making in risk management. *Sci. Total. Environ.* **2017**, *598*, 593–603. [CrossRef]
21. Kappes, M.; Gruber, K.; Frigerio, S.; Bell, R.; Keiler, M.; Glade, T. The MultiRISK platform: The technical concept and application of a regional-scale multihazard exposure analysis tool. *Geomorphol.* **2012**, *151–152*, 139–155. [CrossRef]
22. Calka, B.; Da Costa, J.N.; Bielecka, E. Fine scale population density data and its application in risk assessment. *Geomatics. Nat. Hazards Risk* **2017**, *8*, 1440–1455. [CrossRef]
23. Hirabayashi, Y.; Mahendran, R.; Koirala, S.; Konoshima, L.; Yamazaki, D.; Watanabe, S.; Kim, H.; Kanae, S. Global flood risk under climate change. *Nat. Clim. Chang.* **2013**, *3*, 816–821. [CrossRef]
24. Kolen, B.; Kutschera, G.; Helsloot, I. A Comparison Between the Netherlands and Germany of Evacuation in Case of Extreme Flooding. In Proceedings of the Urban Flood Conference, Paris, France, 26–27 September 2010; Available online: https://www.hkv.nl/wp-content/uploads/2020/07/A_Comparison_between_The_Netherlands_and_Germany_BK_verkortwebsite.pdf (accessed on 1 February 2021).
25. Zhu, S.; Dai, Q.; Zhao, B.; Shao, J. Assessment of Population Exposure to Urban Flood at the Building Scale. *Water* **2020**, *12*, 3253. [CrossRef]
26. Darabi, H.; Haghighi, A.T.; Mohamadi, M.A.; Rashidpour, M.; Ziegler, A.D.; Hekmatzadeh, A.A.; Kløve, B. Urban flood risk mapping using data-driven geospatial techniques for a flood-prone case area in Iran. *Hydrol. Res.* **2020**, *51*, 127–142. [CrossRef]
27. Messner, F.; Meyer, V. Guidelines for Direct, Tangible Flood Damage Evaluation. Evaluating Flood Damages: Guidance and Recommendations on Principles and Methods. Report No. T09-06-01. 2007. Available online: http://www.floodsite.net/html/grenoble_workshop/documents/Floodsite_Task9Review_Feb2008_short.pdf (accessed on 24 February 2021).
28. Oliveri, E.; Santoro, M. Estimation of urban structural flood damages: The case study of Palermo. *Urban. Water* **2000**, *2*, 223–234. [CrossRef]
29. Gutry-Korycka, M.; Magnuszewski, A.; Suchożebrski, J.; Jaworski, W.; Marcinkowski, M.; Szydłowski, M. Numerical estimation of flood zones in the Vistula River valley, Warsaw, Poland. In Proceedings of the 5th FRIEND World Conference (Climate Variability and Change—Hydrological Impacts), Havana, Cuba, 10–16 November 2006; IAHS Publ. 308: Wallington, UK, 2006.
30. De Moel, H.; Aerts, J.C.J.H. Effect of uncertainty in land use, damage models and inundation depth on flood damage estimates. *Nat. Hazards* **2011**, *58*, 407–425. [CrossRef]
31. Park, K.; Won, J.-H. Analysis on distribution characteristics of building use with risk zone classification based on urban flood risk assessment. *Int. J. Disaster Risk Reduct.* **2019**, *38*, 101192. [CrossRef]
32. Nriagu, J. Encyclopedia of Environmental Health, 2nd ed.Elsevier: Amsterdam, The Netherlands, 2019; ISBN 978-0-444-63952-3.
33. Zabini, F.; Grasso, V.; Crisci, A.; Gozzini, B. How do people perceive flood risk? Findings from a public survey in Tuscany, Italy. *J. Flood Risk Manag.* **2021**, *14*. [CrossRef]
34. Mol, J.M.; Botzen, W.J.W.; Blasch, J.E.; De Moel, H. Insights into Flood Risk Misperceptions of Homeowners in the Dutch River Delta. *Risk Anal.* **2020**, *40*, 1450–1468. [CrossRef]
35. Kellens, W.; Terpstra, T.; De Maeyer, P. Perception and Communication of Flood Risks: A Systematic Review of Empirical Research. *Risk Anal.* **2013**, *33*, 24–49. [CrossRef]
36. Hagemeier-Klose, M.; Wagner, K. Evaluation of flood hazard maps in print and web mapping services as information tools in flood risk communication. *Nat. Hazards Earth Syst. Sci.* **2009**, *9*, 563–574. [CrossRef]
37. ISOK. Country's Protection Against Extreme Hazards. Available online: https://imgw.isok.gov.pl/index.html (accessed on 4 November 2020).
38. Directive 2007/60/EC of the European Parliament and of the Council of 23 October 2007 on the Assessment and Management of Flood Risks. Official Journal of the European Union, L 288/27, 06 November 2007. Available online: https://eur-lex.europa.eu/legal-content/EN/TXT/PDF/?uri=OJ:L:2007:288:FULL&from=EN (accessed on 4 January 2021).
39. Water Act, the Act of July 20, 2017. *J. Law* **2017**, 1566. Available online: https://isap.sejm.gov.pl/isap.nsf/download.xsp/WDU20170001566/U/D20171566Lj.pdf (accessed on 4 January 2021).
40. Regulation of Ministry of 21 November 2012 on the Development of Flood hazard Maps and Flood Risk Maps. *J. Laws* **2013**, 104. Available online: http://isap.sejm.gov.pl/isap.nsf/download.xsp/WDU20130000104/O/D20130104.pdf (accessed on 19 November 2020).
41. Birkmann, J.; Welle, T. Assessing the risk of loss and damage: Exposure, vulnerability and risk to climate-related hazards for different country classifications. *Int. J. Glob. Warm.* **2015**, *8*, 191–212. [CrossRef]
42. Kreimer, A. Social and Economic Impacts of Natural Disasters. *Int. Geol. Rev.* **2001**, *43*, 401–405. [CrossRef]
43. Magnuszewski, A.; Moran, S. Vistula river bad erosion processes and their influence on Warsaw's flood safety. In Proceedings of the Sediment Dynamics from the Summit to the Sea Symposium, New Orleans, LA, USA, 11–14 December 2014; p. 367. [CrossRef]
44. Cyberski, J.; Grześ, M.; Gutry-Korycka, M.; Nachlik, E.; Kundzewicz, Z. History of floods on the River Vistula. *Hydrol. Sci. J.* **2006**, *51*, 799–817. [CrossRef]
45. Bielecka, E.; Calka, B.; Bitner, A. Spatial distribution of urban greenery in Warsaw. A quantitative approach. In *Proceedings of 7th International Conference on Cartography and GIS.; Sozopol, Bulgaria, 18–23 June 2018*; Bandrova, T., Konečný, M., Eds.; Bulgarian Cartographic Association: Sofia, Bulgaria, 2018; pp. 408–416. Available online: https://iccgis2018.cartography-gis.com/proceedings (accessed on 24 February 2021).

46. Zmudzka, E.; Kulesza, K.; Lenartowicz, M.; Leziak, K.; Magnuszewski, A. Assessment of modern hydro-meteorological hazards in a big city—Identification for Warsaw. *Meteorol. Appl.* **2019**, *26*, 500–510. [CrossRef]
47. Bielecka, E.; Dukaczewski, D.; Janczar, E. Spatial Data Infrastructure in Poland—Lessons learnt from so far achievements. *Geod. Cartogr.* **2018**, *67*, 3–23. [CrossRef]
48. The Polish Spatial Infrastructure Geoportal. Available online: https://mapy.geoportal.gov.pl/imap/Imgp_2.html?gpmap=gp0 (accessed on 5 November 2020).
49. Matczak, P.; Lewandowski, J.; Choryński, A.; Szwed, M.; Kundzewicz, Z.W. Doing more while remaining the same? Flood risk governance in Poland. *J. Flood Risk Manag.* **2018**, *11*, 239–249. [CrossRef]
50. Council of Ministers. Regulation of the Council of Ministers of December 15, 1998 on the detailed rules for maintaining, ap-plying and making available the national official register of territorial division of the country and the related obligations of government administration bodies and local government units. *J. Law* **1998**, *1031*.
51. Local Data Bank, Central Statistical Office, Warsaw, Poland. Available online: https://bdl.stat.gov.pl/BDL/dane/podgrup/temat (accessed on 4 January 2021).
52. Voss, P.R.; Long, D.D.; Hammer, R.B. *When Census Geography Doesn't Work: Using Ancillary Information to Improve the Spatial Interpolation of Demographic Data*; CDE Working Paper No. 99–26; Center for Demography and Ecology, University of Wisconsin: Madison, WI, USA, 1999.
53. Thompson, C.M.; Frazier, T.G. Deterministic and probabilistic flood modeling for contemporary and future coastal and inland precipitation inundation. *Appl. Geogr.* **2014**, *50*, 1–14. [CrossRef]
54. Calka, B.; Bielecka, E.; Zdunkiewicz, K. Redistribution population data across a regular spatial grid according to buildings characteristics. *Geod. Cartogr.* **2016**, *65*, 149–162. [CrossRef]
55. Jenks, G.F. The Data Model Concept in Statistical Mapping. *Int. Yearb. Cartogr.* **1967**, *7*, 186–190.
56. Messner, F.; Meyer, V. Flood damage, vulnerability and risk perception—challenges for flood damage research. In *Flood Risk Management: Hazards, Vulnerability and Mitigation Measures*; Schanze, J., Zeman, E., Marsalek, J., Eds.; Springer: Dordrecht, The Netherlands, 2005; Volume 67, pp. 149–167.
57. De Almeida, L.Q.; Welle, T.; Birkmann, J. Disaster risk indicators in Brazil: A proposal based on the world risk index. *Int. J. Disaster Risk Reduct.* **2016**, *17*, 251–272. [CrossRef]
58. Da Costa, J.N.; Bielecka, E.; Calka, B. Uncertainty Quantification of the Global Rural-Urban Mapping Project over Polish Census Data. In Proceedings of the 10th International Conference Environmental Engineering; Vilnius Gediminas Technical University, Vilnius, Lithuania, 27–28 April 2017.
59. Calka, B.; Bielecka, E. Reliability Analysis of LandScan Gridded Population Data. The Case Study of Poland. *ISPRS Int. J. Geo-Inf.* **2019**, *8*, 222. [CrossRef]
60. Calka, B.; Bielecka, E. GHS-POP Accuracy Assessment: Poland and Portugal Case Study. *Remote Sens.* **2020**, *12*, 1105. [CrossRef]
61. Chen, K. An approach to linking remotely sensed data and areal census data. *Int. J. Remote Sens.* **2002**, *23*, 37–48. [CrossRef]
62. Wu, C.; Murray, A.T. Population Estimation Using Landsat Enhanced Thematic Mapper Imagery. *Geogr. Anal.* **2007**, *39*, 26–43. [CrossRef]
63. Tomás, L.; Fonseca, L.M.G.; Almeida, C.; Leonardi, F.; Pereira, M.N. Urban population estimation based on residential buildings volume using IKONOS-2 images and lidar data. *Int. J. Remote Sens.* **2016**, *37*, 1–28. [CrossRef]
64. Lwin, K.; Murayama, Y. A GIS Approach to Estimation of Building Population for Micro-spatial Analysis. *Trans. GIS* **2009**, *13*, 401–414. [CrossRef]
65. ElFouly, M.; Labetski, A. Flood damage cost estimation in 3D based on an indicator modelling framework. *Geomat. Nat. Hazards Risk* **2020**, *11*, 1129–1153. [CrossRef]
66. Merz, B.; Kreibich, H.; Thieken, A.; Schmidtke, R. Estimation uncertainty of direct monetary flood damage to buildings. *Nat. Hazards Earth Syst. Sci.* **2004**, *4*, 153–163. [CrossRef]
67. Merz, B.; Kreibich, H.; Schwarze, R.; Thieken, A. Review article Assessment of economic flood damage. *Nat. Hazards Earth Syst. Sci.* **2010**, *10*, 1697–1724. [CrossRef]
68. Bell, H.M.; Tobin, G.A. Efficient and effective? The 100-year flood in the communication and perception of flood risk. *Environ. Hazards* **2007**, *7*, 302–311. [CrossRef]
69. WHO. *Floods: Climate Change and Adaptation Strategies for Human Health. Report on a WHO Meeting, London, United Kingdom, 30 June–2 July 2002*; EUR/02/5036813; WHO Regional Office for Europe: Copenhagen, Denmark, 2002.

resources

MDPI

Article

Worry about Climate Change and Urban Flooding Risk Preparedness in Southern Italy: A Survey in the Simeto River Valley (Sicily, Italy)

Paola Nanni *, David J. Peres, Rosaria E. Musumeci and Antonino Cancelliere

Department of Civil Engineering and Architecture, University of Catania, 95123 Catania, Italy; djperes@dica.unict.it (D.J.P.); rosaria.musumeci@unict.it (R.E.M.); antonino.cancelliere@unict.it (A.C.)
* Correspondence: paola.nanni@unict.it

Abstract: Intensive urbanization and related increase of impervious surfaces, causes negative impacts on the hydrological cycle, amplifying the risk of urban floods. These impacts can get even worse due to potential climate change impacts. The urban areas of the Simeto River Valley (SRV), the largest river valley in Sicily (Italy), have been repeatedly hit by intense rainfall events in the last decades that lead to urban flooding, causing several damages and, in some instances, threats to population. In this paper, we present the results of a 10-question survey on climate change and risk perception in 11 municipalities of the SRV carried out within the activities of the LIFE project SimetoRES, which allowed to collect 1143 feedbacks from the residents. The survey investigated: (a) the level of worry about climate change in relation to extreme storms, (b) elements of urban flooding risk preparedness: the direct experience of the residents during heavy rain events, their trust in a civil protection regional alert system, and their knowledge of the correct behavior in case of flood, and (c) the willingness of citizens to implement sustainable drainage actions for climate change adaptation in their own municipality and real estates. The results show that more than 52% of citizens has inadequate knowledge of the correct behavior during flooding events and only 30% of them feel responsible for mitigation of flooding risk. There is a modest willingness by the population to support the construction of sustainable urban drainage infrastructures. A statistical cross-analysis of the answers to the different questions, based on contingency matrices and conditional frequencies, has shown that a greater worry about climate change has no significant impact either on the behavior of people in dangerous situations occurring during flooding events or on the willingness to support financially sustainable solutions. These results suggest that to build a higher worry about climate change and related urban flooding risk is not sufficient to have better preparedness, and that more direct educative actions are necessary in the area.

Keywords: risk preparedness; urban flooding; resilience; climate change adaptation; community involvement

Citation: Nanni, P.; Peres, D.J.; Musumeci, R.E.; Cancelliere, A. Worry about Climate Change and Urban Flooding Risk Preparedness in Southern Italy: A Survey in the Simeto River Valley (Sicily, Italy). *Resources* **2021**, *10*, 25. https://doi.org/10.3390/resources10030025

Academic Editor: Nicoletta Santangelo

Received: 17 February 2021
Accepted: 11 March 2021
Published: 14 March 2021

Publisher's Note: MDPI stays neutral with regard to jurisdictional claims in published maps and institutional affiliations.

1. Introduction

Climate change (CC) is a major societal risk issue and there are increasing calls for urgent mitigation and adaptation actions [1]. Over the last decade, many studies have highlighted the importance of adaptation by testing ecosystem-based approaches as a means of understanding and improving the integration of such approaches into climate change adaptation and mitigation strategies [2–5]. The traditional approach to urbanization based exclusively on impervious paving of surfaces and stormwater management relying on grey infrastructures (sewers), is not sustainable and thus is no longer compatible with climate change adaptation strategies [6–8]. The increasing urbanization leads to a greater share of impervious areas that result in increased flood risk and overloaded storm water pipe systems. For this reason, blue-green storm water and nature-based solutions have come to be seen as efficient measures against increasing flood risk in urban areas [9–11].

Flood risk may be defined as the product between the probability of flood hazard and the consequence of occurrence of flood event [12] according to

$$\text{Flood risk} = \text{probability of flood hazard} \times \text{consequence of occurrence of flood event}$$

where consequence of occurrence of flood event is a function of hazard × vulnerability, the latter here including both exposure and susceptibility of harm. Several studies state that current understanding of flood risk focuses on two main factors: climate change and socioeconomic growth [11–13].

The risk of flooding for city population has been generally increasing in the past decades, and not sufficiently contrasted in terms of retrofitting urban drainage systems to urban expansion, mainly because of the significant monetary investments needed, which are not sufficiently stimulated by citizens and local administrators due to low awareness of the issue [14,15]. Hence, soft measures (i.e., non-infrastructural) oriented to increase risk awareness and preparedness of the population at all levels are of key importance, also given the comparatively low investments needed with respect to hard (i.e., infrastructural) urban flooding mitigation measures. In fact, education to flood risk awareness and preparedness has led to many benefits in several cases [16]. Several episodes in Italy have demonstrated that inadequate preparedness to urban flooding risk is a factor that contributed significantly to many casualties. Many news and videos show an incautious exposure to dangerous situations by people, which demonstrates their low levels of risk awareness. For instance, while torrents within a town were flooding with water levels near to the intrados of a bridge, people crossed it and stood upon it for mere curiosity and to shoot videos with their smartphones. Similar situations have occurred with respect to underpasses. As a confirmation that this issue does exist and is of particular concern, it can be mentioned that the Italian Civil Protection has promoted an educational campaign named "Io non rischio" (I don't take risks) in order to help people to understand which is the correct behavior during floods and other natural hazards (http://iononrischio.protezionecivile.it/en/homepage/, last accessed on 15 February 2021).

1.1. Natural Hazard Risk and Climate Change Perception

Early analyses of risk from natural hazards focused on the search for physical and tangible causes, while recently risk awareness has been gradually incorporated in several studies [17–21]. Focus has been put, particularly, on the risk of floods and landslides [16,22–25].

The spectrum of risk perception in natural hazards includes three distinct elements: worry, awareness, and preparedness [24,26–29]. In particular, according to [24], the following definitions can be given, which we use within this study: *worry* is the level of dread or concern associated with the given risk (climate change or urban flooding); *awareness* can be defined as knowledge or consciousness of the risk that an individual or a group of individuals is exposed to; *preparedness* is both the capability of coping with a flood throughout the inundation period, and post-flood recovery capability and strategies, and can be described in social, technical, economic and institutional dimensions.

Bubeck et al. (2012) [30] suggest that the relationship between individual flood risk perceptions and mitigation behavior is hardly observed in empirical studies. Other research has included the social perception of risk by using approaches that combine data on physical processes with individual interpretations of the risk [31–33]. At a national scale, investigators have estimated the individual and collective risk posed by landslides and floods to the population [34], though the assessment of public perception of the risk posed by landslides and floods in Italy remains mostly unexplored. A number of studies have been focused on the use of specific surveys to investigate natural hazard risk perception. For example, Avvisati et al. (2019) [17] carried out a study of multi-risk perception in 12 municipalities and 2 territorial unions of Campania Region characterized by different risks: seismic, volcanic, hydrogeological (floods and landslides). The results showed that historical memory plays a crucial role in the perception of natural hazards.

On the other hand, looking at studies related to Europe, Diakakis et al. (2018) [22] administered questionnaires to the population of the Attica Region in Greece, to obtain basic information on how individuals understand flood risk, risk mitigation and to what degree they take protection measures, investigating on which degree they trust relevant institutions and their awareness of flood warning and flood protection actions. Their results showed that respondents rank floods third in terms of importance—behind earthquakes and forest fires—among the more relevant risks in the region, despite the clear majority believed the risk is increasing, mostly due to anthropogenic factors. Responses illustrated low levels of trust in authorities and low levels of knowledge of protection actions and awareness regarding floods, as well as low levels of preparedness, in terms of undertaking private mitigation measures.

Other studies claim that the communication of information about natural hazard risks to the public is a difficult task for decision-makers. Feldman et al. (2016) [35] suggest that newer forms of technology present useful options for building disaster resilience and that age is the central factor in predicting the sources people use to receive risk information.

The literature concerning the perception of climate change has developed mainly in the last decade. S. Van Der Linden (2014) [36] claims that climate change compared with many other hazards is therefore relatively unique: not only because of its scope and breadth but also in the sense that it is not directly "situated" in our daily environment [37]. Nevertheless, an increasing amount of research has shown that people can (to some extent) accurately detect changes in their local climate and relate this perceptual experience to climate change [38]. Moreover, the rising incidence rate of extreme weather events is now increasingly being associated with climate change [39]. In fact, a number of studies have indicated that personal experience with extreme weather events is a significant predictor of climate change risk perceptions [38,40–42].

The link between the various facets of risk perception (worry, awareness, and preparedness) is difficult to capture. In particular, as reviewed by [43], the literature reports either indifference or positive association between worry about risk and preparedness against it. Hence, further contributions to this aspect are important.

1.2. Aim of the Study

This study aims at understanding, with reference to the Simeto River Valley (SRV) area in Sicily, Italy:

(a) what is the current level of worry of the population about the climate change issue and to which extent they link urban flooding to climate change;
(b) the level of individuals' risk preparedness (short-term preparedness), specifically with reference to the way a person behaves during urban flooding events;
(c) long-term preparedness, specifically, people's willingness to invest as individuals and as a community in climate change adaptation infrastructures for sustainable urban drainage.

We also want to explore some of the links between the three listed aspects and in particular, the link between the level or worry about climate change and the short-term and long-term preparedness to urban flooding issues potentially exacerbated by climate change. To investigate these issues, a survey has been administered to the population, as part of the activities of EU LIFE project SimetoRES (www.lifesimetores.it, accessed on 15 February 2021). In order to involve all age categories of the local population, the survey has been conceived to be simple and short. Given the characteristics of the population, the survey constituted also a "hook" for involving the citizens in more intensive and active initiatives. The survey was open for about three months and 1143 responses were received, which constitutes a large dataset in comparison to many other studies. The survey, consistent with the aims of the study, was articulated in three respective sections exploring each of the above-mentioned aspects.

The collected data can be considered representative of the perception of climate change effects on flood risk within urban contexts typical of Southern Italy. In this geographical

area, urbanization has developed quite often with low attention to storm water management and urban planning in general; also, the seniors may have a quite low degree of education, given the predominantly agricultural vocation of the past economy in the area. Given these characteristics of the area, existing literature on the subject, and relative to other sites in the globe, may not be enough representative.

2. Materials and Methods

2.1. Description of Survey Area

The Simeto River basin (Figure 1) is located on the Southwest of Mount Etna, the largest active volcano in Europe, and is therefore characterized by quite unique natural features [44]. The basin extends in the territories of the provinces of Catania, Enna, and Messina, with a surface that measures approximately 4030 km^2. The SRV is an area located along the central stretch of the Simeto River, which is the main river in Sicily, a few kilometers west of the Catania Metropolitan Area. Approximately 150,000 people live in the SRV area, distributed in 10 medium-small towns: the largest community is the city of Paternò with 50,000 residents, while the smallest is Ragalna with around 4000 [45]. In the last two decades, part of this community has been involved in participatory actions for the sustainable development of the area. In particular, thanks to the cooperation between local groups of citizens, organized in an association named Participatory Presidium of the Simeto River Agreement (PSRA) [46], local administration bodies and the University of Catania, in 2015 the municipalities of Paternò, Ragalna, S.M. di Licodia, Motta Sant'Anastasia, Belpasso, Biancavilla, Adrano, Centuripe, Troina, and Regalbuto, for a total of about 100,000 inhabitants, the PSRA and the University of Catania have signed the Simeto River Agreement (SRA), a river contract aiming at encouraging local development through participatory approaches (Figure 2). Figure 2 shows the location of the municipalities involved in the SRA along with the location of Catania, where the University of Catania is based, and where the present survey was also administered.

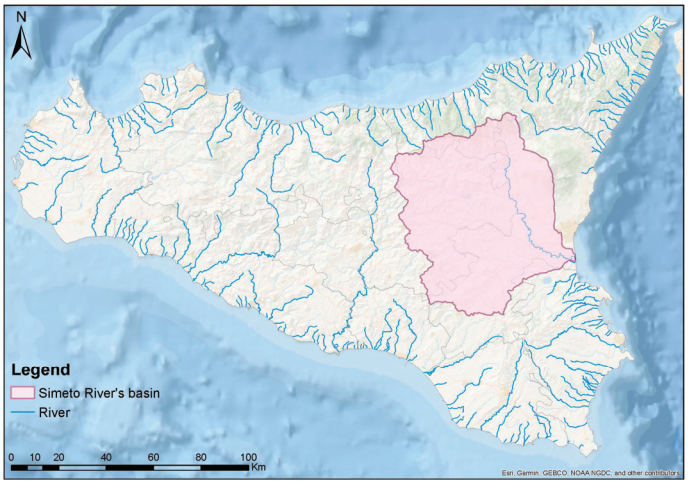

Figure 1. Location of the Simeto River basin on the east of Sicily (Italy).

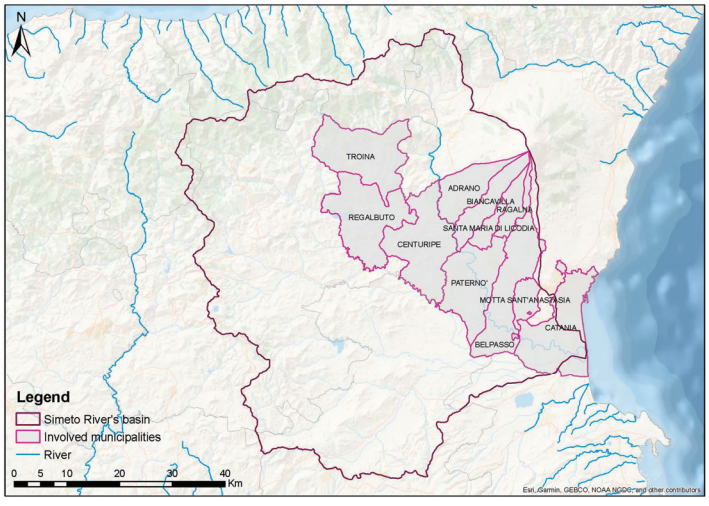

Figure 2. Location of the municipalities involved in the Simeto River Agreement, plus the city of Catania.

The pluviometric regime in the Simeto River basin is characterized by maximum average values in the month of December and, progressively smaller, in the months of January, November, and October and the minimum average values in July or in August. The Simeto River basin, particularly in the central area at higher elevations, is subject to heavy rainfall events in autumn and spring [47]. With the increase of urban sprawl, impervious surfaces replaced the more permeable ancient streets, small retention areas have been covered, and new roads interrupted the hillslopes or new constructions have been introduced. This intensive urbanization has not been accompanied by adequate retrofitting for urban flood control. In the case of the municipalities on the slopes of Etna, the situation is further complicated by the need for an inter-municipal view of stormwater management, which is seldom fostered. The development of commercial, industrial, and urbanization services along the road axes realized a real urbanized continuum. It follows that this area is particularly vulnerable to changes induced by geomorphological and hydrogeological processes, which may exacerbate if solutions are not properly implemented. The current Basin Plan technical documentation quantifies the hazard and risk related to geo-hydrological hazards for the municipalities of the Simeto Valley. A summary of the figures for hydraulic and geo-hydrological hazard is shown in Tables 1 and 2. These data can be an element of comparison with the results of the survey, i.e., to see how risk awareness of the population corresponds to the expert knowledge of flooding hazard in the area. It is worthwhile to mention that, in such technical documentation, geo-hydrological risk is defined as the risk connected to the instability of the slopes, due to particular geological and geomorphological processes, while the hydraulic risk is linked to large river flooding following particular environmental, atmospheric, or meteorological and climatic conditions affecting rainwater and their hydrological cycle, with possible consequences on the safety of the population and on the safeguard of services and activities. As shown in the table of geomorphological hazard (Table 1), the municipalities with the highest surface area at risk are Centuripe, Regalbuto, and Troina, while the ones with the highest surface at hydraulic risk (Table 2) are Catania, Paternò, and Belpasso.

Table 1. Extension of the areas with different levels of geomorphological hazard, as quantified by the plan for the Simeto River basin, P4 indicates the highest level of hazard, P1 the lowest [47].

Municipality	Total Surface (ha)	Geomorphological Hazard Surfaces (ha)			
		P4	P3	P2	P1
Centuripe	17,419.7	15.66	40.95	822.43	74.41
Regalbuto	17,029.4	185.75	45.78	606.05	151.33
Troina	16,828.0	38.30	31.72	964.58	331.71
Adrano	8322.2	22.47	46.48	49.44	14.40
Belpasso	16,632.8	0.00	0.00	50.37	0.00
Biancavilla	7027.6	21.00	28.19	0.00	0.00
Catania	18,290.0	11.95	2.73	42.95	5.47
Motta Sant'Anastasia	3570.6	1.37	17.08	187.76	5.06
Paternò	14,468.2	5.46	14.96	196.39	4.95
Santa Maria di Licodia	2627.6	1.73	6.76	0.00	0.00
Ragalna	3952.8	0.00	0.00	0.00	0.00

Table 2. Extension of the areas at different levels of hydraulic hazard for the Simeto River basin, P3 indicates the highest level of hazard, P1 the lowest [47].

Municipality	Total Surface (ha)	Hydraulic Hazard Surfaces (ha)		
		P3	P2	P1
Centuripe	17,419.7	162.76	195.65	406.48
Regalbuto	17,029.4	31.78	84.25	100.66
Troina	16,828	0.00	0.00	0.00
Adrano	8322.2	0.00	0.00	0.00
Belpasso	16,632.8	639.47	3270.93	4970.44
Biancavilla	7027.6	90.29	98.84	103.67
Catania	18,290	4104.72	8821.15	9192.27
Motta Sant'Anastasia	3570.6	57.04	192.02	197.39
Paternò	14,468.2	1043.63	1583.98	2191.85
Santa Maria di Licodia	2627.6	0.00	0.00	0.00
Ragalna	3952.8	0.00	0.00	0.00

In addition to these figures, it should be mentioned that the SRV has been repeatedly hit in recent years by intense pluvial flooding events, caused by heavy rain in combination with an overwhelmed drainage system. These events proved that it is important to develop strategies with different time horizons and priorities for management alternatives to mitigate pluvial flooding risk.

The city of Paternò, which has about 50,000 residents, has experienced several times pluvial flooding episodes that affected the entire city. For instance, in the fall of 2009 and subsequently, in November 2011, March 2013, and August 2015, this city has been hit by intense rainfall and the city drainage system proved insufficient, with the consequence of flooding of the roadways and damages to public and private buildings. More recently, in October 2018, a flood caused a dangerous situation near the riverbed of the Simeto River, where some houses that fall along the banks had already been invaded by water and mud. The greatest damages recorded were those caused by the overflow of the Simeto River. The waters of the river invaded the Catania-Siracusa Highway, which was temporarily closed. Another event occurred in October 2019, when Paternò and the surrounding cities were hit by a heavy storm. The situation appeared critical and the peripheral roads were invaded by water and mud, a person was trapped in an underpass. Another person was rescued in extremis by a truck driver after his car was left at the mercy of the river of mud with no possibility of movement. These episodes are just a few of the many signs that reveal the need for a better understanding of the potential risks for people's lives during intense rainfall and consequent flooding. Figure 3 shows some images of floods of recent years in the cities of Paternò and Catania.

Figure 3. Images of the floods of recent years: (**a**) street of Paternò during the flood of August 2015, (**b**) square of Paternò during the flood of March 2013, (**c**) Via Etnea of Catania during the flood of October 2018, (**d**) Piazza Università of Catania during the flood of October 2018.

It is important to specify that insurance against flood damages is not so common among citizens. The Ministry of infrastructure and transport and the Ministry of the Environment and Land and Sea Protection, as well as local departments, allocate funds for hard and soft measures against floods and other natural disasters. State and Regional special laws are emanated in case of catastrophic natural disasters for compensating flood damages and for reconstruction of damaged areas.

2.2. Study Design

The design of the survey considered some other works, both Italian and foreign, which have a similar structure. For example, the municipality of Ferrara (Italy) in 2010 conducted a study based on nine multiple-choice questions to better understand knowledge, sensitivity, and interest in climate change through the population [48]. The Joint Disaster Management Risk Assessment and Preparedness in the Danube Macro-region project [49] conducted a study to evaluate climate change perception, submitting to citizens multiple-choice questions, as in our case, about the involvement by the media on the treatment of the topic, the perception of climate change compared to past decades (especially for the adult population) and the actual derived risks, including extreme precipitation events and floods. A study by Yale University estimates U.S. climate change beliefs, risk perceptions, and policy preferences at State and local scale using the Yale Climate Opinion Maps based on 2018 data [50]. This survey, with its about 20 questions with Likert scale [51], tried to investigate the opinions of the community regarding climate change and the risks deriving from it.

In 2017, the European Commission published the special Eurobarometer 459, with the result of a large-scale survey proposed in some European countries. The key topic was, again, the perception of climate change, but with a focus on the responsibilities of national governments [52].

The survey here in question, reported entirely in the Appendix A, consisted of 10 questions, some of them structured with answers requiring a numerical value, following the Likert scale [51]. The questions were formulated independently against each other and their number was reduced to the minimum in order to keep it less tedious for respondents, in order to reach a high number of participants.

As already mentioned, the survey is divided into three sections. In detail, the first part of the survey recalled recent episodes of severe flooding occurred in the Simeto Valley in the autumn of 2018. We asked if such events were related to climate change, or if they could be considered frequent events during the fall season or else if they were isolated phenomena. Subsequently, we asked how often they heard about climate change and through which channels. The central part of the questionnaire started by analyzing the day-life experience of citizens, by asking if they pass or live close to places frequently flooded during extreme rain events. Then we asked, using a Likert scale, how worried they feel about weather alerts, to understand how much confidence the citizen have in the Civil Protection and local authorities, which are responsible for issuing such alerts. Finally, we investigated their individual preparedness, i.e., their tendency to behave correctly during urban flooding, asking them what they would do in three distinct possible scenarios: they are at work or at school, they have to go through an underpass or they have to pass a bridge.

The last part of the questionnaire concerned the community's willingness to adapt to climate change, as a further measure of long-term preparedness. First, we asked about the best practices for adapting to climate change according to citizens, to investigate whether they really knew the meaning of this type of practice. Finally, we investigated how much they would be willing to spend to implement measures for climate change adaptation. In this sense, they were asked whether they were willing to accept a municipal expense for the purpose and whether they were willing to invest in new adaptation works on their private properties. This last part has been automatically submitted only to adults (over 19 years old), as for the children these questions are of difficult understanding or not relevant. The survey had anonymous answers, but prior to the 10 illustrated questions, the participants had to fill some general information on their age, gender, main occupation, education level, and city of residence in order to socio-geographically characterize the answers.

It should be pointed out that this survey has been carried out in a local context where various community involvement actions are already active. As mentioned above, recently part of this community has been involved in participatory actions for the sustainable development of the area, therefore some citizens are already somehow sensible to some of the topics of the survey. In a context such as this, the present questionnaire aims to serve not only as a statistical and investigative tool but also represents a training opportunity for citizens, bringing their attention to its topics, as well as the possibility of encouraging and strengthening community involvement within the SRA.

2.3. Distribution of the Survey and Sample Characterization

The survey was published and distributed mainly electronically through the web-platform EU Survey (https://ec.europa.eu/eusurvey, accessed on 15 February 2021), for a period of about three months and was advertised through the social channels of the LIFE SimetoRES Project IT-LIFE17_CCA_IT_000115, Simeto River Agreement, and the University of Catania social channels (Facebook, Twitter, institutional websites). Such distribution was supported by the active work of volunteers from the Participatory Presidium of the Simeto river agreement, the umbrella of volunteer organizations deeply involved in several aspects of the project. Instant messaging (mainly WhatsApp) was also effectively used, sharing the link to the questionnaire in chatting groups of local community associations, school (parents and classes), professional orders, and others. A paper hardcopy version of the survey was also distributed during some public events in order to involve even those that may have been reached by social media only marginally. The answers were 1143 in total, 1078 collected electronically, and 65 hardcopies formats, distributed per municipality as shown in Table 3, and by individuals' characteristics as illustrated in Figure 4. The percentage of women is slightly higher than the percentage of men, the age groups are adequately represented except for the group of children (younger than 14 years old) who are only about 1% of the respondents. Almost 38% of the participants are high school graduates and approximately one-third are university graduates. Most of the participants study or work, only 11% are unemployed, and just slightly more than 4% are retired.

Table 3. Number of responses received from each municipality and percentage of responses out of the total answers to the survey.

Municipality	Inhabitants (2018)	Number of Answers	Percentage of Answers to the Survey
Adrano	35,633	53	4.64%
Belpasso	28,126	38	3.33%
Biancavilla	23,948	33	2.89%
Catania	31,1620	128	11.21%
Centuripe	5373	130	11.38%
Motta Sant'Anastasia	12,189	4	0.35%
Paternò	47,827	329	28.81%
Ragalna	3960	66	5.78%
Regalbuto	7190	98	8.58%
Santa Maria di Licodia	7691	90	7.88%
Troina	9202	17	1.49%
Other		156	13.66%

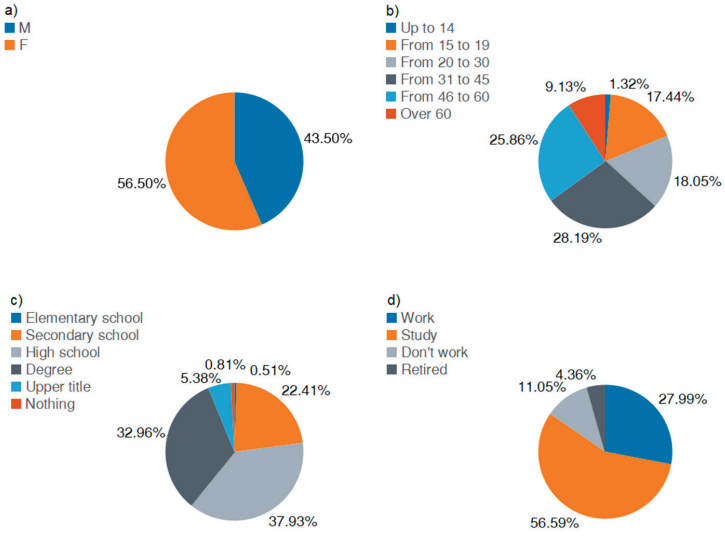

Figure 4. Social characterization of the participants to the survey in terms of (**a**) gender, (**b**) age, (**c**) education, (**d**) work.

3. Results

3.1. Worry about Climate Change

There has been lengthy debate in the scholarly community about whether individuals can "experience" climate change on a first-hand basis [38]. Some studies claim that global climate change is effectively invisible to laypeople, as climate change, by scientific definition, relies on statistical data compiled over long periods of time [53,54]. Ethnographic and survey results, however, have suggested that some members of the public believe that they have experienced climate change through seasonal changes, or living through extreme weather events [38,55,56].

In this case, in particular, around 84% of interviewees responded that the extreme rainfall events that hit Sicily in 2018 were mainly due to climate change. Only 8.7% of respondents believe that these phenomena have occurred as they are extreme events due to natural climate of the area. As a matter of fact, the study area has experienced even more severe events in the

past, therefore the link with climate change is highly uncertain, so this question contributes by measuring the level of worry by the population. It is interesting to note that the likely correct interpretation (heavy rainfall events occur quite often in autumn, so there are quite normal in this season) is more frequent within the age group of over-60s, as the 20% of them answered so, while in the other age groups the percentage remains less than 10%. Additionally, rather a considerable percentage of school-age students (30.77%) are not able to decide whether such events are due to natural climate variability or to changed conditions, i.e., they are not able to identify a possible cause for this type of events (Figure 5).

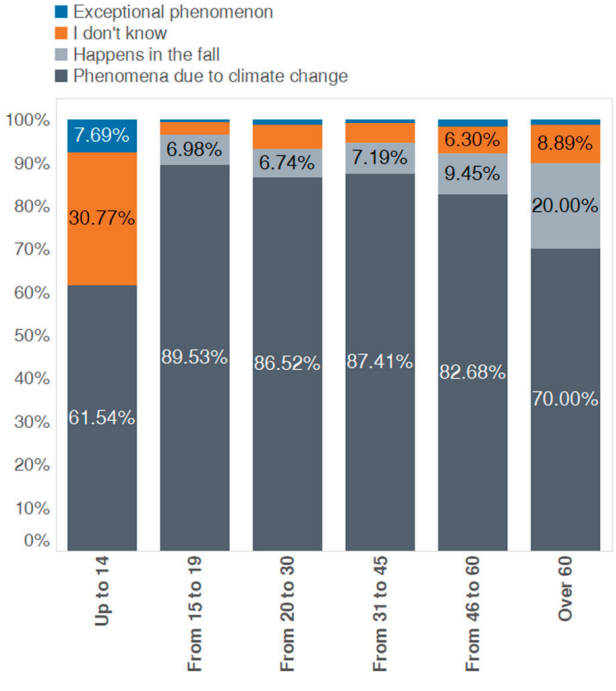

Figure 5. Results for the question: 'During the autumn of 2018, Sicily was hit by heavy rains in both the eastern and western parts, what do you think these phenomena are due?' Answers classified according to different age groups.

Regarding the exposure to information on climate change, over 44% of participants answered that they hear about climate change "at least once a week" and almost 30% even "once a day" (Figure 6). This indicates that the population is quite interested and worried about climate change as it is discussed in usual conversations, within all age groups. Table 4 shows the different information sources through which the inhabitants declared to "hear about" climate change. For this question, multiple answers were allowed. The table shows that the most frequent source of information on climate change is newspapers, radio, and television (77.89%), followed by social media and the internet in general (66.53%).

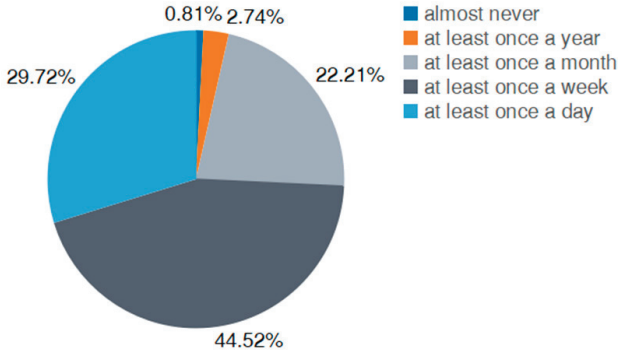

Figure 6. Responses to question 'In the last years, how often have you heard about climate change?'

Table 4. Sources from which population responded to hear about climate change. Respondents could select more than one answer (percentages do not sum up to 100% as multiple answers were accepted).

Source	Percentage of Answers
Talking with friends and family	44.12%
Social network/Internet	66.53%
Newspapers, Radio, TV	77.89%
At school/work	33.87%
During events/conferences	23.83%
Never heard of it	0.01%

3.2. Direct Experience of Urban Flooding and Risk Preparedness

More than 62% of the respondents answered that they cross areas prone to flooding during heavy rainfall events. This could be related to the fact that the problem is diffused within a large area. Figure 7 shows the answers divided into the different municipalities. The chart shows that the municipalities where the higher number of respondents declared to cross floodable areas are Catania, Biancavilla, and Adrano. Instead, the less interested in floods are Centuripe, Troina, and Regalbuto, cities which are located at the top of mountain areas. However, even in these municipalities, more than 50% of participants stated that they cross dangerous areas during intense storms: this could is related to the fact that these cities have many commuters that move out of their town for work/school on a daily basis, for example, it is possible that many citizens need to go to Catania for work, study or other needs, which is the closest city with services. After this question, participants were asked to indicate their degree of concern during weather alerts. Table 5 shows that most respondents (around 45%) have a "medium" level of concern and only 32% have a high or very high level of concern (the sum of 23% and 9%). This happens probably because of the relatively large spatial and temporal uncertainty of the weather alerts in the region, which remains significant to a degree that may induce a partial distrust about them—a phenomenon also known as *cry wolf syndrome* [57]. In fact, in recent years, there have been several cases in which weather warnings have been issued without any rain occurring, other times there have been very intense rain events without there being any weather warnings: these situations contribute to confuse citizens, who lose confidence in the weather alert service.

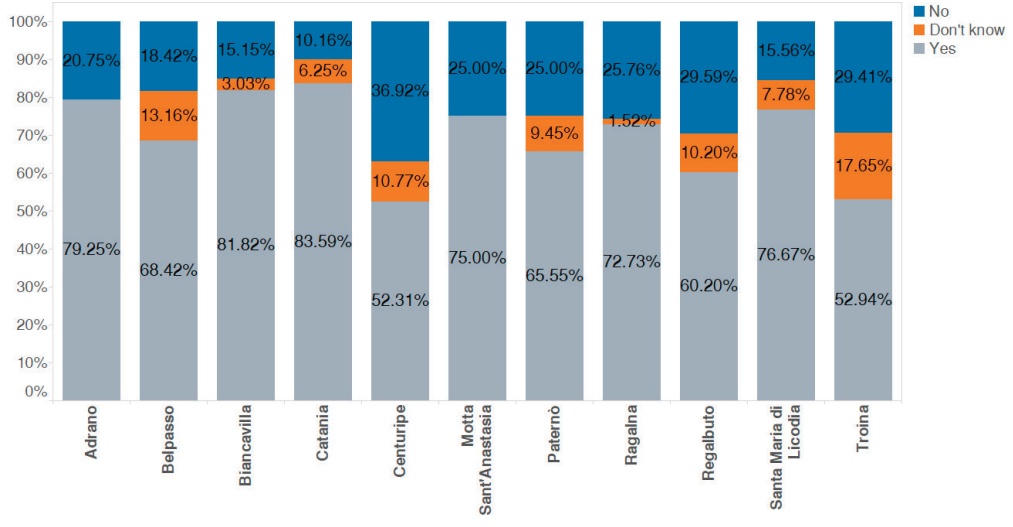

Figure 7. Responses to question 'Do you cross areas that are likely to be flooded during a rain event?' The size of the indicator represents the quantity of responses coming from individual municipalities, while the color indicates the type of response.

Table 5. Level of concern during a weather alert.

Level of Concern	Percentage of Answers
very low level of concern	5.17%
low level of concern	16.53%
medium level of concern	45.84%
high level of concern	23.23%
very high level of concern	9.23%

Regarding risk preparedness, the charts in Figure 8 show the answers on the behavior during potentially dangerous scenarios in three different cases. In the first question, we asked how the citizens would behave in case of a storm if they were indoors at school, work or gym. The chart shows that almost 74% know the right behavior to take; in the second question, we asked what behavior they would have if they were in the situation to decide to cross an underpass, even in this case almost 74% of the interlocutors answered correctly; instead, the third question asked about their choice in case of crossing of a bridge during an exceptional rain event. In this case, only about 48% of participants gave the answer corresponding to the correct behavior. As it can be seen from the graph, 20% of people would not actually know how to behave and about 33% of participants would have risky behavior. It is also interesting to investigate the answers according to the different age groups (Figures 9–11). We note that young people are actually the least aware about what to do in the case of an extreme rain event. Only 15% of children (up to 14) and 35% of teenagers (from 15 to 19) answered correctly.

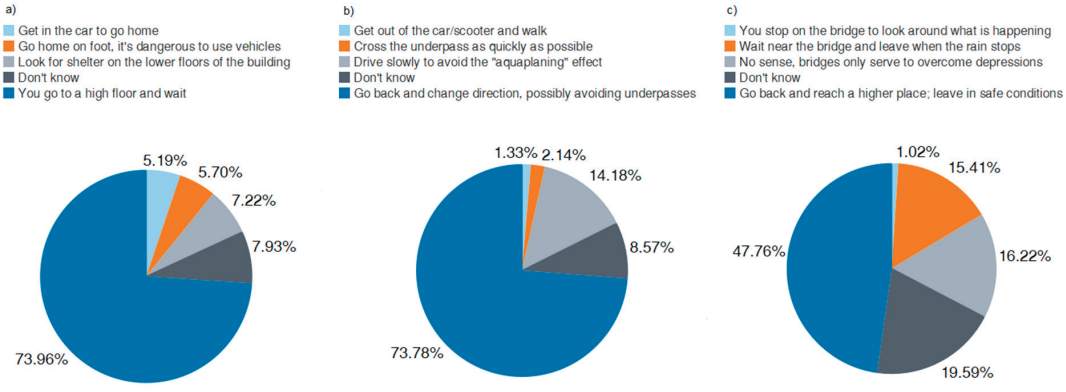

Figure 8. (**a**) Answers to the question: "What do you do if there is a storm and you are at work/school/gym?" (**b**) Answers to the question: "What do you do if there is a storm and you are in your car/scooter and you have to pass an underpass?" (**c**) Answers to the question: "What do you do if there is a storm and you are in your car/scooter and you have to pass a bridge?".

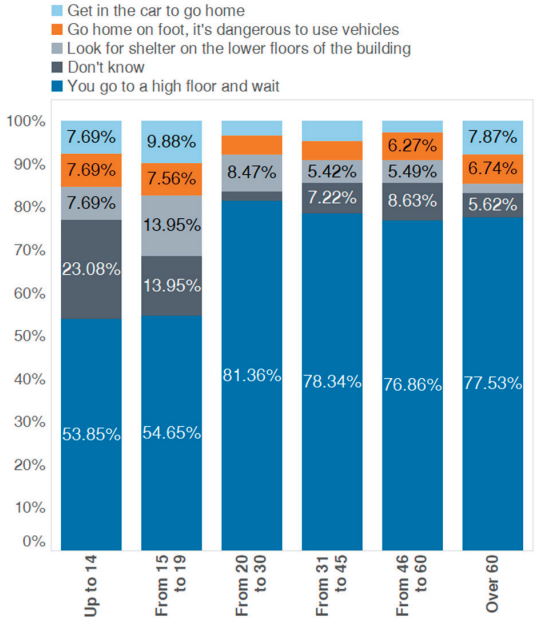

Figure 9. Responses to question 'What do you do if there is a storm and you are at work/school/gym?'.

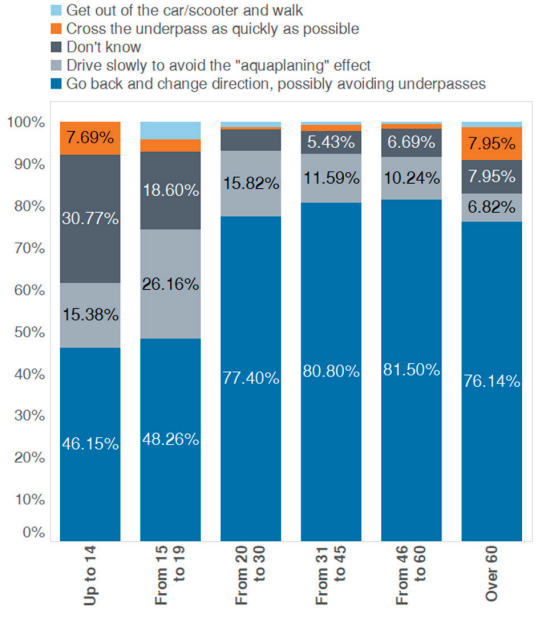

Figure 10. Responses to question 'What do you do if there is a storm and you are in your car/scooter and you have to pass an underpass?'.

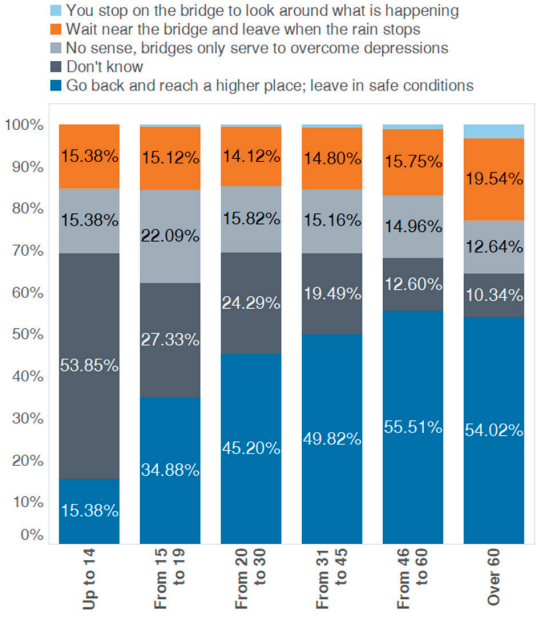

Figure 11. Responses to question 'What do you do if there is a storm and you are in your car/scooter and you have to pass a bridge?'.

Moreover, we asked if they feel personally responsible for flood prevention, and how much they think other public bodies are responsible for protection from the induced risk. The citizen had the possibility to assign a score based on the degree of assigned

responsibility in the case of flood event for the different bodies indicated. Using a Likert scale the responsibilities were divided into low, medium, or high. The result shows that only 35.5% of citizens consider themselves to have a responsibility in flood prevention, while almost 30% believe they have a very low responsibility. It also shows that there is a high tendency to attribute most of the responsibility to public bodies, in particular to the Central Government (Figure 12).

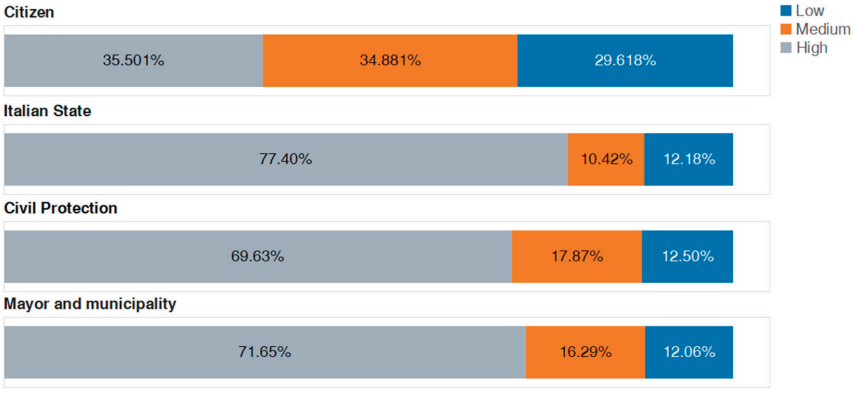

Figure 12. Answer to the question concerning the attribution of responsibility for the prevention of flood risk.

3.3. Willingness to Adaptation

The first question of this section asked the participants to identify the best practices for adapting to climate change, in order to investigate whether respondents know the meaning of adaptation and how it differs from the concept of mitigation. Knowledge of this difference is fundamental to the population to be a catalyst for the implementation of adaptation actions, as these are of different nature than the mitigation actions. In fact, the former does not focus on a reduction of greenhouse gas emissions, while the latter is mainly oriented to that scope, thus requiring totally different strategies.

The outcomes of the survey show that citizens are mostly confused about this point (Table 6). Almost 44% of the interviewees answered that waste sorting is an adaptation measure and over 58% indicated renewable energy production, while both should be mainly considered mitigation measures. Then, more direct questions on the willingness for adaptation were asked. In particular, participants were first asked if they would be favorable to an increase of investments in sustainable drainage infrastructures by their municipality. The answers have been represented in Figure 13, as a function of the age group. Overall, almost 80% of the answers indicated willingness to accept an increase in public costs if well justified; however, mainly adult groups (i.e., over 30 years old) seemed more favorable to this type of initiative. Then, the question was oriented to a more individual statement: citizens were asked whether while restructuring their own properties, they would be willing to increase their expenses to put in place sustainable drainage practices, such as increasing the surrounding pervious surfaces (Figure 14). Over 82% of young adults in the age between 31 and 45 years have responded to be willing to do that, while people aged less than 30 years seem to be the less willing to make such an investment.

Table 6. Responses to question 'Which of these are good practices for adaptation?'.

Good Practices for Adaptation	Percentage of Answers
Waste sorting	43.61%
Improve the quality of weather alerts	17.78%
Sewer maintenance	51.75%
Avoid wasting water	19.81%
Build infrastructures for flood protection	60.07%
Production and use of energy from renewable sources	58.23%

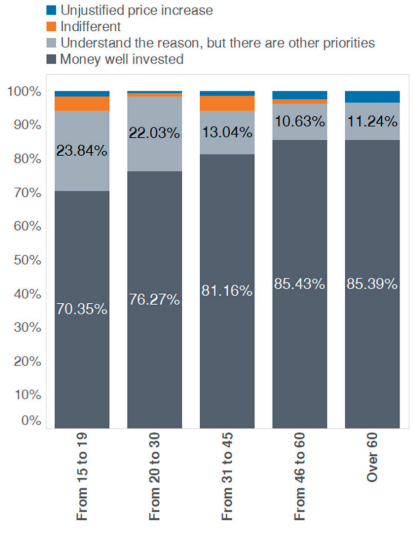

Figure 13. Answer to the question: "Your municipality is investing funds for the construction of a new parking and decides to spend 10% more for make it with pervious materials that allow stormwater retention and therefore reduce urban flooding. What do you think about that?".

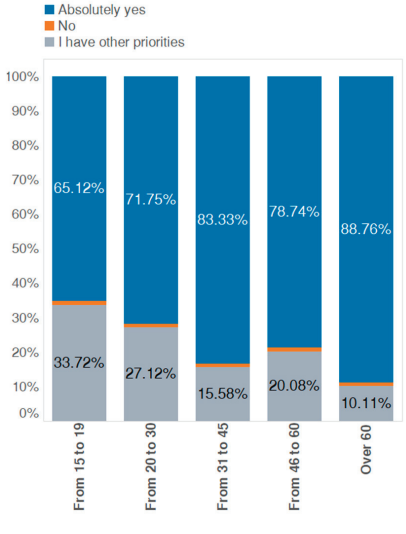

Figure 14. Answer to question: "In building or renovating your home would you be willing to spend more to introduce more green areas and less asphalted surfaces to better adapt to climate change?".

4. Discussion

4.1. Analysis of Direct Results

In this section we firstly present an overall summary of the direct results of the survey, we briefly compare our results with those presented in related studies in the literature, and finally, we carry out some cross-analysis of the various factors explored with the survey, and in particular the possible links between the worry of population about climate change and how this may influence their preparedness.

Table 7 presents a short overview of the main direct results of the survey, which were presented in detail in the Results section. With "direct results" we mean those that can be derived from one single question, without analyzing possible relationships between the answers.

Table 7. Summary table with main direct results of the survey.

Question	Overall Results
Link between climate change and floods	Present for over 80%
How often you hear about climate change	At least once a week
What sources discuss about climate change	Radio/TV/Newspaper/Social
Direct experience with floodable areas	Present for over 50%
Confidence in weather alert	Medium/Low
Good practices during floods	Not always correct
Responsibility for the prevention of flood risk	Italian State and other institutions
Good practices for adaptation	Little knowledge of adaptation actions
Public adaptation actions	Modestly favorable
Private adaptation actions	Modestly favorable

Our investigation indicated that most of the citizens are worried about climate change and confirmed that they are highly interested in the topic, as they follow information coming from multiple media streams and discuss it prevalently on a weekly (44%) or daily basis (30%). The predominant perception is that there is a link between floods in the last decade and climate change (84%). With reference to the direct experience of residents during heavy rain events and related urban flooding, most citizens agree that the urban areas of the SRV are prone to flooding, as many of them report to cross flooded streets. However, they are quite sceptical regarding the weather alerts, as they perceive them more as a problem in their daily activities rather than a protection of their safety. A significant percentage of the population is unaware of the basic rules for individual safety during a heavy rainfall event, as more than 1 out of 4 persons would have wrong behavior during urban flooding risky situations. Finally, it seems that there is a modest willingness of citizens to implement adaptation actions in their own municipality and real estate. Although it is not possible to know if citizens actually carry out works (public or private), the answers to the last questions reveal a certain desire of the population to accept new measures if it means adapting to climate change and thus improving safety.

4.2. Comparison and European and National Studies

We attempted to compare these direct results with those of other areas, as reported in recent similar studies, in order to find possible divergences, which we discuss in the following. For example, at the European scale, according to the 2017 Eurobarometer Report [52], it is clear that 74% of citizens actually consider climate change as a serious problem, while in our case over 83% of respondents believe that climate change is responsible for exceptional phenomena that cause serious problems and damage, showing potentially a higher degree of concern. As regards responsibilities, in Europe, only 43% of the responsibility for preventing the risks associated with climate change is attributed to the government, while in the SRV the percentage of citizens of the SRV who hold the government responsible is higher than 77.4%. On the other hand, European citizens that feel personally responsible for the prevention of the flood risk are only 22% against the 35%

of our respondents. This in general indicates that the population agrees on the fact that the local and national administrators do not take sufficient actions for protection of the territory against urban flooding. At a national level, the only survey deemed to have comparable questions with ours is the one conducted for the Municipality of Ferrara [48], in the north of Italy, in which however only 164 questionnaires were analyzed (approximately 0.1% of the population). The analysis found that about 61% of citizens perceive the evidence of climate change (vs. 83% in our case, based on question 1) and about 58.5% believe that it is very important to take actions to mitigate the impacts of climate change (vs. 79.9% for the SRV). In the Municipality of Ferrara, 20% of the responsibility for preventing the risks associated with climate change is attributed to the State and over 55% to the Municipality, while the citizens of the SRV hold the State the most responsible (77.4%). The percentage that feels directly involved and responsible for risk prevention is more or less the same in the two areas, around 35%. Citizens of Ferrara that are moderately willing to invest in adaptation measures are about 37.5%, while 37% are very willing. Regarding SRV citizens, more than 77% of them are very willing to personally support the costs for adaptation measures.

Of course, the presented comparison is subject to some limitations mainly due to the fact that not the exact questions and methodologies have been done and applied. Nevertheless, the differences are quite high and potentially significant also taking into account the possible influence of the above-mentioned limitation. Hence the comparison confirms the relevance of investigating the SRV, as it presents specific features that other studies do not allow to infer.

4.3. Cross-Analysis: Link between Worry about Climate Change and Urban Flooding Preparedness

In many parts of the industrially-developed world, efforts in the media and in schools are mainly oriented to build awareness of the climate change issue, as also stimulated by several activist movements, such as Extinction Rebellion (https://extinctionrebellion.uk/the-truth/, accessed on 15 February 2021) and Fridays for Future (https://fridaysforfuture.org/, accessed on 15 February 2021), whose real impacts and advantages are under study by several scholars [58–60]. Here, we wanted to explore, the possible linkages between building an awareness of the risks related to climate change and the advantages in terms of a possible increase in the awareness of related urban flooding risk and the willingness to adaptation. This is allowed by the data collected in our survey by cross-analysis of part 2 (direct experience of urban flooding and risk awareness) and 3 (willingness to adaptation) vs. part 1 (concern of climate change and connection with urban flooding). To investigate these aspects, two contingency matrices have been derived linking respectively relevant questions of part 1 with part 2 (Table 8) and part 1 with part 3 (Table 9) of the survey. This approach is similar to that applied in the case of prediction problems where the use of the contingency matrix (also termed as confusion matrix) allows the understanding of the performance of the predictor in terms of Receiver Operating Characteristics (ROC) [61,62]. In particular, the following assumptions were made in computing the quantities in Tables 8 and 9:

- Degree of interest and concern for climate change:
    - A partial score of 1 was assigned when the interviewee answered "These are phenomena due to climatic changes taking place on the planet" to question 1, a score of 0 otherwise
    - A partial score of 1 for who hears about climate change at least once a day, 0 otherwise
    - The degree was classified as "higher" if total score (sum first and second item) was at least 1, "lower" otherwise
- Correct behavior during urban flooding:
    - A partial score of 1 was assigned to each answer corresponding to correct behavior (questions 6a–c), and 0 to a wrong behavior
    - A "likely" correct behavior was assigned to individuals that had a total score of 2 or more, while it was deemed "unlikely" otherwise

- Willingness to invest in adaptation actions (sustainable drainage):
  - A partial score equal to 1 was attributed to answers "It's well-spent money, the Municipality has done a good thing" (question 9) and "Absolutely yes" (question 10)
  - A "higher" willingness level to individuals that had a total score of 1 or more, "lower" otherwise

Table 8. Contingency table for exploring link between concern for climate change and the possible correct behavior of individuals during urban flooding.

		Degree of Worry about Climate Change	
		Higher	**Lower**
Correct behavior during urban floods	**Likely**	707 (A)	93 (C)
	Unlikely	293 (B)	49 (D)
	Total	1000 ($A + B$)	142 ($C + D$)
	Conditional frequencies	$A/(A + B) = 0.71$	$C/(C + D) = 0.66$

Table 9. Contingency table for exploring link between concern for climate change and the possible willingness to invest in adaptation actions.

		Degree of Worry about Climate Change	
		Higher	**Lower**
Willingness to invest in adaptation actions	**Higher**	915 (A)	123 (C)
	Lower	85 (B)	19 (D)
	Total	1000 ($A + B$)	142 ($C + D$)
	Conditional frequencies	$A/(A + B) = 0.92$	$C/(C + D) = 0.87$

Once the categorization has been done and entries of the contingency tables have been counted, conditional frequencies have been computed to test whether the degree of interest and concern for climate change is related to a variation of the likelihood of correct behavior during urban flooding events and a higher willingness to invest in adaptation. In particular, to test whether there is a significant variation the following conditional frequencies have been computed: frequency that a person behaves correctly during urban floods (is willing to invest in adaptation actions) given that he is highly concerned about climate change, and frequency that a person behaves correctly during urban floods (is willing to invest in adaptation actions) given that he is lowly concerned about climate change. These two conditional frequencies correspond to $A/(A + B)$ and $C/(C + D)$.

$$H = A/(A + B) - C/(C + D) \quad (1)$$

The difference provides an indication whether the conditioning factor is important or not: if H is significantly greater than zero the concern about climate change positively affects behavior during floods (increases willingness to invest in adaptation actions), if is significantly less than zero than the influence is negative, if H is approximately zero then there is no influence. We consider a threshold of $|H| = 0.2$ for significance. In the context of ROC analysis, H is also termed as true skill statistic or Hanssen–Kuipers discriminant [63–65]. As can be derived from Tables 8 and 9, the difference in both cases is 0.05, i.e., non-significant. This means that to be concerned by climate change does not give any advantage in resilience, i.e., does not induce a better behavior against the climate-related hazard of urban flooding, nor on the willingness to invest in a sustainable solution for adaptation to climate change increases. In other words, people are not as willing to take actions as they are to be concerned when it comes to climate change.

5. Conclusions

The results of a survey exploring worry about climate change and its possible relation with the behavior during urban floods and the willingness to invest in adaptation actions have been presented, relatively to the Simeto River Valley area in Sicily. The data collection that was made is quite relevant with respect to other studies, as here more than 1000 persons were interviewed, while it is difficult to find regional studies with more than a few hundreds of participants involved. The simplicity of the survey was a crucial factor for collecting such a high number of answers, but, on the other hand, has not undermined the possibility to arrive at important conclusions about the issues explored. The overall picture deriving from the present analysis highlights how there is a high concern for the possible impacts of climate change, specifically in connection to urban flooding. The climate change issue entered in almost every-day conversations by the population. However, this high level of concern does not correspond to a comparable level of knowledge of the correct behavior during climate-related extreme events—specifically urban flooding—and the willingness to invest in adaptation measures. In fact, the population tends to attribute increasingly intense events to climate change but does not know the correct behavior to take during the emergencies, does not correctly attribute the responsibility for flood-caused damage, and does not trust authorities that are in charge of human safety. The cross-analysis that we carried out, shows that there is no gain for these two resilience factors associated with a higher degree of concern about climate change. Overall, the outcomes of the survey suggest that the information that is conveyed by the media and taught in schools is mainly oriented to increase the worry about climate change and that this is not significantly useful for an increase in the resilience of the populations, i.e., specifically a higher risk awareness during urban flooding events and of the importance of investment in sustainable drainage practices. Hence, greater efforts should be spent through media and education to build a greater risk preparedness rather than prevalently a greater worry about climate change.

Author Contributions: Conceptualization, all authors; Formal analysis, P.N. and D.J.P.; Funding acquisition, A.C., R.E.M. and D.J.P.; Investigation, all authors; Methodology, all authors; Project administration, A.C. and R.E.M.; Resources, A.C. and R.E.M.; Supervision, D.J.P., A.C. and R.E.M.; Visualization, P.N. and D.J.P.; Writing—original draft, P.N. and D.J.P.; Writing—review & editing, all authors. All authors have read and agreed to the published version of the manuscript.

Funding: This work has been partly funded by the EU project LIFE SimetoRES (IT-LIFE17_CCA_IT_000115), whose partners are the municipalities of Paternò, Ragalna, Santa Maria di Licodia and the Department of Civil and Environmental Engineering of the University of Catania.

Institutional Review Board Statement: Not applicable.

Informed Consent Statement: Not applicable.

Data Availability Statement: Data are available by request to the authors.

Acknowledgments: The Participatory Presidium of the Simeto River Agreement is strongly acknowledged for its active support in all the communication activities of the project, and in the dissemination and collection of the questionnaires. The authors thank Laura Saija for the fruitful discussions and Gabriele Gugliuzzo for the collaboration in organizing the results. This work is in partial fulfilment of the Ph.D. activities of P.N.

Conflicts of Interest: The authors declare no conflict of interest.

Appendix A

The survey consists of a combination of 10 questions, including some multiple choice and others using the Likert scale (1932), preceded by 5 questions related to the characterization of the sample. The questions were formulated to be independent of each other and each of them is aimed at extrapolating precise information. The survey was administered in Italian language. Below we show the questions translated in English.

Sample characterization:
Gender

- M
- F

How old are you?

- Up to 14 years
- Between 15 and 19 years old
- Between 20 and 30 years
- Between 31 and 45 years old
- Between 46 and 60 years old
- Over 60 years old

Education

- None
- Primary school diploma
- Middle School diploma
- High school diploma
- Graduation
- Higher qualification (Ph.D., Master, etc.)

What is your current occupation?

- Student
- Worker
- Unemployed
- Retired

Where do you live?

- Adrano
- Belpasso
- Biancavilla
- Catania
- Centuripe
- Motta Sant'Anastasia
- Paternò
- Ragalna
- Regalbuto
- Santa Maria di Licodia
- Troina
- Other

Perception of climate change:
Question No. 1
During the autumn of 2018, Sicily was hit by heavy rains in both the eastern and western parts, what do you think these phenomena are due?

- Heavy rainfall events occur quite often in autumn, so there are quite normal in this season;
- These are phenomena due to climatic changes taking place on the planet;
- It was an isolated phenomenon;
- I do not know.

Question No. 2
In the last years, how often have you heard about climate change?

- At least once a day;
- At least once a week;
- At least once a month;

- At least once a year;
- Almost never;
- Never.

Question No. 3
Where did you hear about climate change? (More options can be selected)

- Talking to friends, family;
- Social networks/internets;
- Newspapers/magazines/TV/Radio;
- At school/university/work;
- During events/conferences;
- I don't remember hearing about it.

Perception of flood events, behaviour during weather alerts and related responsibilities:

Question No. 4
Do you cross areas that are likely to be flooded during a rain event?

- Yes;
- No;
- I do not know.

Question No. 5
The news talks about a serious weather alert for tomorrow, how do you feel? Indicate your degree of worry (1 means "very little", 5 means "very much")

- 1;
- 2;
- 3;
- 4;
- 5.

Question No. 6
In the event of a flood what do you do if:
a. you are at work/school/gym

- Make sure you get in the car to go home;
- You go to a mezzanine floor of a building, and wait for the return to normality before going out;
- Go home by feet as quickly as possible because it could be dangerous to use any means of transport;
- You take shelter on the lower floors of a building, and wait for the return to normality before going out;
- I do not know.

b. you are in your car/scooter and you have to pass an underpass?

- You go through the underpass as fast as possible to get into safety;
- You go back and change directions, possibly avoiding other underpasses;
- You cross slowly to avoid the danger of "aquaplaning";
- Get off the car/scooter and cross on foot;
- I do not know.

c. you are in your car/scooter and you have to pass a bridge?

- You stop on the bridge to check what's going on;
- Go back and reach a higher place; leave only after the situation has returned to normal;
- The question makes little sense, bridges only serve to overcome dips of the soil that have little relationship with water;
- Wait near the bridge and leave when it stops raining;
- I do not know.

Question No. 7

Indicates the degree of responsibility for the prevention of flood risk of the following figures where 1 means very little and very much 5.

The citizens

- 1;
- 2;
- 3;
- 4;
- 5.

The Mayor and the Municipality

- 1;
- 2;
- 3;
- 4;
- 5.

Civil Protection and Firefighters

- 1;
- 2;
- 3;
- 4;
- 5.

The State

- 1;
- 2;
- 3;
- 4;
- 5.

Willingness to adapt to climate change

Question No. 8

What are good practices for adaptation? (Choose max 3 options)

- Waste sorting
- Improve the quality of weather warnings
- Sewer maintenance
- Avoid wasting water
- Build infrastructures that help to avoid flooding
- Production and use of energy from renewable sources

Question No. 9

Your municipality is investing funds for the construction of a new parking and decides to spend 10% more for make it with pervious materials that allow stormwater retention and therefore reduce urban flooding. What do you think about that?

- It's well-spent money, the Municipality has done a good thing;
- I understand the reason, but there are other priorities to invest in;
- It seems absurd to me; it is an unjustified increase of public expenditures;
- Indifferent.

Question No. 10

In building or renovating your home would you be willing to spend more to introduce more green areas and less asphalted surfaces to better adapt to climate change?

- Absolutely yes;
- Maybe, as I have other priorities;
- No.

References

1. Spence, A.; Poortinga, W.; Pidgeon, N. The Psychological Distance of Climate Change. *Risk Anal.* **2012**, *32*, 957–972. [CrossRef] [PubMed]
2. Naumann, S.; Gerardo, A.; Berry, P. *Assessment of the Potential of Ecosystem-Based Approaches to Climate Change Adaptation and Mitigation in Europe*; Final report to the European Commission, DG Environment, Contract no. 070307/2010/580412/SER/B2; Ecologic institute and Environmental Change Institute, Oxford University Centre for the Environment: Oxford, UK, 2011.
3. Prutsch, A.; Felderer, A.; Balas, M.; Konig, M.; Clar, C.; Steurer, R. *Methods and Tools for Adaptation to Climate Change. A Handbook for Provinces, Regions and Cities*; Climate ADAPT: Vienna, Austria, 2014; ISBN 9783990042977.
4. Demski, C.; Capstick, S.; Pidgeon, N.; Sposato, R.G.; Spence, A. Experience of extreme weather affects climate change mitigation and adaptation responses. *Clim. Chang.* **2017**, *140*, 149–164. [CrossRef]
5. Sussams, L.W.; Sheate, W.R.; Eales, R.P. Green infrastructure as a climate change adaptation policy intervention: Muddying the waters or clearing a path to a more secure future? *J. Environ. Manag.* **2015**, *147*, 184–193. [CrossRef] [PubMed]
6. Du, J.; Qian, L.; Rui, H.; Zuo, T.; Zheng, D.; Xu, Y.; Xu, C.Y. Assessing the effects of urbanization on annual runoff and flood events using an integrated hydrological modeling system for Qinhuai River basin, China. *J. Hydrol.* **2012**, *464–465*, 127–139. [CrossRef]
7. Palla, A.; Sansalone, J.J.; Gnecco, I.; Lanza, L.G. Storm water infiltration in a monitored green roof for hydrologic restoration. *Water Sci. Technol.* **2011**, *64*, 766–773. [CrossRef] [PubMed]
8. Haghighatafshar, S.; Becker, P.; Moddemeyer, S.; Persson, A.; Sörensen, J.; Aspegren, H.; Jönsson, K. Paradigm shift in engineering of pluvial floods: From historical recurrence intervals to risk-based design for an uncertain future. *Sustain. Cities Soc.* **2020**, *61*, 102317. [CrossRef]
9. Hammond, M.J.; Chen, A.S.; Djordjević, S.; Butler, D.; Mark, O. Urban flood impact assessment: A state-of-the-art review. *Urban Water J.* **2015**, *12*, 14–29. [CrossRef]
10. Haaland, C.; van den Bosch, C.K. Challenges and strategies for urban green-space planning in cities undergoing densification: A review. *Urban For. Urban Green.* **2015**, *14*, 760–771. [CrossRef]
11. Berndtsson, R.; Becker, P.; Persson, A.; Aspegren, H.; Haghighatafshar, S.; Jönsson, K.; Larsson, R.; Mobini, S.; Mottaghi, M.; Nilsson, J.; et al. Drivers of changing urban flood risk: A framework for action. *J. Environ. Manag.* **2019**, *240*, 47–56. [CrossRef]
12. Saidu, I.; Lal, M.D. Flood risk inevitability and flood risk management in urban areas: A review. *J. Geogr. Reg. Plan.* **2015**, *8*, 205–209. [CrossRef]
13. Jongman, B.; Ward, P.J.; Aerts, J.C.J.H. Global exposure to river and coastal flooding: Long term trends and changes. *Glob. Environ. Chang.* **2012**, *22*, 823–835. [CrossRef]
14. Petry, B. Keynote lecture: Coping with floods: Complementarity of structural and non-structural measures. *Flood Def.* **2002**, 60–70.
15. Meyer, V.; Priest, S.; Kuhlicke, C. Economic evaluation of structural and non-structural flood risk management measures: Examples from the Mulde River. *Nat. Hazards* **2012**, *62*, 301–324. [CrossRef]
16. Salvati, P.; Bianchi, C.; Fiorucci, F.; Giostrella, P.; Marchesini, I.; Guzzetti, F. Perception of flood and landslide risk in Italy: A preliminary analysis. *Nat. Hazards Earth Syst. Sci.* **2014**, *14*, 2589–2603. [CrossRef]
17. Avvisati, G.; Bellucci Sessa, E.; Colucci, O.; Marfè, B.; Marotta, E.; Nave, R.; Peluso, R.; Ricci, T.; Tomasone, M. Perception of risk for natural hazards in Campania Region (Southern Italy). *Int. J. Disaster Risk Reduct.* **2019**, *40*, 101164. [CrossRef]
18. Davis, M.S.; Ricci, T.; Mitchell, L.M. Perceptions of risk for volcanic hazards at Vesuvio and Etna, Italy. *Australas. J. Disaster Trauma Stud.* **2005**, *2005*, 21.
19. Paton, D.; Johnston, D. Disasters and communities: Vulnerability, resilience and preparedness. *Disaster Prev. Manag. An Int. J.* **2001**, *10*, 270–277. [CrossRef]
20. Ricci, T.; Nave, R.; Barberi, F. Vesuvio civil protection exercise MESIMEX: Survey on volcanic risk perception. *Ann. Geophys.* **2013**, *56*. [CrossRef]
21. Wachinger, G.; Renn, O. Risk perception of natural hazards. WP3-Report of the CapHaz-Net Projekt. 2010, pp. 1–111. Available online: http://www.caphaz-net.org (accessed on 15 February 2021).
22. Diakakis, M.; Priskos, G.; Skordoulis, M. Public perception of flood risk in flash flood prone areas of Eastern Mediterranean: The case of Attica Region in Greece. *Int. J. Disaster Risk Reduct.* **2018**, *28*, 404–413. [CrossRef]
23. Gravina, T.; Figliozzi, E.; Mari, N.; De Luca Tupputi Schinosa, F. Landslide risk perception in Frosinone (Lazio, Central Italy). *Landslides* **2017**, *14*, 1419–1429. [CrossRef]
24. Raaijmakers, R.; Krywkow, J.; van der Veen, A. Flood risk perceptions and spatial multi-criteria analysis: An exploratory research for hazard mitigation. *Nat. Hazards* **2008**, *46*, 307–322. [CrossRef]
25. Shen, X. *Flood Risk Perception and Communication within Risk Management in Different Cultural Contexts a Comparative Case Study between Wuhan, China and cologne, germany Xiaomeng Shen Beijing, VR China*; UNU-EHS: Bonn, Germany, 2009.
26. Lechowska, E. What determines flood risk perception? A review of factors of flood risk perception and relations between its basic elements. *Nat. Hazards* **2018**, *94*, 1341–1366. [CrossRef]
27. Bouman, T.; Verschoor, M.; Albers, C.J.; Böhm, G.; Fisher, S.D.; Poortinga, W.; Whitmarsh, L.; Steg, L. When worry about climate change leads to climate action: How values, worry and personal responsibility relate to various climate actions. *Glob. Environ. Chang.* **2020**, *62*, 102061. [CrossRef]
28. Whitmarsh, L.; Capstick, S. *Perceptions of Climate Change*; Elsevier Inc.: Amsterdam, The Netherlands, 2018; ISBN 9780128131305.

29. van der Linden, S.; van der Linden, S. *Determinants and Measurement of Climate Change Risk Perception, Worry, and Concern*; Oxford University Press: Oxford, UK, 2017; ISBN 9780190228620.
30. Bubeck, P.; Botzen, W.J.W.; Aerts, J.C.J.H. A Review of Risk Perceptions and Other Factors that Influence Flood Mitigation Behavior. *Risk Anal.* **2012**, *32*, 1481–1495. [CrossRef] [PubMed]
31. Capstick, S.B.; Pidgeon, N.F.; Corner, A.J.; Spence, E.M.; Pearson, P.N. Public understanding in Great Britain of ocean acidification. *Nat. Clim. Chang.* **2016**, *6*, 763–767. [CrossRef]
32. Morton, T.A.; Rabinovich, A.; Marshall, D.; Bretschneider, P. The future that may (or may not) come: How framing changes responses to uncertainty in climate change communications. *Glob. Environ. Chang.* **2011**, *21*, 103–109. [CrossRef]
33. Johannesson, M.P.; Gjerstad, Ø.; Nordø, Å.D.; Tvinnereim, E.; Fløttum, K. Citizens' preferences for tackling climate change. Quantitative and qualitative analyses of their freely formulated solutions. *Glob. Environ. Chang.* **2017**, *46*, 34–41. [CrossRef]
34. Guzzetti, F.; Stark, C.P.; Salvati, P. Evaluation of flood and landslide risk to the population of Italy. *Environ. Manag.* **2005**, *36*, 15–36. [CrossRef]
35. Feldman, D.; Contreras, S.; Karlin, B.; Basolo, V.; Matthew, R.; Sanders, B.; Houston, D.; Cheung, W.; Goodrich, K.; Reyes, A.; et al. Communicating flood risk: Looking back and forward at traditional and social media outlets. *Int. J. Disaster Risk Reduct.* **2016**, *15*, 43–51. [CrossRef]
36. Van Der Linden, S. On the relationship between personal experience, affect and risk perception: The case of climate change. *Eur. J. Soc. Psychol.* **2014**, *44*, 430–440. [CrossRef]
37. Helgeson, J.; van der Linden, S.; Chabay, I. The role of knowledge, learning and mental models in public perceptions of climate change related risks. *Learn. Sustain. Times Accel. Chang.* **2012**, 381–394. [CrossRef]
38. Akerlof, K.; Maibach, E.W.; Fitzgerald, D.; Cedeno, A.Y.; Neuman, A. Do people "personally experience" global warming, and if so how, and does it matter? *Glob. Environ. Chang.* **2013**, *23*, 81–91. [CrossRef]
39. Coumou, D.; Rahmstorf, S. A decade of weather extremes. *Nat. Clim. Chang.* **2012**, *2*, 491–496. [CrossRef]
40. Brody, S.D.; Zahran, S.; Vedlitz, A.; Grover, H. Examining the Relationship Between Physical Vulnerability and Public Perceptions of Global Climate Change in the United States. *Environ. Behav.* **2007**, *40*, 72–95. [CrossRef]
41. Krosnick, J.A.; Holbrook, A.L.; Lowe, L.; Visser, P.S. The origins and consequences of democratic citizens' policy agendas: A study of popular concern about global warming. *Clim. Chang.* **2006**, *77*, 7–43. [CrossRef]
42. Spence, A.; Poortinga, W.; Butler, C.; Pidgeon, N.F. Perceptions of climate change and willingness to save energy related to flood experience. *Nat. Clim. Chang.* **2011**, *1*, 46–49. [CrossRef]
43. Miceli, R.; Sotgiu, I.; Settanni, M. Disaster preparedness and perception of flood risk: A study in an alpine valley in Italy. *J. Environ. Psychol.* **2008**, *28*, 164–173. [CrossRef]
44. Raciti, A.; Saija, L. From ecosystem services to Ecological Devices: The CoPED Summer School experience in the Simeto River Valley, Italy. *J. Urban Manag.* **2018**, *7*, 161–171. [CrossRef]
45. ISTAT. *Sistema Statistico Nazionale Istituto Nazionale Di Statistica*; ISTAT: Rome, Italy, 2018; Volume 1, ISBN 9788845818660.
46. Saija, L.; De Leo, D.; Forester, J.; Pappalardo, G.; Rocha, I.; Sletto, B.; Corburn, J.; Mwau, B.; Magnaghi, A. Learning from practice: Environmental and community mapping as participatory action research in planning. *Plan. Theory Pract.* **2017**, *18*, 127–153. [CrossRef]
47. Italiana, R. Piano Stralcio di Bacino per l' Assetto Idrogeologico della Regione Siciliana. *PAI*. 2004. Available online: http://www.osservatorioacque.it/documenti/pta/allegati/18/all.18%20-%20pai.pdf (accessed on 15 February 2021).
48. Comune di Ferrara & Servizio Ambiente—Ufficio Agenda 21L. L'adattamento ai Cambiamenti Climatici. Esito Delle Indagini Condotte nel Comune di Ferrara (No. 1). Comune di Ferrara. December 2010. Available online: https://servizi.comune.fe.it/4786/cambiamenti-climatici (accessed on 15 February 2021).
49. SEERISK Joint Disaster Management Risk Assessment and Preparedness in the Danube Macro-region (SEERISK) project—Social awareness questionnaire. *Jt. Disaster Manag. Risk Assess. Prep. Danube Macro-Region Proj.* **2013**, *1*, 84–86.
50. Howe, P.; Mildenberger, M.; Marlon, J.; Leiserowitz, A. Geographic variation in opinions on climate change at state and local scales in the USA. *Nat. Clim. Chang.* **2015**. [CrossRef]
51. Likert, R. A technique for the measurement of attitudes. *Arch. Psychol.* **1932**, *22*, 140–155.
52. European Commission, Directorate-General for Climate Action, & Directorate-General for Communication. Special Eurobarometer 459—Climate Change (No. 459). Wave EB87.1—TNS Opinion & Social. September 2017. Available online: https://ec.europa.eu/clima/sites/clima/files/support/docs/report_2017_en.pdf (accessed on 15 February 2021).
53. Moser, S.C.; Dilling, L. Making climate hot. *Environment* **2004**, *46*, 32–46. [CrossRef]
54. Weber, E.U. What shapes perceptions of climate change? New research since 2010. *Wiley Interdiscip. Rev. Clim. Chang.* **2016**, *7*, 125–134. [CrossRef]
55. Ballew, M.T.; Leiserowitz, A.; Roser-Renouf, C.; Rosenthal, S.A.; Kotcher, J.E.; Marlon, J.R.; Lyon, E.; Goldberg, M.H.; Maibach, E.W. Climate change in the american mind: Data, tools, and trends. *Environment* **2019**, *61*, 4–18. [CrossRef]
56. Osaka, S.; Bellamy, R. Natural variability or climate change? Stakeholder and citizen perceptions of extreme event attribution. *Glob. Environ. Chang.* **2020**, *62*, 102070. [CrossRef]
57. Breznitz, S. *Cry Wolf*; New York Psychol. Press: New York, NY, USA, 1984.
58. Marris, E. Why young climate activists have captured the world's attention. *Nature* **2019**, *573*, 471–472. [CrossRef] [PubMed]
59. Feldman, L.; Hart, P.S. Using Political Efficacy Messages to Increase Climate Activism. *Sci. Commun.* **2016**, *38*, 99–127. [CrossRef]

60. Roser-Renouf, C.; Maibach, E.W.; Leiserowitz, A.; Zhao, X. The genesis of climate change activism: From key beliefs to political action. *Clim. Chang.* **2014**, *125*, 163–178. [CrossRef]
61. Staley, D.M.; Kean, J.W.; Cannon, S.H.; Schmidt, K.M.; Laber, J.L. Objective definition of rainfall intensity-duration thresholds for the initiation of post-fire debris flows in southern California. *Landslides* **2013**, *10*, 547–562. [CrossRef]
62. Peres, D.J.; Cancelliere, A. Derivation and evaluation of landslide-triggering thresholds by a Monte Carlo approach. *Hydrol. Earth Syst. Sci.* **2014**, *18*, 4913–4931. [CrossRef]
63. Peirce, C.S. The numerical measure of the success of predictions. *Science* **1884**, *4*, 453–454. [CrossRef] [PubMed]
64. Wilks, D.S. Chapter 8—Forecast Verification. In *Statistical Methods in the Atmospheric Sciences*; Wilks, D.S.B.T.-I.G., Ed.; Academic Press: New York, NY, USA, 2011; Volume 100, pp. 301–394. ISBN 0074-6142.
65. Marino, P.; Peres, D.J.; Cancelliere, A.; Greco, R.; Bogaard, T.A. Soil moisture information can improve shallow landslide forecasting using the hydrometeorological threshold approach. *Landslides* **2020**, *17*, 2041–2054. [CrossRef]

resources

MDPI

Article

The Flash Floods Risk in the Local Spatial Planning (Case Study: Lublin Upland, E Poland)

Bogusława Baran-Zgłobicka [1], Dominika Godziszewska [2] and Wojciech Zgłobicki [2,*]

[1] Institute of Socio-Economic Geography and Spatial Management, Maria Curie-Skłodowska University, Kraśnicka Av. 2d, 20-718 Lublin, Poland; bbaran@umcs.pl
[2] Institute of Earth and Environmental Sciences, Maria Curie-Skłodowska University, Kraśnicka Av. 2d, 20-718 Lublin, Poland; d.godziszewska@interia.pl
* Correspondence: wojciech.zglobicki@umcs.pl; Tel.: +48-81-537-6884

Abstract: Flash floods pose a significant threat to humans but the state of our knowledge on the occurrence and related risk of such phenomena is insufficient. At the same time, many climate change models predict that extreme rainfall events will occur more and more frequently. Identifying areas susceptible to flash floods is more complicated that in the case of floods occurring in the valley bottoms of large rivers. Flood risk maps in Poland have not been developed for small catchments. The study objective was to assess whether the threat related to flash floods is taken into account in the spatial planning system of municipalities. Studies were conducted in the Lublin Upland, E Poland (an area of about 7200 km^2). A preliminary assessment of susceptibility of 369 catchments to flash floods was carried out in a GIS environment using multi criteria analysis. The susceptible catchments cover about 30% of the area. Existing planning documents, flood hazard and flood risk maps were analyzed for municipalities located in the catchments with highest susceptibility to this phenomenon. Our results show that flash flood risk is usually not recognized at the level of local governments even when it is significant. Local planning documents do not take into account the existence of this threat.

Keywords: floods; GIS; natural hazards; risk management; spatial management

Citation: Baran-Zgłobicka, B.; Godziszewska, D.; Zgłobicki, W. The Flash Floods Risk in the Local Spatial Planning (Case Study: Lublin Upland, E Poland). *Resources* **2021**, *10*, 14. https://doi.org/10.3390/resources10020014

Academic Editors: Brunella Bonaccorso and David J. Peres

Received: 28 December 2020
Accepted: 8 February 2021
Published: 11 February 2021

1. Introduction

Flash floods are among natural hazards to which more and more attention is devoted due to their social and economic impact [1–6]. The term is applied to a rapid rise in water level, characterized by short duration and high intensity of maximum flows posing a threat to people [7,8]. According to Ostrowski et al. (2012) [9], a flash flood is a flood with a high water-volume lasting for a short time and occurring after a sudden, intensive rainfall (usually a rainstorm). Initially, the term applied to phenomena related to floods resulting from the breaking of reservoir dams. Flash floods pose a significant threat to humans because they are triggered by torrential rainfall that can occur almost anywhere [1,10,11]. It is estimated that 40% of flood victims in Europe between 1950 and 2006 suffered because of flash floods [12]. At the same time, some climate change models predict that such extreme rainfall events will occur more and more frequently [13], hence the risk posed by flash floods is probably going to increase. Nonetheless, the problem requires further study [14,15].

In agricultural areas, intensive surface runoff after heavy rainfall causes strong gully erosion that leads to the destruction of crops and roads [16,17]. The accumulated material silts up fields, roads and farms. The flood wave rapidly forming in the valley bottoms is a threat to human health and life and causes considerable material losses. Such floods pose a significant problem to local governments as they usually have to deal with repairing the flood damage on their own [7]. Typical flash floods in Poland affect catchments covering less than 40 km^2. They result from rainfall usually lasting up to two hours and having an

intensity of 20–80 mm h^{-1}. Phenomena of this type occur most often in July and May and June [18].

Local flash floods occur in Poland and in other parts of Europe mainly in upland and mountain areas. Their spatial distribution is determined by two factors—climate and topographic conditions [1,2,19]. High slope gradients, higher density of the river network and shallower soil cover quickly lead to the development of intensive surface runoff [7,20]. The state of our knowledge on the occurrence, determinants, and course of such phenomena is insufficient [21]. Flash floods can thus occur in unexpected and totally unprepared locations (Figure 1). Identifying areas vulnerable to flash floods is more complicated that in the case of floods occurring in the valley bottoms of large rivers. Rapid runoff and flooding can occur in areas practically devoid of permanent drainage and not covered by the network of standard meteorological and hydrological measurements.

Figure 1. Effects of a flash flood in Fajsławice municipality (June 2016) (source http://www.krasnostawska.pl/siedliska-znowu-pod-woda/; accessed on 20 December 2020).

Studies on flash floods in Poland focus mainly on mountain areas. Based on the analysis of selected characteristics of the natural environment of small catchments of the Foothills (Carpathian Mountains), Bryndal (2011) [22] identified areas susceptible to the occurrence of such phenomena. Ostrowski et al. (2012) [9] prepared a catalogue of flash floods in the years 1971–2010, assessed the dynamics, cyclic nature and frequency of these phenomena, and identified regions at particular risk of flooding. Several studies describe the hydrological and geomorphological effects of these phenomena [14,23–25].

The identification of catchments at risk of flash floods is most frequently carried out by analyzing a number of various criteria by means of GIS (geographic information systems) [26–30]. These studies encompass individual cities [31] or entire countries [30,32]. In the case of studies concerning small areas, detailed data and advanced models difficult to use for larger areas are often employed. Studies encompassing entire countries are usually based on data and maps in small scales. Particular attention is devoted to this threat in urban areas, especially those with numerous underground structures, such as the metro (subway) [33,34].

The appropriate use of spatial resources is one of the ways for humanity to adapt to the expected climate changes [35,36]. Assessing the inclusion of areas exposed to such hazards in the spatial planning process was an important aspect of the conducted research [7,37]. This is particularly important in the context of the present-day changes in land cover and development of the settlement network taking place. Spatial planning is regarded as one of

the main instruments for managing adaptation to climate change and managing the effects of climate change in the spatial context [35,38,39], also with regard to limiting the negative effects of floods [40–42]. Flood risk management is a matter of cross-sector collaboration controlled, at different levels of territorial division of countries, by various institutions and state administration bodies [43]. The full coordination between government bodies and entities competent in risk management, i.e., protection of the population, spatial planning and sectoral programs (e.g., in the field of water management) is a systemic challenge not only in Poland. For the already developed areas in the valleys of smaller rivers, risk reduction can be achieved by educating the residents, preparing warning systems and effective crisis response plans and protective measures for individual buildings [44]. Another matter is the spatial chaos and crisis of spatial planning, which constitute a major obstacle to the sustainable development of the country [45].

The study objective was to assess to what extent the threat related to the potential risk of flash floods is taken into account in the spatial planning system of municipalities. The first step was the identification of catchments susceptible to flash floods in the agricultural area of the Lublin Upland (E Poland). Results of the assessment allow one to identify areas (catchments and municipalities) exposed to a potentially greater flash flood hazard if heavy rainfall occurs (higher hazard). Then, planning documents and existing flood maps were analyzed in terms of identifying the flash flood risk. For the valleys of large and medium rivers, flood hazard maps and flood risk maps are developed in Poland in accordance with the European Flood Directive. In the case of smaller valleys, however, areas at risk of flash floods were not prepared [7,16]. The results of studies on the inclusion of phenomena such as flash floods in the spatial planning system have not been published in Poland so far. This problem has not been more widely discussed in international literature either.

2. Materials and Methods

2.1. Study Area

The Lublin Upland is located in the south-east of Poland (Figure 2). The region, covering 7200 km^2, is divided into nine physical geographical regions In terms of the administrative division, the Lublin Upland is located in Lubelskie Province. The substrate of the Lublin Upland consists of lithologically varied Cretaceous and Paleogene carbonate rocks. They are overlain by tertiary limestone and various Pleistocene deposits: till, sand, gravel and periglacial loess. The Lublin Upland reaches the highest elevation in its central and eastern parts (up to 300 m a.s.l.), from where it descends to the north-east and north-west to an elevation of about 200 m a.s.l. The plate structure of the Cretaceous and Paleogene bedrock is reflected in land relief—vast, flat top plateaus are common in the area. The general outline of the area is influenced by the properties of Upper Cretaceous rocks that form area of the hilly type. The diverse land relief is reflected in the names of the mesoregions: Małopolska Vistula Gap, Nałęczów Plateau, Bełżyce Plateau, Chodel Basin, Urzędów Elevation, Świdnik Plateau, Giełczew Elevation, Grabowiec Elevation and Zamość Depression. Diversified landscapes may be found here: monotonous plateaus, hilly areas dissected by deep and narrow river valleys, residual hills, dense gully networks, escarpments, karst depressions and sandy planes with dunes.

The annual precipitation is about 550–600 mm, the mean annual air temperatures range from 7.0 to 7.6 °C and the mean specific runoff rate is about 4.0 $dm^3/s{\cdot}km^2$. Precipitation in this region occurs most often in the summer season, frequently in the form of downpours and storms. The period of intensive precipitation lasts about 210 days, i.e., longer than in other regions of Poland [46].

The rivers of the Lublin Upland are small. The river network in the southern part of the Upland is sparse while it is a bit denser in the northern part. The main river flowing across the Lublin Upland is the Wieprz; it also drains the greatest amount of water, the mean flow at its estuary being about 17 m^3/s. The Bystrzyca, the biggest tributary of the Wieprz, carries about 5 m^3/s while the flow of other rivers in the region does not exceed 2 m^3/s. Groundwaters occur in Cretaceous, Tertiary and Quaternary formations. The

main aquifer is mainly in the Upper Cretaceous deposits [46]. Outside of river valleys, groundwaters occur deep (30–50 m and more) below the ground surface.

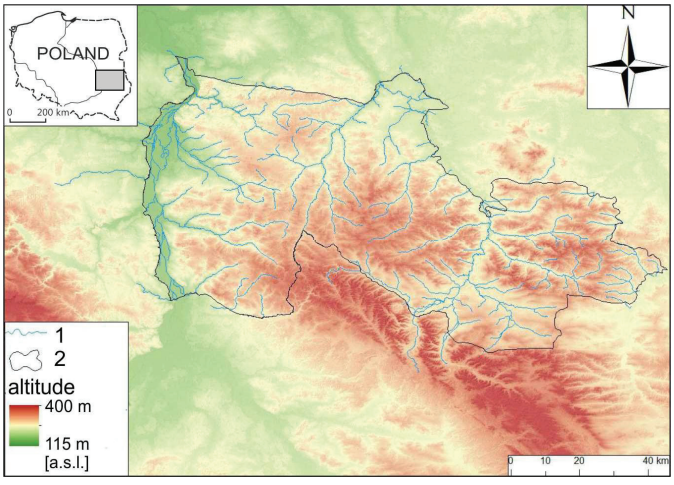

Figure 2. Location and topography of the Lublin Upland; 1—the main rivers, 2—boundary of the Lublin Upland.

The Lublin Upland is a region where torrential rains, heavy rains or hail storms occur relatively frequently. The amount of rainfall reaches about 20–30 mm each time, and in some cases as much as 100 mm. The duration of such rainfall events can be short: from a few to several dozen minutes. These phenomena result in intensive surface runoff that leads to rapid rises in water levels. These phenomena occur locally, often affecting areas between ten to several dozen square kilometers, with 70% of the precipitation occurring in June and July. In the 1951–2000 period, between 10 and 20 rainfall events with a daily volume of more than 100 mm were recorded. The best-known events from that period included the heavy rains in Piaski Szlacheckie in 1956, in Dzierzkowice in 1969 and in Kazimierz Dolny in 1981 [14].

The Lublin Upland is a typically agricultural region where arable land usually covers 70–80% of the area of the individual counties. The population density, ranging from 70 to 90 persons per km^2, is slightly lower than the national average for Poland. A characteristic feature of the region is the occurrence of numerous family farm holdings with an average area of about 5 ha. Despite such a high fragmentation of production, the Lublin Upland is an important area of agricultural production in Poland due to the presence of fertile soils (Cambisols and Luvisols) [47]. Recent years, however, have seen a decrease in the agriculturally used areas resulting from the socioeconomic changes occurring here [48].

2.2. Local Spatial Planning in Poland in Relation to Flood Risk Management

A flood is a natural disaster (Act of 18 April 2002 on a State of Natural Disaster) [49]. Minimizing flood risk, ensuring safety during its occurrence and removing the effects of flooding requires the cooperation of state and local government administration with various institutions. It is also necessary to ensure a coherent formal and legal system concerning flood control, water management, spatial planning and crisis management. At the local level, it is the municipality's own responsibility to ensure "public order and safety of citizens as well as fire and flood protection, including the equipment and maintenance of a municipal flood protection warehouse" (article 7 § 1 (14) of the Act of 8 March 1999 on municipal government [50]. Pursuant to the Crisis Management Act of 26 April 2007 [51],

the basic crisis management instrument of a planning character is the National Crisis Management Plan along with the provincial, county and municipal plans [52–54].

Spatial planning is a key instrument for the appropriate and rational design of spatial development. In Poland, the legal basis for this process is provided by the Act of 27 March 2003 on Spatial Planning and Development [55] that defines (article 1 § 1) "the scope and modes of procedure in land use designation for specific purposes and establishing the rules of land development, with spatial order and sustainable development regarded as the basis for these actions".

The local level of spatial planning that encompasses a spatial development conditions and directions study for a municipality ("study") and a local spatial development plan ("local plan") is the most important from the point of view of flood hazard management. A study is an act of internal management and cannot be the basis for administrative decisions. Its preparation is obligatory for the entire area of a municipality (town). A local plan, on the other hand, is an act of local law and, with certain exceptions, it is not obligatory. It can be prepared for an entire municipality and an individual plot of land. The provisions of a local plan must conform to the provisions of the study. In the absence of a local plan to determine the development requirements, a decision on development conditions and land use is issued [56,57].

The Act on Spatial Planning and Development [53] indicates the minimum scope of problems included in planning studies. A study should take into account conditions resulting from, inter alia, "the threat to the safety of people and their property" and, in relation to water "flood control requirements" (art. 10 § 1 of the Act on Spatial Planning and Spatial Development). A study should specify, among others, "areas particularly exposed to flood risk" (art. 10 § 2). A local plan must specify (art. 15 § 2) "the boundaries and ways of developing [...] areas particularly exposed to flood risk" and "detailed area development conditions and use restrictions, including the prohibition of building development".

In 2011 the provisions of the European Flood Directive were implemented (Directive 2007/60/EC of the European Parliament and of the Council) [58] in Polish law whereby spatial planning has been very strongly integrated into the process of reducing the negative effects of floods. The identification of the flood hazard is now formally regulated by the Water Law Act of 20 July 2017 [59], which makes Wody Polskie (State Water Management Company) and state and local government administration bodies responsible for flood control (protection) [60–62]. This protection is provided "while taking into account flood hazard maps, flood risk maps and flood risk management plans". Flood risk management includes, "in particular, prevention, protection, preparedness and responding when flood occurs, dealing with the effects of floods, restoration and drawing conclusions in order to reduce the potential adverse effects of floods on human health, the environment, cultural heritage and economic activity." (art. 163).

According to the European Flood Directive flood hazard maps (FHMs) and flood risk maps (FRMs) are drawn up for areas identified in the preliminary flood risk assessment. The purpose of preparing this preliminary flood risk assessment is to identify areas at risk of flooding, those with a significant flood risk or with a high probability of a high flood risk. The first assessment was carried out in the period 2010–2015 as part of an EU-funded project—the IT System for the Protection of the Country against Extreme Hazards (ISOK), which provides access to, among others, flood hazard maps and flood risk maps [63]. The final versions of flood hazard maps and flood risk maps were submitted to local government units in April 2015. Eventually, after protests of local governments (especially of cities), which often questioned the flood water extent presented on the maps and did not want to bear the high costs of changes in planning documents, optionality was introduced (art. 88f § 5, 6 of the Water Law Act of 2001, [64]). In 2016, a review and updating of the preliminary flood risk assessment was begun.

2.3. Methods

The assessment of the susceptibility of catchments to flash floods was divided into five steps: (a) identifying the characteristics of the catchment environment influencing this phenomenon; (b) collecting the necessary spatial data; (c) spatial analysis of the parameters; (d) quantifying the individual characteristics and (e) carrying out a synthetic assessment of susceptibility (Figure 3).

The fundamental part of the study consisted of the analysis of the existing planning documents for local government units located within the catchments with high susceptibility to flash floods. It was assessed whether this threat is recognized in these documents and reflected in spatial planning. It was also examined whether they are covered by the flood risk maps and flood hazard maps prepared as part of the implementation of the EU Flood Directive. Twelve studies (spatial development conditions and directions study for a municipality) and over 60 local plans (spatial development plans) or their changes were analyzed (Figure 3).

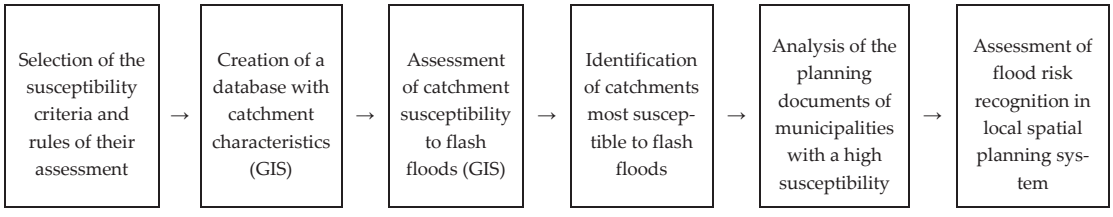

Figure 3. Scheme of research procedure.

Based on the analysis of the available literature on the determinants of the catchments' susceptibility to flash floods, it was found that, in the case of a study area of more than 7200 km^2 (369 catchments), it would be advisable to use the following catchment characteristics: (A) catchment area; (B) circularity index; (C) mean catchment gradient; (D) density of the river network; (E) mean length of first-order watercourses; (F) forest cover; (G) built-up areas and (H) road density. A study prepared by Bryndal (2011) [20] for Carpathian catchments proved to be particularly valuable. In the study, he carried out a detailed analysis of catchment parameters influencing their susceptibility to rapid rises in water levels.

The catchment area is a significant parameter because flash floods usually occur in small catchments, covering from a dozen or so to 40 km^2 [9,20]. Therefore, the following rule was adopted: the smaller the area of a catchment, the greater its susceptibility to the occurrence of flash floods. The shape of a catchment (expressed by the circularity index) is important from the perspective of the speed of water supply to the watercourses. The higher the value of the index—and the shape of a catchment closer to a circle—the smaller the risk. With a more circular shape, the supply of water to the primary valley is more spread over time. The higher the slope gradients, the faster the formation of runoff occurs [17]. The formation of a flood wave is also more likely when the density of a permanent drainage network is greater and the length of first-order watercourses is smaller. The agricultural use of an area results in a quick formation of surface runoff. Thus, the susceptibility of a catchment to flash floods decreases with increased forest cover. On the other hand, a greater proportion of built-up areas (smaller infiltration) and roads (accelerated runoff) increases the flash flood hazard [65].

Land relief analysis was based on a digital terrain model with a spatial resolution of 30 m (SRTM). Data were sourced from the USGS Earth Explorer website [66]. Fourteen scenes connected with each other were used to obtain coverage of the entire area of the Lublin Upland. Watercourses in the form of the vector layer were obtained from the website of the Head Office of Geodesy and Cartography (GUGiK) [67]. The study used a layer containing the boundaries of catchments with permanent drainage. It was obtained from

the resources of the Faculty of Earth Sciences and Spatial Management, UMCS. The study also used land cover vector data prepared as part of the CORINE Land Cover 2018 project. They were obtained from the resources of the Copernicus Land Monitoring Service [68]. The study used data related to built-up areas and forests. The road network (all roads) in the vector Esri shapefile format was generated from the OpenStreetMap [69] using the QuickOSM plugin in QGIS 3.4.4 software. All the analyses were carried out in ArcMap version 10.2.1. They were primarily based on the creation of maps presenting the spatial variation of the individual parameters and the susceptibility assessment results.

Digital maps were prepared showing the diversity of parameters within the catchments under study. Then the susceptibility of catchments was quantified according to the selected assessment criteria. For each catchment, eight parameters were rated separately on a 6-point scale. Varied weights of criteria, proposed by authors, were used depending of their role in formation of flash floods (Table 1). Setting the weights we used the information available in the literature on the impact of individual factors on the intensity of flash floods [2,4,6,11]. For each parameter, separate maps were created showing the spatial variation of its values in the catchments according to the adopted assessment criteria (divided into five classes of partial susceptibility). The synthetic susceptibility of catchments was calculated based on the following formula:

$$FF = \sum_{i=1}^{n} (w_i x_i)$$

FF: susceptibility to flash flood formation;
w_i: weight of parameter;
x_i: parameter;
n: number of parameters.

Based on the partial assessments, the total susceptibility index expressed with a numerical value with a theoretical variation of 0–48 was obtained. Four classes of susceptibility to the occurrence of flash floods were distinguished:

- Class I (from 25 to 30 points): insusceptible catchments;
- Class II (from 31 to 36 points): catchments with low susceptibility;
- Class III (from 37 to 42 points): susceptible catchments;
- Class IV (from 43 to 48 points): highly susceptible catchments.

To assess the impact of particular features (parameters) of the catchment on the final assessment results Pearson's correlation coefficients between the synthetic, point assessment result and the catchment parameters was calculated.

Table 1. Criteria of susceptibility assessment of catchments to flash floods.

Score	Catchment Area (km^2)	Circularity Index	Mean Catchment Gradient	Density of River Network ($km \cdot km^{-2}$)	Mean Length of First-Order Watercourses (km)	Forest Cover (%)	Built-Up Area (%)	Density of Road Network ($km \cdot km^{-2}$)
1	>60	>0.7	<1.75°	<0.15	>10	>40	<0.1	<0.5
2	30–59	0.6–0.7	1.75–1.9°	0.15–0.19	7.5–9.9	20–39	0.2–1.9	0.5–1.4
3	20–29	0.5–0.59	2–2.4°	0.2–0.29	5.0–7.4	10–19	2–4.9	1.5–2.9
4	10–19	0.4–0.49	2.5–2.9°	0.3–0.49	2.5–4.9	5–9	5–19.9	3–4.9
5	5–9	0.3–0.39	3–3.5°	0.5–0.59	1–2.4	0.2–5	20–40	5–10
6	<5	<0.3	>3.5°	>0.6	< 1	<0.2	>40	>10
Weight	1.5	0.8	2	0.8	1	2	0.8	1.5

The occurrence of the most vulnerable catchments within administrative units was analyzed. Existing planning documents were analyzed for municipalities located within the catchments with high susceptibility to flash floods (more than 50% of the area occupied by the catchments belonging to class III and IV). It was assessed whether this threat is

recognized in them and reflected in spatial planning. Twelve studies (spatial development conditions and directions study for a municipality) and over 60 local plans (spatial development plans) or their changes were analyzed. We also analyzed flood hazard and flood risk maps prepared in accordance with the Flood Directive available at the ISOK website [63]. It was assessed whether they include catchments and municipalities located within them, for which high susceptibility to flash floods was found.

3. Results

Most of the 369 catchments in this study were rather small (Table 2). The area of more than 60% was less than 20 km^2. The biggest proportion of the catchments (30%) covered an area of 10 to 20 km^2. Most of the large catchments were located in the western and central part of the Lublin Upland, while the smallest catchments were located in the east and north of the region (Figure 4).

Table 2. The parameters of the studied catchments (369 in total).

Parameter	Mean	Standard Deviation	Minimum	Maximum
Catchment area (km^2)	19.2	16.7	0.1	98.3
Mean catchment gradient (°)	2.53	0.74	1.27	5.88
Forest cover (%)	14.1	14.2	0.0	81.2
Circularity index	0.506	0.10	0.209	0.803
Density of river network (km·km^{-2})	0.28	0.16	0.1	0.89
Mean length of first-order watercourses (km)	3.13	2.33	0.8	17.4
Built-up area (%)	6.54	11.6	0	99.8
Density of road network (km·km^{-2})	1.86	6.11	0.1	16.5

Most of the catchments (about 50%) had moderate gradients, from 2 to 3 degrees. Catchments with the highest slope gradients were primarily located in the eastern part of the Upland (Figure 4). Three concentrations of catchments with the lowest mean gradients were situated in the southernmost part of the region and in its central-northern part. Most of the catchments (44%) had a forest cover within the 10–20% and 20–40%, range. The most extensive forest cover occurred in areas in the western and eastern part of the Upland. The central part had the smallest forest cover (Figure 4). Most of the catchments (over 50% of all catchments under study) had a river network density of 0.2–0.5 km·km^{-2}. The lowest value of this index occurred in catchments in the south-western and central part of the Upland. The highest density occurred in the north-western, south-eastern and central-northern part of the region. The circularity index of most of the catchments (60%) ranged from 0.4 to 0.6. There were no patterns in the spatial distribution of catchments with various values of this index; they were equally distributed across the entire region. The mean length of first-order watercourses in most of the catchments (30%) ranged from 2.5 to 5 km (Figure 4). Additionally, in this case, there are no distinct patterns in their spatial distribution; catchments with different values of this index form a mosaic-like pattern across the entire area of the Lublin Upland (Figure 4). Built-up areas accounted for 2–5% in 34% of the catchments and 5–20% in 29% of the catchments. Catchments where the road network ranges from 0.5 to 1.5 km·km^{-2} were predominant. The highest road density occurred in the central part of the Upland while the lowest density in the eastern part (Figure 4).

The mean score for all catchments in the Lublin Upland was 36, which was the upper limit of susceptibility class II (Table 3). About 30% of the area belonged to class III and IV. The most susceptible catchments were scattered across the entire area of the Upland. Their biggest concentrations were located near Lublin and in the east of the Upland. The least susceptible catchments predominated in the west and south-west part. Low susceptibility also occurred in the northern part (Figure 5).

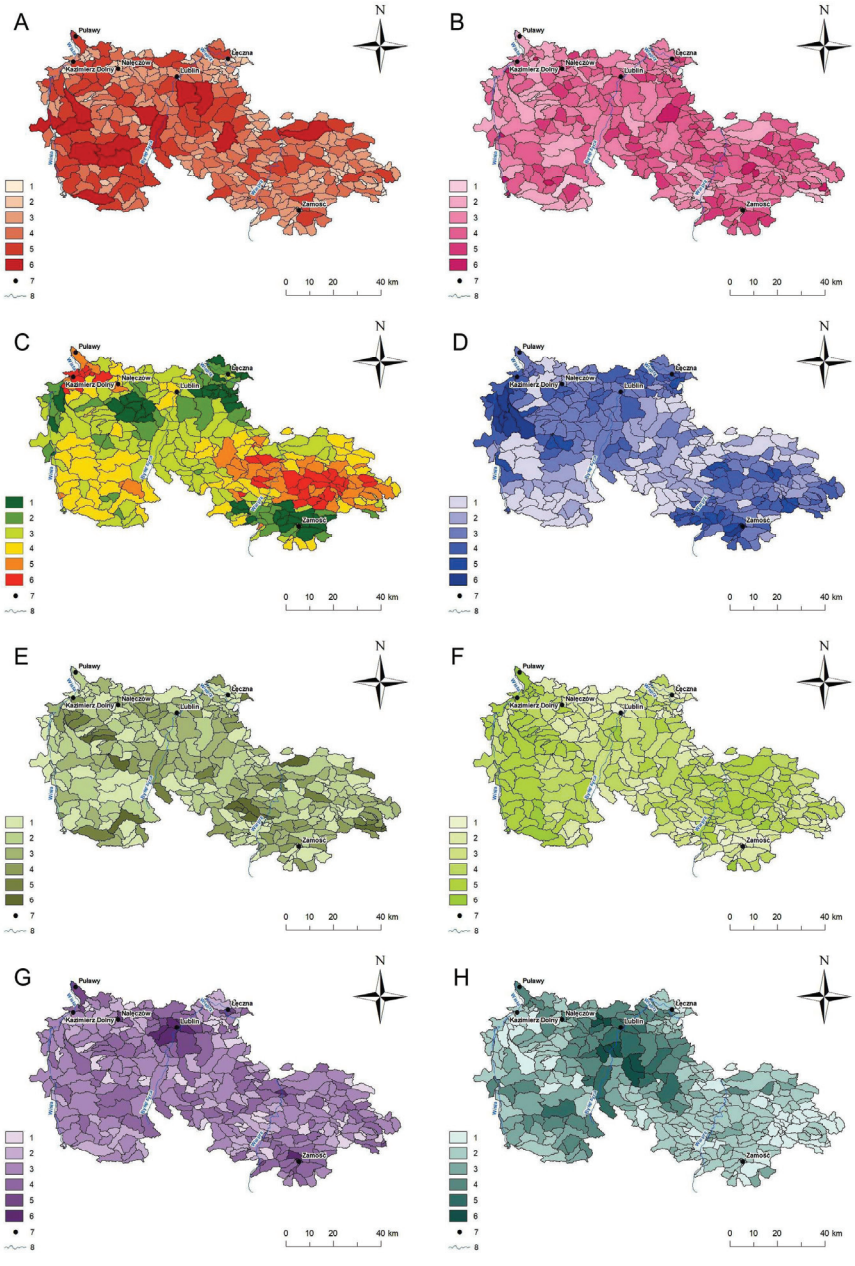

Figure 4. Assessment of susceptibility of catchments to the occurrence of flash floods. (**A**)—catchment area (km^2), 1: <5, 2: 5–9, 3: 10–19, 4: 20–29, 5: 30–59, 6: >60; (**B**)—circularity index, 1: 0.3, 2: 0.3–0.39, 3: 0.4–0.49, 4: 0.5– 0.59, 5: 0.6–0.7, 6: >0.7; (**C**)—mean gradient in catchment (°), 1: <1.75, 2: 1.75 –1.9, 3: 2–2.4, 4: 2.5–2.9, 5: 3–3.5, 6: >3.5; (**D**)—density of river network (km·km^{-2}), 1: <0.15, 2: 0.15–0.19, 3: 0.2–0.29, 4: 0.3–0.49, 5: 0.5–0.59, 6: >0.6; (**E**)—mean length of first-order watercourses (km), 1: >10, 2: 7.5–9.9, 3: 5.0–7.4, 4: 2.5–4.9, 5: 1–2.4, 6< 1; (**F**)—forest cover (%), 1: 0, 2: 0.1–5, 3: 5–9, 4: 10–19, 5: 20–39, 6: >40; (**G**)—built-up area (%),1: 0, 2: 0.1–1.9, 3: 2–4.9, 4: 5–19.9, 5: 20–40, 6: > 40 and (**H**)—road density (km·km^{-2}), 1: <0.5 2: 0.5–1.4, 3: 1.5–2.9, 4: 3–4.9, 5: 5–10, 6>10; 7—main towns, 8—main rivers.

Table 3. Quantitative differences of catchments with different degrees of susceptibility.

Class	Number of Catchments	Area (km^2)	Proportion of Area (%)
I	44	1250.82	17.3
II	165	3654.68	50.7
III	129	1972.14	27.3
IV	31	231.79	3.2

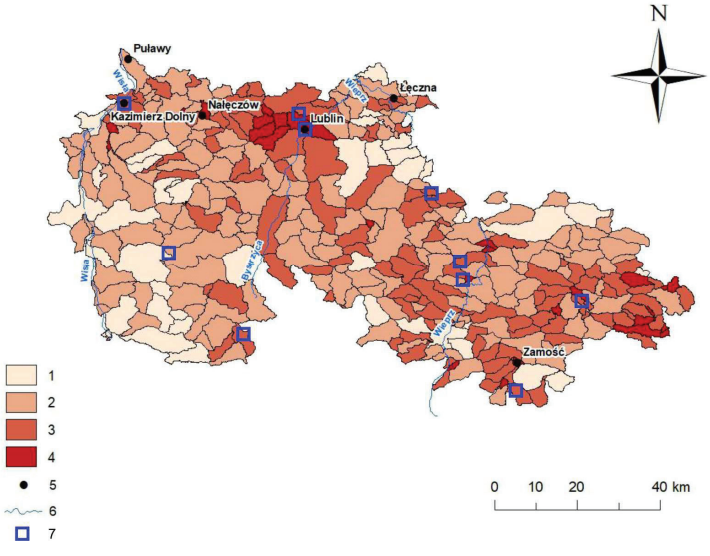

Figure 5. Synthetic assessment of susceptibility of catchments in the Lublin Upland to the occurrence of flash floods. 1—Susceptibility class I, 2—Susceptibility class II, 3—Susceptibility class III, 4—Susceptibility class IV, 5—main towns, 6—main rivers, 7—major flash floods (1960–2020).

Catchments belonging to Class I show a low level of susceptibility to the formation of flash floods. Most of the catchments in this class covered a large area (mean area of 28 km^2) and had a large forest cover (24.7%). The lower mean gradient of the catchment area, 2.1, was a characteristic feature of these catchments. They also had a poorly developed river network, with a density of 0.2 km·km^{-2}, while the length of first-order watercourses was 4.5 km. The mean road density was 1.47 km·km^{-2}, while built-up areas accounted for 2.6% (mean) of the area of these catchments.

Catchments assigned to class II show a low susceptibility to rapid rises in water levels and runoffs. It is the most numerous class, comprising nearly half of the catchments. Catchments in this class typically covered a rather large area (mean area of 22.1 km^2) and had a rather small forest cover (17.4%). The density of their river network as rather low, 0.26 km·km^{-2}, while the mean length of first-order watercourses was 4 km. The road network density was 1.99 km·km^{-2} while built-up areas accounted for 3.9% of these catchments.

Catchments belonging to class III were susceptible to the formation of flash floods. Their area was considerably smaller than those in the previous classes: 15.2 km^2 on average. The slope gradients (2.6° on average) were slightly higher than in class I and class II catchments. The proportion of forests in the land cover of these catchments was small (9.2%). The mean length of first-order watercourses, 2.4 km, was clearly shorter, while the proportion of built-up areas was greater, 7.1%. The density of the road network was similar to the value for class II catchments.

Class IV comprised catchments highly susceptible to flash floods and runoffs. Their area was small, 7.5 km^2 on average. The mean slope gradient, ranging from 1.5 to 0.71, was the highest among all the classes. The proportion of forested areas was very small, 1.8% on average, but that of built-up areas was high, 23%. The density of the river network in these catchments was the highest, 0.6 km·km^{-2}, while the mean length of first-order watercourses was the shortest, 1.9 km.

Table 4 contains correlation coefficients between the synthetic susceptibility (expressed in points) and the characteristics (parameters) of the studied catchments. Table 5 provides information on the basic features and existing planning documents for municipalities with a high degree of susceptibility to flash floods. Table 6 presents the results of the analyses of existing flood hazard and flood risk maps within the surveyed municipalities. It also presents information on the scope of flood hazard and flood risk identified in the planning documents.

Table 4. Correlation coefficients between catchment susceptibility and catchment parameters.

Parameter	Correlation Coefficient
Catchment area	−0.382
Mean catchment gradient	0.218
Forest cover	−0.459
Built-up areas	0.405
Circularity index	−0.020
Density of river network	0.232
Density of road network	0.063
Mean length of first-order watercourses	0.276

Table 5. Selected characteristics of municipalities with high flash flood risk (>50% of the area in class III and IV).

Selected Features	Municipalities												
	Lublin	Zamość	Fajsławice	Głusk	Grabowiec	Jastków	Konopnica	Rudnik	Skierbieszów	Strzyżewice	Trzeszczany	Uchanie	Żółkiewka
	City			Rural Municipality									
Area of the unit (km^2)	147	30	71	64	128	113	93	89	139	109	90	121	130
Population density (persons/km^2)	2303	2103	65	174	31	124	149	34	37	74	46	38	42
Forest cover (%)	11.4	1.6	4.0	7.7	10.3	4.9	5.9	9.2	19.9	15.9	13.5	15.5	8.7
Agricultural land (%) *	36.8	47.1	92.3	85.9	86.8	88.5	88.8	88.1	76.1	81.2	83.1	81.4	88.7
Arable land (%) *	31.1	29.7	84.8	79.8	72.3	75.0	73.4	76.9	61.5	71.0	68.6	67.2	80.7
Built-up and urbanized land (%) **	45.9	49.3	2.8	5.1	2.5	4.5	4.7	1.9	3.4	2.7	8.1	2.4	2.1
Spatial Planning Documents													
Existing Spatial Development Plans													
Local plans (in total) (number)	94	1	1	16	5	25	7	2	4	1	6	2	1
Area covered by local plans (%)	53.7	100	100	7.6	100	94.9	24.2	99.9	6.3	100	99.9	2.8	12.5
Decisions on building conditions and land development issued in 2009–2018													
On determining the location of a public purpose investment	1759	0	0	-	0	60	0	0	38	0	0	33	15
Concerning building conditions (in total)	7588	0	0	-	0	53	3292	1	123	0	0	212	66
Concerning multi-family housing	651	0	0	-	0	0	2	0	0	0	0	13	0
Concerning single-family housing	3241	0	0	-	0	44	2085	1	70	0	0	97	22
Concerning service buildings	1584	0	0	-	0	2	107	0	1	0	0	14	1
Concerning other buildings	2112	0	0	-	0	7	1098	0	52	0	0	88	43

Source: own study based on the Local Data Bank of the Central Statistical Office of Poland (2019), * according to the 2010 Agricultural Census, ** data from 2014, "-" no data.

Table 6. Provisions of planning documents vs. flood hazard in municipalities (>50% of the area in class III and IV).

Municipality	Area Occupied by the III and IV Susceptibility Class (%)	Flash Floods (FF) Risk (Results of the Study) Flood Hazard Flood Hazard Maps (FHM), Flood Risk Maps (FRM)	Planning Documents	
Lublin	85.9	Within the city limits there is a large share of FF risk areas, the highest degree of susceptibility (class IV) covers the catchments of river valleys. Most of the city within the FHM and FRM sheets, small areas are within the water range of Q1% and Q0.2%	The study (2019) delineates the main areas of flood occurrence in river valleys; recommendations for risk areas, the exclusion of buildings in local plans; indicates that flooding may occur locally as a result of torrential rain or thaw (in river valleys and dry valleys).	Local plans (2002, 2005) regulate the problems of flood risk to a small extent. Local plans (2014, 2016, 2018, 2019) indicate areas at risk of flooding with a water range of 1% and 0.2% and at risk of flooding in the event of a dam or flood embankment breakage.
Zamość	58.2	More than half of the city is located in an area of significant FF threat The area entirely within the FHM and FRM sheets, which include river valleys, individual buildings are within Q1% and Q0.2% of water range.	The study (2019) indicates the development of flood protection infrastructure in river valleys, increasing retention and excluding buildings; does not designate areas of particular flood risk.	The local plan (2006) for the entire city does not define the boundaries and ways of management and development of flood-prone areas.
Fajsławice	85.1	Most of the catchment area in the commune is susceptible (class III) to FF. A small fragment of the area is within the FHM and FRM, but apart from the flood risk of 1% and 0.2%	The study (2015) allows for the construction of hydrotechnical structures for water retention or flood protection.	Changes to the local plan (2006, 2014, 2018) do not define the range of flood-prone areas due to the lack of occurrence.
Głusk	78.3	Most of the catchment area in the municipality is susceptible (class III) to FF. River valleys partly within FHM and FRM.	The study (2018) indicates the risk of rainfall and snowmelt floods; defines the boundaries of flood risk areas; excludes from development areas at risk of flooding with water reach of 10%, 1% and 0.2%.	The local plan (1999) for the entire municipality does not indicate the risk of flooding. Changes to the plans (2005, 2006), covering fragments of river valleys, do not indicate a flood risk.
Grabowiec	52.1	More than half of the area is catchment areas susceptible to FF (mainly class III) Fragments of river valleys within the FHM and FRM sheets.	The study (2013) shows that there are no flood risk areas in the municipality.	The local plan (2002) and its changes (2009, 2015) do not define the issues related to flood risk.
Jastków	91.5	Most of the catchments are susceptible (class III) to FF, very susceptible (class IV) are in the S-E part. Partly river valleys within the FHM and FRM sheets, but outside the flood risk of 1% and 0.2%.	The study (2015) prohibits the location of new buildings in river valleys in flood risk areas; sets out the rules of development within plots bordering on riverbanks.	The local plan (2002) does not specify the flood risk. Changes to the local plan apply to small areas and do not include flood risk areas.
Konopnica	67.4	There is a large area of catchments susceptible (class III) and very susceptible (class IV) to FF. Small parts of the area within the FHM and FRM sheets, but outside the flood risk of 1% and 0.2%.	The study (2010) sets the water range of 1% (coincides with the boundaries of the river valley bottoms) and the general principles of management.	The local plan (2002) does not specify the flood risk.

Table 6. *Cont.*

Municipality	Area Occupied by the III and IV Susceptibility Class (%)	Flash Floods (FF) Risk (Results of the Study) Flood Hazard Flood Hazard Maps (FHM), Flood Risk Maps (FRM)	Planning Documents	
Rudnik	81.5	Most of the catchments in the municipality are susceptible (III) to FF. Only N part located within FHM and FRM, but outside the flood hazard area 1% and 0.2%.	The study (2019) identifies the areas of flood risk and inundation related to ground and water conditions as well as snowmelt and torrential rainfall;	Local plan (2004) unavailable, its content has not been analyzed. The change of the plan (2010) indicates that there is no flood risk in the area covered by the plan.
Skierbieszów	61.8	A large proportion of catchments susceptible to FF (mainly class III). Area within the FHM and FRM sheets, buildings beyond the range of Q1% water, while at Q0.2% individual properties at risk of flooding.	Study (2002)—no information on flood risk; indicates the areas for the location of retention reservoirs.	The local plan (2006), in the area of direct flood risk, prohibits the location of buildings and construction of buildings.
Strzyżewice	59.6	There is a large share of FF susceptible catchments (only class III). Most of the area within the FHM and FRM sheets, individual properties within Q1% water and a few farms at Q0.2%.	The study (2010) indicates areas exposed to flooding—mainly river valleys, including areas within 1% of water reach; determines the location of buildings outside the flood hazard areas.	The local plan (2003) indicates the river valley bottoms as potential flood areas. The change of the plan (2011) designates the areas at risk of flooding with a water range of 1%.
Trzeszczany	66.1	The western part of the area—catchments in susceptibility class III and IV. Only the middle-eastern part within the boundaries of the FHM and FRM sheets, but outside the flood risk of 1% and 0.2%.	Study (1999)—document unavailable, not analyzed.	The local plan (2003) does not specify the risks associated with flooding. Amendments to the plan (2009, 2013, 2015) establish that there are no flood-prone areas.
Uchanie	53.9	Main river valley catchment areas endangered by FF (class III and IV). The western part within the FHM and FRM sheets, but outside the flood risk of 1% and 0.2%.	The study (2017) shows that municipality is only exposed to spring snowmelt or rain flooding.	The local plan (2007) concerns the areas to be afforested, and the second (2017) the location of the pipeline, in both there is no reference to flood risk.
Żółkiewka	50.0	Half of the area is covered by catchments susceptible to FF (class III). Most of the area within the FHM and FRM sheets, but outside the flood risk of 1% and 0.2%.	The study (2012) indicates a high water range area with a probability of 1% and 0.5%; determines the location of buildings outside the flood hazard areas.	The local plan (2006), in the area of direct flood risk, prohibits the location of buildings and construction of buildings.

Source: own study based data available at https://wody.isok.gov.pl/imap_kzgw/?gpmap=gpFHM (accessed on 20 December 2020) and planning documents available on the websites of municipal offices (documents were analyzed with areas potentially at risk of flooding).

4. Discussion

The studies conducted so far indicate that the Lublin Upland is an area where flash floods occur [9,14,16]. However, the frequency of these phenomena is not as high as in mountain areas. On the other hand, the degree of spatial development in the Upland was greater. The analysis of maps showing the susceptibility of catchments to flash floods and the locations where heavy rains occur indicates the existence of a real threat [14]. In the second half of the 20th century, heavy rains with a volume of more than 30–40 mm within 1–2 h were estimated to have a frequency of 1 event per 20–30 years in the Lublin Upland [14]. However, flash floods can occur in the same locations with a greater frequency, as it is the case in the catchment of the Sanna river or in the area of Lublin (Figure 6). The question of the spatial distribution of these phenomena requires further investigation because systematic research in this respect has not been conducted so far. Although the applied method of identifying catchments susceptible to flash floods is of a preliminary and de facto qualitative character, it can be useful in the spatial planning process. It allows one to identify the areas where the susceptibility is the highest. Major flash floods of the last 50 years occurred in the catchments of the IV class (Figure 5). The parameters analyzed had a varying impact on the susceptibility of catchments to flash floods. The high proportion of built-up areas, small share of forests and small catchment area had the greatest synthetic susceptibility of catchments to flash floods (Table 4).

In accordance with Polish law, a preliminary flood risk assessment was carried out for the Lublin Upland. Flood risk maps and flood hazard maps were drawn up for the areas at risk. They are available on the ISOK map portal [63]. The sheets of this map encompassed all the major rivers of the region and some of the smaller rivers. The analysis of flood hazard maps and catchments at risk of flash floods showed that these areas were not always reflected in the flood risk maps and flood hazard maps (Table 6). Particularly small catchments, located in the upper reaches of small watercourses, were not taken into account on flood hazard maps even if floods occurred there historically (Figure 5).

Flash floods are a separate problem, particularly in small catchments because their scale and intensity are difficult to predict. The prepared susceptibility assessment revealed catchments at risk of flash floods based on the adopted parameters. A high flash flood hazard in the Lublin Upland results from the specific land relief, high degree of deforestation and considerable share of arable land. Due to these characteristics, along with the prevailing land use pattern (fields perpendicular to the valley axis), water after heavy rainfall is quickly drained from the plateau top and slopes (also via gully systems with hard roads) to flat-bottomed valleys. Buildings, historically located usually along the edge of the valley bottom, are threatened with flooding. The situation within territorial units with a high share of built-up and urbanized areas is particularly difficult. In June 2019, a flood occurred successively in Pasieka, Wierzchowiska Drugie and Wierzchowiska Pierwsze—localities lying in the valley of the small Sanna river in Modliborzyce municipality. Houses and roads were flooded, part of the technical infrastructure was damaged. The valley was outside the scope of the prepared sheets of the flood hazard maps. However, the river had already flooded there before (Figure 6). A similar situation took place in Siedliska Drugie in Fajsławice municipality where, in 2016, a flash flood occurred in the part of the valley not included in the flood hazard maps.

Not all rural municipalities and towns of the Lublin Upland make full use of planning instruments to appropriately manage space, also in the context of flood hazards (Table 5). In the case of 13 units of territorial division with a high level of flash flood hazard (third- and fourth-degree hazard in over 50% of the area), a high percentage of the area is covered by local plans in only six of them. What is more, some of these plans were drawn up a long time ago and do not guarantee a comprehensive approach to flood hazard. In several municipalities, only a few percent of their area are included in the local plans. It is also quite alarming that local plans exist for only half of the territory of the region's capital city Lublin. Detailed analysis of local plans shows to what extent the risk has been identified and how it has been taken into account in planning documents (Table 6).

Figure 6. Effects of a flash flood in the valley of the Sanna River in Modliborzyce municipality (June 2019) (source: https://modliborzyce.pl/2312-miesiąc-po-powodzi-cz-1.html, accessed on 20 December 2020).

The inclusion of 100-year water ranges (Q1%) in planning documents does not fully address the flash flood hazard because with rapid rises in water levels, the flows can even exceed the range of a 500-year water (Q0.2%). The criteria for the preliminary flood risk assessment are not fully effective with regard to small catchments with big elevation differences and agricultural land use. Only a few studied planning documents take into account the phenomenon of flash floods. Its spatial range is indicated only in the case of overlapping with the risk of "classic floods". In the recently developed planning documents, the flood risk is determined on the basis of the FHM and FRM, which do not fully take into account the flash flood hazard. Planners do not know the criteria for separating flood extents, therefore FHM and FRM require a more complete flash flood risk. Even if they have information about the phenomenon (identify the areas of occurrence in the study), the basis for the findings in planning documents, in accordance with the law, are FHM and FRM. No flood hazard maps and flood risk maps have been prepared for many of such areas [7,33]. Such a situation also occurs in the Lublin Upland. Even if such maps exist, spatial development plans do not fully cover areas at risk of flash floods (Table 6). The decisions on development conditions and land management do not always address the hazard adequately.

In Lublin Upland the flood hazard ranges have been specified in the case of areas located in the catchments of larger rivers. However, areas located in the catchments of smaller watercourses are usually regarded as safer while in fact they are particularly exposed to the flood hazard in the case of heavy rains [7,33]. Flood hazard maps and flood risk maps are very important not only for planners, including urban planners, but also for the crisis management cycle: from the prevention phase, through the preparation and response phase, to the reconstruction phase. There is also an issue of connecting the identification of hazards based on natural criteria with the possibility for action at the level of administrative divisions. Spatial planning is the domain of the authorities of territorial units established by way of administrative decisions. The authorities responsible for water management operate within units having natural boundaries. This system needs to be integrated, and this remains a challenge not only in Poland. Flood risk reduction can be achieved through a proper spatial planning process, which is based on reliable information on flood hazards. This enables the designation of areas to be excluded from building development or the identification of technical restrictions and requirements for the location of buildings to be introduced.

A full coordination between spatial development policy and entities responsible for flood risk management is a challenge not only in Poland. The connection between the spatial planning system and flood risk management system needs to be strengthened. As a preliminary step, spatial planning should be aimed at reducing the risk and consequences of natural disasters [40,70]. Gralepois (2020) [38] points out that spatial planning has not been fully used in the prevention of floods and its importance was appreciated to a greater extent only with the implementation of the Flood Directive. However, as the

examples of England and France show, the choice of planning instruments is not always satisfactory, particularly in the context of conflicts between the local tier in spatial planning and national legislation and risk management. In the Netherlands, on the other hand, flood prevention is better integrated into spatial planning, which is a result of greater awareness and better integration of flood management. However, Neuvel and Van Den Brink (2009) [71] indicated that in many cases, even if flood risk information exists, it is not always adequately used.

An important factor in mitigating the risk of flooding is to reduce the vulnerability to flooding, which means the degree to which people, their property and facilities are prepared for flooding, and the ability to repair damage and rebuild after flooding has occurred. Measures related to the reduction of vulnerability include preparing residents for the hazards, i.e., measures related to the protection of buildings at risk of flooding, implementation of flood warning systems and flood education, in the broad sense of the term, among the decision-makers and residents [72]. The episodic nature of flash floods means that residents are not aware of the risks and are not properly prepared for the occurrence of flash floods: they do not know how to properly secure their property or how evacuation is conducted [73]. Fortunately, flood warning systems are used to a greater degree, using devices to signal the danger of flooding when the water level in a watercourse or the amount of precipitation exceed a set limit [7,74,75]. Mobile telephony can also be used to quickly and directly inform people in vulnerable areas.

5. Conclusions

The amount of available data on the occurrence of flash floods in the Lublin Upland is not extensive. The catchments with high susceptibility covered about 30% of the studied area. Most severe flash floods in the second half of 20th century occurred in the catchments of the IV class. It seems, therefore, that the method can be used by local government units.

In Poland currently, areas at risk of flash floods are not fully taken into account in the spatial planning process. Few planning documents take into account the phenomenon of flash floods, and its spatial range is indicated only in the case of overlapping with the risk of "classic floods". It is advisable to include in the legal system the requirement for preliminary and, in justified cases, detailed analyses of this hazard. Planners need spatial information and, therefore, there is a need to expand the areas for which flood hazard maps and flood risk maps are drawn up.

A serious problem in units of territorial division is the lack of local plans in which it would be possible to include appropriate guidelines for development and building in areas at particular risk of flooding because the procedure for preparing them ensures a better level of protection than it is the case with decisions on the site-location of public-purpose investment projects and decisions on development conditions. Additionally, the flood risk management system is undergoing constant legal and structural change, which does not allow its efficiency to be properly assessed.

A very important issue is the question of educating society about this type of phenomena. In addition to the existing recommendations in the legal system, it is necessary to make the inhabitants of areas at risk of flash floods aware of the possibility of such phenomena, even if they are not located in the valleys of large rivers.

Author Contributions: Conceptualization, W.Z., B.B.-Z. and D.G.; methodology, W.Z., D.G. and B.B.-Z.; investigation, D.G. and B.B.-Z.; writing—original draft preparation, W.Z. and B.B.-Z.; writing—review and editing, W.Z. and B.B.-Z.; visualization, W.Z. All authors have read and agreed to the published version of the manuscript.

Funding: This research received no external funding.

Institutional Review Board Statement: Not applicable.

Informed Consent Statement: Not applicable.

Data Availability Statement: All sources of the publicly available datasets are provide in the text as references.

Acknowledgments: The authors wish to thank the Editors and anonymous reviewers for their valuable comments and suggestions to improve the quality of this paper.

Conflicts of Interest: The authors declare no conflict of interest.

References

1. Gaume, E.; Bain, V.; Bernardara, P.; Newinger, O.; Barbuc, M.; Bateman, A.; Blaškovičova, L.; Blöschl, G.; Borga, M.; Dumitrescu, A.; et al. A compilation of data on European flash floods. *J. Hydrol.* **2009**, *367*, 70–78. [CrossRef]
2. Marchi, L.; Borga, M.; Preciso, E.; Gaume, E. Characterization of selected extreme flash floods in Europe and implications for flood risk management. *J. Hydrol.* **2010**, *394*, 118–133. [CrossRef]
3. Borga, M.; Anagnostou, E.N.; Blöschl, G.; Creutin, J.D. Flash flood forecasting, warning and risk management: The HYDRATE project. *Environ. Sci. Policy* **2011**, *14*, 834–844. [CrossRef]
4. Lumbroso, D.; Gaume, E. Reducing the uncertainty in indirect estimates of extreme flash flood discharges. *J. Hydrol.* **2012**, *414–415*, 16–30. [CrossRef]
5. Gourley, J.J.; Hong, Y.; Flamig, Z.L.; Arthur, A.; Clark, R.; Calianno, M.; Ruin, I.; Ortel, T.; Wieczorek, M.E.; Kirstetter, P.-E.; et al. A unified flash flood database across the United States. *Bull. Am. Meteorol. Soc.* **2013**, *94*, 799–805. [CrossRef]
6. Ma, M.; He, B.; Wan, J.; Jia, P.; Guo, X.; Gao, L.; Maguire, L.W.; Hong, Y. Characterizing the Flash Flooding Risks from 2011 to 2016 over China. *Water* **2018**, *10*, 704. [CrossRef]
7. Bryndal, T. Powodzie błyskawiczne w małych zlewniach karpackich—Wybrane aspekty zarządzania ryzykiem powodziowym. *Ann. Univ. Paedagog. Crac. Studia Geogr.* **2014**, *170*, 69–80.
8. Pociask-Karteczka, J.; Żychowski, J.; Bryndal, T. Zagrożenia związane z wodą—Powodzie błyskawiczne. *Gospod. Wodna* **2017**, *2*, 37–42.
9. Ostrowski, J.; Czarnecka, H.; Glowacka, B.; Krupa-Marchlewska, J.; Zaniewska, M.; Sasim, M.; Moskwicki, T.; Dobrowolski, A. Nagłe powodzie lokalne (flash flood) w Polsce i skala ich zagrożeń. In *Wpływ Zmian Klimatu na Środowisko, Gospodarkę i Społeczeństwo. Tom 3, Klęski Żywiołowe a Bezpieczeństwo Wewnętrzne Kraju*; Lorenc, H., Ed.; Wydawnictwo IMGW-PIB: Warszawa, Poland, 2012; pp. 123–149.
10. Parczewski, J. Warunki występowania gwałtownych wezbrań na małych ciekach. *Wiadomości Służby Hydrol. Meteorol.* **1960**, *8*, 1–159.
11. Gaume, E.; Borga, M. Post-flood field investigations in upland catchments after major flash floods: Proposal of a methodology and illustrations. *J. Flood Risk Manag.* **2008**, *1*, 175–189. [CrossRef]
12. Barredo, J.I. Major flood disasters in Europe: 1950–2005. *Nat. Hazards* **2007**, *42*, 125–148. [CrossRef]
13. Christensen, J.H.; Christensen, O.B. Climate modelling: Severe summertime flooding in Europe. *Nature* **2003**, *421*, 805–806. [CrossRef]
14. Anagnostopoulos, G.G.; Koutsoyiannis, D.; Christofides, A.; Efstratiadis, A.; Mamassis, N. A comparison of local and aggregated climate model outputs with observed data. *Hydrol. Sci. J.* **2010**, *55*, 1094–1110. [CrossRef]
15. Kundzewicz, Z.W.; Stakhiv, E.Z. Are climate models "ready for prime time" in water resources management applications, or is more research needed? *Hydrol. Sci. J.* **2010**, *55*, 1085–1089. [CrossRef]
16. Rodzik, J.; Janicki, G.; Zagórski, P.; Zgłobicki, W. Deszcze nawalne na Wyżynie Lubelskiej i ich wpływ na rzeźbę obszarów lessowych. *Dok. Geogr.* **1998**, *11*, 45–68.
17. Rodzik, J.; Janicki, G. Local downpours and their erosion effects. *Glob. Chang.* **2003**, *10*, 49–66.
18. Bryndal, T. Local flash floods in Central Europe: A case study of Poland. *Nor. Geogr. Tidsskr. Nor. J. Geogr.* **2015**, *69*, 288–298. [CrossRef]
19. Mertz, R.; Blöschl, G. A process typology of regional floods. *Water Resour. Res.* **2003**, *39*, 1340.
20. Weingartner, R.; Barben, M.; Spreafico, M. Floods in mountain areas—An overview based on examples from Switzerland. *J. Hydrol.* **2003**, *282*, 10–24. [CrossRef]
21. Creutin, J.D.; Borga, M. Radar hydrology modifies the monitoring of flashflood hazard. *Hydrol. Process.* **2003**, *17*, 1453–1456. [CrossRef]
22. Bryndal, T. Identyfikacja małych zlewni podatnych na formowanie gwałtownych wezbrań (na przykładzie Pogórza Dynowskiego, Strzyżowskiego i Przemyskiego. *Przegląd Geogr.* **2011**, *83*, 27–49. [CrossRef]
23. Ziemnicki, S. Skutki deszczu nawalnego we wsi Piaski Szlacheckie pod Krasnymstawem. *Gospod. Wodna* **1956**, *11*, 476–480.
24. Gil, E. Spływ wody i procesy geomorfologiczne w zlewniach fliszowych podczas gwałtownej ulewy w Szymbarku w dniu 7 czerwca 1985 roku. *Dok. Geogr.* **1998**, *11*, 85–107.
25. Bryndal, T.; Cabaj, W.; Ciupa, T. Gwałtowne wezbrania małych cieków w Niecce Nidziańskiej. *Przegląd Geogr.* **2008**, *80*, 127–146.
26. Abdelkareem, M. Targeting flash flood potential areas using remotely sensed data and GIS techniques. *Nat. Hazards* **2017**, *85*, 19–37. [CrossRef]
27. Costache, R.; Zaharia, L. Flash-flood potential assessment and mapping by integrating the weights-of-evidence and frequency ratio statistical methods in GIS environment—Case study: Bâsca Chiojdului River catchment (Romania). *J. Earth Syst. Sci.* **2017**, *126*, 59. [CrossRef]
28. Liu, C.; Li, Y. GIS-based dynamic modelling and analysis of flash floods considering land-use planning. *Int. J. Geogr. Inf. Sci.* **2017**, *31*, 481–498. [CrossRef]

29. Costache, R.; Pham, Q.B.; Sharifi, E.; Linh, N.T.T.; Abba, S.; Vojtek, M.; Vojteková, J.; Nhi, P.T.T.; Khoi, D.N. Flash-Flood Susceptibility Assessment Using Multi-Criteria Decision Making and Machine Learning Supported by Remote Sensing and GIS Techniques. *Remote Sens.* **2020**, *12*, 106. [CrossRef]
30. Pham, B.T.; Avand, M.; Janizadeh, S.; Phong, T.V.; Al-Ansari, N.; Ho, L.S.; Das, S.; Le, H.V.; Amini, A.; Bozchaloei, S.K.; et al. GIS Based Hybrid Computational Approaches for Flash Flood Susceptibility Assessment. *Water* **2020**, *12*, 683. [CrossRef]
31. Elkhrachy, I. Flash Flood Hazard Mapping Using Satellite Images and GIS Tools: A case study of Najran City, Kingdom of Saudi Arabia (KSA). *Egypt. J. Remote Sens. Space Sci.* **2015**, *18*, 261–278. [CrossRef]
32. Xiong, J.; Li, J.; Cheng, W.; Wang, W.; Guo, L. A GIS-Based Support Vector Machine Model for Flash Flood Vulnerability Assessment and Mapping in China. *ISPRS Int. J. Geo Inf.* **2019**, *8*, 297. [CrossRef]
33. Lyu, H.-M.; Shen, S.-L.; Zhou, A.; Yang, J. Perspectives for flood risk assessment and management for mega-city metro system. *Tunn. Undergr. Space Technol.* **2019**, *84*, 31–44. [CrossRef]
34. Lyu, H.-M.; Zhou, W.-H.; Shen, S.-L.; Zhou, A.-N. Inundation risk assessment of metro system using AHP and TFN-AHP in Shenzhen. *Sustain. Cities Soc.* **2020**, *56*, 202103. [CrossRef]
35. Wilson, E. Adapting to Climate Change at the Local Level: The Spatial Planning Response. *Local Environ.* **2006**, *11*, 609–625. [CrossRef]
36. Onur, A.Z.; Tezer, A. Ecosystem services based spatial planning decision making for adaptation to climate changes. *Habitat Int.* **2015**, *47*, 267–278. [CrossRef]
37. Franczak, P.; Listwan-Franczak, K.; Działek, J.; Biernacki, W. Planowanie przestrzenne na obszarach zalewowych w zlewniach górskich różnego rzędu w dorzeczu górnej Wisły oraz górnej i środkowej Odry. *Prace Studia Geogr.* **2016**, *61*, 25–45.
38. Rannow, S.; Loibl, W.; Greiving, S.; Gruehn, D.; Meyer, B.C. Potential impacts of climate change in Germany—Identifying regional priorities for adaptation activities in spatial planning. *Landsc. Urban Plan.* **2010**, *98*, 30. [CrossRef]
39. Greiving, S.; Fleischhauer, M. National Climate Change Adaptation Strategies of European States from a Spatial Planning and Development Perspective. *Eur. Plan. Stud.* **2012**, *20*, 27–48. [CrossRef]
40. Neuvel, J.M.M. Geographical Dimensions of Risk Management. In *The Contribution of Spatial Planning and Geo-ICT to Risk Reduction*; Thesis Wageningen University: Wageningen, The Netherlands, 2009.
41. Ran, J.; Nedovic-Budic, Z. Integrating spatial planning and flood risk management: A new conceptual framework for the spatially integrated policy infrastructure. *Comput. Environ. Urban Syst.* **2016**, *57*, 68–79. [CrossRef]
42. Gralepois, M. What Can We Learn from Planning Instruments in Flood Prevention? Comparative Illustration to Highlight the Challenges of Governance in Europe. *Water* **2020**, *12*, 1841. [CrossRef]
43. Sapountzaki, K.; Wanczura, S.; Casertano, G.; Greiving, S.; Xanthopoulos, G.; Ferrara, F.F. Disconnected policies and actors and the missing role of spatial throughout the risk management cycle. *Nat. Hazards* **2011**, *59*, 1445–1474. [CrossRef]
44. Biernacki, W.; Bokwa, A.; Dziadek, J.; Padło, T. *Społeczności Lokalne Wobec Zagrożeń Przyrodniczych i Klęsk Żywiołowych*; Wyd. UJ: Kraków, Poland, 2009.
45. Śleszyński, P.; Kowalewski, A.; Markowski, T.; Kobus-Legutko, P.; Nowak, M. The Contemporary Economic Costs of Spatial Chaos: Evidence from Poland. *Land* **2020**, *9*, 214. [CrossRef]
46. Uziak, S.; Turski, R. (Eds.) *Środowisko Przyrodnicze Lubelszczyzny*; Lubelskie Towarzystwo Naukowe: Lublin, Poland, 2009.
47. Bański, J. *Rozwój Obszarów Wiejskich*; PWE: Warszawa, Poland, 2017.
48. Zgłobicki, W.; Karczmarczuk, K.; Baran-Zgłobicka, B. Intensity and Driving Forces of Land Abandonment in Eastern Poland. *Appl. Sci.* **2020**, *10*, 3500.
49. Ustawa z dnia 18 kwietnia 2002 r. o stanie klęski żywiołowej. Dziennik Ustaw 62/2002 poz. 558 (tekst jednolity Dz. U. 2017 poz. 1897). Issued by Prime Minister of Republic of Poland. 2002. Available online: http://isap.sejm.gov.pl/isap.nsf/DocDetails.xsp?id=wdu20020620558 (accessed on 20 December 2020).
50. Ustawa z dnia 8 marca 1990 r. o samorządzie gminnym. Dziennik Ustaw 16/1999 poz. 95 (tekst jednolity Dz. U. 2020, poz. 713). Issued by Prime Minister of Republic of Poland. 1990. Available online: https://isap.sejm.gov.pl/isap.nsf/DocDetails.xsp?id=WDU19900160095 (accessed on 20 December 2020).
51. Ustawa z dnia 26 kwietnia 2007 r. o zarządzaniu kryzysowym. Dziennik Ustaw 89/2007 poz. 590 (tekst jednolity Dz. U. 2020 poz. 1856). Issued by Prime Minister of Republic of Poland. 2007. Available online: https://isap.sejm.gov.pl/isap.nsf/DocDetails.xsp?id=WDU20070890590 (accessed on 20 December 2020).
52. Poskrobko, B.; Poskrobko, T. *Zarządzanie Środowiskiem w Polsce*; PWE: Warszawa, Poland, 2012.
53. Wróblewski, D. (Ed.) *Zagadnienia Ogólne z Zakresu Zarządzania Ryzykiem i Zarządzania Kryzysowego*; Analiza wybranych przepisów; Wyd. CNBOP-PIB: Józefów, Poland, 2014.
54. Wróblewski, D. (Ed.) *Zarządzanie Ryzykiem. Przegląd Wybranych Metodyk*; Wyd. CNBOP-PIB: Józefów, Poland, 2018.
55. Ustawa z dnia 27 Marca 2003 r. o Planowaniu i Zagospodarowaniu Przestrzennym; Dziennik Ustaw 84/2001 poz. (tekst jednolity Dz. U. 2020 poz. 293). Issued by Prime Minister of Republic of Poland. 2003. Available online: https://isap.sejm.gov.pl/isap.nsf/DocDetails.xsp?id=WDU20030800717 (accessed on 20 December 2020).
56. Nowak, M.J. *Decyzje o Warunkach Zabudowy i Zagospodarowania Terenu w Gospodarowaniu i Zarządzaniu Przestrzenią*; CeDeWu: Warszawa, Poland, 2012.
57. Nowak, M.J. *Planowanie i Zagospodarowanie Przestrzenne: Komentarz Do Ustawy i Przepisów Powiązanych*; Wydawnictwo C.H. Beck: Warszawa, Poland, 2019.

58. Dyrektywa 2007/60/WE Parlamentu Europejskiego i Rady z dnia 23 października 2007 r. w sprawie oceny ryzyka powodziowego i zarządzania nim. Publisher: Dziennik Urzędowy Unii Europejskiej, L. 228 z 06.11.2007 r. Available online: https://eur-lex.europa.eu/legal-content/PL/TXT/PDF/?uri=OJ:L:2007:288:FULL&from=FI (accessed on 20 December 2020).
59. Ustawa z dnia 17 lipca 2017 r. Prawo wodne. Dziennik Ustaw 2017 poz. 1566 (tekst jednolity Dz. U. 2020 poz. 310). Issued by Prime Minister of Republic of Poland. 2017. Available online: https://isap.sejm.gov.pl/isap.nsf/DocDetails.xsp?id=WDU20170001566 (accessed on 20 December 2020).
60. Głosińska, E. Spatial planning in floodplains for implementation by the floods directive in Poland. *Geogr. Pol.* **2014**, *87*, 127–142. [CrossRef]
61. Dutkowiak, I. *Prawo Wodne w Procesie Inwestycyjnym*; Presscom: Wrocław, Poland, 2018.
62. Rakoczy, B. *Prawo Wodne. Praktyczny Przewodnik*; Wolters Kluwer: Warszawa, Poland, 2018.
63. IT System for the Protection of the Country against Extreme Hazards. Available online: https://wody.isok.gov.pl/imap_kzgw/?gpmap=gpMZP (accessed on 20 December 2020).
64. Ustawa z dnia 18 lipca 2001 r. Prawo wodne. Dziennik Ustaww 115/2001 poz. 1229 (Dz. 2015 poz. 2295, tekst jednolity 2017 poz. 1121). Issued by Prime Minister of the Republic of Poland. 2001. Available online: https://isap.sejm.gov.pl/isap.nsf/DocDetails.xsp?id=WDU20011151229 (accessed on 20 December 2020).
65. Boardman, J.; Vandaele, K.; Evans, R.; Foster, I.D.L. Off-site impacts of soil erosion and runoff: Why connectivity is more important than erosion rates. *Soil Use Manag.* **2019**, *35*, 245–256. [CrossRef]
66. USGS Earth Explorer. Available online: https://earthexplorer.usgs.gov/ (accessed on 20 December 2020).
67. GUGiK. Available online: http://www.gugik.gov.pl/pzgik (accessed on 20 December 2020).
68. Copernicus Land Monitoring Service. Available online: https://land.copernicus.eu/pan-european/corine-land-cover/clc2018 (accessed on 12 December 2020).
69. OpenStreetMap. Available online: https://www.openstreetmap.org/ (accessed on 20 December 2020).
70. Meng, M.; Dabrowski, M.; Stead, D. Enhancing Flood Resilience and Climate Adaptation: The State of the Art and New Directions for Spatial Planning. *Sustainability* **2020**, *12*, 7864. [CrossRef]
71. Neuvel, J.M.M.; Van Den Brink, A. Flood risk management in Dutch local spatial planning practices. *J. Environ. Plan. Manag.* **2009**, *52*, 865–880. [CrossRef]
72. Kron, W. Flood Risk = Hazard. Values. Vulnerability. *Water Int.* **2005**, *30*, 58–68. [CrossRef]
73. Martins, B.; Nunes, A.; Lourenço, L.; Velez-Castro, F. Flash Flood Risk Perception by the Population of Mindelo, S. Vicente (Cape Verde). *Water* **2019**, *11*, 1895. [CrossRef]
74. Konieczny, R.; Siudak, M.; Bogdańska-Warmuz, M.; Madej, P.; Walczykiewicz, T. Opracowanie systemu zapobiegania i sposoby ograniczenia skutków powodzi oraz zasad funkcjonowania systemu ostrzeżeń. In *Wpływ Zmian Klimatu na Środowisko, Gospodarkę i Społeczeństwo. Tom 3, Klęski Żywiołowe a Bezpieczeństwo Wewnętrzne Kraju*; Lorenc, W.H., Ed.; Wydawnictwo IMGW-PIB: Warszawa, Poland, 2012; pp. 281–303.
75. Acosta-Coll, M.; Ballester-Merelo, F.; Martinez-Peiró, M.; De la Hoz-Franco, E. Real-Time Early Warning System Design for Pluvial Flash Floods—A Review. *Sensors* **2018**, *18*, 2255. [CrossRef]

resources

MDPI

Article

A Short-Time Repeat TLS Survey to Estimate Rates of Glacier Retreat and Patterns of Forefield Development (Case Study: Scottbreen, SW Svalbard)

Waldemar Kociuba *, Grzegorz Gajek and Łukasz Franczak

Institute of Earth and Environmental Sciences, Faculty of Earth Sciences and Spatial Management, Maria Curie-Sklodowska University in Lublin, al. Krasnicka 2 D, 20-718 Lublin, Poland; gajcy@umcs.pl (G.G.); lukasz.franczak@umcs.pl (Ł.F.)

* Correspondence: waldemar.kociuba@umcs.pl

Abstract: The study presents findings from comparative analyses of high-resolution differential digital elevation models (DEM of Difference—DoD) based on terrestrial laser scanning (TLS) surveys. The research was conducted on the 0.2 km^2 Scottbreen valley glacier foreland located in the north-western part of Wedel-Jarlsberg Land (Svalbard) in August of 2013. The comparison between DTMs at 3-week intervals made it possible to identify erosion and depositional areas, as well as the volume of the melting glacier's terminus. It showed a considerable recession rate of the Scottbreen (20 m $year^{-1}$) while its forefield was being reshaped by the proglacial Scott River. A study area of 205,389 m^2, 31% of which is occupied by the glacier (clear ice zone), was included in the repeated TLS survey, which was performed from five permanent scan station points (registered on the basis of five target points—TP). The resultant point clouds with a density ranging from 91 to 336 pt m^{-2} were converted into DEMs (at a spacing of 0.1 m). They were then put together to identify erosion and depositional areas using Geomorphic Change Detection Software (GCD). During the 3-week interval, the retreat of the glacier's snout ranged from 3 to 9 m (mean of 5 m), which was accompanied by an average lowering of the surface by up to 0.86 m (±0.03 m) and a decrease of ice volume by 53,475 m^3 (±1761 m^3). The deglaciated area increased by 4549 m^2 (~5%) as a result of the recession, which resulted in an extensive reshaping of the recently deglaciated area. The DEM of Difference (DoD) analyses showed the following: (i) lowering of the glacial surface by melting and ii) predominance of deposition in the glacier's marginal zone. In fact, 17,570 m^3 (±1172 m^3) of sediments were deposited in the glacier forefield (41,451 m^2). Also, the erosion of sediment layers having a volume of 11,974 m^3 (±1313 m^3) covered an area equal to 46,429 m^2 (53%). This occurrence was primarily based on the washing away of banks and the deepening of proglacial stream beds, as well as the washing away of the lower parts of moraine hillocks and outwash fans.

Keywords: repeated TLS surveys; DEM of Difference (DoD), sediment budgeting; glacial and postglacial surface features; Svalbard

Citation: Kociuba, W.; Gajek, G.; Franczak, Ł. A Short-Time Repeat TLS Survey to Estimate Rates of Glacier Retreat and Patterns of Forefield Development (Case Study: Scottbreen, SW Svalbard). *Resources* **2021**, *10*, 2. https://doi.org/10.3390/resources10010002

Received: 23 October 2020
Accepted: 22 December 2020
Published: 25 December 2020

1. Introduction

Over the past few decades, it has been observed that changes to the environment of High-Arctic regions result in a negative glacier mass balance, which leads to an increased recession [1–8]. Glacier surface changes that have been recorded since the end of the Little Ice Age (LIA), which affect the development of the glacier's forelands in this part of the Arctic, have been mostly measured by glaciological methods [4,5,9–11]. However, geodetic methods and non-invasive remote sensing methods have been used more and more often in recent decades [12–16].

Seasonal measurements along the set of longitudinal or/and cross profiles have been employed to measure glacier surface elevation changes and its retreat rates. This simple and popular method makes use of ablation stakes, which are anchored to the glacier, and

allows for monitoring the rising or lowering of the ice surface along the set transects. Additionally, the precise establishment of the stakes' transect position by means of the real time kinematic Global Navigation Satellite Systems (rtk-GNSS) facilitates specifying the horizontal component of the glacier's movement. It also makes it easier to monitor changes to the reach of the glacier terminus at the point where visible contact is made between ice and initial sediment-landform assemblages e.g., [4,17–19]. However, using this method to assess changes to Scottbreen's volume only generates very approximate numerical values, a relatively small amount of data (number of point measurements), and results that are exclusively limited to selected measurement cross-sections [19]. Moreover, the said method fails to provide information about the possibility of surface changes in the entire glacier area. Typically, findings obtained by this method present only the horizontal component of changes in the terminus position, and that simply gives a very general idea about the movement of the glacier surface, the velocity of which is estimated to be approx. 1 m year^{-1}. This is the case because of the method's relatively low accuracy (0.05–0.1 m) as well as a considerable bias error that is connected with the measuring stake's deviation in the measurement process [20].

Employing remote sensing tools leads to considerably greater possibilities. Tele-detection methods, which include satellite radar and photogrammetry measurement [12,21,22], are most often used in assessing recent transformations of the glacier land system. These methods provide the means to assess changes in the geometry (width, length, surface, and height) of the surface [23], as well as the volume [12]. However, such methods are mostly used for measuring ice caps and large valley glaciers [15] due to the low resolution of available data.

Furthermore, methods based on data obtained from low- and medium-altitude flights are equally popular. A photogrammetric analysis of stereo-pairs of an air photo was used to assess frontal position changes e.g., [5,23–25]. Also, ground-based photogrammetry was used to measure the ice cliff's position [26–28]. Moreover, on the basis of terrestrial photogrammetry in the 1980s, a hypsometric map of the Scottbreen tongue and foreland was made and used as a background for thematic maps [29]. At present, particularly in research on small valley glaciers or their parts, small autonomous Unmanned Aerial Vehicle Systems (UAS/UAVS) equipped with digital cameras [30] are utilised more and more often, along with Structure from Motion (SfM)—a terrestrial photogrammetric range imaging technique—which is employed in estimating three-dimensional structures from two-dimensional image sequences at a small-scale [31–33].

Light detection and ranging LiDAR have become the more frequently used methods among the group of remote sensing techniques. Airborne laser scanning (ALS), which is based on the data obtained from medium-altitude flights, provides data of considerably higher resolution than satellite data (up to several pt m^{-2}) [34–37]. ALS-based DEMs feature spacing that ranges from a few decimetres to a metre and it facilitates comparative analyses of medium- and small-size glaciers. Nonetheless, due to infrequent flights, this method fails to provide the possibility of assessing changes occurring at short temporal intervals, which might be caused by phenomena such as extreme weather. Intensive precipitation or a considerable increase in temperature (or both of these phenomena coinciding) may trigger a thaw of the snow cover in the central and upper part of the glacier, which could in turn cause an intensive surface runoff. Should such flows have large energies, both the glacier's tongue and the whole marginal zone may be remodelled. In such cases, Terrestrial Laser Scanning (TLS) guarantees a good measurement efficacy [38,39]. This ground-based, active imaging method yields rapidly acquired, accurate, dense 3D point clouds of surfaces by high-precision laser rangefinder. Employing repeated stationary multi-station surveys facilitates both measurements of geometric parameters and an advanced interpretation of the development of landforms [40–45].

The aim of this paper is the estimation of short time changes within the scope of the terminus and the forefield of the Scottbreen using TLS-based high-resolution surveys. This technique provides data on the topographic surface with an average density reaching over

1000 pt m^{-2}, while the DEM of difference analysis allows assessing of surface changes and sediment budgeting of the valley glacier as well as the inner marginal zone, which has been newly unveiled as a result of the glacier's intensive recession e.g., [46–49].

2. Study Area

The research into changes to the glacier terminus zone was performed in the catchment area of the valley glacier located in the NW of Wedel-Jarlsberg Land in the Bellsund region of Spitsbergen (Figure 1A). The glacial catchment of the Scottbreen covers an area of 10.1 km^2 (Figure 1B). The catchment is 40% covered by the valley glacier. At present, the Scottbreen is in the phase of intensive recession, it is 3.1 km in length, and its width ranges from 1.1 to 1.8 km (Figure 1C, Table 1). The Scottbreen shares its firn field with Blomlibreen (Figure 1B). In 2013, the glacier's highest areas peaked at 502 m a.s.l., whereas its concave terminus fell between 85–89 m a.s.l. This is reflected in the longitudinal profile (Figure 1C). The equilibrium-line altitude (ELA) for the glaciers of Spitsbergen's west coast was estimated by Hagen et al. [50] at approximately 400 m a.s.l. The equilibrium line, according to field observations made in the ablation season of 2013, was situated at a height of approximately 530 m a.s.l. In light of georadar profiling done in the spring of 2009, the Scottbreen was confirmed to be a typical polythermal, subpolar glacier of high geographic latitude [51] with its terminus frozen to the bed. The layer of cold ice at a thickness of approximately 75 metres stretches along the longitudinal profile of the radar scan (up to 470 m a.s.l.) (unpublished). The relief of the upper section of the valley shows two different parts, which are clearly recognizable and can be distinguished as: (1) the upper part covering the mountain valley glacier and (2) the recently-deglaciated inner marginal part (an area limited by the terminal moraine rampart) with a system of distribution channels within the outwash plain, which is separated from the east by the terminal moraine ridge [52,53] (Figure 1B). An englacial and subglacial drainage was concentrated in the main outflow located in the southern part of the glacier terminus. It is here that the Scott River begins with a glacial regime as follows: glacial feed (90%), snow melting (4%), precipitation (4%), and permafrost feed (2%), which drains the non-frozen part of the basin [54].

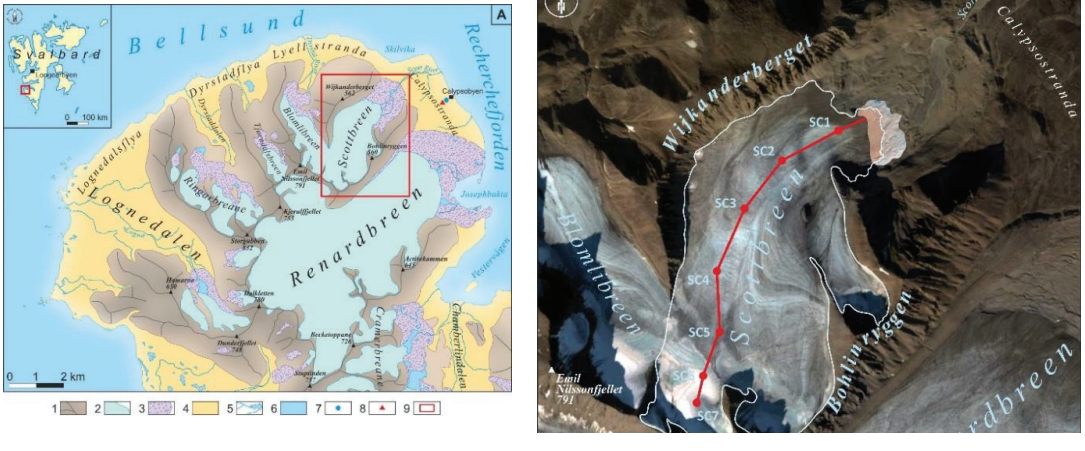

Figure 1. *Cont.*

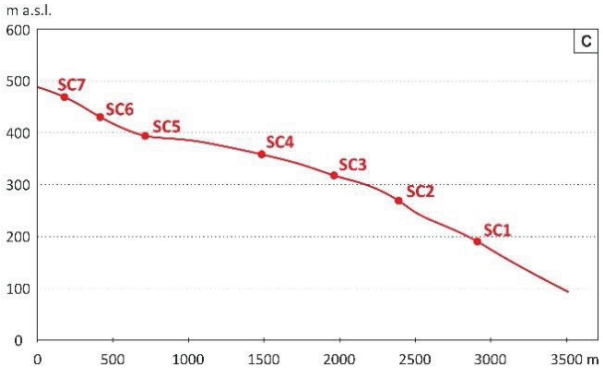

Figure 1. (**A**) Location of the research area in Spitsbergen: (1) ridges and slopes; (2) glaciers; (3) glacier forefield; (4) marine terraces; (5) rivers and lakes; (6) sea; (7) Calypsobyen Meteorological Station; (8) rtkGNSS base station; (9) study area. (**B**) Aerial photo with study area of the Scottbreen forefield: (1) Scottbreen outline on 7 August 2013; (2) study area; (3) longitudinal profile line with a set of the ablation stakes. Source of the aerial photo: Google Earth Pro; the stage on 17 August 2013. (**C**) Scottbreen's longitudinal profile with a set of the ablation stakes.

Table 1. Main features of Scottbreen.

Morphometric		Mass Balance and Geometric Changes	
glacier basin area (km^2)	ca. 6	mass balance (w.e.)	−0.81 (1990–2012)
glacier area (km^2)	4.4 (2012)	avg. terminus position change (m year^{-1})	−15 (1895–2012)
length (m)	3100 (2013)	observed surges (year)	ca. 1880
width (m)	1100–1800	area changes (km^2)	−1.52 (1895–2012)
max. elevation (m a.s.l.)	502	average thickness changes (m year^{-1})	−57 (1936–2005)
		ablation area (>350 m a.s.l.)	−58 (2005–2012)
min. elevation (m a.s.l.)	85 (2013)	average thickness changes (m year^{-1})	0 (1936–1990)
		accumulation area (>350 m a.s.l.)	−0.62 (1990–2019)
accumulation area (km^2)	1.6	flow velocity (m year^{-1})	ca. 1
ELA (m a.s.l.)	400 (2003) 530 (2013)		
aspect	N (accumulation area) NE (tongue)	**Glacier type**	
max. thickness (m)	ca. 160	drainage	supraglacial, inglacial, subglacial
volume (km^3)	ca. 0.301 (2009) [55]	thermal regime	polythermal
avg. slope (°)	ca. 5	morphologic	valley, subpolar high latitudes, ground based

The study was performed in an area spanning 205,389 m^2, within the actively transforming glacier terminus's deglaciation zone (31% of the analysed area) and its forefield (69%) (Figure 1B).

Geomorphology

Glacier zone (clear ice zone). The analysed area covers the front of the glacier (100 m to 200 m in width) with an area of 62,558 m^2 (1.6% of the whole glacier area). The constantly tilted glacier zone has an average slope of 10° (Figure 1C) and is deeply cut through by subglacial outflow channels (winding, meandering development patterns, 100 to 160 m in length). Depositional landforms are represented by numerous polygenetic ridges of glacial sediments, which originate from complicated glacitectonic processes within the area of the cold-based glacier terminus. The inventory of the forms within the terminus area includes

concentrations of cryoconite holes, which remain on the ice surface as small cones after the snow cover has melted.

Glacier forefield. The marginal zone of the Scottbreen features a number of polygenetic landforms (terminal and lateral moraines, ground and fluted moraine, rôche moutonnée covered with a thin layer of the ground moraine), fluvioglacial (inner marginal outwash plain, eskers, kame terraces) and periglacial (as solifluction covers). This part of the glacier base is characterised by the greatest dynamics in morphogenetic processes due to the rate of the glacier's recession [52]. Between 2012 and 2013, this resulted in the annual merging of the uncovered, 10 to 20 metres wide area [53], which was being intensively reshaped by fluvioglacial processes, with the non-glaciated part of the catchment (Figure 2).

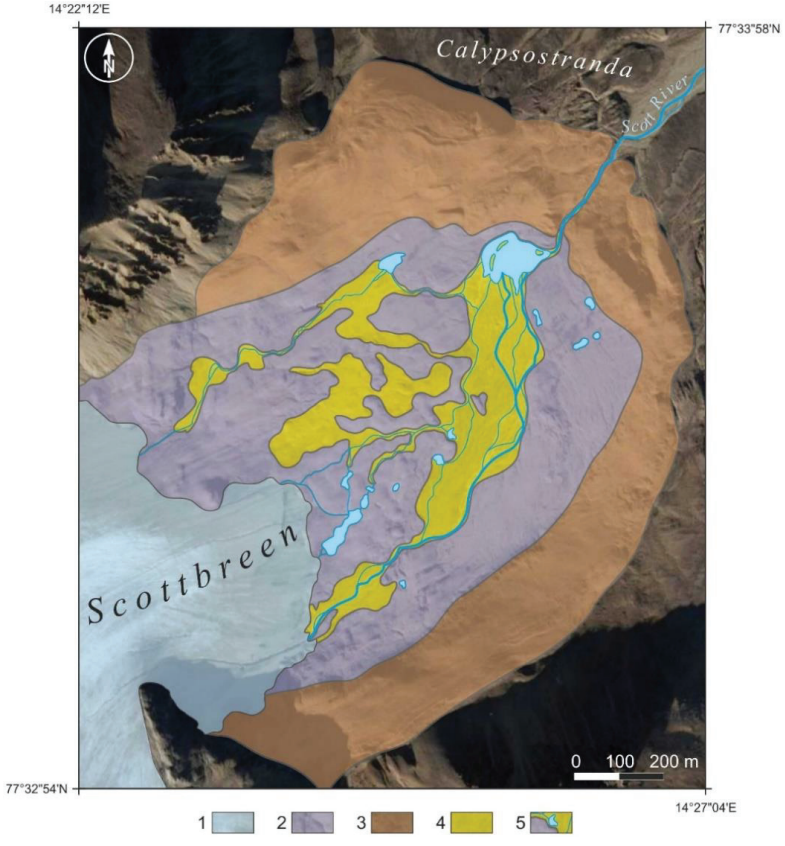

Figure 2. A geomorphic sketch of the actively transforming glacier's forefield zone: (1) clear ice zone (photo date: 17 August 2013); (2) ground moraine; (3) terminal- and lateral-moraine; (4) outwash plain; (5) rivers and lakes. Source of the aerial photo: Google Earth Pro.

A constant build-up of the inner marginal outwash plain, which has been observed since the 1930s to have a 20-m annual recession, has caused the present glacier terminus to be separated from the terminal moraine ridge by approximately 700 m (Figure 2). This area is characterised by modern geomorphic processes transforming glacigenic landforms left after the glacier had receded (a particularly well-developed ground moraine with the forms of subglacial transportation: e.g., fluted moraine, supraglacial debris stripes emerging from longitudinal foliation and the ablation moraine) as well as fluvioglacial (outwash plains, kame terraces, eskers, subglacial glaciofluvial channel filling, kettle holes etc. (Figure 2)).

The area is being intensively reshaped as a result of the action of proglacial waters that are distributed by a system of channels into the area of the inner marginal outwash plain [56]. The effect of the annual changes in the range of the main source of sediment is a multilayer occurrence of cones of various age levels. The youngest, which stretches at the gate outlet in the ice-moraine ridge, is shaped by the braided system, whereas older levels (located lower) are flat and diversified with paleochannels. Beds that cover the channel of the Scott River distribute large amounts of mineral material deposited in the form of oblong intra-bed screes [57,58].

3. Methods

3.1. Data Acquisition. TLS and rtkGPS Surveys

The analyses of short-term changes of physical/geometric parameters within the glacier terminus and its marginal zone, including the assessment of the changes to the ice budget and sediments, were performed using Terrestrial Laser Scanning (TLS) technology. Comparative field research was done by means of the Leica ScanStation C10 mid-range laser scanner at 3-week intervals between July and August of 2013 (i.e., in the period of the Scottbreen's greatest ablation activity). This device facilitates stationary laser measurement of 3D positioning with a maximum speed of 50,000 points per second [pt s^{-1}] and within a maximum range of 300 m [59]; it also uses a green impulse laser (with the wave length of 532 mm), which can penetrate small depths of water [60]. Furthermore, measurement data obtained in the form of a single 'point cloud' makes up a 'model space' that is characterised by 3D position accuracy of up to 6 mm at distances up to 100 m [59]. In the course of the research, the measurement was made using pre-set spacings of 'middle resolution' (0.1/0.1m at 100 m), which mapped the measured area with approximately 5 million points [M pt] (from each of the measurement sites). The average density of the points for the 'model space' reached 360 points per square metre [pt m^{-2}]. Both measurement campaigns employed the known coordinates (KC) method described by Kociuba [53,58], where each measurement is taken from a known coordinate point and the scanner's rangefinder is oriented towards one of the target points (belonging to a network of fixed coordinates). The analysed area was scanned from five measurement stands positioned on stable roche moutonnée culminations so as to obtain full information concerning the topographic area. The network of measurement points was marked permanently by means of seven ablation stakes (Figure 1C) whose position was established with rtkGPS measurements (TopCon Hiper II was used in the Base/Rover system). Lastly, the points were used alternately as measurement stands and reference points for connecting individual 'model spaces' into the integrated Digital Surface Model (DSM).

3.2. DEM Parameters and Data Analysis

Using the KC method allowed passing over both the time-consuming process of transforming the system from the local to the geographic, and also the 'manual' registration process for individual 'model spaces' [61]. Predefining the scanner's position before commencing the measurements makes it possible for the obtained 'point clouds' to be georeferenced and thus automatically merged into a single 3D model during the import process of the Leica Cyclone 8.1 software (Leica Geosystems AG, Heerbrugg, Switzerland). The accuracy of the model integration was determined by the precision of rtkGPS measurements. The position was established on the basis of a signal from at least nine satellites of the Global Positioning System (GPS) and the Global Navigation Satellite System (GPS+GLONASS; both a Global Positioning System (GPS) and its Russian equivalent named Globalnaya Navigacionaya Sputnikovaya Sistema (GLONASS)) by averaging out five measurement epochs (the number of samples used for averaging out the coordinates). Also, the range of the measurement ambiguity of the predefined receiver was set so as to make sure that vertical and horizontal deviation did not exceed 0.02 m [62]. DMSs that contained from 19,308,739 M pt to 71,535,423 M pt were obtained, which corresponds to a density of 336 to 90 pt m^{-2}.

The first measurement was made on 28 July, and the next one on 18 August 2013 following a 3-day heavy rainfall, which was caused by an inflow of south-west air masses. Both DSMs were further transformed into high-resolution digital elevation models (DEMs) that made up the basis for further quantitative analyses of: (i) transformations of the topographic surface and (ii) balancing the erosion-deposition budget. The TLS points (DSMs) were imported and processed to the DEM by means of the LP360 4.4 software (GeoCue Group Inc., Huntsville, AL, USA) with a mean spacing of 0.1 m. Research into the physical parameters (differences of height and volume) and the analysis of the differences of the topographic surface were made by means of the Geomorphic Change Detection (GCD 7.4.4) plug-in version for ArcGIS 10.8 software (ESRI, Redlands, CA, USA). In order to calibrate the DoD calculation, an approach based on the spatially variable assessment of the error was applied. The DEM quality was strictly related to the quality of the survey data [63]. Since the maximum TLS survey error for each measurement (0.006 m on 50 m) was lower than the rtkGPS reference points network location error (0.02 m) (both scanner and target points), the highest value was taken as the minimum level of detection (minLoD) for both DEMs, and it was used as a uniform error to calculate the surface error of each DEM. Thus, any predicted elevation changes below 0.02 m were not included in the results of the DoD analysis. Finally, the 'propagated error' function was used to detect changes between DEMs [63,64]. Comparative studies involving the application of the DEM of Difference (DoD) method [63] were applied in calculating erosion and deposition (volume and area) e.g., [65–67].

3.3. Meteorological Measurements

Meteorological observations were made between 10 July and 18 August in the 2013 melt season. Main meteorological parameters (temperature, humidity, pressure, wind) were recorded with a 10-min sampling frequency using the Campbell measurement station located 2 m above ground level. The Calypso Meteorological Station was located on a raised sea terrace within the Calyspostranda plain (in the close neighbourhood of the abandoned Calypsobyen settlement) (Figure 1A).

3.4. Direct Glaciological Measurements

Measurements of surface ablation were made every 5 days between 13 July and 17 September of 2013. Said measurements were taken at seven points on the glacier surface (Figure 1B,C). The ablation stake's position by rtk-GNSS along with the pole's height above the glacier surface were both sampled.

4. Results

4.1. Meteorological Conditions

Temporal variations of the meteorological conditions are illustrated in Figure 3. Minimum and maximum temperature values were recorded over a period spanning the glacier's morphological changes (from 28 July to 18 August 2013) and were respectively noted as 2.7 °C (on 13 August) and 8.6 °C (on 17 August). In the same time span, a considerable increase in temperature was accompanied by above-average precipitation. The highest daily precipitation of 16.8 mm was recorded on 14 August. Total rainfall on four consecutive days between 13 and 16 August amounted to 46.9 mm, i.e., 43% of the total precipitation in the analysed summer season and 66% in the period covering measurements of the glacier's morphological changes (28 July–18 August).

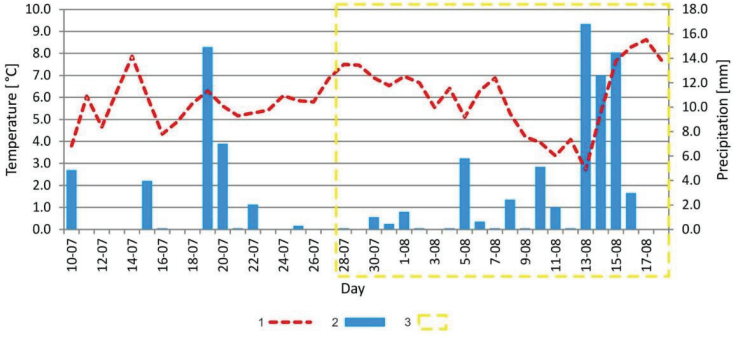

Figure 3. Comparison of changes in mean daily air temperature and mean daily precipitation during 2013 melt season: (1) average temperature, (2) daily precipitation sum, (3) analysed period.

4.2. Geomorphic Change Detection Analysis by TLS-Based DEMs

Differential analyses of DEMs show significant changes to the topographic surface both of the glacier and its forefield, which suggests there to be extensive dynamics of geomorphic processes during the measurement period. The analysed area may be considered to be comprised of three cascade-positioned zones, which differ in the type of dominating geomorphic processes, and which refer to the morphological and genetic division of the basin: (1) glacier's front zone, which undergoes intensive surface ablation; (2) recently deglaciated area, a dynamic, unstable narrow zone with intensive morphological transformations that was created in the analysed period as a result of glacier retreat; and (3) inner marginal zone, a stable zone with an equilibrium of erosional and depositional processes (Appendix A; Figure 4).

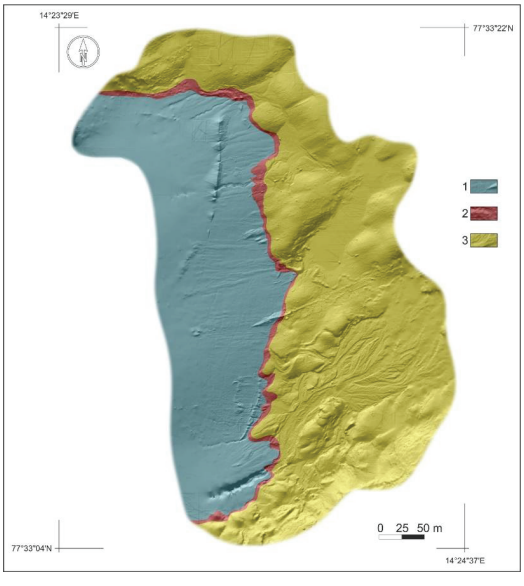

Figure 4. High-resolution hillshades model of study area from 28 July 2013. (1) clear ice zone, (2) recently-deglaciated zone, (3) glacier forefield—inner marginal area.

4.3. Morphological Changes

4.3.1. Glacier Zone (Clear Ice Zone)

Nearly all of the Scottbreen tongue's area underwent a dynamic lowering in the analysed period. Over the area ~63,000 m^2 of the glacier ice, the decrease of its surface dominated (99%). The volume of melted ice was 53,475 m^3 (±1761 m^3) in the 3-week timespan (Appendix A. The surroundings of the main meltwater channel situated in the southern section of the glacier tongue, which drains into the Scott River, were affected by the greatest changes in thickness (Table A2; Figure 5(Ba)). What is more, these changes were connected to an intensification of vertical erosion within the superglacial channel in the time of the precipitation-ablation flood. The maximum channel depth reached 4.0 m. The DoD of Scottbreen's glacial zone also shows an intensive surface ablation with a lowering in the related area of the surface. However, the observed lowering of the glacier's tongue does not show any major differentiations within the study area. Ultimately, the depth of the lowering in Scottbreen's tongue surface was on average 0.86 m (±0.03 m) and its average net thickness difference was 0.84 m (±0.02 m) (Table A2).

Only 1% of area (731 m^2) containing a positive vertical component (surface rise) was registered within the designated ablation zone (Table A2). The greatest accretion in the area was observed in the northern part of the tongue, within the debris outcrop, which stretched crosswise for approximately 120 m in relation to the movement of the glacier (Figure 5(Bb)). The greatest increase there was registered at ~1 m. Additionally, a small feature was noted in the central part of the ablation area, approximately 130 m to the west of the Scottbreen's tongue, which rose to 0.5 m in the analysed period. It may be supposed that the feature is probably an initial outcrop of the surface moraine, whose continuation could be observed in the zone at the tongue's edge. This represents an interesting effect of the transport of supraglacial morainic material along the area's longitudinal foliation.

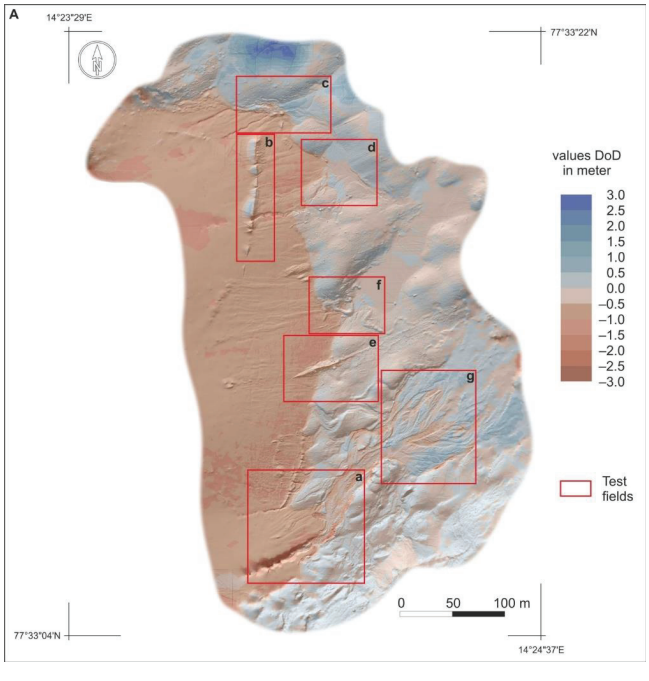

Figure 5. *Cont.*

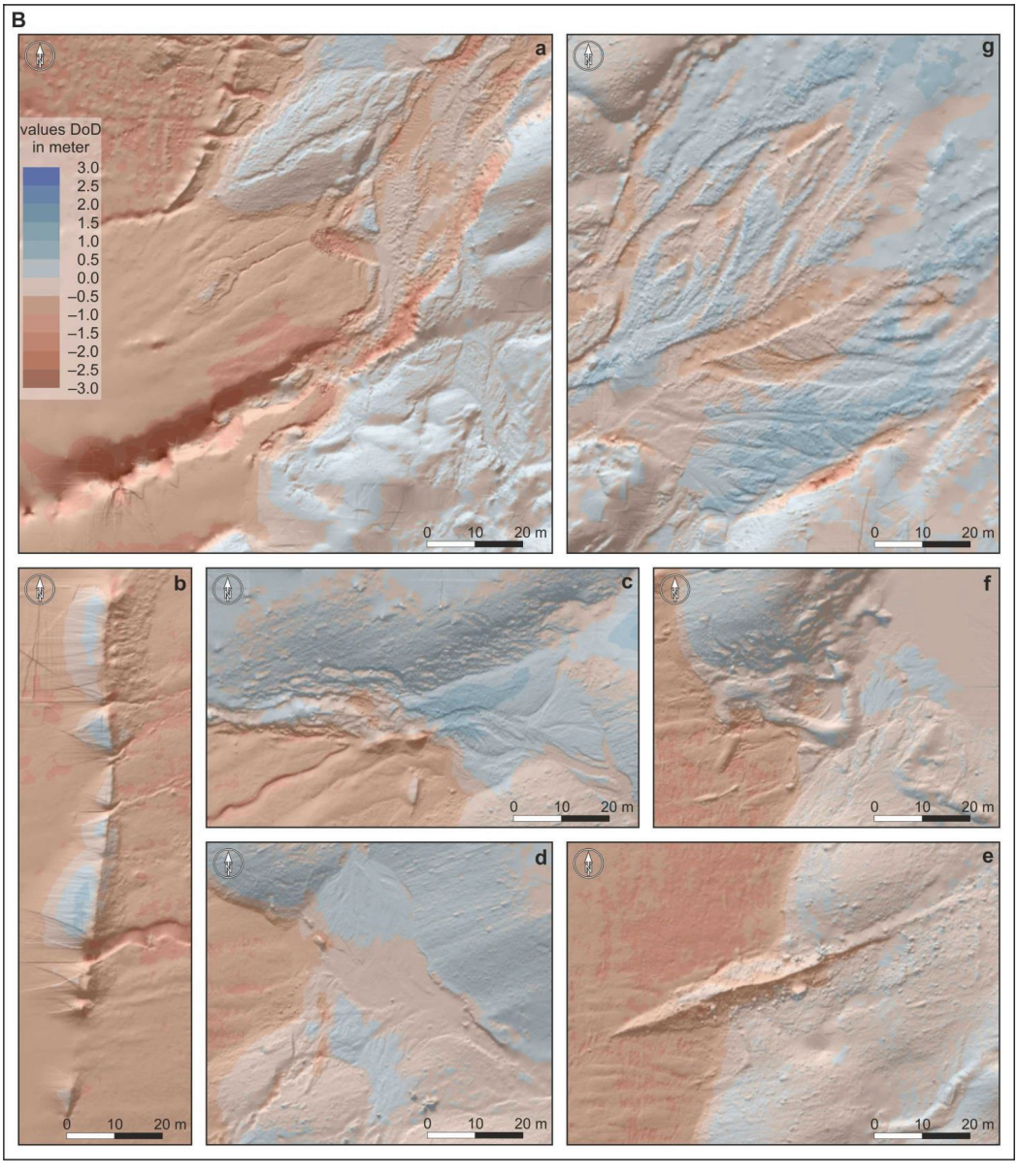

Figure 5. (**A**) DEM of Difference (DoD) for test area. Hillshades from the more recent survey in the DoD are shown behind the DoD for context. Landforms in the actively reshaped glacier terminus zone; described landforms marked by rectangles (from a to g). (**B**) Glacigenic and fluvioglacial landforms (from a to g).

4.3.2. Recently-Deglaciated Area (Zone)

In the relief of the narrow, newly uncovered area, a number of new landforms created by the glacier were mapped. Around 94% of the surface in this zone lowered by 0.58 m (±0.03 m) (as a result of melting ice, retreat of the terminus or thawing of buried ice), while

the total volume of melted ice was 2494 m^3 (±122 m^3) (Table A3). The width of the zone varies with the intensity of morphogenetic processes within the glacier's tongue (Figure 4). Due to the registered changes, the zone's width may be assessed to be approximately 10–12 m in the northern part of the research area, around 5–7 (max 12.0 m) in its middle part, and roughly 8–10 m in the southern part. The rate of the glacier's retreat, which was recorded in the TLS measurements, seems to confirm earlier information about the average annual recession rate of Scottbreen's terminus. Based on juxtaposing of the available photogrammetric material and field studies, the recession rate was noted to be 23 m per year in the 1990–2012 period. Correspondingly, Zagórski and Bartoszewski [19], Reder and Zagórski [57] and Reder [68] obtained similar research results for Scottbreen's recession rate.

The detection of changes in such a narrow zone is very difficult due to the area's intensive morphodynamics taking place over a very short time span, and the instability of the landforms in the deglaciation area caused by successively melting buried ice. In the northern part of the area, the deglaciation resulted in overbuilding the eastern zone of the one recently deglaciated, and also the simultaneous lowering of the area that directly converged with the terminus. The development of a small alluvial cone (at approximate maxima: height—1.0 m, width—20.0 m, length—10.0 m) as well as a visible increase in material fraction (clearly seen in the DSM) were the effect of an increase in both the energy and the flow of the glacier's small marginal outflow (Figure 5(Bc)). To the south of this area, intensive ablation and retreating of the glacier terminus led to an almost complete blurring of about 1.0 m of the high ridge on the surface moraine (Figure 5(Bd)). This area is characterised by the development of small fluvial channels (approximately 2.0 m in width), the washing away of the bed's surface, and, in its central zone, the simultaneous overbuilding of the alluvial fans found in the adjacent marginal zone. The next test area (Figure 5(Be)) suggests a domination of glacigenic processes, which developed the inner marginal zone. The degradation of buried ice resulted in the lowering of the surface. Forms that were consolidated by the morainic material show a variety of surface changes—a small rising or lowering (the ridge of the surface moraine along the longitudinal foliation). Subglacial accumulation esker forms (built of loose sediments, mostly sand and gravels) of several metres in length were uncovered in the middle area as a result of the glacier's front retreat (Figure 5(Bf)). These forms ranged from 4 to 5 m in width and their height did not exceed 0.5 m. The esker ridge was cut by small supraglacial currents where it came in direct contact with the glacier's terminus. Within this area, erosion processes driven by fluvioglacial processes dominate, despite noting distinct accumulation forms there. However, the greatest changes were registered in the southern part of the research area (Figure 5(Ba)). There the proglacial river bed developed laterally in a northern direction as a result of the fluvioglacial processes intensifying. Moreover, there was degradation of the surface moraine ridge, which was found to be transversing the direction of the glacier's movement. As a result, debris cones of several meters in width developed. Further, an area that exhibited features of dead ice was recorded in the southern part of the test area—it underwent a morphogenesis that differed from that of the active glacier's terminus. A recession rate similar to the one in the specified test areas was not registered within the dead ice, however, intensive lowering of the surface (1.5–2.0 m) was observed, which was accompanied by modelling of the sheet's edge by ablation waters.

4.3.3. Glacier Forefield—Inner Marginal Zone

In the analysed period, the recorded marginal zone was reshaped both by erosion and by deposition processes. The detected surface changes indicate a slight dominance of areas with surface lowering at 46,429 m^2 (62%) in relation to areas of surface rising at 41,451 m^2. This trend is reversed for volume, with deposition at 17,570 m^3 (±1172 m^3) and erosion of 11,974 m^3 (±1313 m^3). The above-mentioned were accompanied by average elevation changes ranging from +0.42 m (±0.03 m) to −0.21 m (±0.02 m), respectively (Table A4). The erosion mostly covered the concentration zone of the glacier waters' main

draining system in the research area's southern part, which contains a system of beds distributing proglacial outflow to the NE. The northward shift of the main outflow zone was accompanied by the development of small alluvial fans, a mid-channel, and lateral bars in the abandoned channels as well as in the central and southern part of the valley floor. (Figure 5(Ba,Bg)). Moreover, intensified side erosion was created as a result of the Scott River's multi-current proglacial braided patterns towards the north. These processes resulted in an intensive undercutting of the southern edges of the ground moraine's middle sheet. The deposition of sediment with its thickness of 0.3 m caused the overbuilding of the glacigenic landform complex—an ice-moraine ridge and a lateral moraine separated by fluvioglacial landforms i.e., a sandur cone with two outwash hollows. The eastern part of the main zone, which drained the glacier, and the NW part of the cone, which contained the outwash hollows, were both overbuilt. Small changes took place within the culmination of moraine hillocks in the N and SE parts of the cone (Figure 5(Ba,Bg)). Nearly the whole area, which was predominated by forms both of the bed and the lateral moraine, was reshaped by mass processes characteristic of the periglacial environment.

5. Discussion

The inner marginal outwash fan, which is separated by terminal moraine ridges, makes up an interesting research object for studies on contemporary morphogenesis as well as activities of glacial and fluvioglacial processes. However, research work in this zone typically concerns the recession/advance rates of the glacier terminus e.g., [11,52,57], but it seldom refers to the quantitative assessment of the effects of glacial retreat e.g., [35,47,48,69,70]. Research findings to date have suggested that the present direction of geomorphic changes in the glacial forefield zone of the High Arctic results from the following factors: (i) global (climate-driving factors), (ii) regional (geographic latitude, location with respect to land areas and seas, exposure to predominant winds), and foremost, (iii) local (structural conditions, lithology of sediments, genesis, the glacier's type and thickness, exposition and tilting of the firn zone, and the glacier's trough). These factors are decisive in the development and the functioning of temporal or periodical sediment deposition zones, which occur in front of the quickly retreating glacier terminus. The growth rate of glacier-uncovered surfaces significantly affects the contemporary dynamics of the geomorphic processes in the entire inner marginal zone [44].

This study shows short-term erosion and deposition distributions for each analysed area. In the clean ice zone, surface lowering is dominant (99%) due to rapid ice melting. In the 3-week period, the average lowering of the glacier terminus surface was recorded to be 0.84 m (0.04 m per day). By contrast, this is much higher than the average (2.2 m per year; 0.13 m per 3-week period; and 0.006 m per day, respectively), which was noted over a 3-year span between 2010 and 2013 [44]. By comparison, a slightly lower rate (0.39 m per 3-week period and 0.02 m per day, respectively) was determined for the retreat of the Sólheimajökull glacier over a period of 14 years [16]. Furthermore, surface lowering also dominates (95%) in the narrow zone of the recently-deglaciated area, which results in an average decrease of 0.54 m (3-week rate) and 0.026 m (daily rate), respectively. It is worthy to note that a slight predomination of surface rising (53%) was only recorded in the glacier's forefield zone. This slight advantage of deposition equates to an average increase of 0.064 m over the 3-week period (0.004 m per day). In the above-mentioned 3-year span, some much lower average rates had been determined for Scottbreen's near forefield (0.025 m—annual; 0.001 m—3-week; and 0.0001 m—daily, respectively), whereas these rates were comparatively two-times higher for its intramarginal outwash fan (0.059 m; 0.003 m and 0.0002 m, respectively) [44]. However, this zone was observed to have different trends in its various cold regions. Similar average values but of surface lowering (−0.05 m—annual; 0.003 m—3-week; and 0.0001 m—daily, respectively) were determined for the Midtre Lovénbreenand (NW Svalbard) forefield over a 2-year period, and these were based on comparisons between LiDAR-derived DEMs/DoD. In reference to those values, average surface lowering was even higher (0.7 m per year; 0.04 m per 3-week

period; and 0.002 m per day, respectively) for the moraine downwasting [37]. Quantitative analyses (Tables A1–A4) show a dominance of surface lowering in the clear ice zone (ice-melting) and in the recently deglaciated zone (erosion). In the inner marginal zone, where there is a considerable balance of surface elevation changes, erosion is roughly equal to deposition. It is also where periodic sediment deposition is generally separated from the lower parts of the valleys by the terminal and lateral moraine rampart. The river valley that cuts this rampart crosswise performs a transit role in this system, however, it traps the coarsest fractions of the sediments [71]. Dislodged pebbles and boulders feed the sediment load of the river but are transported over small distances only, which causes aggradation to predominate on the bottoms of proglacial rivers [44]. This study shows that an intensive deglaciation was accompanied by considerable changes in the morphology of the uncovered ice areas [72], which resulted in erosion (most often) as well as deposition (less frequently), within the landforms that had already existed and the newly created landforms—often very ephemeral. The area's overbuilding, which was recorded in the ablation zone (in the northern part of the terminus) at the outlet of the debris, refers to zones of thrust faults. The fault zones create a discontinuity along which some debris is transported to the glacier surface. However, an increase within the area of the analysed scree crest is not connected to increased sediment transport from the glacier's bedrock, but is rather caused by the fact that ice, which is devoid of its rock cover, undergoes an intensive ablation. Such a mechanism of sediment transmission and formation of crosswise ridges in the surface moraine, which has been widely described in literature e.g., [73,74], is characteristic of polythermal glaciers with a base of frozen terminus. The analysed landform is ephemeral and its functioning time depends on the permanence of an ice core covered with supraglacial debris. An analogous form at a later developmental stage was recorded in the southern part of the terminus. Only a small-area, maximally 0.5 m high elevation took place within the area of the ridge whose length is approximately 80 m. This is connected to the fact that the form situated closer to the edge of the terminus underwent intensive washing away processes.

Meteorological observations recorded throughout the summer melting period together with ablation measurements at the Scottbreen show an asynchronism between precipitation as well as ablation volumes within the glacier's area and the 'morphological effect' in the newly uncovered areas. A precipitation episode, which had been noted at the beginning of the observation period (approximately 35% of the volume of recorded precipitation), resulted in a small area lowering (0.2 m) in a part of the Scottbreen's terminus. Between 7–18 August 2013, the glacier surface at stake SC1 (Figure 1B) decreased by 29 cm and at stake SC2 by 33 cm. That same year in the period from 13 July to 18 August, before the rainfall episode, SC1 showed that the surface decreased at a fairly constant pace, which averaged a max of 20.3 cm. In the same period of time, SC2 (Figure 1B) showed that the mean value of the glacier surface descent was 18.8 cm. The causes of such a state might be found in an increased capacity to retain precipitation waters in the Scottbreen's accumulation zone and water percolation in empty areas of the snow, firn, and ice [75–78]. Percolation is a slow process that efficiently stopped the surface flow of ablation-precipitation waters down the glacier's surface. The rainfall episode (from 13 to 16 August) contributed to an increased surface ablation of the glacier, in particular in its terminus part (registered area lowering at SC1—0.75 m (Figure 1B,C), and by comparison of the average area lowering at DoD—1.1–1.5 m). In fact, such an extensive area lowering was caused not only by record precipitation together with a considerable increase in the average air temperature, but it is also influenced by the release of water retained in snow and firn that were stored in higher glacial zones. This was accompanied by a simultaneous intensive flow down the glacier's surface area within the ablation zone.

The methodology of comparative studies showed considerable development of glacial and proglacial landforms located in the glacier's recently deglaciated and inner marginal areas, which resulted from above-average weather conditions. The effects of the 3-day rainfall with its volume being close to the multi-annual sum (registered in the melt period)

suggest that events of an above-average character within a very brief timescale may diametrically alter the short-term transformation trend. The glacier's ablation rate, the range of area lowering, or the changes in the volume of forefield landforms, which occur as a result of these episodic events, may equal or even exceed annual mean values that have been registered. Research to date [19,57,68] has documented the glacier's terminus retreat to be at a rate of 3 to 22 m annually (Figure 2). Moreover, Kociuba [56] estimated the annual (2010–2013) mean ice loss in this zone at 2.2 m year^{-1}, which corresponds to the water equivalent of 2.0 m^3 from each square meter. The intensive ice-melting leads to concentrated runoff of sub- as well as supraglacial waters and results in a considerable reshaping of ephemeral landforms within the newly uncovered parts of the valley. Corresponding research that was performed using the glaciological method on the intensive ablation zone of the glacier's terminus confirmed the value of the mean lowering of the glacier's surface, which was registered as per the DoD results. In the analysed period, the mean lowering registered at SC1 (Figure 1B,C), in a location approximately 70 m over the glacier's longitudinal profile, equalled 0.75 m. All these values were additionally confirmed by the juxtaposition of numerical terrain models, which had been obtained from the available photogrammetric depictions and terrain studies (by GPS of the glacier's surface) over the 1990–2012 period. In that same period, the glacier's surface in its terminus part lowered by approximately 58 m and averaged out at an annual value of 2.3 m. These values are fully compatible with the results obtained at the time of field studies in 2012. Then, during the 5 weeks of the ablation period, the glacier's area lowered by 1.2 m in its terminus zone.

6. Conclusions

- The foreland of the Scottbreen—a typical valley glacier that has undergone dynamic transformations connected with its terminus, which in turn have retreated at a rate of 22 m year^{-1}—makes up an interesting research study into the contemporary development of newly deglaciated areas. Comparative measurements in the 3-week period at the turn of July and August of 2013 introduce a new quality into spatial analyses of glacial areas. They have made it possible to perform quantitative and qualitative evaluations on the range and direction of landform development. The spatial analysis on the dynamics of geomorphic processes that shape said zone has given rise to tracing short-term landform transformations under conditions of progressive degradation of the glacial catchment's cryosphere in the sensitive High-Arctic environment.
- Three zones were distinguished with respect to the differences in the dynamics of geomorphological processes: (i) the glacier front zone, which is characterised by a glacier surface lowering rate of 2 m year^{-1}; (ii) the recently deglaciated zone with dynamic geomorphic processes, which worsens during extreme and above-average meteorological events (e.g., heavy rainfall, rapid increase in air temperature); and (iii) the inner marginal zone, which is relatively stable and characterised by an erosion/deposition balance.
- The range of transportation of supraglacial debris is limited. The majority of newly provided debris that comes from the glacier's ablation is deposited in a narrow, recently deglaciated zone (up to 12 m). Here, a predominance of aggradation was registered in the analysed 3-week period. Moreover, redeposition of sediments into the inner marginal zone is restricted by a range of hills in the terminus and lateral moraines located at the foot of the zone, which includes numerous intramoraine fluvial basins (or, less frequently, basins that are not drained by any outflow) catching the supraglacial debris. However, during the period of above-average floods, the scree deposited in the basins may be channelled to the basins' lower parts where it overbuilds the landform of the inner marginal outwash plain.
- It has been shown that in a very short timescale, rapid meteorological phenomena can result in relief changes that are diametrically different from the rates and directions of annual and perennial changes. The occurrence of events characterised as above-average, i.e., high precipitation and an increase in temperature during the 3-week

comparative period (July–August 2013), cause the glacier's area to lower by up to 3.5 m—this is nearly two times more than the annual mean (2 m year^{-1}) in the 2010–2013 period.

- The conducted analysis on the dynamics of spatial changes in the proglacial zone may contribute to a better understanding of the way modern processes shape the forefield of the glacier's terminus. Detailed comparative analyses confirmed the high precision and efficiency of high-resolution TLS-based DEM as a tool for inventorying and tracking high-dynamic development of glacial and proglacial landforms. This tool is particularly useful in analysing ephemeral landforms (from several days to several weeks long). This study's adopted methodology for performing both measurements and comparative analyses on high-resolution models of investigated areas is far more universal and effective than methods that have been traditionally used in glaciology. Consequently, the amount of data provided during a single measurement cycle and the comparability of the findings should be the basis for implementing the TLS-based DEM analysis as a standard tool in a new comprehensive approach to conducting glaciological and geomorphological research into glacier forefields.

Author Contributions: Conceptualization: W.K.; methodology, W.K., G.G. and Ł.F.; field study, high-resolution survey W.K., G.G. and Ł.F.; writing—original draft preparation, W.K., G.G. and Ł.F.; visualization, W.K., G.G. and Ł.F., writing—review and editing, W.K. and G.G.; visualization, Ł.F. All authors have read and agreed to the published version of the manuscript.

Funding: This research received no external funding.

Institutional Review Board Statement: Not applicable.

Informed Consent Statement: Not applicable.

Data Availability Statement: Data is contained within the article.

Acknowledgments: The study was carried out in the Scott River catchment in the summer season of 2013 with the participation of the University of Maria Curie-Skłodowska's Polar Expeditions Team. The study was supported by: the scientific project of the National Science Centre 2011/01/B/ST10/06996 'Mechanisms of fluvial transport and sediment supply to channels of Arctic rivers with various hydrological regimes (SW Spitsbergen)', and the statutory research of FESSM MCSU 'Application of the TLS in the geomorphological research'. The authors would like to thank the reviewers for their valuable comments which helped to make the improvements that were essential to the successful completion of this work. The authors are also grateful for the English language proofreading by Luke Boczkowski.

Conflicts of Interest: The authors declare no conflict of interest.

Appendix A

Changes in spatial parameters of the studied area calculated volumetrically with reference to the total volume of ice/material net change recorded by the DoD (both melting/erosion and deposition) from 28 July to 18 August 2013. [Table A1] The entire analysed area; [Table A2] the terminus of the Scottbreen in the range of 28 July 2013; [Table A3] the area uncovered to 18 August 2013 (recent-deglaciated area); [Table A4] the glacier forefield—inner marginal zone.

Table A1. The entire analysed area.

Attribute	Raw	Thresholded DoD Estimate:		
Areal Metrics				
Total Area of Surface Lowering (m^2)	143,326	108,948		
Total Area of Surface Raising (m^2)	62,063	42,225		
Total Area (m^2)	205,389	151,173	74%	
Total Volumetric Metrics			± Error Volume	% Error
Total Volume of Surface Lowering (m^3)	66,049	65,647	±3082	5%
Total Volume of Surface Raising (m^3)	17,945	17,741	±1194	7%
Total Volume of Difference (m^3)	83,994	83,388	±4276	5%
Total Net Volume Difference (m^3)	−48,103	−47,905	±3305	−7%
Vertical Averages:				
Average Depth of Surface Lowering (m)	0.46	0.60	±0.03	5%
Average Depth of Surface Raising (m)	0.29	0.42	±0.03	7%
Average Total Thickness of Difference (m) for Area of Interest	0.41	0.41	±0.02	5%
Average Net Thickness Difference (m) for Study Area	−0.23	−0.23	±0.02	−7%
Percentages (by volume)				
Percent Elevation Lowering	79%	79%		
Percent Surface Raising	21%	21%		
Percent Imbalance (departure from equilibrium)	−29%	−29%		

Table A2. The terminus of the Scottbreen in the range of 28 July 2013.

Attribute	Raw	Thresholded DoD Estimate:		
Areal Metrics				
Total Area of Surface Lowering (m^2)	62,558	62,250		
Total Area of Surface Raising (m^2)	911	731		
Total Area (m^2)	63,469	62,981	99%	
Total Volumetric Metrics			± Error Volume	% Error
Total Volume of Surface Lowering (m^3)	53,479	53,475	±1761	3%
Total Volume of Surface Raising (m^3)	164	162	±21	13%
Total Volume of Difference (m^3)	53,643	53,637	±1781	3%
Total Net Volume Difference (m^3)	−53,315	−53,313	±1761	−3%
Vertical Averages:				
Average Depth of Surface Lowering (m)	0.85	0.86	±0.03	5%
Average Depth of Surface Raising (m)	0.18	0.22	±0.03	7%
Average Total Thickness of Difference (m) for glacier terminus	0.85	0.85	±0.02	5%
Average Net Thickness Difference (m) for Area of Interest	−0.84	−0.84	±0.02	−7%
Percentages (by volume)				
Percent Elevation Lowering	79%	79%		
Percent Surface Raising	21%	21%		
Percent Imbalance (departure from equilibrium)	−29%	−29%		

Table A3. The area uncovered to 18 August 2013 (recent-deglaciated area)

Attribute	**Raw**	**Thresholded DoD Estimate:**		
Areal Metrics				
Total Area of Surface Lowering (m^2)	4495	4302		
Total Area of Surface Raising (m^2)	356	247		
Total Area (m^2)	4851	4549	94%	
Total Volumetric Metrics			± Error Volume	%Error
Total Volume of Surface Lowering (m^3)	2497	2494	±122	5%
Total Volume of Surface Raising (m^3)	55	54	±7	13%
Total Volume of Difference (m^3)	2552	2549	±129	5%
Total Net Volume Difference (m^3)	−2441	−2440	±122	−5%
Vertical Averages:				
Average Depth of Surface Lowering (m)	0.56	0.58	±0.03	5%
Average Depth of Surface Raising (m)	0.16	0.22	±0.03	13%
Average Total Thickness of Difference (m) for Area of Interest	0.53	0.53	±0.03	5%
Average Net Thickness Difference (m) for Recent-Deglaciated Area	−0.50	−0.50	±0.03	−5%
Percentages (by volume)				
Percent Elevation Lowering	98%	98%		
Percent Surface Raising	2%	2%		
Percent Imbalance (departure from equilibrium)	−48%	−48%		

Table A4. The glacier forefield—inner marginal zone.

Attribute	**Raw**	**Thresholded DoD Estimate:**		
Areal Metrics				
Total Area of Surface Lowering (m^2)	80,495	46,429		
Total Area of Surface Raising (m^2)	61,106	41,451		
Total Area (m^2)	141,601		62%	
Total Volumetric Metrics			± Error Volume	% Error
Total Volume of Surface Lowering (m^3)	12,372	11,974	±1313	11%
Total Volume of Surface Raising (m^3)	17,773	17,570	±1172	7%
Total Volume of Difference (m^3)	30,145	29,545	±2486	8%
Total Net Volume Difference (m^3)	5400	5596	±1760	31%
Vertical Averages:				
Average Depth of Surface Lowering (m)	0.15	0.26	±0.03	11%
Average Depth of Surface Raising (m)	0.29	0.42	±0.03	7%
Average Total Thickness of Difference (m) for Area of Interest	0.21	0.21	±0.02	8%
Average Net Thickness Difference (m) for Glacier Forefield	0.04	0.04	±0.01	31%
Percentages (by volume)				
Percent Elevation Lowering	41%	41%		
Percent Surface Raising	59%	59%		
Percent Imbalance (departure from equilibrium)	9%	9%		

References

1. Hagen, J.O.; Liestøl, O.; Roland, E.; Jørgensen, T. *Glacier Atlas of Svalbard and Jan Mayen*; Norsk Polarinstitutt Meddelelser: Oslo, Norway, 1993; p. 141.
2. Jania, J.; Hagen, J.O. *Mass Balance of Arctic Glaciers*; University of Silesia: Sosnowiec-Oslo, Poland, 1996; p. 62.
3. Hagen, J.O.; Melvold, K.; Pinglot, F.; Dowdeswell, J.A. On the net mass balance of the glaciers and ice caps in Svalbard, Norwegian. *Arct. Antarct. Alp. Res.* **2003**, *35*, 264–270. [CrossRef]
4. Hagen, J.O.M.; Eiken, T.; Kohler, J.; Melvold, K. Geometry changes on Svalbard glaciers: Mass-balance or dynamic response? *Ann. Glaciol.* **2005**, *42*, 255–261. [CrossRef]
5. Błaszczyk, M.; Jania, J.A.; Hagen, J.O. Tidewater glaciers of Svalbard: Recent changes and estimates of calving fluxes. *Polar Res.* **2009**, *30*, 85–142.
6. Zemp, M.; Hoelzle, M.; Haeberli, W. Six decades of glacier mass-balance observations: A re-view of the worldwide monitoring network. *Ann. Glaciol.* **2009**, *50*, 101–111. [CrossRef]
7. Pachauri, R.K.; Meyeer, L.A. (Eds.) IPCC Climate Change 2014: Synthesis Report. In *Contribution of Working Groups I, II and III to the Fifth Assessment Report of the Intergovernmental Panel on Climate Change*; IPCC: Geneva, Switzerland, 2014.
8. Christianson, K.; Kohler, J.; Alley, R.B.; Nuth, C.; Van Pelt, W. Dynamic perennial firn aquifer on an Arctic glacier. *Geophys. Res. Lett.* **2015**, *42*, 1418–1426. [CrossRef]
9. Nuth, C.; Schuler, T.V.; Kohler, J.; Altena, B.; Hagen, J.O. Estimating the long-term calving flux of Kronebreen, Svalbard, from geodetic elevation changes and mass-balance modeling. *J. Glaciol.* **2012**, *58*, 119–133. [CrossRef]
10. Sobota, I. Selected methods in mass balance estimation of Waldemar Glacier Spitsbergen. *Pol. Polar Res.* **2007**, *28*, 249–268.
11. Sobota, I.; Nowak, M.; Weckwerth, P. Long-term changes of glaciers in north-western Spitsbergen. *Glob. Planet. Chang.* **2016**, *144*, 182–197. [CrossRef]
12. Connor, L.N.; Laxon, S.W.; Ridout, A.L.; Krabill, W.B.; McAdoo, D.C. Comparison of Envisat radar and airborne laser altimeter measurements over Arctic sea ice. *Remote Sens. Environ.* **2009**, *113*, 563–570. [CrossRef]
13. Barnhart, T.B.; Crosby, B.T. Comparing Two Methods of Surface Change Detection on an Evolving Thermokarst Using High-Temporal-Frequency Terrestrial Laser Scanning, Selawik River, Alaska. *Remote Sens.* **2013**, *5*, 2813–2837. [CrossRef]
14. Carrivick, J.L.; Berry, K.; Geilhausen, M.; James, W.H.; Williams, C.; Brown, L.E.; Rippin, D.M.; Carver, S.J. Decadal-scale changes of the ödenwinkelkees, central Austria, suggest increasing control of topography and evolution towards steady state. *Geogr. Ann.* **2015**, *97*, 543–562. [CrossRef]
15. Papasodoro, C.; Berthier, E.; Royer, A.; Zdanowicz, C.; Langlois, A. Area, elevation and mass changes of the two southernmost ice caps of the Canadian Arctic Archipelago between 1952 and 2014. *Cryosphere* **2015**, *9*, 1535–1550. [CrossRef]
16. Staines, K.E.H.; Carrivick, J.L.; Tweed, F.S.; Evans, A.J.; Russell, A.J.; Jóhannesson, T.; Roberts, M. A multi-dimensional analysis of pro-glacial landscape change at Sólheimajökull, southern Iceland. *Earth Surf. Process. Landf.* **2014**, *40*, 809–822. [CrossRef]
17. Sobota, I.; Lankauf, K.R. Recession of Kaffiøyra Region Glaciers, Oscar II Land, Svalbard. *Bull. Geogr.* **2010**, *3*, 27–45. [CrossRef]
18. Lankauf, K.R. *The Retreat of the Glaciers in the Kaffiøyra Region (Oscar II Land-Spitsbergen) in the Twentieth Century*; Polish Academy of Science: Warsaw, Poland, 2002; p. 221.
19. Zagórski, P.; Bartoszewski, S. An Attempt at the Estimation of the Recession of the Scott Glacier (Spitsbergen) on the Basis of Archival Materials and GPS Measurements. In *Polish Polar Studies*; Styszyńska, A., Marsz, A.A., Eds.; Katedra Meteorologii i Oceanografii Nautycznej AM: Gdynia, Poland, 2004; pp. 415–423.
20. Brasington, J.; Rumsby, B.T.; McVey, R.A. Monitoring and modelling morphological change in a braided gravel-bed river using high resolution GPS-based survey. *Earth Surf. Process. Landf.* **2000**, *25*, 973–990. [CrossRef]
21. Bolch, T.; Shea, J.M.; Liu, S.; Azam, F.M.; Gao, Y.; Gruber, S.; Immerzeel, W.W.; Kulkarni, A.; Li, H.; Tahir, A.A.; et al. Status and Change of the Cryosphere in the Extended Hindu Kush Himalaya Region. In *The Hindu Kush Himalaya Assessment: Mountains, Climate Change, Sustainability and People*; Wester, P., Ed.; Springer International Publishing: Chem, Switzerland, 2019; pp. 209–255.
22. Zhang, G.; Bolch, T.; Allen, S.; Linsbauer, A.; Chen, W.; Wang, W. Glacial lake evolution and glacier–lake interactions in the Poiqu River basin, central Himalaya, 1964–2017. *J. Glaciol.* **2019**, *65*, 347–365. [CrossRef]
23. Kääb, A.; Lefauconnier, B.; Melvold, K. Flow field of Kronebreen, Svalbard, using repeated Landsat 7 and ASTER data. *Ann. Glaciol.* **2005**, *42*, 7–13. [CrossRef]
24. Dowdeswell, J.A.; Benham, T.J. A surge of Perseibreen, Svalbard, examined using aerial photography and ASTER high−Resolution satellite imagery. *Polar Res.* **2003**, *22*, 373–383. [CrossRef]
25. Luckman, A.; Benn, D.I.; Cottier, F.; Bevan, S.; Nilsen, F.; Inall, M. Calving rates at tidewater glaciers vary strongly with ocean temperature. *Nat. Commun.* **2015**, *6*, 8566. [CrossRef]
26. Vieli, A.; Jania, J.; Kolondra, L. The retreat of a tidewater glacier: Observations and model calculations on Hansbreen, Spitsbergen. *J. Glaciol.* **2002**, *48*, 592–600. [CrossRef]
27. Kolondra, L. The centenary of Hans Glacier front position change measurements (S-Spitsbergen). *Arch. Fotogram. Kartogr. Teledetekcji* **2007**, *17*, 375–384.
28. Wangensteen, B.; Eiken, T.; Ødegård, R.S.; Sollid, J.L. Measuring coastal cliff retreat in the Kongsfjorden area, Svalbard, using terrestrial photogrammetry. *Polar Res.* **2007**, *26*, 14–21. [CrossRef]

29. Szczęsny, R.; Dzierżek, J.; Harasimiuk, H.; Nitychoruk, J.; Pękala, K.; Repelewska-Pękalowa, J. *Photogeological Map of the Renardbreen, Scottbreen and Blomlibreen Forefield (Wedel Jarls-berg Land, Spitsbergen), Scale 1:10,000*; Wydawnictwa Geologiczne: Warszawa, Poland, 1989.
30. Colomina, I.; Molina, P. Unmanned aerial systems for photogrammetry and remote sensing: A review. *ISPRS J. Photogramm. Remote Sens.* **2014**, *92*, 79–97. [CrossRef]
31. Westoby, M.J.; Brasington, J.; Glasser, N.F.; Hambrey, M.J.; Reyonds, M.J. Structure from Motion photogrammetry: A low-cost, effective tool for geoscience applications. *Geomorphology* **2012**, *179*, 300–314. [CrossRef]
32. Lucieer, A.; Turner, D.; King, D.H.; Robinson, S.A. Using an Unmanned Aerial Vehicle (UAV) to capture micro-topography of Antarctic moss beds. *Int. J. Appl. Earth Obs. Geoinf.* **2014**, *27*, 53–62. [CrossRef]
33. Ryani, J.C.; Hubbard, A.L.; Box, J.; Todd, J.; Christoffersen, P.; Carr, J.R.; Holt, T.O.; Snooke, N. UAV photogrammetry and structure from motion to assess calving dynamics at Store Glacier, a large outlet draining the Greenland ice sheet. *Cryosphere* **2015**, *9*, 1–11. [CrossRef]
34. Charlton, M.E.; Large, A.R.G.; Fuller, I.C. Application of airborne LiDAR in river environments: The river Coquet, Northumberland, UK. *Earth Surf. Process. Landf.* **2003**, *28*, 299–306. [CrossRef]
35. Bamber, J.L.; Krabill, W.; Raper, V.; Dowdeswel, J.A.; Oerlemans, J. Elevation changes measured on Svalbard glaciers and ice caps from airborne LiDAR data. *Ann. Glaciol.* **2005**, *42*, 202–208. [CrossRef]
36. Arnold, N.S.; Ress, W.G.; Devereux, B.J.; Amable, G.S. Evaluating the potential of high resolution airborne LiDAR data in glaciology. *Int. J. Remote Sens.* **2006**, *27*, 1233–1251. [CrossRef]
37. Irvine-Fynn, T.D.L.; Barrand, N.; Porter, P.; Hodson, A.; Murray, T. Recent High-Arctic glacial sediment redistribution: A process perspective using airborne lidar. *Geomorphology* **2011**, *125*, 27–39. [CrossRef]
38. Heritage, G.L.; Hetherington, D. Towards a protocol for laser scanning in fluvial geomorphology. *Earth Surf. Process. Landf.* **2007**, *32*, 66–74. [CrossRef]
39. Heritage, G.L.; Milan, D.J.; Large, A.R.G.; Fuller, I.C. Influence of survey strategy and interpolation model on DEM quality. *Geomorphology* **2009**, *112*, 334–344. [CrossRef]
40. Lichti, D.D.; Gordon, S.J.; Tipdecho, T. Error Models and Propagation in Directly Georeferenced Terrestrial Laser Scanner Networks. *J. Surv. Eng.* **2005**, *131*, 135–142. [CrossRef]
41. Milan, D.J.; Heritage, G.L.; Hetherington, D. Application of a 3D laser scanner in the assess-ment of erosion and deposition volumes and channel change in a proglacial river. *Earth Surf. Process. Landf.* **2007**, *32*, 1657–1674. [CrossRef]
42. Kenner, R.; Phillips, M.; Danioth, C.; Denier, C.; Thee, P.; Zgraggen, A. Investigation of rock and ice loss in a recently deglaciated mountain rock wall using terrestrial laser scanning: Gemsstock, Swiss Alps. *Cold Reg. Sci. Technol.* **2011**, *67*, 157–164. [CrossRef]
43. Kociuba, W. Application of Terrestrial Laser Scanning in the assessment of the role of small debris flow in river sediment supply in the cold climate environment. *Ann. UMCS* **2014**, *69*, 79–91. [CrossRef]
44. Kociuba, W. Assessment of sediment sources throughout the proglacial area of a small Arctic catchment based on high-resolution digital elevation models. *Geomorphology* **2017**, *287*, 73–89. [CrossRef]
45. Kociuba, W. Analysis of geomorphic changes and quantification of sediment budgets of a small Arctic valley with the application of repeat TLS surveys. *Z. Geomorphol. Suppl. Issues* **2017**, *61*, 105–120. [CrossRef]
46. Ewertowski, M.W.; Evans, D.J.A.; Roberts, D.H.; Tomczyk, A.M.; Ewertowski, W.; Pleksot, K. Quantification of historical landscape change on the foreland of a receding polythermal glacier, Hørbyebreen, Svalbard. *Geomorphology* **2019**, *325*, 40–54. [CrossRef]
47. Ewertowski, M.W.; Tomczyk, A.M.; Evans, D.J.A.; Roberts, D.H.; Ewertowski, W. Operational Framework for Rapid, Very-high Resolution Mapping of Glacial Geomorphology Using Low-cost Unmanned Aerial Vehicles and Structure-from-Motion Approach. *Remote Sens.* **2019**, *11*, 65. [CrossRef]
48. Chandler, B.M.; Lovell, H.; Boston, C.M.; Lukas, S.; Barr, I.D.; Benediktsson, Í.Ö.; Benn, D.I.; Clark, C.D.; Darvill, C.M.; Evans, D.J.; et al. Glacial geomorphological mapping: A review of approaches and frameworks for best practice. *Earth Sci. Rev.* **2018**, *185*, 806–846. [CrossRef]
49. Chandler, B.M.; Evans, D.J.; Chandler, S.J.; Ewertowski, M.W.; Lovell, H.; Roberts, D.H.; Schaefer, M.; Tomczyk, A.M. The glacial landsystem of Fjallsjökull, Iceland: Spatial and temporal evolution of process-form regimes at an active temperate glacier. *Geomorphology* **2020**, *361*, 107192. [CrossRef]
50. Hagen, J.O.; Kohler, J.; Melvold, K.; Winther, J.G. Glaciers in Svalbard: Mass balance, runoff and fresh water flux. *Pollut. Res.* **2003**, *22*, 145–159. [CrossRef]
51. Baranowski, S. *Subpolarne Lodowce Spitsbergenu na tle Klimatu Tego Regionu*; Acta Universitatis Wratislaviensis: Wrocław, Poland, 1977; pp. 1–157.
52. Rodzik, J.; Gajek, G.; Reder, J.; Zagórski, P. Glacial Geomorphology. In *Geographical Environment of NW Part of Wedel Jarlsberg Land (Spitsbergen, Svalbard)*; Zagórski, P., Harasimiuk, M., Rodzik, J., Eds.; MCSU Press: Lublin, Poland, 2013; pp. 36–165.
53. Kociuba, W.; Janicki, G. Changeability of movable bed-surface particles in natural, gravel-bed channels and its relation to bedload grain size distribution (scott river, svalbard). *Geogr. Ann.* **2015**, *97*, 507–521. [CrossRef]
54. Bartoszewski, S. *Outflow Regime of the Rivers of the Wedel Jarlsberg Land*; Wydawnictwo UMCS: Lublin, Poland, 1998; pp. 1–167.
55. Navarro, F.; Martín-Español, A.; Lapazaran, J.; Grabiec, M.; Otero, J.; Vasilenko, E.V.; Puczko, D. Ice Volume Estimates from Ground-Penetrating Radar Surveys, Wedel Jarlsberg Land Glaciers, Svalbard. *Arct. Antarct. Alp. Res.* **2014**, *46*, 394–406. [CrossRef]

56. Kociuba, W. *The Mechanism and Dynamics of Sediment Supply and Fluvial Transport in a Glacial Catchment*; MCSU Press: Lublin, Poland, 2015; p. 151.
57. Reder, J.; Zagórski, P. Recession and development of marginal zone of the Scott Glacier. *Landf. Anal.* **2007**, *5*, 175–178.
58. Kociuba, W.; Krząstek, P.; Superson, J. Combining GPS-RTK and rephotographic methodolo-gies for the assessment of transfor-mations of the ephemeral landforms of the near foreland of a valley glacier (Scottbreen, Svalbard). *Z. Geomorphol.* **2016**, *60*, 29–44. [CrossRef]
59. Leica-geosystems. Leica ScanStation C10—Datasheet. 2012. Available online: http://www.leica-geosystems.co.uk/downloads123/hds/hds/ScanStation%20C10/brochures-datasheet/Leica_ScanStation_C10_DS_en.pdf (accessed on 22 October 2020).
60. Smith, M.W.; Vericat, D. Evaluating shallow-water bathymetry from through-water terres-trial laser scanning under a range of hydraulic and physical water quality conditions. *River Res. Appl.* **2014**, *30*, 905–924. [CrossRef]
61. Kociuba, W.; Kubisz, W.; Zagórski, P. Use of terrestrial laser scanning (TLS) for monitoring and modelling of geomorphic processes and phenomena at a small and medium spatial scale in Polar environment (Scott River—Spitsbergen). *Geomorphology* **2014**, *212*, 84–96. [CrossRef]
62. Kociuba, W. Different Paths for Developing Terrestrial LiDAR Data for Comparative Analyses of Topographic Surface Changes. *Appl. Sci.* **2020**, *10*, 7409. [CrossRef]
63. Wheaton, J.M.; Brasington, J.; Darby, S.E.; Sear, D.A. Accounting for uncertainty in DEMs from repeat topographic surveys: Improved sediment budgets. *Earth Surf. Process. Landf.* **2009**, *35*, 136–156. [CrossRef]
64. Brasington, J.; Langham, J.; Rumsby, B. Methodological sensitivity of morphometric esti-mates of coarse fluvial sediment transport. *Geomorphology* **2003**, *53*, 299–316. [CrossRef]
65. Heritage, G.; Large, A.R.G. *Laser Scanning for the Environmental Sciences*; Wiley-Blackwell: Chichester, UK, 2009; p. 288.
66. Milan, D.J.; Heritage, G.L.; Large, A.R.G.; Fuller, I.C. Filtering spatial error from DEMs: Implications for morphological change estimation. *Geomorphology* **2011**, *125*, 160–171. [CrossRef]
67. Schwendel, A.C.; Fuller, I.C.; Death, R.G. Assessing DEM interpolation methods for effective representation of upland stream morphology for rapid appraisal of bed stability. *River Res. Appl.* **2012**, *28*, 567–584. [CrossRef]
68. Reder, J. Ewolucja Stref Marginalnych Lodowców NW Części Ziemi Wedela Jarlsberga. In *XX Lat Badań Polarnych Instytutu Nauk o Ziemi UMCS na Spitsbergenie*; Superson, J., Zagórski, P., Eds.; MCSU Press: Lublin, Poland, 2006; pp. 45–51.
69. Nuth, C.; Kohler, J.; Aas, H.F.; Brandt, O.; Hagen, J.O. Glacier geometry and elevation changes on Svalbard (1936–90): A baseline dataset. *Ann. Glaciol.* **2007**, *46*, 106–116. [CrossRef]
70. Ewertowski, M.W.; Tomczyk, A.M. Quantification of the ice-cored moraines' short-term dynamics in the high-Arctic glaciers Ebbabreen and Ragnarbreen, Petuniabukta, Svalbard. *Geomorphology* **2015**, *234*, 211–227. [CrossRef]
71. Westoby, M.J.; Glasser, N.F.; Hambrey, M.J.; Brasington, J.; Reyonds, M.J.; Hassan, M.A.A. Reconstructing historic Glacial LakeOutburst Floods through numerical modelling and geomorphological assessment: Extreme events in the Himalaya. *Earth Surf. Process. Landf.* **2014**, *39*, 1675–1692. [CrossRef]
72. Carrivick, J.L.; Heckmann, T. Short-term geomorphological evolution of proglacial systems. *Geomorphology* **2017**, *287*, 3–28. [CrossRef]
73. Hambrey, M.J.; Glasser, N.F. The Role of Folding and Foliation Development in the Genesis of Medial Moraines: Examples from Svalbard Glaciers. *J. Geol.* **2003**, *111*, 471–485. [CrossRef]
74. Bennett, M.R.; Glasser, N.F. *Glacial Geology: Ice Sheets and Landforms*, 2nd ed.; Wiley-Blackwell: Oxford, UK, 2009; pp. 1–385.
75. Colbeck, S.C. A theory of water percolation in snow. *J. Glaciol.* **1972**, *1*, 369–385. [CrossRef]
76. Conway, H.; Benedict, R. Infiltration of water into snow. *Water Resour. Res.* **1994**, *30*, 641–649. [CrossRef]
77. Bales, R.C.; Harrington, R.F. Resent progress in snow hydrology. *Rev. Geophys.* **1995**, *33*, 1011–1020. [CrossRef]
78. Cuffey, K.M.; Paterson, W.S.B. *The Physics of Glaciers*, 4th ed.; Elsevier: Oxford, UK, 2010; pp. 1–674.

resources

MDPI

Article

Hydrological Response to Drought Occurrences in a Brazilian Savanna Basin

Rubens Junqueira *, Marcelo R. Viola, Jhones da S. Amorim and Carlos R. de Mello

Programa de Pós-Graduação em Recursos Hídricos, Departamento de Recursos Hídricos, Universidade Federal de Lavras, Lavras 3037, Brazil; marcelo.viola@ufla.br (M.R.V.); jhonesamorim@gmail.com (J.d.S.A.); crmello@ufla.br (C.R.d.M.)

* Correspondence: rubensjunqueira@live.com

Received: 29 August 2020; Accepted: 14 October 2020; Published: 16 October 2020

Abstract: The Brazilian savanna is one of the world's 25 biodiversity hotspots. However, droughts can decrease water availability in this biome. This study aimed to analyze meteorological and hydrological droughts and their influence on the hydrological behavior in a Brazilian savanna basin. For that, hydrological indicators were calculated to analyze the hydrological behavior in the Pandeiros river basin (PRB). The Standardized Precipitation Index (SPI) and Standardized Streamflow Index (SSI) were calculated for the hydrological year and rainy season from 1977 to 2018. The propagation of the meteorological to hydrological drought was studied by means of the Pearson coefficient of correlation between the SSI and SPI with 0, 3, 6, 9, and 12-month lags. A longer meteorological drought was observed from 2014/15 to 2017/18 which caused a reduction in the groundwater recharge, besides potentially reducing the ecological functions of the Brazilian savanna. This drought was intensified by an increase in the average annual temperature, resulting in the increasing of evapotranspiration. Regarding drought propagation, there is no significant difference among the coefficients of correlation from 0 to 6-month lags. For the lags of 9 and 12 months, the correlation decreases, indicating a greater influence of the current rainy season than the past ones.

Keywords: extreme events; hydrological indicators; SPI; water resources management

1. Introduction

The Brazilian savanna (known as "Cerrado") is the second-largest biome in South America, covering an area of 2 million km^2. It is one of the world's 25 biodiversity hotspots due to the endemic species concentration and the high degree of threat [1,2]. Moreover, this biome plays an important role in providing water, maintaining its ecohydrological functionality for industry, agriculture, navigation, tourism, and hydroelectricity in several Brazilian and South American basins, including the São Francisco river basin (SFRB) [3]. Therefore, it is important to conduct hydrological studies for better assisting water resource management in the Brazilian savanna aiming to maintain its eco-hydrological services [4].

Hydrological indicators, such as the aquifer restitution rate (ARR) and the surface runoff rate (SRR), have been widely used to evaluate the hydrological behavior of Brazilian river basins [4–6]. Nevertheless, during extreme events, for example, floods and droughts, the basin may present different behavior. Extreme drought events can abnormally reduce the streamflow, agricultural production, lake and reservoir levels, and groundwater recharge [7].

Recently, several studies on drought have been developed in Brazil focused on meteorological droughts [8–10]. According to Van Loon [7], this drought is associated with a deficiency in precipitation, and possibly an increase in evapotranspiration. However, few studies have attempted to analyze the influence of meteorological drought on the streamflow (hydrological drought).

Although the origin of hydrological drought is commonly related to meteorological drought, other factors can influence it, highlighting lithology, vegetation, and human influence [11]. Junqueira et al. [12] reported a longer hydrological drought than meteorological ones from 2015 to 2017 due to the reduction in groundwater recharge in previous seasons in the Tocantins river basin, Brazil. As a result, the effects on irrigation, hydroelectricity, and urban supply were prolonged.

To analyze the occurrence, duration, and intensity of droughts, several indexes have been developed in recent years. The Standardized Precipitation Index (SPI) [13] has been widely used in Brazil and worldwide [12,14–16]. According to the World Meteorological Organization (WMO) [17], this index is considered standard due to its accuracy and simplicity. Several indexes have emerged from the SPI, such as the Standardized Streamflow Index (SSI) [11], a hydrological drought index with the same characteristics as the SPI. These indexes represent anomalies from a normal situation and allow for comparison in different regions [7].

To calculate a standardized index, a Probability Distribution Function (PDF) is required. McKee et al. [13] applied the two parameters of Gamma distribution for SPI. Nevertheless, to be more accurate in estimating droughts, Vicente-Serrano et al. [11] suggested it the most suitable PDF rather than adopting a single distribution for all situations. An inappropriate PDF may over- or underestimate the magnitude of the drought, as the extreme events are in the tail of the PDF [16]. Therefore, researchers have analyzed several PDFs to calculate standardized drought indexes and found different results worldwide [11,18,19].

In this context, this study aimed to analyze the occurrence, intensity, duration, and propagation of meteorological to hydrological droughts and their influence on the hydrological behavior in a Brazilian savanna basin.

2. Materials and Methods

2.1. Study Area

The Pandeiros river basin (PRB), located in the north Minas Gerais State, is inserted in the Brazilian savanna and has an area of 3220 km^2. Due to its ecological relevance for the Brazilian savanna and for the SFRB, the Pandeiros River Environmental Protection Area was created through State Law n° 11,901 to protect the native fish species, which represent 70% of the reproduction and development fish from the middle São Francisco River [20,21]. Figure 1 shows the PRB location, the streamflow and rain gauge stations, and the Digital Elevation Model (DEM) ALOS (Advanced Land Observing Satellite) PALSAR (Phased Array L-band Synthetic Aperture Radar), with a spatial resolution of 12.5 m.

The elevation ranges from 496 to 847 m, with an average of 677 m. The climate, according to Köppen type-climate classification, is Aw (tropical with wet summers and dry winters) [22]. The average precipitation for the hydrological year (October to September) is 1085 mm, of which 92% occurs during the rainy period (October to March).

The predominant soil in the PRB is the Latosol, which covers 88.3% of its area [23], and the natural pasture, typical of the Brazilian savanna, is the land use predominant, covering 96.3% of the basin's area [24].

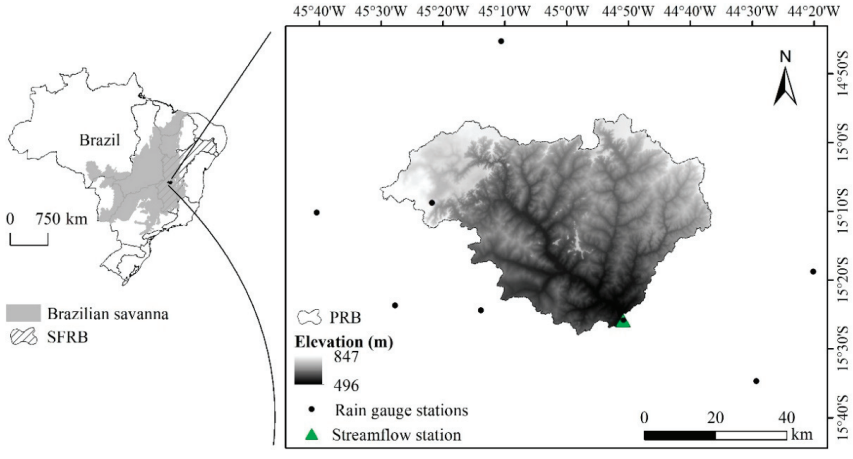

Figure 1. Locations of the PRB, streamflow and rain gauge stations, and DEM.

2.2. Input Data

Daily streamflow and precipitation datasets were obtained from the Brazilian National Water Agency (ANA) from October 1977 to September 2018 (41 hydrological years), using only those with up to 10% of gaps, aiming to meet the data quality standards for carrying out drought analysis [19]. The double mass curve was used to analyze the homogeneity and consistency of the precipitation series [25]. Then, gap filling was carried out on a monthly time scale using the Inverse Squared Distance Weighted method. The basin-scale precipitation was obtained using the area-weighted procedure with the eight rain gauge stations available (Figure 1) [26].

2.3. Hydrological Behavior

2.3.1. Baseflow

To appraise the hydrological behavior of the PRB, the baseflow was taken using the recursive digital filters method, which divides the streamflow into direct surface runoff and baseflow (Equation (1)) [27].

$$y_k = f_k + b_k \quad (1)$$

where y is the total streamflow ($m^3\ s^{-1}$); f is the direct surface runoff ($m^3\ s^{-1}$); b is the baseflow ($m^3\ s^{-1}$); and k is the time step (day).

For b_k calculation, the methodology proposed by Eckhardt [27] for the general form of the recursive filter with one parameter is given by Equation (2).

$$b_k = \frac{(1 - BFI_{max}) \times a \times b_{k-1} + (1 - a) \times BFI_{max} \times y_k}{1 - a \times BFI_{max}} \quad (2)$$

where BFI_{max} is the maximum value of the baseflow index that can be assumed equal to 0.8 as recommended by Eckhardt [27] for perennial streams; and a corresponds to the groundwater recession constant (0.8925), dimensionless. This model assumes that the aquifer outflow is linearly proportional to its storage, which means an exponential recession of baseflow during the period without groundwater recharge [27].

2.3.2. Hydrological Indicators

The hydrological indicators adopted to study the hydrological behavior in the PRB are presented in Table 1.

Table 1. Hydrological indicators used in this study.

Hydrological Indicator	Abbreviation	Unit
Depletion coefficient	α	day^{-1}
Water depth stored in the aquifer at the end of the hydrological year	A_f	mm
Baseflow index	BFI	-
Aquifer restitution rate	ARR	%
Evapotranspiration rate	ETR	%
Surface runoff rate	SRR	%
Long-term streamflow	Q_{mean}	$m^3\ s^{-1}$
Minimum streamflow	Q_{min}	$m^3\ s^{-1}$
Maximum streamflow	Q_{max}	$m^3\ s^{-1}$
Minimum streamflow that occurs in 90% of the time	$Q_{90\%}$	$m^3\ s^{-1}$
Minimum streamflow that occurs in 95% of the time	$Q_{95\%}$	$m^3\ s^{-1}$
Minimum streamflow in seven consecutive days and a return period of 10 years	$Q_{7,10}$	$m^3\ s^{-1}$
Specific yield (SY) related to Q_{mean}, Q_{min}, Q_{max}, $Q_{90\%}$, $Q_{95\%}$, and $Q_{7,10}$	SY_{mean}, SY_{min}, SY_{max}, $SY_{90\%}$, $SY_{95\%}$, and $SY_{7,10}$, respectively	$L\ s^{-1}\ km^{-2}$

BFI is the long-term ratio between baseflow and total streamflow and the closer to 1 it is, the greater the contribution of baseflow to the streamflow. The ARR was obtained by the long-term ratio between baseflow and precipitation and indicates the precipitation rate that contributes to aquifer restitution. The evapotranspiration was calculated based on annual water balance (ET = precipitation − total streamflow, in mm), and then the ETR was calculated as ET divided by precipitation. The SRR consists of the long-term ratio between direct surface runoff (SR = total streamflow − baseflow) and precipitation. The α and A_f are described in Equations (3) and (4). According to Silva et al. [28], α values close to zero indicate higher natural regularization capacity.

$$Q_t = Q_0 \times e^{-\alpha.t} \tag{3}$$

$$A_f = \frac{Q_i \times 86.4}{\alpha \times A_b} \tag{4}$$

where Q_0 was the streamflow at the beginning of the recession, in $m^3\ s^{-1}$; Q_t is the streamflow after t days of the beginning of the recession, in $m^3\ s^{-1}$; Q_i is the streamflow at the end of the hydrological year, in $m^3\ s^{-1}$; and A_b is the basin's area, in km^2.

The Q_{mean} was obtained from the average of the daily streamflow, while the Q_{min} and Q_{max} were obtained from the average of the minimum and maximum daily annual streamflow, respectively. To obtain $Q_{7,10}$, 10 PDFs fitted using the L-moments were analyzed [29]: the 3-parameter log-normal (LN3), 3-parameter Pearson (PE3), the Gumbel extreme value, the Generalized Extreme Values (GEV), Gamma, Weibull, the 4-parameter Kappa, the 5-parameter Wakeby, the generalized logistic (GLO), and the generalized Pareto (GPA). The PDF was then selected based on the best fitting according to the Anderson–Darling (AD) test. The $Q_{90\%}$ and $Q_{95\%}$ were obtained based on the flow-duration curve. The SY is the result of the calculated streamflows ($Q_{90\%}$, $Q_{95\%}$, etc.) divided by the basin's area, which allows comparing them among different regions or sub-basins.

2.4. Meteorological and Hydrological Droughts

To analyze the occurrence, intensity, and duration of the droughts in the PRB, the SPI [13] and SSI [11] were calculated by year, considering the hydrological year (October to September), and for half-year time scales, considering the rainy season (October to March).

For the SPI and SSI calculation, the basin-scale precipitation and streamflow series, respectively, were accumulated for the studied period and a PDF was fitted. Following that, they were transformed into a normal distribution, with mean and variance, respectively, equal to zero and one. The analysis of the most suitable PDF was performed in a similar way to the $Q_{7,10}$. This procedure, according to Vicente-Serrano et al. [11], allows higher precision in obtaining drought indexes. Afterward, the indexes were classified following the WMO [17] classification (Table 2).

Table 2. Classification for the SPI and SSI values.

Classification	Indexes Values	Probability (%)
Extremely dry (ED)	SPI and SSI ≤ −2.0	2.3
Severely dry (SD)	−2.0 < SPI and SSI ≤ −1.5	4.4
Moderately dry (MD)	−1.5 < SPI and SSI ≤ −1.0	9.2
Near normal (NN)	−1.0 < SPI and SSI < 1.0	68.2
Moderately wet (MW)	1.0 ≤ SPI and SSI < 1.5	9.2
Very wet (VW)	1.5 ≤ SPI and SSI < 2.0	4.4
Extremely wet (EW)	SPI and SSI ≥ 2.0	2.3

The Pearson correlation of the coefficient (r) with a statistical significance of 5% ($\alpha = 0.05$) was used to analyze the correlation between the SPI and SSI on different time scales. In addition, to assess the propagation of meteorological to hydrological drought, the correlations between the 0, 3, 6, 9, and 12-month lags with both the SSI and SPI were performed on an annual scale.

3. Results and Discussion

3.1. Hydrological Behavior

Figure 2A presents the average monthly precipitation, streamflow, and baseflow for the PRB. Surface runoff occurs predominantly in the rainy season, whereas in the dry season, it is the baseflow. The BFI indicator was equal to 0.80, which is a characteristic of perennial rivers [27], showing the importance of baseflow over the total streamflow in the studied basin. The ARR for the PRB was 14.9%, a high value when considering that 81.4% of the precipitation returns to the atmosphere by evapotranspiration (ETR). Besides, only 3.7% of the total precipitation is converted to surface runoff (SRR). The high ARR and low SRR values are associated with the predominance of Latosol, which is a deep soil with a high infiltration capacity [30], occurring in a flatter topography (average slope of 5.9%). Moreover, the PRB is part of an environmental protection area and its vegetation has been preserved, which favors the soil-water infiltration and reduces direct surface runoff.

The SY_{mean} obtained for the PRB was 6.46 L s^{-1} km^{-2}, while the SY_{min} and SY_{max} were 3.6 and 24.8 L s^{-1} km^{-2}, respectively. These values are low when compared to others obtained for Brazilian savanna basins such as by Rodrigues et al. [4] in the Manual Alves da Natividade river basin. However, the ETR obtained by Rodrigues et al. [4] was 69.1%, lower than that obtained in the PRB (81.4%). Therefore, the high evapotranspiration contributed to the reduction of the streamflow in the PRB.

Regarding $Q_{7,10}$ (6.9 m^3 s^{-1}), for the streamflow that is used as a basis for granting water resources in the region, the PDF that presented the best fitting was Wakeby, with AD equal to 0.30. Amorim et al. [29] found a similar result in the Mortes River, Southeastern Brazil, demonstrating the satisfactory performance of this PDF for the Q_7 series. The $SY_{7,10}$ was equal to 2.1 L s^{-1} km^{-2}, similar to that obtained by Silva et al. [6] in the Minas Gerais State. According to the Euclydes et al. [31] classification, the PRB has a high natural regularization capacity once $SY_{7,10}$ corresponds to 33% of

SY_{mean}, which follows the α value close to zero (0.0073). The α is close to that obtained by Freitas and Bacellar [32] in sub-basins of the upper São Francisco River and by Junqueira et al. [12] in the Tocantins river basin. From the flow-duration curve (Figure 2B), $Q_{90\%}$ and $Q_{95\%}$ was equal to 9.7 and 7.7 $m^3\ s^{-1}$, respectively, which generated SY_{90} equal to 3.0 L s^{-1} km^{-2} and SY_{95} equal to 2.4 L s^{-1} km^{-2}, higher than $SY_{7,10}$.

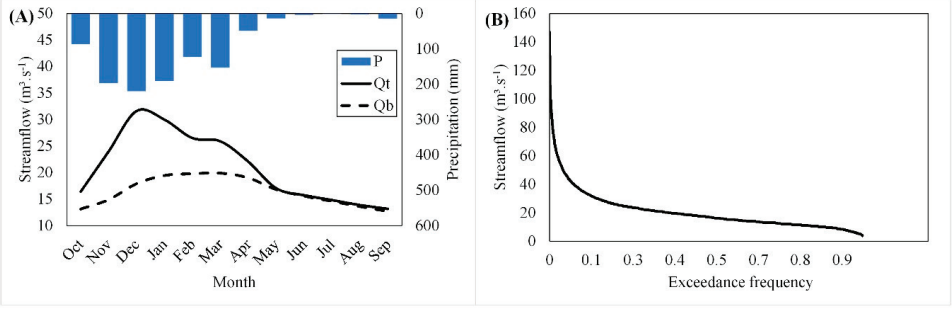

Figure 2. Hydrograph containing average monthly precipitation (P), total streamflow (Qt), and baseflow (Qb) (**A**); and permanent flow curve (**B**).

3.2. Meteorological and Hydrological Droughts

Among the PDFs analyzed, Weibull presented a better fit in two historical series, whereas Wakeby showed better performance in six. Although McKee et al. [13] have used Gamma for the SPI calculation, this PDF did not produce the best fit in either case. GPA presented unsatisfactory results for the basin-scale precipitation and streamflow series, not being approved in the AD test in both time scales. Table 3 presents the AD test results for the basin-scale precipitation and streamflow series for the hydrological years and rainy seasons obtained from each PDF.

Table 3. AD test results for the basin-scale precipitation and streamflow for the PRB.

PDF	Precipitation						Streamflow	
	Hy	L3	L6	L9	L12	Rs	Hy	Rs
Gumbel	0.929	0.874	0.690	0.886	0.249	0.527	0.348	0.462
Gamma	0.562	0.452	0.386	0.376	0.250	0.262	0.381	0.524
GEV	0.552	0.421	0.387	0.320	0.216	0.258	0.350	0.465
Kappa	0.537	0.398	0.368	0.318	0.217	0.243	0.359	0.520
GLO	0.612	0.492	0.456	0.359	0.244	0.341	0.423	0.567
GPA	-	-	-	-	-	-	-	-
Weibull	0.528 *	0.397 *	0.358	0.300	-	0.239	-	-
Wakeby	0.711	0.467	0.325 *	0.279 *	0.202 *	0.206 *	0.281 *	0.388 *
PE3	0.552	0.424	0.385	0.315	0.229	0.260	0.363	0.478
LN3	0.553	0.425	0.388	0.315	0.222	0.262	0.356	0.470

Note: * Best fit, Hy = Hydrological year, L3 = 3 months lag, L6 = 6 months lag, L9 = 9 months lag, L12 = 12 months lag, Rs = Rainy season.

The SPI and SSI results for the hydrological years and rainy seasons, calculated according to the most suitable PDF, can be observed in Figure 3. There is an agreement between the SPI values for the hydrological year and the rainy season (r = 0.96). A similar result is observed in the SSI, where r = 0.99. However, when comparing the SPI against the SSI at the two-time scales, the correlation decreases (r = 0.64). This is due to the complexity of the factors associated with the hydrological cycle in the basins, where the response to precipitation depends on factors such as vegetation, lithology, and topography [11].

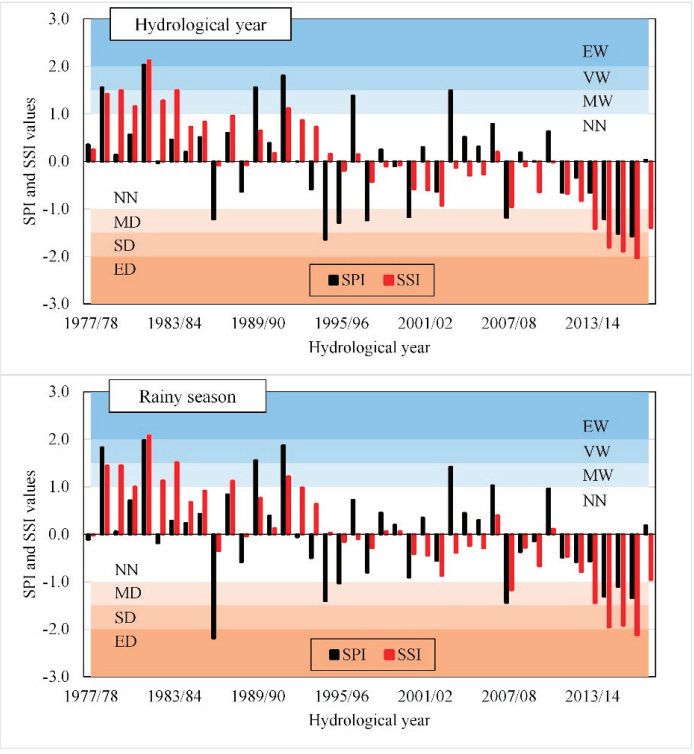

Figure 3. SPI and SSI results for hydrological years and rainy seasons in the PRB.

The most significant meteorological droughts occurred during the hydrological years of 1986/87, 1994/95, 1995/96, 1997/98, 2007/08, and between 2014/15 and 2016/17 in the PRB. Similar behavior was observed for the rainy season, however, with some differences concerning intensity. Although the dry season accounted for only 8% of annual precipitation, the total precipitation in this period for the hydrological year of 1986/87 was 171.1 mm, approximately twice the average (89.5 mm). Therefore, the attenuation of drought on a hydrological year scale may have occurred due to increased precipitation in the dry season.

As a result of some years with below-average precipitation, the hydrological years between 2013/14 to 2017/18 presented a long and intense hydrological drought. In these years, there was a high reduction in the long-term mean streamflow, from 20.8 $m^3\ s^{-1}$ in the whole period to 10.3 $m^3\ s^{-1}$ for the drought period (2013/14 to 2017/18), which is lower than the minimum streamflow for the entire studied period (11.5 $m^3\ s^{-1}$). Also, there was a significant reduction in ARR (14.9 to 9.2%), SSR (3.7 to 2.4%), SY_{mean} (6.5 to 3.2 L $s^{-1}\ km^{-2}$), SY_{min} (3.6 to 1.5 L $s^{-1}\ km^{-2}$), and SY_{max} (24.8 to 17.4 L $s^{-1}\ km^{-2}$).

Besides the reduction in precipitation, the increase in temperature and, consequently, in evapotranspiration, contributed to the hydrological drought intensification, as highlighted by Van Loon [7] and Junqueira et al. [12]. According to data obtained from the Brazilian National Institute of Meteorology (INMET) using a weather station close to the basin (Januária station), the daily annual average temperature from 1977/78 to 2012/13 was 23.4 °C, however, from 2013/14 to 2017/18 there was an increase of 1.3 °C. Thus, the ETR in this period was equal to 88.4%, higher than the average observed in the studied period (81.4%).

Studies suggest an increase in the intensity and frequency of droughts by the end of the century worldwide due to atmospheric evaporative demand increases, reducing water availability, soil water

storage, and agricultural production [15,33,34]. Yet, Santos et al. [35] observed a reduction in the water table in the PRB wetlands, downstream of the streamflow gauge station of this study, due to a reduction in precipitation and an increase in temperature in recent years, affecting vegetation dynamics in the wetland.

During the period 2013/14 to 2017/18, similar events were found in other Brazilian regions such as the Doce river basin [14], Tocantins river basin [12], Northeastern Brazil [36], Amazon [36], Paraná river basin [37], the metropolitan region of São Paulo [38], and Ceará State [9], affecting the hydropower generation and urban supply. Besides, droughts can affect the ecological functions of the Brazilian savanna [34], as well as reduce the native fish species and increase exotic species [39].

According to Azevedo et al. [40], after a long period of drought, the Sobradinho hydropower plant reservoir, located in SFRB and responsible for almost 60% of the water resources in Northeastern Brazil, presented a reduction of up to 50% in surface water in 2015/16. In that year, hydropower generation was only 170 MW (its total installed power is 1050 MW).

Some researchers associate drought occurrence with anomalies in sea surface temperatures in the Pacific and the Atlantic Oceans [9,12,36]. Santos et al. [41] reported that anomalies in the El Niño-Southern Oscillation (ENSO) phenomenon are related to the cycle of meteorological droughts in the region in which the PRB is located, however, the Pacific Decadal Oscillation (PDO) influence has not been identified as having a clear influence on drought events in this region. El Niño (positive phase of the ENSO) occurred during all the years in which there was a meteorological drought in the PRB, except for 2007/08 and 2016/17, when the La Niña phenomenon (negative phase of the ENSO) took place for some months. Junqueira et al. [12] and Marengo et al. [36] also found the influence of the ENSO on the drought occurrences in the Tocantins river basin and Northeastern Brazil. According to Garreaud et al. [42], although the PDO-related precipitation and temperature anomalies have the same behavior as the ENSO in South America, their effects seem to be less intense in the PRB region.

3.3. Drought Propagation

Table 4 presents the correlation results between the SSI and SPI with a lag of 0, 3, 6, 9, and 12 months, both on an annual scale. There is no difference between the r values from a 0 to 6-month lag. However, a higher correlation was obtained for the 3-month lag, indicating a lag in the propagation of the meteorological drought to the hydrological one. A similar result was found by Rodrigues et al. [34] in sub-basins of the Tocantins River, where the correlation between the indices was higher in the period from 0 to 3 months.

Table 4. r results between the SSI and the SPI with a lag of 0, 3, 6, 9, and 12 months.

SPI Lags (Months)	0	3	6	9	12
R	0.64	0.65	0.64	0.47	0.39

Furthermore, the correlation is lower for 9 and 12-month lags, that is, changes in streamflow are more influenced by the current than the past rainy season. According to Van Loon [7], rainfall deficit in the rainy season can influence following dry season conditions. In cases of longer meteorological drought, there may be a reduction in groundwater recharge, affecting the streamflow even after the meteorological conditions return to normal, as also reported by Jesus et al. [14] in the Doce river basin and by Junqueira et al. [12] in the Tocantins river basin. As an example, in the hydrological year 2017/18, the SPI was classified as near normal, however, the SSI was classified as moderately dry. This increase in precipitation from one year to the next attenuated the hydrological drought but was not enough to fill the recharge deficit from previous years.

According to Junqueira et al. [12], baseflow depends on the precipitation/recharge rate in previous months, as well as on aquifer characteristics. As the streamflow in the PRB is strongly influenced by baseflow (BFI = 0.80), the deficiency in groundwater recharge has a prolonged effect on the streamflow. This deficiency is confirmed by the A_f values, where, from 2013/14 to 2017/18, the average was 21.1 mm,

less than half the historical average (48.9 mm). The recharging deficiency increased during the drought until it reached its lowest value at the end of 2016/17 (A_f = 16.3 mm). After the 2017/18 hydrological year, there was a slight recovery of water storage in the aquifer (A_f = 20.0 mm) due to the increase in precipitation, however, it remained below the historical average.

4. Conclusions

The SPI allowed us to identify the main droughts that hit the PRB (1986/87, 1994/95, 1995/96, 1997/98, 2000/01, 2007/08, 2014/15, 2015/16, and 2016/17). These events may be related to the occurrence of macro-scale climatic phenomena such as the ENSO, as observed in other Brazilian regions. Although the droughts observed in hydrological years presented a high correlation with the drought during the rainy season, the dry season can occasionally influence the drought intensity.

The hydrological drought from 2013/14 to 2017/18 occurred mainly due to a prolonged reduction in precipitation, reducing water availability, and affecting the fish reproduction in the PRB and SFRB and the ecological functions of the Brazilian savanna. In addition to the reduction in precipitation, the increase in temperature and, consequently, in evapotranspiration contributed to the intensification of the hydrological drought in the cited period.

Based on the hydrological indicators, a high influence of baseflow on the total streamflow (BFI = 0.8) and evapotranspiration (81.4% of the total precipitation) on the hydrological behavior of the PRB was observed. Moreover, the analysis of hydrological indicators highlighted the influence of droughts on groundwater recharge, evidenced by a reduction in A_f values.

The propagation of meteorological to hydrological drought occurred in shorter lags (0 to 6 months), with greater correlation in 3-month lag. However, for the lags of 9 and 12 months, the correlation decreased, indicating that changes in streamflow are more influenced by the current than previous rainy seasons.

Author Contributions: Conceptualization, R.J., M.R.V. and J.d.S.A.; methodology, R.J., M.R.V. and J.d.S.A.; software, R.J. and J.d.S.A.; validation, R.J.; formal analysis, R.J. and M.R.V.; investigation, R.J.; resources, R.J., M.R.V. and J.d.S.A.; data curation, R.J. and J.d.S.A.; writing—original draft preparation, R.J.; writing—review and editing, R.J., M.R.V., J.d.S.A. and C.R.d.M.; visualization, R.J. and M.R.V.; supervision: M.R.V.; project administration, R.J., M.R.V. and J.d.S.A.; funding acquisition, R.J., M.R.V. and J.d.S.A. All authors have read and agreed to the published version of the manuscript.

Funding: This study was funded by the Coordenação de Aperfeiçoamento de Pessoal de Nível Superior—CAPES (grant numbers 88882.446869/2019-01 and 88882.446854/2019-01) and the Conselho Nacional de Desenvolvimento Científico e Tecnológico (CNPq) with the grant for authors, and Universidade Federal de Lavras (UFLA) through public notice PRPG/UFLA n° 046/2020 with the support for publication.

Acknowledgments: We greatly acknowledge the Brazilian National Water Agency (ANA) and the Brazilian National Institute of Meteorology (INMET) for providing the input data to develop this study.

Conflicts of Interest: The authors declare no conflict of interest.

References

1. Myers, N.; Mittermeier, R.A.; Mittermeier, C.G.; da Fonseca, G.A.B.; Kent, J. Biodiversity hotspots for conservation priorities. *Nature* **2000**, *403*, 853–858. [CrossRef] [PubMed]
2. Hunke, P.; Mueller, E.N.; Schröder, B.; Zeilhofer, P. The Brazilian Cerrado: Assessment of water and soil degradation in catchments under intensive agricultural use. *Ecohydrology* **2015**, *8*, 1154–1180. [CrossRef]
3. Oliveira, P.T.S.; Nearing, M.A.; Moran, M.S.; Goodrich, D.C.; Wendland, E.; Gupta, H.V. Trends in water balance components across the Brazilian Cerrado. *Water Resour. Res.* **2014**, *50*, 7100–7114. [CrossRef]
4. Rodrigues, J.A.M.; Andrade, A.C.O.; Viola, M.R.; Morais, M.A.V. Indicadores hidrológicos para a gestão de recursos hídricos na bacia hidrográfica do rio Manuel Alves Da Natividade, Tocantins. *Sci. Agrar.* **2016**, *16*. [CrossRef]
5. Mello, C.R.; Viola, M.R.; Beskow, S. Vazões máximas e mínimas na região do Alto Rio Grande, MG. *Ciência e Agrotecnologia* **2010**, *34*, 494–501. [CrossRef]

6. Silva, L.A.; Silva, A.M.; Coelho, G.; Pinto, L.C.; Eduardo, E.N. Minimum and reference discharges and specific yield for the state of Minas Gerais, Brazil. *Rev. Bras. Ciencias Agrar.* **2017**, *12*, 543–549. [CrossRef]
7. Van Loon, A.F. Hydrological drought explained. *Wiley Interdiscip. Rev. Water* **2015**, *2*, 359–392. [CrossRef]
8. Rocha Júnior, R.L.; Santos Silva, F.D.; Costa, R.L.; Gomes, H.B.; Pinto, D.D.C.; Herdies, D.L. Bivariate assessment of drought return periods and frequency in brazilian northeast using joint distribution by copula method. *Geosciences* **2020**, *10*, 135. [CrossRef]
9. Pontes Filho, J.D.; Souza Filho, F.D.A.; Martins, E.S.P.R.; de Studart, T.M.D.C. Copula-Based Multivariate Frequency Analysis of the 2012–2018 Drought in Northeast Brazil. *Water* **2020**, *12*, 834. [CrossRef]
10. Juliani, B.H.T.; Okawa, C.M.P. Application of a standardized precipitation index for meteorological drought analysis of the semi-arid climate influence in Minas Gerais, Brazil. *Hydrology* **2017**, *4*, 26. [CrossRef]
11. Vicente-Serrano, S.M.; López-Moreno, J.I.; Beguería, S.; Lorenzo-Lacruz, J.; Azorin-Molina, C.; Morán-Tejeda, E. Accurate Computation of a Streamflow Drought Index. *J. Hydrol. Eng.* **2012**, *17*, 318–332. [CrossRef]
12. Junqueira, R.; Viola, M.R.; de Mello, C.R.; Vieira-Filho, M.; Alves, M.V.G.; Amorim, J.d.S. Drought severity indexes for the Tocantins River Basin, Brazil. *Theor. Appl. Climatol.* **2020**, *140*. [CrossRef]
13. McKee, T.B.; Doesken, N.J.; Kleist, J. The relationship of drought frequency and duration to time scales. *Proc. Conf. Appl. Climatol.* **1993**, *17*, 179–183.
14. Jesus, E.T.; Amorim, J.S.; Junqueira, R.; Viola, M.R.; Mello, C.R. Meteorological and hydrological drought from 1987 to 2017 in Doce River Basin, Southeastern Brazil. *Rev. Bras. Recur. Hídricos* **2020**, *25*, 1–12. [CrossRef]
15. Vicente-Serrano, S.M.; Domínguez-Castro, F.; McVicar, T.R.; Tomas-Burguera, M.; Peña-Gallardo, M.; Noguera, I.; López-Moreno, J.I.; Peña, D.; El Kenawy, A. Global characterization of hydrological and meteorological droughts under future climate change: The importance of timescales, vegetation-CO2 feedbacks and changes to distribution functions. *Int. J. Climatol.* **2020**, *40*, 2557–2567. [CrossRef]
16. Sienz, F.; Bothe, O.; Fraedrich, K. Monitoring and quantifying future climate projections of dryness and wetness extremes: SPI bias. *Hydrol. Earth Syst. Sci.* **2012**, *16*, 2143–2157. [CrossRef]
17. WMO—World Meteorological Organization. *Standardized Precipitation Index User Guide*; WMO-No. 1090; World Meteorological Organization: Geneva, Switzerland, 2012; Volume 21, p. 24.
18. Pieper, P.; Düsterhus, A.; Baehr, J. Global and regional performances of SPI candidate distribution functions in observations and simulations. *Hydrol. Earth Syst. Sci. Discuss.* **2020**, 1–33. [CrossRef]
19. Jahangir, M.H.; Abolghasemi, M. Determining the most appropriate probability distribution function for calculate and compare the SPEI and SPI drought index in Tehran. *Desert Ecosyst. Eng. J.* **2019**, *8*, 1–16. [CrossRef]
20. Santos, U.; Silva, P.C.; Barros, L.C.; Dergam, J.A. Fish fauna of the Pandeiros River, a region of environmental protection for fish species in Minas Gerais state, Brazil. *Check List* **2015**, *11*, 1507. [CrossRef]
21. Nunes, Y.R.F.; Azevedo, I.F.P.; Neves, W.V.; Veloso, M.D.D.M.; Souza, R.d.A.; Fernandes, G.W. Pandeiros: O Pantanal Mineiro. *MG Biota* **2009**, *2*, 4–17.
22. Alvares, C.A.; Stape, J.L.; Sentelhas, P.C.; de Moraes Gonçalves, J.L.; Sparovek, G. Köppen's climate classification map for Brazil. *Meteorol. Zeitschrift* **2013**, *22*, 711–728. [CrossRef]
23. Minas Gerais State Environmental Foundation (FEAM) Mapa de solos do Estado de Minas Gerais 2010. Available online: http://www.feam.br/-qualidade-do-solo-e-areas-contaminadas/mapa-de-solos (accessed on 6 November 2019).
24. Brazilian Institute of Geography and Statistics (IBGE) Mapa de Cobertura e Uso da Terra do Brasil 2010 2018. Available online: https://www.ibge.gov.br/geociencias/informacoes-ambientais/cobertura-e-uso-da-terra/15831-cobertura-e-uso-da-terra-do-brasil.html?edicao=16023&t=sobre (accessed on 7 November 2019).
25. Gao, P.; Li, P.; Zhao, B.; Xu, R.; Zhao, G.; Sun, W.; Mu, X. Use of double mass curves in hydrologic benefit evaluations. *Hydrol. Process.* **2017**, *31*, 4639–4646. [CrossRef]
26. Gao, C.; Li, X. Precipitation thresholds of drought disaster for maize in areas in front of Bengbu Sluice, Huaihe River Basin, China. *Water* **2018**, *10*, 1395. [CrossRef]
27. Eckhardt, K. How to construct recursive digital filters for baseflow separation. *Hydrol. Process.* **2005**, *19*, 507–515. [CrossRef]

28. Silva, R.F.G.; Bacellar, L.d.A.P.; Fernandes, K.N. Estimativa de parâmetros de aquíferos através do coeficiente de recessão em áreas de embasamento cristalino de Minas Gerais. *Rem Rev. Esc. Minas* **2010**, *63*, 465–471. [CrossRef]
29. Amorim, J.D.S.; Junqueira, R.; Mantovani, V.A.; Viola, M.R.; de Mello, C.R.; Bento, N.L. Streamflow regionalization for the Mortes River Basin upstream from the Funil Hydropower Plant, MG. *Ambient. Água* **2020**, *15*, 1–11. [CrossRef]
30. Junqueira Junior, J.A.; Mello, C.R.; Owens, P.R.; Mello, J.M.; Curi, N.; Alves, G.J. Time-stability of soil water content (SWC) in an Atlantic Forest—Latosol site. *Geoderma* **2017**, *288*, 64–78. [CrossRef]
31. Euclydes, H.P.; Ferreira, P.A.; Faria Filho, R.F. *Atlas digital das águas de Minas*, 1st ed.; UFV: Viçosa, Brazil, 2005.
32. Freitas, S.; Bacellar, L. Avaliação da Recarga de Aquíferos em Microbacias do Alto Rio das Velhas, Minas Gerais. *Rev. Bras. Recur. Hídricos* **2013**, *18*, 31–38. [CrossRef]
33. Dai, A.; Zhao, T.; Chen, J. Climate Change and Drought: A Precipitation and Evaporation Perspective. *Curr. Clim. Chang. Reports* **2018**, *4*, 301–312. [CrossRef]
34. Rodrigues, J.A.M.; Viola, M.R.; Alvarenga, L.A.; Mello, C.R.; Chou, S.C.; Oliveira, V.A.; Uddameri, V.; Morais, M.A.V. Climate change impacts under representative concentration pathway scenarios on streamflow and droughts of basins in the Brazilian Cerrado biome. *Int. J. Climatol.* **2019**, 1–16. [CrossRef]
35. Santos, G.L.; Pereira, M.G.; Delgado, R.C.; Magistrali, I.C.; Silva, C.G.; Oliveira, C.M.M.; Teodoro, P.E. Anthropogenic and climatic influences in the swamp environment of the Pandeiros River basin, Minas Gerais-Brazil. *Environ. Monit. Assess.* **2020**, *192*. [CrossRef] [PubMed]
36. Marengo, J.A.; Alves, L.M.; Alvala, R.C.S.; Cunha, A.P.; Brito, S.; Moraes, O.L.L. Climatic characteristics of the 2010-2016 drought in the semiarid northeast Brazil region. *An. Acad. Bras. Cienc.* **2018**, *90*, 1973–1985. [CrossRef] [PubMed]
37. Melo, D.C.D.; Scanlon, B.R.; Zhang, Z.; Wendland, E.; Yin, L. Reservoir storage and hydrologic responses to droughts in the Paraná River basin, south-eastern Brazil. *Hydrol. Earth Syst. Sci.* **2016**, *20*, 4673–4688. [CrossRef]
38. Nobre, C.A.; Marengo, J.A.; Seluchi, M.E.; Cuartas, L.A.; Alves, L.M. Some Characteristics and Impacts of the Drought and Water Crisis in Southeastern Brazil during 2014 and 2015. *J. Water Resour. Prot.* **2016**, *8*, 252–262. [CrossRef]
39. Ramírez, A.; Gutiérrez-Fonseca, P.E.; Kelly, S.P.; Engman, A.C.; Wagner, K.; Rosas, K.G.; Rodríguez, N. Drought facilitates species invasions in an urban stream: Results from a long-term study of tropical island fish assemblage structure. *Front. Ecol. Evol.* **2018**, *6*, 1–11. [CrossRef]
40. Azevedo, S.C.D.; Cardim, G.P.; Puga, F.; Singh, R.P.; Silva, E.A.D. Analysis of the 2012–2016 drought in the northeast Brazil and its impacts on the Sobradinho water reservoir. *Remote Sens. Lett.* **2018**, *9*, 438–446. [CrossRef]
41. Santos, M.S.; Costa, V.A.F.; Fernandes, W.D.S.; de Paes, R.P. Time-space characterization of droughts in the São Francisco river catchment using the Standard Precipitation Index and continuous wavelet transform. *Rev. Bras. Recur. Hidricos* **2019**, *24*, 1–12. [CrossRef]
42. Garreaud, R.D.; Vuille, M.; Compagnucci, R.; Marengo, J. Present-day South American climate. *Palaeogeogr. Palaeoclimatol. Palaeoecol.* **2009**, *281*, 180–195. [CrossRef]

resources

MDPI

Article

The Soil Moisture during Dry Spells Model and Its Verification

Małgorzata Biniak-Pieróg [1,*], Mieczysław Chalfen [2], Andrzej Żyromski [1], Andrzej Doroszewski [3] and Tomasz Jóźwicki [3]

[1] Institute of Environmental Development and Protection, Wrocław University of Environmental and Life Sciences, Plac Grunwaldzki 24, 50-363 Wrocław, Poland; andrzej.zyromski@upwr.edu.pl
[2] Department of Mathematics, Wrocław University of Environmental and Life Sciences, Grunwaldzka Street 53, 50-357 Wrocław, Poland; mieczyslaw.chalfen@upwr.edu.pl
[3] Department of Agrometeorology and Applied Informatics, Institute of Soil Science and Plant Cultivation—State Research Institute, Czartoryskich Street 8, 24-100 Puławy, Poland; ador@iung.pulawy.pl (A.D.); tjozwicki@iung.pulawy.pl (T.J.)
* Correspondence: malgorzata.biniak-pierog@upwr.edu.pl

Received: 19 May 2020; Accepted: 7 July 2020; Published: 9 July 2020

Abstract: The objective of this study was the development and verification of a model of soil moisture decrease during dry spells—SMDS. The analyses were based on diurnal information of the occurrence of atmospheric precipitation and diurnal values of soil moisture under a bare soil surface, covering the period of 2003–2019, from May until October. A decreasing exponential trend was used for the description of the rate of moisture decrease in six layers of the soil profile during dry spells. The least squares method was used to determine, for each dry spell and soil depth, the value of exponent α, which described the rate of soil moisture decrease. Data from the years 2003–2015 were used for the identification of parameter α of the model for each of the layers separately, while data from 2016–2019 were used for model verification. The mean relative error between moisture values measured in 2016–2019 and the calculated values was 3.8%, and accepted as sufficiently accurate. It was found that the error of model fitting decreased with soil layer depth, from 8.1% for the surface layer to 1.0% for the deepest layer, while increasing with the duration of the dry spell at the rate of 0.5%/day. The universality of the model was also confirmed by verification made with the use of the results of soil moisture measurements conducted in the years 2009–2019 at two other independent locations. However, it should be emphasized that in the case of the surface horizon of soil, for which the process of soil drying is a function of factors occurring in the atmosphere, the developed model may have limited application and the obtained results may be affected by greater errors. The adoption of calculated values of coefficient α as characteristic for the individual measurement depths allowed calculation of the predicted values of moisture as a function of the duration of a dry spell, relative to the initial moisture level adopted as 100%. The exponential form of the trend of soil moisture changes in time adopted for the analysis also allowed calculation of the duration of a hypothetical dry spell t, after which soil moisture at a given depth drops from the known initial moisture θ_0 to the predicted moisture θ. This is an important finding from the perspective of land use.

Keywords: soil moisture; dry spells; time domain reflectometry; moisture decrease model; Poland

1. Introduction

Soil water resources play an important role in the water cycle in the plant-soil-atmosphere system, and particularly in the surface layer of soil [1–5]. This system affects energy flux and supplies water vapor to the atmosphere as a result of the process of evaporation from bare soil, or evapotranspiration from areas covered with vegetation of diverse kinds. This leads to the exhaustion of water resources in

soil, while supplying the atmosphere with water vapor, thereby creating the basis for the formation of precipitation, which is the main source of the water supply of the soil profile independently of human influence. The important elements are the amount of precipitation, its intensity, and its distribution in time. The effect of precipitation is particularly visible in the surface layer of soil, where moisture exhibits a significant variation over time and decreases with greater depths [6–9]. As soil moisture is a key variable in the climate system, it plays a major role in climate change projections [5]. As a consequence of predicted global warming, changes in terrestrial water storage are expected [10–13]. As reported by Giorgi et al. [14] an increase of the intensity of precipitation and of the duration of non-rainfall periods, with simultaneous limitation of the reach of precipitation and shortening of the duration of wet periods, can have an impact on the time, location, and availability of water. As follows from the study by Huang et al. [15], at a global scale, arid areas could constitute more than 50% of the Earth's total landmass, the majority of which could be found in developing countries.

According to Grillakis [16], changes to soil water resources in the European region are expected as a consequence of predicted climate change. In this regard, in recent years, the occurrence of increasingly long series of rainless days, lasting for as long as several weeks, have been observed, representing atmospheric anomalies. The direct effect of such events is a disturbed water balance in a given area, caused by rainfall deficit, which leads to the occurrence of the phenomenon of so-called atmospheric drought (also called meteorological drought). Poland is situated in a zone of a moderate climate of the transitional type, and destructive droughts occur within its territory, causing a depletion of water resources and, thus, a major economic, environmental, and societal problem. According to the climate-soil moisture regime described by Budyko (after [2,5]), the region belongs to a transitional climate regime, where soil moisture constrains evapotranspiration variation. Drought occurs in Poland at several-year intervals, and results in serious economic losses.

Agriculture is the most sensitive element of the economy in many countries. Atmospheric drought lasting for several weeks results in the exhaustion of water resources in the soil, which leads to the appearance of a soil drought. In such conditions, the growth of plants is hampered; thus a distinct drop in soil water resources is later reflected in low yields of crop plants [17,18]. The occurrence of soil drought can be accelerated or delayed by individual properties of soil, in particular, its particle size distribution. In the case of heavy soils, in which capillary rise replenishes water resources in the root zone from deeper layers, that process delays the occurrence of soil drought. In light gavel and sandy soils, no such possibilities exist, and soil drought will appear much sooner. Rainfall deficit causes strong crusting of the surface layer of soil, hindering the infiltration of water into deeper soil layers, in which the rate of infiltration is dependent on the moisture status of the soil [19–21]. In agriculture, it is difficult to clearly separate soil drought from agricultural drought. In the simplest terms, soil drought is treated as a deficit of soil water for plants, while the effect on plant growth is taken into account in the case of agricultural drought [17].

Droughts are a threat to correct plant growth and development, but studies conducted by the authors of the present paper indicate that the occurrence of non-rainfall periods in certain inter-phase periods of crop plants can have a positive effect in the form of increased yields [22–24]. However, droughts represent a primary threat to the water balance of a given area. Among the relevant variables relating to drought impacts, the intensity of atmospheric drought occurrence is the easiest to estimate. Input data used in the calculation of a meteorological drought index are predominantly total precipitation and, less frequently, evaporation. Due to information availability, the most frequently used indicators for the estimation of meteorological drought are the series of non-rainfall days, relative precipitation index (RPI), effective drought index (EDI), climatic water balance (CWB), or standardized climatic water balance (SCWB), and the well-known and commonly used Sielianinov coefficient [25–32]. At the global scale, many indices for the estimation of meteorological drought exist, but the most frequently used is the standardized precipitation index (SPI), based on atmospheric precipitation. This index allows both short- and long-term prediction of the effects of drought and permits comparative analyses of drought intensity in various regions of the world [33–37].

Due to the fact that direct measurements of soil moisture are time and labor consuming, as well as costly, many indirect methods are used for the identification and estimation of the intensity of soil drought. Such indices are formulated on the basis of meteorological factors and soil moisture conditions for various time intervals, and, in the case of crop plants, for the periods between different plant development phases. The most sensitive interphase periods for crop plants are referred to as the critical periods. Indices based on the meteorological elements allow the identification of periods of potential drought threat, which does not always translate directly into soil drought. In turn, indices based on soil moisture require direct measurements, with short time periods, e.g., one day. Such a short time interval requires costly specialized equipment, and, for this reason, the measurements are usually made at the scale of a single measurement point. As reported by Łabędzki and Bąk [27], the most popular indices of this type used globally include the crop drought index (CDI), soil moisture index (SMI), crop yield reduction (CYR), Palmer drought severity index (PDSI), crop moisture index (CMI), Z index, drought severity index (DSI), and soil moisture deficit index (SMDI) [16,38–43], amongst many others. Their detailed review, together with description of the required input data and of application limitations, is given in the Word Meteorological Organization (WMO) manual. In spite of such a large number of existing tools, research continues to be undertaken to develop new indices, and into possibilities for their use for the estimation of meteorological drought and the occurrence of soil drought [44–47]. Independently from that direction of research, complex models have also been developed, allowing the estimation of soil moisture on the basis of a broad spectrum of meteorological elements and soil characteristics [48–51]. In the search for methods of estimation of the spatial occurrence of soil drought, remote sensing techniques have also been employed [52–58].

Nonetheless, methods developed and used to date, despite their numerous advantages, have limitations, as they do not provide information on the actual status of soil moisture during dry spells. Such information can only be obtained at the cost of labor-consuming field measurements, as changes in soil moisture relate to the impact of atmospheric conditions and plant cover, and are determined by the retention capacity of soil, which, in turn, is a function of the soil particle size distribution. Twenty-four-hour monitoring of the state of soil moisture under bare soil as a reference surface has been conducted since 2003 at the Institute of Environmental Development and Protection, Wrocław University of Environmental and Life Sciences, Poland. The reference status of this surface results from the fact that the bare surface directly intercepts the effect of atmospheric elements and is the background for assessing the impact of plant cover on soil water balance. Studies on soil moisture under bare soil have been conducted for years in many research centers [59–62].

Given the above, the objective of the current study was the development and verification of a model of soil moisture decrease during dry spells (SMDS). The analyses were based on diurnal information on the occurrence of atmospheric precipitation and diurnal values of soil moisture under bare soil. These allowed the development of a simple mathematical model describing the rate of moisture decrease in the soil profile at various depths during dry spells. Theoretical mathematical models describing soil moisture, based on a deterministic description of the phenomenon, such as the Richards equation, e.g., [63], are frequently used. The diffusion coefficient in the Richards equation depends on soil characteristics. However, these models require continuous measurement of soil moisture in the surface layer (boundary condition), or the artificial assumption that soil moisture on the surface is constant, invariable over time. In this paper, the authors' intention was to find an operational model of soil moisture decrease only on the basis of the duration of dry spells, eliminating the need for conducting soil moisture measurements. This type of model is much easier to apply in agricultural practice. The developed model is a methodological contribution for further analysis taking into consideration plant-covered surfaces, e.g., those covered by grass.

2. Materials and Methods

2.1. Site Description

Soil moisture measurements were conducted in the area of the Faculty Agro and Hydrometeorology Observatory, Wrocław University of Environmental and Life Sciences, Poland, during the summer half-year (May until October), in the years 2003–2019. Data from 2003–2015 (13 years) were used to determine the model parameter, while those from 2016–2019 (4 years) were used to verify the model. The observatory is situated in the north-eastern part of the city, and is separated from the urban heat island by a complex of parks, stadiums, meadows, and fields, and the Odra-Widawa Canal (Figure 1). The observatory is situated at an elevation of 120.7 m a.s.l., latitude 51°07′, longitude 17°07′.

Figure 1. Location of the Faculty Agro and Hydrometeorology Observatory, Wrocław University of Environmental and Life Sciences, and stations used for additional verification: Jelcz Laskowice and Baborówko.

In addition, for model verification, the authors used data from soil moisture measurements conducted in the period 2009–2019 (11 years) at two other locations: Jelcz Laskowice (Dolnośląskie Province, ca. 25 km south-east from Wrocław, 51°02′07″ N, 17°20′28″ E) and Baborówko (Wielkopolskie Province, ca. 150 km north from Wrocław, 52°35′09″ N, 16°37′54″ E) (Figure 1). These stations are included in the network of soil moisture measurements within the scope of the Agricultural Drought Monitoring System (ADMS) in Poland, conducted by the Institute of Soil Science and Plant Cultivation—State Research Institute (IUNG-PIB) on behalf of the Ministry of Agriculture and Rural Development.

2.1.1. Soil

In the surface layers, the soils in the area of the observatory are characterized by the occurrence of fine-grain loamy sands, which in deeper layers change to weakly loamy and loose sands with intrusions of mainly loamy sands and sandy loams (Table 1). The sand layer has thickness from 90 to 150 cm overlaying the loam. At the depth of 100–120 cm, the soils are completely saturated with water for several months a year. Periodically, as a result of capillary rise or in periods of intense rainfall, the saturation can reach the level of 50–70 cm below the surface of the ground. Typologically, the soils

are proper fluvisols. In the international classification of FAO-WRB [64], these are cultured soils with preserved features of alluvial deposits. Most frequently, they are classified in the group of Phaeozems (Fluvic Gleyic Phaeozems (Anthric, Arenic)). Total porosity of the soils is in the range of 40–45%. Hydraulic conductivity in the sandy layers varies from 2.9×10^3 to 4.6×10^3 cm/s, while in the sandy loam at the depth of 120–150 cm, it attains the lowest value of 1.9×10^3 cm/s. The soils in the area of the observatory are characterized by low retention capacity. The field water capacity in the sandy layers with suction force pF = 2.0 varies from 6.0% to 12.5% [65].

Table 1. Particle size distribution (PSD) of the soils in the area of the observatory [65].

Depth	Percentage Share of Fraction With Diameter (mm)									PSD Group
cm	>2	2.0–1.0	1.0–0.5	0.5–0.25	0.25–0.1	0.1–0.05	0.05–0.02	0.02–0.002	<0.002	
0–28	0	2	8	23	42	8	8	7	2	loamy sand
28–39	0	1	9	24	43	6	10	6	1	loamy sand
39–77	0	2	9	20	48	11	6	3	1	weakly-loamy sand
77–106	0	2	16	33	43	2	2	1	1	loose sand
106–122	2	4	17	23	42	3	1	1	9	loose sand
122–150	2	1	5	18	35	7	7	9	18	sandy loam

2.1.2. Agroclimate

Characterization of the agrometeorological conditions in the area of the observatory was conducted on the basis of the normative multi-year period of 1971–2000, due to the fact that the currently valid norm recommended by WMO—that is, the 30-year period of 1981–2010—includes the years adopted for the analyses [66]. Figure 2 presents the characteristics of the summer half-years adopted for the analyses. The characteristics include such elements as air temperature, atmospheric precipitation, and the level of the ground water table.

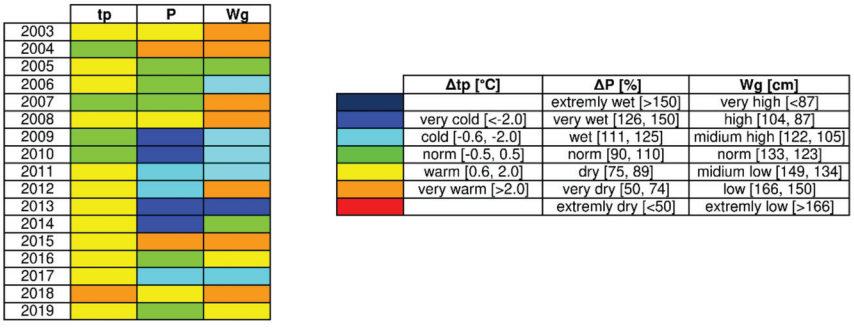

Figure 2. Agrometeorological characterization (air temperature, tp; precipitation, P; ground water level, Wg) of the summer half-year in the years 2003–2019 in relation to the normative multi-year period of 1971–2000.

The mean half-year values of air temperature, with the exception of 2018, were characterized by small variation, as they varied from 15.1 °C in 2007 and 2010 to 16.5 °C in 2006. The exception was the mentioned 2018, with an average temperature of 17.6 °C, classified as a very warm period. In a vast majority of cases, deviations from the norm for the multi-year period of 1971–2000 of 14.8 °C [67] were classified as warm periods. Only in the years 2004, 2007, 2009, and 2010 did the values of the deviations not exceed 0.5 °C, and thus corresponded to normal conditions.

The analyzed summer half-years were characterized by notably greater variation of the rainfall conditions, which basically results from the random character of this factor and its large variation year to year. The half-year precipitation totals varied from 259 mm in 2004 and 264 mm in 2015, to 541 mm

in 2013, while the mean value for the normative multi-year period is 369 mm. Their interpretation was conducted on the basis of the RPI (relative precipitation index) [27]. As can be seen in Figure 2, the period adopted for the analyses covered years with precipitation totals conforming to the norm, as well as years with either a precipitation deficit or excess. Note should be taken of the outstanding period of 2009–2014, with an accumulation of summer half-years with precipitation totals corresponding to wet and very wet periods, and the period of 2005–2007 with normal precipitation totals.

The depths of the ground water table level were characterized on the basis of the norm proposed by Biniak-Pieróg [59]. From the ground surface, the mean half-year depths of the ground water table level varied from 164 cm in 2008 and 2018 to 100 cm in 2013, and the mean multi-year value was 126 cm. The most frequently observed were half-year periods with ground water levels corresponding to low states (7 cases), followed by medium-high states (5 cases).

The summer half-years of 2016–2019 adopted for verification of the model parameter were characterized by variability of the agrometeorological conditions, in particular, taking into account rainfall conditions (Figure 2). They included both warm periods with excess precipitation and a medium-high groundwater level (2017), or warm periods with normative precipitation but a medium-low groundwater level (2016 and 2019).

2.2. Data

The analyses were based on diurnal values of soil moisture under the bare surface, adopted as the reference surface, and information on the occurrence of atmospheric precipitations. Soil moisture was measured every day, at the time of morning observations, i.e., at 6.00 UTC, in the hydrological summer half-year, lasting 1 May–31 October, in the years 2003–2019, using the TDR (time domain reflectometry) method. This approach is one of the most modern methods of measurement, consisting of the generation of an electromagnetic wave pulse, which, entering the analyzed medium—in this case, soil—is reflected, and recording of the moment of return of the attenuated reflected pulse. The value of attenuation of the reflected wave that is returned depends primarily on the content of water in the soil, in addition to the concentration of electrolytes and the content of clays [68]. The main advantages of the method include its high temporal and spatial resolution; high measurement accuracy, reaching 1–2% of volumetric moisture; minimized calibration requirements; zero risk of radiation, as is the case when using the gammametric or neutron methods; and the possibility of conducting continuous, rapid, and non-destructive measurements with any chosen time interval [69,70]. In the current study, a modern apparatus was used, in the form of TDR/MUX/mpts instruments and data loggers MIDL_GPRS for field installation, the sole manufacturer of which in Poland is the Institute of Agrophysics PAS in Lublin [71]. These instruments allow continuous measurement of soil moisture, temperature, and salinity at the same point. They work together with a set of TDR probes installed at depths of 10, 20, 30, 40, 50, 60, 80, and 100 cm under the bare soil surface (Figure 3), calibrated at the beginning of each measurement season by means of the software provided by the manufacturer [71].

Figure 3. Measurement of soil moisture with the use of TDR/MUX/mpts and MIDL_GPRS data acquisition loggers at the Faculty Agro and Hydrometeorology Observatory.

Soil moisture values in the layers of 0–10, 10–20, 20–40, 40–60, 60–80, and 80–100 cm were used for the analyses, for the summer half-years of 2003–2019. Table 1 presents the extreme and mean values of soil moisture from the layers adopted for the analyses. The years in which the lowest values were observed are differentiated in relation to the soil layer. For the surface layers of 0–10 and 10–20 cm, the lowest values of soil moisture were noted in 2004 at 0.019 and 0.035, respectively. This year was classified as very dry, with the ground water table at low states (Figure 2). Whereas, for the layers of 20–40 and 40–60 cm, the lowest values of soil moisture were noted in 2003—a warm and dry year, with a low state of the ground water table at 0.052 and 0.062, respectively. In the case of the deepest layers of 60–80 and 80–100 cm, the lowest values were observed in 2015 and 2016, respectively. In this case, the medium-low and low states of the ground water table were important. Irrespective of the analyzed soil layer, under bare soil, the maximum values were observed in 2013. This was a normal half-year in terms of air temperatures, and with above-norm rainfalls corresponding to a very wet period with a medium state of the ground water table. In addition, in several preceding years, the summer half-years were characterized by above-norm rainfalls and ground water table states, which allowed replenishment of the water resources in the soil profile, and their maintenance (Table 2).

Table 2. Extreme and average values of soil moisture in summer half-years in the period of 2003–2019.

		Soil Depth (cm)					
		0–10	**10–20**	**20–40**	**40–60**	**60–80**	**80–100**
2003	min	0.022	0.045	0.052 *	0.062 *	0.085	0.102
	max	0.078	0.091	0.084	0.093	0.124	0.185
	average	0.047	0.063	0.066 *	0.073 *	0.102	0.122
2004	min	0.019 *	0.035 *	0.062	0.087	0.087	0.101
	max	0.080	0.083	0.116	0.164	0.169	0.209
	average	0.038 *	0.053 *	0.087	0.111	0.120	0.136
2005	min	0.022	0.045	0.091	0.103	0.114	0.124
	max	0.134	0.101	0.133	0.157	0.171	0.215
	average	0.058	0.066	0.103	0.122	0.137	0.159
2006	min	0.035	0.039	0.078	0.087	0.107	0.128
	max	0.158	0.102	0.165	0.177	0.198	0.232
	average	0.065	0.061	0.102	0.115	0.141	0.171
2007	min	0.033	0.070	0.096	0.092	0.104	0.126
	max	0.109	0.131	0.141	0.137	0.155	0.182
	average	0.055	0.089	0.111	0.108	0.122	0.145
2008	min	0.062	0.060	0.092	0.113	0.138	0.153
	max	0.116	0.101	0.152	0.190	0.214	0.235
	average	0.076	0.072	0.105	0.131	0.158	0.179
2009	min	0.054	0.055	0.108	0.133	0.161	0.181
	max	0.216	0.280	0.267	0.257	0.255	0.258
	average	0.086	0.090	0.142	0.167	0.187	0.202
2010	min	0.057	0.074	0.110	0.132	0.158	0.176
	max	0.309	0.296	0.281	0.270	0.273	0.272
	average	0.100	0.118	0.151	0.171	0.191	0.204
2011	min	0.042	0.061	0.065	0.088	0.120	0.152
	max	0.183	0.197	0.315	0.296	0.299	0.299
	average	0.086	0.097	0.095	0.121	0.153	0.179
2012	min	0.065	0.061	0.072	0.078	0.097	0.118
	max	0.161	0.157	0.129	0.135	0.154	0.176
	average	0.080	0.078	0.083	0.087	0.107	0.133

Table 2. *Cont.*

		Soil Depth (cm)					
		0–10	**10–20**	**20–40**	**40–60**	**60–80**	**80–100**
2013	min	0.070	0.072	0.083	0.091	0.129	0.154
	max	0.329 *	0.309 *	0.321 *	0.328 *	0.310 *	0.305 *
	average	0.124 *	0.135 *	0.152 *	0.177*	0.187	0.197
2014	min	0.066	0.068	0.076	0.089	0.101	0.111
	max	0.103	0.107	0.109	0.124	0.162	0.172
	average	0.081	0.082	0.088	0.101	0.114	0.125
2015	min	0.051	0.050	0.062	0.067	0.078	0.081 *
	max	0.140	0.095	0.089	0.085	0.098	0.112
	average	0.066	0.063	0.070	0.073	0.087 *	0.097 *
2016	min	0.051	0.052	0.058	0.066	0.072 *	0.108
	max	0.084	0.082	0.088	0.132	0.160	0.188
	average	0.066	0.065	0.070	0.099	0.116	0.144
2017	min	0.053	0.071	0.063	0.093	0.168	0.235
	max	0.102	0.122	0.100	0.161	0.249	0.275
	average	0.065	0.090	0.081	0.117	0.213	0.260
2018	min	0.064	0.061	0.101	0.128	0.175	0.177
	max	0.154	0.141	0.139	0.165	0.243	0.256
	average	0.085	0.093	0.108	0.141	0.202	0.221
2019	min	0.076	0.076	0.089	0.139	0.193	0.204
	max	0.170	0.140	0.157	0.224	0.258	0.245
	average	0.109	0.096	0.107	0.159	0.215 *	0.225

* absolute values.

Diurnal information on atmospheric precipitation was acquired by means of the standard Hellmann rain gauge. With regard to the scope of the analyses, the important information was the occurrence or lack of atmospheric precipitation. The number of non-rainfall days varied from 80 in the very wet summer half-year of 2012 to 121 in the dry half-year of 2018. Due to the random character of rainfall and its high variation, the number of days with no rainfall did not correspond with the characteristics of the precipitation conditions. For example, similar numbers of non-rainfall days (approximately 110) were observed in a normal year (2006), a dry year (2015), and a wet year (2011).

The information acquired as described above was the basis for the determination of the start and end points of non-rainfall periods. It was assumed that a series of non-rainfall days was defined as 1 day with rainfall below 1 mm or 2 successive days with combined precipitation total below 1 mm, while one day with precipitation of 1 mm and above was not counted as belonging to such a series [72]. The diurnal values of the moisture of bare soil were referenced to the series of non-rainfall days determined in this way for each of the 6 soil layers from 0–10 to 80–100 cm.

2.3. Exponential Model SMDS

The soil moisture decrease in dry spells can be described by means of various relationships. The adoption of the simplest linear relationship between soil moisture and the duration of a dry spell is equivalent to the hardly acceptable assumption that the decrease of moisture on every day is constant and independent of the initial soil moisture of that day. In addition, when constructing a longer forecast of soil moisture based on the decreasing linear trend, one could obtain negative values of soil moisture. Similar problems are encountered in the case of polynomial and exponential models—lack of physical foundations and lack of monotonicity of solutions for longer time horizons. In addition, the authors wanted to create a model that would not be overly complicated while also being universally applicable, and that would describe the decrease of the moisture of bare soil for various locations with similar soil and atmospheric conditions by means of a single functional relationship with parameters that have

subject-matter justification. Such initial assumptions are met by a single-parameter exponential model. It has a substantiated physical basis (Equation (1)), the single parameter of the model has a clear physical interpretation, and the model produces credible monotonic solutions and is universally applicable.

In consideration of these factors, a decreasing exponential trend was applied for the description of the rate of soil moisture decrease during dry spells, for each of the six layers of 0–10, 10–20, 20–40, 40–60, 60–80, and 80–100 cm. The exponential form of the trend results from the prior assumption adopted that the value of the diurnal drop of soil moisture is proportional to the initial moisture of each day, according to the formula:

$$\theta(t+1) - \theta(t) = k \cdot \theta(t), \tag{1}$$

where:

$\theta(t)$—volumetric moisture (-),
t—time (day), and
k—coefficient of proportionality, $-1 < k < 0$.

Coefficient k is negative because soil moisture decreases during dry spells. Similarly, $k > -1$ because the decrease of moisture during one day cannot be greater that the moisture at the beginning of this day.

The truth of the assumption of a linear relationship between the moisture drop and the initial moisture according to Equation (1) is substantiated statistically in Section 3.2.

From the assumption of Equation (1), one can infer the exponential form of soil moisture as a function of time:

$$\theta(t) = \theta_0 e^{-\alpha t}, \tag{2}$$

where θ_0—moisture on the initial day of the dry spell, and:

$$\alpha = -\ln(1+k). \tag{3}$$

Coefficient $\alpha > 0$ is a numerical characteristic of the rate of moisture decrease: α close to zero means that the rate of moisture decrease is very low, $\alpha = 0$ would mean that soil moisture does not decrease at all during a dry spell and is constant. On the other hand, an increase of the value of parameter α characterizes a dynamic decrease of soil moisture during a dry spell. Coefficient α characterizes the kind of soil, and in this paper, a method is proposed for its determination for each soil layer separately.

For further analysis, only those dry spells were selected that lasted at least 10 days. For each dry spell and for each soil layer separately, the value of α was determined with the method of least squares, minimizing the value of the root of the mean square error (RMSE) according to the formula:

$$\partial_d(\alpha) = \sqrt{\frac{1}{n}\sum_{i=1}^{n}(obs_d - cal_d(\alpha))^2}, \tag{4}$$

where:

$\partial_d(\alpha)$—RMSE,
n—dry spell duration (days),
obs_d—*moisture* measurement at depth d (-), and
$cal_d(\alpha)$—*moisture* at depth d (-) calculated from Equation (2).

Data from the years 2003–2015 were used for the identification of parameter α of the model for each soil layer separately, while independent data from 2016 to 2019 were used for model verification.

Additionally, in the following section of this article, a mean absolute percentage error (*MAPE*) is calculated according to the formula:

$$MAPE = \frac{1}{n}\sum_{i=1}^{n}\frac{|obs_i - cal_i|}{obs_i}100\%. \quad (5)$$

3. Results

3.1. Characterization of Dry Spells

In the years 2003–2015, there were 39 series of observations covering dry spells lasting at least 10 days, but their frequency in the individual months of the year was not uniform (Table 3).

Table 3. Number of dry spells in particular months of the summer half-year.

Months	V	VI	VII	VIII	IX	X
Number of dry spells	8	4	3	3	12	9

The largest number of dry spells was noted in the spring and autumn months (May, September, and October), and the smallest in the summer (June to August). In addition, the duration distribution of individual dry spells was not homogeneous. Notably, the largest number of dry spells lasted for 10–12 days, with the longest lasting for 38 days (Figure 4). The mean duration of dry spells within the analyzed group of dry spells of at least a 10-day duration was 13.67 days.

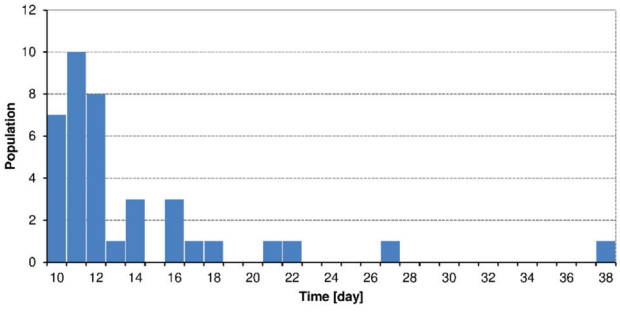

Figure 4. Histogram of dry spell duration.

In each dry spell, soil moisture in the analyzed layers, with a few exceptions, decreased monotonously with the passage of time (Figure 5).

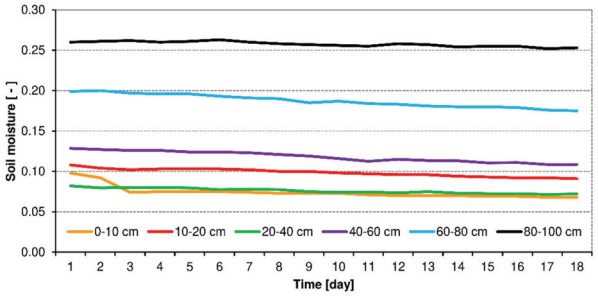

Figure 5. Decrease of soil moisture on consecutive days and sequential soil layers for an exemplary dry spell lasting 18 days.

Appendix A presents soil moisture characteristics for the individual dry spells, i.e., soil moisture on the first day of the dry spell (SMb), % decrease of soil moisture in relation to the initial value (SM%), and % decrease of soil moisture per day (SM%/d). The infrequent negative values (in bold) mean that, during a dry spell, the final value of moisture was higher than the initial value. Such a situation occurs sporadically at greater depths, where the effect of changes of the ground water table on soil moisture in the aeration zone becomes observable. Table 4 presents average values and standard deviations of SM% and SM%/d for the soil depths adopted for the analyses.

Table 4. Average values and standard deviations of SM% and SM%/d for the analyzed soil depths.

Soil Layer (cm)	0–10	10–20	20–40	40–60	60–80	80–100
SM%	26.20	15.93	7.69	5.07	2.38	2.99
SM%/d	2.10	1.26	0.62	0.39	0.19	0.23
St. dev SM%	12.62	10.93	7.77	4.08	3.80	4.78
St. dev SM%/d	1.20	0.99	0.72	0.29	0.28	0.38

3.2. Statistical Substantiation of Assumption (Equation (1))

The truth of the assumption of the linear character of Equation (1) was statistically substantiated. For each of the 39 dry spells and for each of the 6 analyzed soil layers, the coefficient of correlation r between the initial moisture of each day $\theta(t)$ and moisture decrease during one day $\theta(t+1) - \theta(t)$ was calculated. The mean values of r for the depths and the statistics of the student's t-test used for testing the significance of the coefficient of correlation are given in Table 5.

Table 5. Mean values of r for the adopted soil depths and the statistics of the student's t-test used for testing the significance of the coefficient of correlation.

Soil Layer (cm)	0–10	10–20	20–40	40–60	60–80	80–100	Average
Correlation coefficient r	0.66	0.48	0.41	0.31	0.41	0.46	0.46
Student's t-test	4.22	2.37	1.73	1.21	1.80	1.91	2.21

The limit value of the student's t-test statistic for the mean dry spell duration of 13.67 days at a significance level of 0.05 is 2.15, and at a significance level 0.1, it is 1.76. In the conducted correlation analysis, the mean value of the t-test statistic for all dry spells was 2.21, which, at the significance level 0.05, confirms the significance of the coefficient of correlation, and thus confirms the initial assumption in Equation (1). Only in the case of the layer of 40–60 cm was the assumption of linear correlation not met at a significance level of 0.1.

3.3. Identification of the SMDS Model Parameter

In the next stage of the study, for each dry spell and for each soil layer, in accordance with Equation (4), coefficient α in Equation (2) was determined, which describes the rate of moisture decrease. The variation of coefficient α for each of the 39 dry spells for the analyzed soil layers is illustrated in Figure 6.

At this point, it is worthwhile to explain the cause of the very high values of coefficient α for dry spells 11 and 12 (see Figure 6a). These were 10-day dry spells, which started on 11 June 2013 and 30 June 2013. On 9 June 2013, a very strong rainfall was noted, amounting to 28.4 mm, which resulted in a high increase of moisture in the surface horizon of the soil. In the case of dry spell 11, this value was 0.0329, and for dry spell 12, 0.0245. In the summer months, the moisture in the soil layer of 0–10 cm usually did not exceed 0.01 at the start of a dry spell. In consequence, the moisture in the soil layer of 0–10 cm decreased during the 10 days of dry spell 11 by 49%, and, in the case of dry spell 12,

by 48%. Similarly, high decreases of soil moisture were noted in the layers of 10–20 cm (45% and 43%, respectively, for dry spell 11 and 12), 20–40 cm (41% and 35%, respectively, for dry spell 11 and 12).

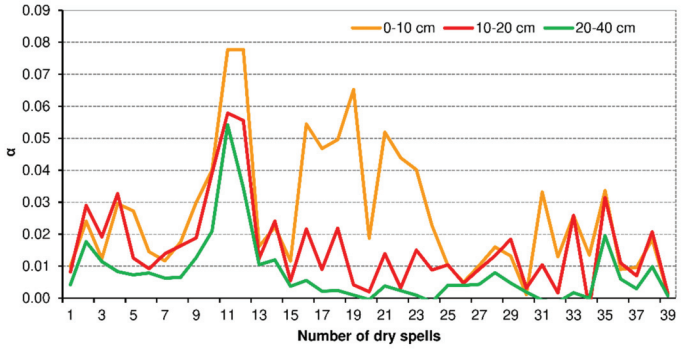

(**a**)

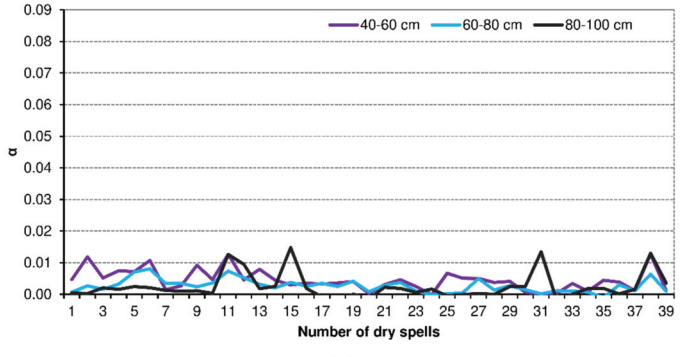

(**b**)

Figure 6. Fluctuation of coefficient α at the adopted soil layers: (**a**) 0–10, 10–20, 20–40 cm; (**b**) 40–60, 60–80, 80–100 cm.

The greatest variation of parameter α was noted for the layer of 0–10 cm, and the oscillations of coefficient α decreased with increasing depth. This supports the decrease of moisture variation with depth. Detailed values are given in Table 6. The third column presents the mean values of coefficient α, which are adopted in a later analysis of this paper as a characteristic of the particular depths in the soil profile. Table 7 presents the decrease of the values of the correlation coefficient r with increasing depth in the soil profile.

Table 6. Values of the coefficient α at subsequent measuring depths.

Soil Layer (cm)	Variability of Coefficient α	Mean Values of Coefficient α
0–10	0.02–0.08 (VI–VIII) <0.03 (V, IX, X)	0.0426 0.0208
10–20	0.01–0.03 (VI 0.055)	0.0159
20–40	<0.01 (VI 0.055)	0.0077
40–60	<0.01	0.0045
60–80	<0.01	0.0027
80–100	<0.01	0.0025

Table 7. Mean values of correlation coefficient r between the model and the measured values and standard deviations with the adopted soil depth.

Soil Layer (cm)	0–10	10–20	20–40	40–60	60–80	80–100
Correlation coefficient r	0.89	0.87	0.78	0.81	0.75	0.60
Standard deviation	0.19	0.28	0.32	0.30	0.31	0.33

Due to the large variation of parameter α obtained for the surface horizon of the soil, in particular the layer of 0–10 cm (Figure 6a), two mean values of this parameter were calculated for that soil layer: $\alpha = 0.0208$ for the months of May, September, and October, and for the typically summer months of June–August, the calculated value was $\alpha = 0.0426$.

For each of the 39 dry spells, the correlation coefficient r was also determined, for the correlation between the soil moisture calculated from Equation (2) and the series of measured moisture values, for each soil layer separately. For each soil depth, a significant correlation was obtained between the model and the measured values ($r > 0.60$), with mean values of r decreasing with depth (Table 7). This indicates that the soil moisture in soil layers down to 60 cm is strongly dependent on moisture conditions on the surface of the ground. At depths from 60 to 100 cm, the meteorological conditions on the ground surface play a lesser role, although they are still statistically significant. At these depths, the effect of the ground water table becomes apparent, but this was not taken into account in the model.

Detailed results of parameter α identification and approximation errors are given in Table 8.

Table 8. Detailed results of parameter α identification and approximation errors.

Soil Layer (cm)	0–10	10–20	20–40	40–60	60–80	80–100
α	0.0208 (V, IX, X) 0.0426 (VI–VIII)	0.0159	0.0077	0.0045	0.0027	0.0025
r	0.892	0.866	0.782	0.806	0.746	0.601
MAPE (%)	2.936	1.364	0.777	0.551	0.526	0.837
RMSE	0.003	0.002	0.001	0.001	0.001	0.002

It is worth noting that *MAPE* (Equation (5) did not exceed 10% for any dry spell and any soil layer. It can be assumed, therefore, that the values of parameter α given in Tables 5 and 7 describe the dynamics of moisture decrease during dry spells well.

3.4. Verification of SMDS Model

Model verification was performed following two pathways:

1. With the use of independent moisture measurements, conducted at the same points as the measurements used for the construction of the model, in the area of the Faculty Agro and Hydrometeorology Observatory of the Wrocław University of Environmental and Life Sciences, taken in 2016–2019; and
2. With the use of moisture measurements of bare soil, taken at the two additional measurement locations, i.e., Jelcz Laskowice and Baborówko (Section 2.1), in the years 2009–2019.

3.4.1. Verification Based on Data from Wrocław (Faculty Agro and Hydrometeorology Observatory)

During the 4-year period 2016–2019, 12 dry spells of at least 10 days were identified, according to the adopted methodology. Figure 7 presents the dependences between the measured and calculated values.

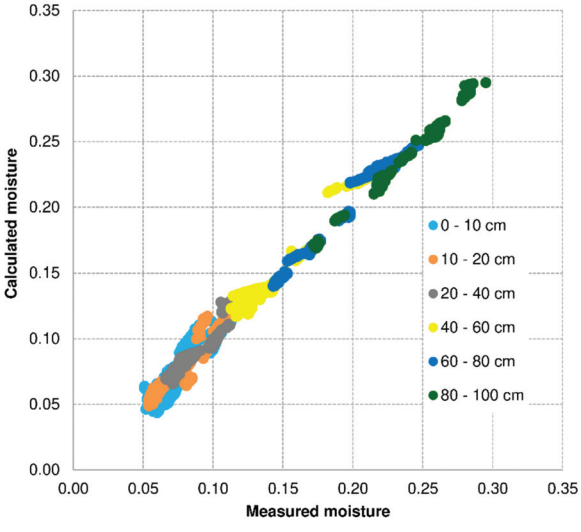

Figure 7. Dependences between the measured and calculated values of soil moisture for the verified years 2016–2019 for Wrocław.

Table 9 presents the values of *MAPE* (%) for each measurement depth separately and the mean value for the entire soil profile, calculated with the use of the data from measurements conducted in the area of the Faculty Agro and Hydrometeorology Observatory.

Table 9. Variability of *MAPE* (%) and parameters of regression and correlation with depths for verified dry spells for Wrocław.

Soil Layer (cm)	0–10	10–20	20–40	40–60	60–80	80–100	Mean
MAPE (%)	8.1	5.3	3.7	3.0	2.1	1.0	3.8
a	1.13	1.09	1.06	1.09	1.09	1.04	1.08
b	−0.01	−0.01	−0.00	−0.01	−0.01	−0.01	−0.01
r^2	0.83	0.93	0.91	0.95	0.98	0.99	0.93

a, b—parameters of regression line Cal = a × Obs + b; Cal—calculated moisture; Obs—measured moisture; r^2—square of correlation coefficient.

The *MAPE* error for all soil layers between moisture values observed in these years and values calculated using Equation (2) was 3.8%. This value was accepted as sufficiently accurate. It was found that the model fitting error decreased with the soil layer depth, from 8.1% for the surface layer to 1.0% for the deepest layer (Table 9). In other words, the accuracy of the exponential model improves with depth in the profile. This results from moisture stabilization at greater soil depths during dry spells. At the same time, the fitting error increased with the duration of the dry spell, at the rate of about 0.5%/day (Figure 8).

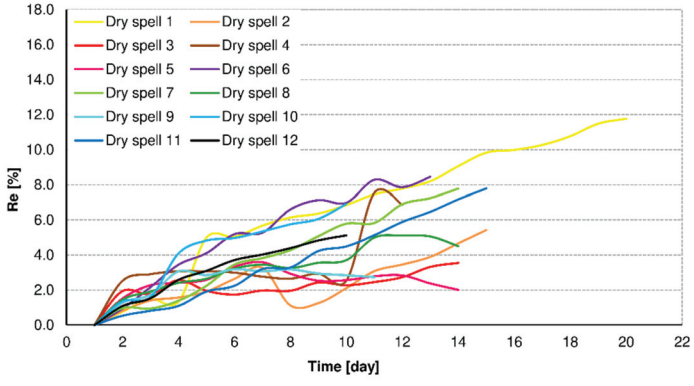

Figure 8. Variability of relative errors $Re = \frac{|Cal-Obs|}{Obs} \cdot 100\%$ with time for verified dry spells for Wrocław.

The drastic increase of the relative error *Re* (%) for dry spell 4 between days 10 and 11 of its duration was caused by sporadic errors in the measurement data. In this case, the measuring apparatus recorded a high decrease of the soil moisture between days 10 and 11 of the duration of the dry spell (i.e., between15 and 16 September 2016) only in the layers of 0–10 and 40–60 cm. It is surprising that in the remaining layers, the soil moisture changed only minimally or not at all (Table 10). The authors did not apply any corrections to the doubtful data, nor did they eliminate those data from the data base.

Table 10. Soil moisture values with depths on the 15th and 16th of September 2016.

Day	0–10 cm	10–20 cm	20–40 cm	40–60 cm	60–80 cm	80–100 cm
15 September 2016	0.063	0.056	0.072	0.140	0.146	0.222
16 September 2016	0.051	0.055	0.072	0.124	0.146	0.220

3.4.2. Verification Based on Data from Jelcz Laskowice and Baborówko

Model verification was also performed with the use of the results of soil moisture measurements conducted in the years 2009–2019 at two other locations in Poland, Jelcz Laskowice and Baborówko (Figure 1). As mentioned in Section 2.1, these stations are included in the soil moisture measurement network within the scope of the Agricultural Drought Monitoring System (ADMS) in Poland, conducted by the Institute of Soil Science and Plant Cultivation—State Research Institute (IUNG-PIB). They represent light soils, accounting for nearly 70% of all soils in Poland and in central Europe. From the viewpoint of particle size distribution, they are light loamy sands and light silty sands, and strong loamy sands and strong loams. In terms of susceptibility to droughts, the soils are classified in category II with a particle size distribution of light silty loamy sand [73]. Moisture measurements at these locations were taken by means of the profile probe PR2 Delta-T® at 5 depths in the soil profile: 10, 20, 40, 60, and 100 cm [74].

During the period of 2009–2019, 20 dry spells in Jelcz Laskowice and 35 in Baborówko were identified, in conformance with the adopted method, each lasting at least 10 days. The locality of Baborówko is situated in the Wielkopolskie Province, classified as one of the driest regions in Poland. This was also supported by the more frequent identification of dry spells numbering longer than 20 days at this measurement location. It should be mentioned that the verified model of soil drying during dry spells was created on the basis of dry spells that lasted, in the vast majority, for 10–20 days, which resulted from the duration of dry spells in Wrocław in the 13-year period adopted for the analyses. SMDS model verification performed on the basis of this material also allowed an assessment of the response of the model to dry spells lasting for longer than 20 days.

Figures 9 and 10 present the relationships between the measured and the calculated values of soil moisture for Jelcz Laskowice and Baborówko, respectively.

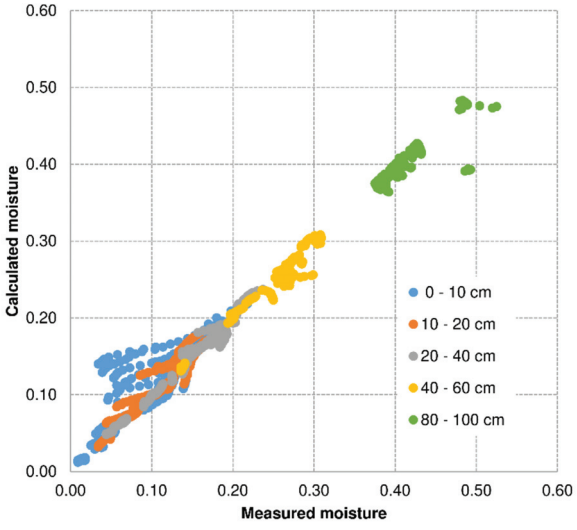

Figure 9. Relationship between measured and calculated values of soil moisture for the verified years 2009–2019 for Jelcz Laskowice.

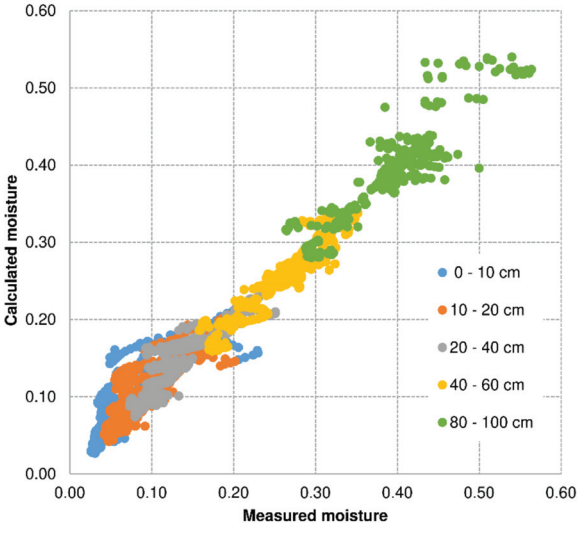

Figure 10. Relationship between measured and calculated values of soil moisture for the verified years 2009–2019 for Baborówko.

Table 11, on the other hand, presents the values of *MAPE* (%) for each of the measurement depths separately, and the mean value for the entire soil profile, calculated with the use of data from both measurement locations that were used for the verification.

Table 11. Variability of *MAPE* (%) and parameters of regression and correlation with depths for verified dry spells for Jelcz Laskowice and Baborówko.

Soil Layer (cm)	0–10	10–20	20–40	40–60	60–80	80–100	Mean
Laskowice *MAPE* (%)	27.7	7.5	3.4	2.6	-	2.2	8.7
a	0.89	0.98	0.98	0.97	-	0.76	9.92
b	0.02	0.00	0.00	0.00	-	0.00	0.00
r^2	0.75	0.93	0.98	0.96	-	0.74	0.87
Baborówko *MAPE* (%)	37.5	16.6	8.4	4.2	-	3.5	14.4
a	0.85	0.92	0.91	0.92	-	0.89	0.90
b	0.03	0.02	0.02	0.02	-	0.04	0.03
r^2	0.75	0.78	0.90	0.91	-	0.84	0.84

a, b—parameters of regression line; Cal = a × Obs + b; Cal—calculated moisture; Obs—measured moisture; r^2—square of correlation coefficient.

Model verification performed with the use of the data from Jelcz Laskowice and Baborówko demonstrated that the model, apart from the surface horizon of the soil, yielded results with errors smaller than 10%, which should be accepted as satisfactory results. This supports the conclusion that the model is a universal one and can be used for other objects characterized by soil conditions similar to those of the Faculty Agro and Hydrometeorology Observatory in Wrocław. In the surface soil horizons, in particular in the layer of 0–10 cm, the errors of verification reached or exceeded 30%. This results from the fact that during dry spells, soil moisture in those layers is also affected by other meteorological factors that influence the dry spell duration not accounted for in the model.

3.5. Prediction

The adoption of the values of the coefficient α given in Tables 6 and 8 as a characteristic for the particular soil layers allows calculation, using Equation (2), of the predicted moisture values in relation to the duration of the dry spell, relative to the initial moisture accepted as 100%. Examples of predicted values are given in Table 12. For example, for a dry spell lasting for 15 days, in the layer of 20–40 cm, the moisture predicted according to the model will decrease to 89% of the initial moisture.

Table 12. Prediction of soil moisture (%) depending on time and soil layer.

α	0.0208	0.0426	0.0159	0.0077	0.0045	0.0027	0.0025
Time (Day)	Soil Layer (cm)						
	0–10	0–10	10–20	20–40	40–60	60–80	80–100
0 d	100	100	100	100	100	100	100
10 d	81	65	85	93	96	97	98
15 d	73	53	79	89	93	96	96
20 d	66	43	73	86	91	95	95
25 d	60	34	67	82	89	94	94
30 d	54	28	62	79	87	92	93
35 d	48	22	57	76	85	91	92
40 d	43	18	53	73	84	90	91

The exponential form of the trend of moisture changes over time adopted for the analyses also allows the calculation, using Equation (2), of the duration of the dry spell t after which soil moisture at

a selected depth will decrease from the known value of the initial moisture θ_0 to moisture θ, which is important for the land use of the area:

$$t = -\frac{1}{\alpha} \ln\left(\frac{\theta}{\theta_0}\right). \quad (6)$$

Obviously, time t depends on the value of the decrease rate coefficient α and on the ratio of the expected moisture θ and the initial moisture θ_0. Examples of such lead times are given in Table 13. For example, in the layer of 20–40 cm, characterized by parameter α = 0.0077, soil moisture will decrease to 80% of the initial value after a dry spell lasting for 28 days.

Table 13. Time (days) required to achieve values of soil moisture θ at the adopted soil layers.

Soil Layer (cm)	α	θ/θ_0 (%)				
		90	**80**	**70**	**60**	**50**
0–10	0.0208	5	10	17	24	33
0–10	0.0426	2	5	8	11	16
10–20	0.0159	6	14	22	32	43
20–40	0.0077	13	28	46	66	90
40–60	0.0045	23	49	79	113	154
60–80	0.0027	39	82	132	189	256
80–100	0.0025	42	89	142	204	277

4. Discussion

Extreme phenomena—in this case droughts—appear in various regions of the world and many research teams are looking for methods of closer elucidation of those phenomena. However, this research is most frequently conducted with the use of known tools and methods. The simple and non-standard method developed and described in detail herein can help agricultural science and practice, and expand knowledge on the dynamics of drought. The permanent layout of measurement points and round-the-clock monitoring of the state of soil moisture at various depths allow the acquisition of highly valuable information on soil water resources. The innovative approach, i.e., simplicity of the model and departure from the standards, consisting in estimating the amount of soil moisture changes through indirect methods based on various available sets of meteorological elements, can contribute to a certain progress in the development of knowledge on drought as an extreme phenomenon.

The proposed exponential SMDS model of soil moisture decrease in dry spells allows estimation of the reduction of soil water content only on the basis of information on the state of soil moisture on the first day of a dry spell and its duration. In practice, this means that on the basis of available information on the lack of rainfall, obtained in the form of a prediction, it is possible to determine the potential decrease of soil moisture without any need for direct labor-consuming and costly measurements of the state of soil moisture. The developed SMDS model relates to bare soil because it is the standard reference surface and allows spatial comparison of results irrespective of the location of studies. The only significant factor differentiating the analyzed bare surfaces is the particle size composition of the soils. Soil drying occurs and is observably faster in light soils, while in compact soils the process proceeds more slowly and has a smaller range at greater soil thicknesses. This results from the fact that such soils have a potentially greater water folding capacity. An absence of vegetation cover on the soil creates such conditions that its moisture is the sole resultant of the effect of agro and hydrometeorological factors. In the literature, the authors of numerous publications indicate the justifiability of referencing the results obtained to surfaces of this type [75–79].

The process of soil drying is no more than the transfer of moisture from one medium to another (soil–air) [80]. The process begins when there is a demand for moisture in the atmosphere, when there

is an influx of radiant energy to the ground surface, and when there is wind, which allows air mass exchange above the area where the process of evaporation takes place. In such a situation, the decrease of soil moisture is a function of factors occurring in the atmosphere. Soil evaporation models have been developed for many years, e.g., [81–83]. They are characterized by various degrees of complexity and various numbers of parameters. Wang et al. [81] proposed a normalized soil water index (NSWI) based on the water balance equation. Teng et al. [82] developed an analytical model consisting of three partial differential equations that respectively govern the vapor flow, liquid water flow, and heat transfer. Merlin et al. [83] proposed a model for soil evaporative efficiency (SEE) estimation defined as the ratio of actual to potential soil evaporation. According to Brutsaert [63], the soil drying process can be described as isothermal linear diffusion in a finite depth domain. The soil drying model proposed in this paper is based on the results of detailed long-term monitoring of the state of soil moisture as a function of agrometeorological factors represented by the single coefficient α.

It is also difficult to confront the results obtained in this study with those of other authors addressing similar subject matter, due to the fact that the estimation of the extent of soil drying is most frequently referenced to the commonly used indicators of meteorological drought [45–47]. A similar problem was also addressed by Miler et al. [84]. Their study on the change of volumetric moisture of soil under a forest in non-rainfall periods in the years 2013–2016 demonstrated an average decrease, without taking into account the duration of the dry spells, of approximately 40% at the depth of 85 cm. At greater depths, the observed changes were only slight. The results of the current study for a bare soil surface were different. In the current case, irrespective of the duration of dry spells, the average moisture decrease varied from 3% for 10-day dry spells to 10% for those lasting for 40 days. The most sensitive to the lack of rainfall are bare soil layers with a thickness down to 40 cm. The results of the analyses demonstrated that, after a dry spell lasting for only 10 days, the moisture decrease varied from 7% for the layer of 20–40 cm to 19% and 35%, respectively, for the adopted α coefficient for the layer of 0–10 cm, while a 40-day non-rainfall period caused soil moisture to decrease by 27% for the layer of 20–40 cm and 57% and 82%, respectively, for the layer of 0–10 cm (Table 12). According to the research of Flammini et al. [79] on the dynamics of evaporation in bare soil in dry summer periods, the initial soil moisture affects the drying process. Gomboš et al. [85] indicate, on the basis of simulated soil moisture values, that during non-rainfall periods, water retention in soil under vegetation cover largely depends on the value of actual evapotranspiration. The level of limitation of the process in dry spell conditions can be an indicator of the drying of the soil profile. Drying begins when water migration towards plant roots becomes reduced. The results, however, should also be referenced to a bare soil surface, as, depending on the plant species and the active depth of the root zone, the process of water loss in the form of evapotranspiration is strongly diversified in the period of vegetation. In contrast, as mentioned earlier, a bare soil surface, as a result of the process of evaporation, responds primarily to a lack of precipitation water influx. At the same time, surface dynamics are also dependent on the degree of saturation of the atmosphere layer close to soil surface with water vapor, and on the dynamics of the movement of air masses adjacent to the ground surface. This indicates the need for conducting the analyses discussed herein to acquire knowledge about other aspects of soil drought with the use of non-standard tools.

In this study, SMDS model verification was conducted with the use of independent data originating from the measurement point on the basis of which the model was created. This verification demonstrated, for a model based only on a number of consecutive days with no rainfall produced, an error of 8% in the surface horizon of the soil (0–10 cm). Furthermore, only in this zone can the potential effect of other factors (e.g., other meteorological elements, such as air temperature and humidity, wind, soil properties, and soil cultivation treatments) be discussed. In the deeper layers of the soil profile, the developed model produces errors in the range of 1–5%, which shows that potential inclusion of the abovementioned other factors does not have any justifiable significance. This regularity was supported by the results of verification conducted for two other independent locations (Section 3.4.2), with the exception of the surface horizon of the soil, with a depth of 0–10 cm.

It should be emphasized that in the case of this layer, for which the process of soil drying is a function of factors occurring in the atmosphere, the developed model may have limited application and the obtained results may be affected by greater errors. The initiation of this process is possible only when the following conditions are met—there is a demand for moisture in the atmosphere (deficit of air humidity), there is an influx radiant energy to the ground surface (solar radiation), and there is wind, which stimulates the dynamics of air mass exchange over the area from which the process of evaporation takes place. It should be assumed that including these elements in the model would certainly improve the quality of the estimated decrease in soil moisture in this layer. On the other hand, the absence of a direct bond between the model and the local meteorological conditions enhances its universal character, at the expense of a small loss of accuracy, especially in the surface horizon of soil. However, from the viewpoint of agricultural cultivations, this layer is of slight importance, yet is nonetheless the most sensitive to the effect of external factors. The results of the verification also confirmed the correct behavior of the model for dry spells of longer duration.

The current authors recognize a number of potential modifications for improving the accuracy of the model, while taking into account the model's fundamental purpose of being easy to use in operational conditions. Firstly, it is possible to determine the value of parameter α separately for every layer and for every month, which will make the model bigger and more complex. One can expect, however, that with such a treatment, the errors will be smaller than those obtained in the presented study, especially in the soil layer of 0–10 cm, which is exposed directly to the effect of meteorological factors. Another solution would be to adopt the assumption that the value of coefficient α also depends on the state of soil moisture on the first day of a dry spell. A third variant could take into account soil temperature as a secondary element of energy influx to the soil, with a significant effect on the rate of soil drying, especially at its surface horizon. Such methods of making the model more general could improve its accuracy.

The proposed SMDS model of the dynamics of soil moisture during dry spells, as opposed to dedicated soil drought indicators based on many meteorological elements, water balance, or evapotranspiration appears to be uncomplicated and with high application possibilities. It can be used to impart greater precision to models of water balance with various levels of complexity and is much easier to apply in agricultural practice.

5. Conclusions

The presented analyses, conducted on original and extensive measurement material containing information on non-rainfall periods and water resources of bare soil, permit the formulation of the following conclusions:

1. The analyses of observation materials and the calculations performed indicate that the exponential trend describes well the decrease of soil moisture during dry spells. Its goodness of fit decreases with increasing depth of measurement.
2. The coefficient of the moisture decrease rate α decreases with depth. Its greatest variation was noted for the depth of 10 cm, and with increasing depth, smaller oscillations of the coefficient were observed.
3. The developed Equation (6) allows determination of the duration of a dry spell after which the soil moisture will decrease to an expected value.
4. As a result of the analyses performed, satisfactory results were obtained at the stage of verification of the developed SMDS model using data originating from the same station as the data used for the determination of the parameters of the model. The mean relative error was 3.8%. It was found that the error of model fitting decreases with increasing depth, from 8.1% for the surface layer to 1.0% for the deepest soil layer, while increasing with the time of the dry spell duration at the rate of 0.5%/day.

5. The verification performed using the measurement material from Jelcz Laskowice and Baborówko also gave satisfactory results. In the case of the deeper soil horizons, the calculated values of *MAPE*% were less than 8%, and only in the layer of 0–10 cm did the error exceed the level of 30%. The results obtained support the possibility of using the SMDS model for other locations.
6. The method of estimation of SMDS model parameters developed in this study and described in detail herein can also be applied for other types of soil. The only condition is the availability of a several-year string of observations of diurnal totals of atmospheric precipitation and values of soil moisture at various depths.

Author Contributions: Conceptualization, M.B.-P., M.C. and A.Ż; methodology, M.B.-P., M.C. and A.Ż.; formal analysis, M.B.-P., M.C.; investigation, M.B.-P.; data curation, M.B.-P., M.C., A.D. and T.J.; writing—original draft preparation, M.B.-P. and M.C.; writing—review and editing, M.B.-P., M.C. and A.Ż.; visualization, M.B.-P. and M.C.; supervision, M.B.-P. All authors have read and agreed to the published version of the manuscript.

Funding: This study was conducted within the project "Technological innovations and system of monitoring, forecasting and planning of irrigation and drainage for precise water management on the scale of drainage/irrigation system (INOMEL)" under the BIOSTRATEG3 program, funded by the Polish National Centre for Research and Development, Contract No. BIOSTRATEG3/347837/11/NCBR/2017. The measurement of soil moisture conducted at Jelcz Laskowice and Baborówko were financed by the Ministry of Agriculture and Rural Development within the scope of the project "Agricultural Drought Monitoring System in Poland in the years 2007–2019".

Acknowledgments: Meteorological data from the Faculty Observatory of Agro- and Hydrometeorology Wrocław-Swojec (WOAiHW-S) were used in this paper.

Conflicts of Interest: The authors declare no conflict of interest.

Appendix A

Table A1. Characteristics for each soil moisture drought adopted for analysis at the stage of model parameter determination.

Dry Spell (Days)	Characteristics	Soil Layer (cm)					
		0–10	**10–20**	**20–40**	**40–60**	**60–80**	**80–100**
22	SMb	0.06	0.10	0.08	0.11	0.22	0.23
	SM%	30.94	19.66	6.38	8.05	0.62	0.14
	SM%/d	1.41	0.89	0.29	0.37	0.03	0.01
11	SMb	0.11	0.09	0.23	0.20	0.26	0.37
	SM%	25.53	25.56	15.80	11.11	2.05	0.36
	SM%/d	2.32	2.32	1.44	1.01	0.19	0.03
12	SMb	0.09	0.09	0.20	0.26	0.29	0.32
	SM%	15.29	18.60	11.22	5.73	2.10	2.18
	SM%/d	1.27	1.55	0.94	0.48	0.17	0.18
11	SMb	0.10	0.10	0.17	0.25	0.28	0.32
	SM%	27.08	28.87	8.67	7.72	2.91	1.58
	SM%/d	2.46	2.62	0.79	0.70	0.26	0.14
11	SMb	0.06	0.09	0.09	0.14	0.25	0.29
	SM%	25.00	10.23	5.75	7.61	6.53	1.74
	SM%/d	2.27	0.93	0.52	0.69	0.59	0.16
18	SMb	0.10	0.11	0.08	0.13	0.20	0.26
	SM%	30.61	15.74	12.20	15.56	12.06	2.69
	SM%/d	1.70	0.87	0.68	0.86	0.67	0.15
11	SMb	0.08	0.08	0.07	0.09	0.16	0.17
	SM%	11.69	13.16	5.84	1.13	2.58	0.00
	SM%/d	1.06	1.20	0.53	0.10	0.23	0.00
10	SMb	0.08	0.08	0.07	0.09	0.15	0.17
	SM%	16.25	12.99	5.97	2.33	3.33	0.00
	SM%/d	1.63	1.30	0.60	0.23	0.33	0.00

Table A1. *Cont.*

Dry Spell (Days)	Characteristics	Soil Layer (cm)					
		0–10	**10–20**	**20–40**	**40–60**	**60–80**	**80–100**
21	SMb	0.12	0.16	0.20	0.24	0.25	0.26
	SM%	46.09	30.77	21.48	16.21	1.57	1.96
	SM%/d	2.19	1.47	1.02	0.77	0.07	0.09
10	SMb	0.07	0.13	0.10	0.14	0.23	0.28
	SM%	35.14	33.33	19.02	4.36	2.65	0.00
	SM%/d	3.51	3.33	1.90	0.44	0.27	0.00
10	SMb	0.33	0.29	0.29	0.28	0.25	0.26
	SM%	47.11	38.19	34.90	10.91	8.33	11.41
	SM%/d	4.71	3.82	3.49	1.09	0.83	1.14
10	SMb	0.25	0.23	0.23	0.25	0.24	0.26
	SM%	46.53	36.48	24.30	4.06	5.76	12.55
	SM%/d	4.65	3.65	2.43	0.41	0.58	1.25
14	SMb	0.12	0.14	0.16	0.24	0.23	0.24
	SM%	22.50	16.31	13.41	9.26	4.37	2.10
	SM%/d	1.61	1.17	0.96	0.66	0.31	0.15
12	SMb	0.09	0.09	0.10	0.13	0.14	0.17
	SM%	24.44	25.53	12.95	5.12	1.42	3.55
	SM%/d	2.04	2.13	1.08	0.43	0.12	0.30
16	SMb	0.06	0.06	0.08	0.08	0.13	0.16
	SM%	16.13	8.93	4.73	3.66	5.30	18.47
	SM%/d	1.01	0.56	0.30	0.23	0.33	1.15
11	SMb	0.07	0.09	0.07	0.08	0.18	0.20
	SM%	45.77	17.12	4.55	3.20	2.58	1.54
	SM%/d	4.16	1.56	0.41	0.29	0.23	0.14
12	SMb	0.04	0.06	0.11	0.14	0.13	0.17
	SM%	43.93	10.29	3.13	4.40	4.64	6.55
	SM%/d	3.66	0.86	0.26	0.37	0.39	0.55
10	SMb	0.07	0.13	0.13	0.10	0.16	0.23
	SM%	40.00	18.66	2.87	4.04	2.74	**−0.88**
	SM%/d	4.00	1.87	0.29	0.40	0.27	**−0.09**
11	SMb	0.10	0.06	0.13	0.14	0.16	0.17
	SM%	33.00	−3.89	0.80	2.92	3.51	**−1.93**
	SM%/d	3.00	−0.35	0.07	0.27	0.32	**−0.18**
16	SMb	0.09	0.06	0.12	0.13	0.15	0.17
	SM%	32.27	3.23	0.54	2.51	2.83	0.58
	SM%/d	2.02	0.20	0.03	0.16	0.18	0.04
11	SMb	0.09	0.06	0.14	0.15	0.23	0.29
	SM%	44.79	12.50	4.33	3.45	2.45	3.29
	SM%/d	4.07	1.14	0.39	0.31	0.22	0.30
11	SMb	0.06	0.05	0.13	0.14	0.22	0.28
	SM%	35.94	5.16	3.75	7.09	3.62	1.05
	SM%/d	3.27	0.47	0.34	0.64	0.33	0.10
12	SMb	0.08	0.13	0.12	0.09	0.15	0.22
	SM%	38.22	16.27	0.56	2.30	0.91	0.47
	SM%/d	3.19	1.36	0.05	0.19	0.08	0.04
12	SMb	0.09	0.06	0.12	0.16	0.22	0.23
	SM%	20.45	5.17	**−1.61**	**−1.27**	**−0.46**	1.32
	SM%/d	1.70	0.43	**−0.13**	**−0.11**	**−0.04**	0.11

Table A1. *Cont.*

Dry Spell (Days)	Characteristics	Soil Layer (cm)					
		0–10	**10–20**	**20–40**	**40–60**	**60–80**	**80–100**
12	SMb	0.07	0.07	0.18	0.21	0.25	0.26
	SM%	10.77	11.59	4.52	7.11	0.00	**−1.54**
	SM%/d	0.90	0.97	0.38	0.59	0.00	**−0.13**
11	SMb	0.06	0.06	0.17	0.19	0.25	0.26
	SM%	5.17	3.39	2.98	4.15	0.00	**−0.38**
	SM%/d	0.47	0.31	0.27	0.38	0.00	**−0.03**
16	SMb	0.10	0.10	0.11	0.17	0.25	0.28
	SM%	13.68	9.90	6.05	7.04	6.85	0.71
	SM%/d	0.86	0.62	0.38	0.44	0.43	0.04
14	SMb	0.13	0.15	0.16	0.22	0.21	0.24
	SM%	20.61	17.12	10.09	4.33	2.34	0.85
	SM%/d	1.47	1.22	0.72	0.31	0.17	0.06
10	SMb	0.09	0.09	0.10	0.13	0.16	0.17
	SM%	12.79	15.73	4.06	3.12	2.58	2.87
	SM%/d	1.28	1.57	0.41	0.31	0.26	0.29
27	SMb	0.06	0.05	0.08	0.07	0.12	0.10
	SM%	8.47	8.00	3.73	1.35	3.48	6.00
	SM%/d	0.31	0.30	0.14	0.05	0.13	0.22
13	SMb	0.04	0.09	0.10	0.12	0.11	0.16
	SM%	34.88	11.76	**−1.68**	**−1.34**	**−2.63**	19.75
	SM%/d	2.68	0.90	**−0.13**	**−0.10**	**−0.20**	1.52
10	SMb	0.07	0.06	0.12	0.13	0.14	0.17
	SM%	13.30	2.21	0.82	0.00	0.69	**−0.60**
	SM%/d	1.33	0.22	0.08	0.00	0.07	**−0.06**
17	SMb	0.08	0.07	0.13	0.13	0.21	0.28
	SM%	28.29	35.21	0.52	2.29	0.64	0.48
	SM%/d	1.66	2.07	0.03	0.13	0.04	0.03
11	SMb	0.08	0.06	0.12	0.16	0.22	0.22
	SM%	12.66	**−5.45**	**−0.81**	0.64	0.46	2.27
	SM%/d	1.15	**−0.50**	**−0.07**	0.06	0.04	0.21
12	SMb	0.15	0.19	0.23	0.24	0.28	0.27
	SM%	35.17	28.04	18.79	5.22	**−1.08**	2.58
	SM%/d	2.93	2.34	1.57	0.43	**−0.09**	0.22
12	SMb	0.09	0.13	0.17	0.22	0.27	0.26
	SM%	11.63	11.02	6.71	4.13	3.75	0.00
	SM%/d	0.97	0.92	0.56	0.34	0.31	0.00
38	SMb	0.12	0.12	0.11	0.16	0.23	0.29
	SM%	31.71	22.03	8.29	3.48	4.80	5.23
	SM%/d	0.83	0.58	0.22	0.09	0.13	0.14
14	SMb	0.10	0.11	0.11	0.15	0.20	0.18
	SM%	26.21	29.91	12.83	13.38	**−14.29**	4.42
	SM%/d	1.87	2.14	0.92	0.96	**−1.02**	0.32
11	SMb	0.06	0.05	0.08	0.07	0.11	0.10
	SM%	1.82	2.13	1.27	1.35	0.89	3.09
	SM%/d	0.17	0.19	0.12	0.12	0.08	0.28
Average	SM%	26.20	15.93	7.69	5.07	2.38	2.99
	SM%/d	2.10	1.26	0.62	0.39	0.19	0.23

SMb—soil moisture on the 1st day of dry spell; SM%—% decrease of soil moisture relative to the initial value; SM%/d—% decrease of soil moisture per day.

References

1. Daniels, E.E.; Hutjes, R.W.A.; Lenderink, G.; Ronda, R.J.; Holtslag, A.A.M. Land Surface Feedbacks on Spring Precipitation in the Netherlands. *J. Hydrometeorol.* **2015**, *16*, 232–243. [CrossRef]
2. Schwingshackl, C.; Hirschi, M.; Seneviratne, S.I. Quantifying Spatiotemporal Variations of Soil Moisture Control on Surface Energy Balance and Near-Surface Air Temperature. *J. Clim.* **2017**, *30*, 7105–7124. [CrossRef]
3. Castelli, G.; Castelli, F.; Bresci, E. Mesoclimate regulation induced by landscape restoration and water harvesting in agroecosystems of the horn of Africa. *Agric. Ecosyst. Environ.* **2019**, *275*, 54–64. [CrossRef]
4. Hauser, M.; Orth, R.; Seneviratne, S.I. Role of soil moisture versus recent climate change for the 2010 heat wave in western Russia. *Geophys. Res. Lett.* **2016**, *43*, 2819–2826. [CrossRef]
5. Seneviratne, S.I.; Corti, T.; Davin, E.L.; Hirschi, M.; Jaeger, E.B.; Lehner, I.; Orlowsky, B.; Teuling, A.J. Investigating soil moisture–climate interactions in a changing climate: A review. *Earth Sci. Rev.* **2010**, *99*, 125–161. [CrossRef]
6. Zhu, B.; Xie, X.; Meng, S.; Lu, C.; Yao, Y. Sensitivity of soil moisture to precipitation and temperature over China: Present state and future projection. *Sci. Total Environ.* **2020**, *705*, 135774. [CrossRef]
7. Biniak-Pieróg, M. *Monitoring of Atmospheric Precipitation and Soil Moisture as Basis for the Estimation of Effective Supply of Soil Profile with Water*; Editorial Office of Wrocław University of Environmental and Life Sciences: Wrocław, Poland, 2017; ISBN 978-83-7717-277-3. (In Polish)
8. Parent, A.-C.; Anctil, F.; Parent, L.-É. Characterization of temporal variability in near-surface soil moisture at scales from 1 h to 2 weeks. *J. Hydrol.* **2006**, *325*, 56–66. [CrossRef]
9. Zhang, Y.; Liu, J.; Xu, X.; Tian, Y.; Li, Y.; Gao, Q. The response of soil moisture content to rainfall events in semi-arid area of Inner Mongolia. *Procedia Environ. Sci.* **2010**, *2*, 1970–1978. [CrossRef]
10. Fu, Q.; Feng, S. Responses of terrestrial aridity to global warming. *J. Geophys. Res.* **2014**, *119*, 7863–7875. [CrossRef]
11. Langridge, R.; Fencl, A. *Implications of Climate Change to Groundwater*; Elsevier: Toronto, ON, Canada, 2019; ISBN 978-0-12-409548-9.
12. Koutroulis, A.G. Dryland changes under different levels of global warming. *Sci. Total Environ.* **2019**, *655*, 482–511. [CrossRef]
13. Girotto, M.; Rodell, M. Chapter Two—Terrestrial water storage. In *Extreme Hydroclimatic Events and Multivariate Hazards in a Changing Environment: A Remote Sensing Approach*; Maggioni, V., Massari, C., Eds.; Elsevier: Amsterdam, The Netherlands, 2019; pp. 41–64. ISBN 978-0-12-814899-0.
14. Giorgi, F.; Coppola, E.; Raffaele, F. A consistent picture of the hydroclimatic response to global warming from multiple indices: Models and observations. *J. Geophys. Res. Atmos.* **2014**, *119*, 11695–11708. [CrossRef]
15. Huang, J.; Yu, H.; Guan, X.; Wang, G.; Guo, R. Accelerated dryland expansion under climate change. *Nat. Clim. Chang.* **2015**, *6*, 166–171. [CrossRef]
16. Grillakis, M.G. Increase in severe and extreme soil moisture droughts for Europe under climate change. *Sci. Total Environ.* **2019**, *660*, 1245–1255. [CrossRef] [PubMed]
17. Łabędzki, L. *Agricultural Droughts. An Outline of Problems and Methods of Monitoring and Classification*; Editoral Office of IMUZ: Falenty, Poland, 2006; ISBN 83-88763-63-6.
18. Przybylak, R.; Oliński, P.; Koprowski, M.; Filipiak, J.; Pospieszyńska, A.; Chorążyczewski, W.; Puchałka, R.; Dąbrowski, H.P. Droughts in the area of Poland in recent centuries in the light of multi-proxy data. *Clim. Past* **2020**, *16*, 627–661. [CrossRef]
19. Liu, Y.; Cui, Z.; Huang, Z.; López-Vicente, M.; Wu, G.-L. Influence of soil moisture and plant roots on the soil infiltration capacity at different stages in arid grasslands of China. *CATENA* **2019**, *182*, 104147. [CrossRef]
20. Darvishan, A.K.; Banasik, K.; Sadeghi, S.H.; Gholami, L.; Hejduk, L. Effects of rain intensity and initial soil moisture on hydrological responses in laboratory conditions. *Int. Agrophysics* **2015**, *29*, 165–173. [CrossRef]
21. Dos Santos, J.C.N.; de Andrade, E.M.; Guerreiro, M.J.S.; Medeiros, P.H.A.; de Queiroz Palácio, H.A.; de Araújo Neto, J.R. Effect of dry spells and soil cracking on runoff generation in a semiarid micro watershed under land use change. *J. Hydrol.* **2016**, *541*, 1057–1066. [CrossRef]
22. Szulczewski, W.; Żyromski, A.; Biniak-Pieróg, M.; Machowczyk, A. Modelling of the effect of dry periods on yielding of spring barley. *Agric. Water Manag.* **2010**, *97*, 587–595. [CrossRef]

23. Szulczewski, W.; Zyromski, A.; Biniak-Pieróg, M. New approach in modeling spring wheat yielding based on dry periods. *Agric. Water Manag.* **2012**, *103*, 105–113. [CrossRef]
24. Żyromski, A.; Szulczewski, W.; Biniak-Pieróg, M.; Zmuda, R. Application of the MoDrY model for the estimation of potato yielding. *Int. J. Plant Prod.* **2013**, *7*, 505–516.
25. Łabędzki, L. Estimation of local drought frequency in central Poland using the standardized precipitation index SPI. *Irrig. Drain.* **2007**, *56*, 67–77. [CrossRef]
26. Ziernicka-Wojtaszek, A. Comparison of selected indices for the assessment of atmospheric drought in the Podkarpackie Province in the years 1901–2000. *Water Environ. Rural Areas* **2012**, *12*, 365–376.
27. Łabędzki, L.; Bąk, B. Meteorological and agricultural drought indices used in drought monitoring in Poland: A review. *Meteorol. Hydrol. Water Manag.* **2015**, *2*, 3–14. [CrossRef]
28. Radzka, E. Periods of days without precipitation during the growing season in central-eastern Poland (1971–2005). *Acta Agrophys.* **2014**, *21*, 483–491.
29. Wójcik, K.; Treder, W.; Zbudniewek, A. Estimation of plant water requirements during sequences of days without precipitation in 2011–2015. *Infrastruct. Ecol. Rural Areas* **2017**, *3*, 1187–1200. [CrossRef]
30. Szyga-Pluta, K. Variability of drought occurrence during growing season in Poland in years 1966–2015. *Przegląd Geofiz.* **2018**, *63*, 51–67.
31. Biniak-Pieróg, M. Occuarance of atmospheric drought in summer half-year in Wroclaw–Swojec during years 1961–2010. *Infrastruct. Ecol. Rural Areas* **2014**, *3*, 945–957.
32. Żyromski, A.; Biniak-Pierog, M.; Szumiejko, F. Spring Drought Estimation in a Point Scale. In *Crisis Management—Restricting the Negative Effects of Extreme Phenomena*; University of Opole: Opole, Poland, 2010; pp. 197–210.
33. Karavitis, C.A.; Alexandris, S.; Tsesmelis, D.E.; Athanasopoulos, G. Application of the Standardized Precipitation Index (SPI) in Greece. *Water Switz.* **2011**, *3*, 787–805. [CrossRef]
34. Caloiero, T. SPI Trend Analysis of New Zealand Applying the ITA Technique. *Geosciences* **2018**, *8*, 101. [CrossRef]
35. Jang, D. Assessment of Meteorological Drought Indices in Korea Using RCP 8.5 Scenario. *Water* **2018**, *10*, 283. [CrossRef]
36. Merabti, A.; Martins, D.S.; Meddi, M.; Pereira, L.S. Spatial and time variability of drought based on SPI and RDI with various time scales. *Water Resour. Manag.* **2018**, *32*, 1087–1100. [CrossRef]
37. Šebenik, U.; Brilly, M.; Šraj, M. Drought analysis using the standardized precipitation index (SPI). *Acta Geogr. Slov.* **2017**, *57*, 31–49. [CrossRef]
38. Bayissa, Y.; Maskey, S.; Tadesse, T.; van Andel, S.J.; Moges, S.; van Griensven, A.; Solomatine, D. Comparison of the performance of six drought indices in characterizing historical drought for the upper Blue Nile Basin, Ethiopia. *Geoscience* **2018**, *8*, 81. [CrossRef]
39. Cammalleri, C.; Micale, F.; Vogt, J. A novel soil moisture-based drought severity index (DSI) combining water deficit magnitude and frequency. *Hydrol. Process.* **2016**, *30*, 289–301. [CrossRef]
40. Narasimhan, B.; Srinivasan, R. Development and evaluation of Soil Moisture Deficit Index (SMDI) and Evapotranspiration Deficit Index (ETDI) for agricultural drought monitoring. *Agric. For. Meteorol.* **2005**, *133*, 69–88. [CrossRef]
41. Palmer, W.C. *Meteorological Drought. Research Paper No. 45*; U.S. Department of Commerce, Weather Bureau: Washington, DC, USA, 1965.
42. Yu, H.; Zhang, Q.; Xu, C.Y.; Du, J.; Sun, P.; Hu, P. Modified Palmer Drought Severity Index: Model improvement and application. *Environ. Int.* **2019**, *130*, 104951. [CrossRef]
43. Rossato, L.; Marengo, J.A.; de Angelis, C.F.; Pires, L.B.M.; Mendiondo, E.M. Impact of soil moisture over Palmer Drought Severity Index and its future projections in Brazil. *Braz. J. Water Resour.* **2017**, *22*, 1–16. [CrossRef]
44. Wu, W.; Geller, M.A.; Dickinson, R.E. The response of soil moisture to long-term variability of precipitation. *J. Hydrometeorol.* **2002**, *3*, 604–613. [CrossRef]
45. Huang, S.; Huang, Q.; Chang, J.; Leng, G.; Xing, L. The response of agricultural drought to meteorological drought and the influencing factors: A case study in the Wei River Basin, China. *Agric. Water Manag.* **2015**, *159*, 45–54. [CrossRef]
46. Gwak, Y.S.; Kim, Y.T.; Won, C.H.; Kim, S.H. The relationships between drought indices (SPI, API) and in-situ soil moisture in forested hillslopes. *WIT Trans. Ecol. Environ.* **2017**, *220*, 217–224. [CrossRef]

47. Halwatura, D.; McIntyre, N.; Lechner, A.M.; Arnold, S. Capability of meteorological drought indices for detecting soil moisture droughts. *J. Hydrol. Reg. Stud.* **2017**, *12*, 396–412. [CrossRef]
48. Sheffield, J.; Goteti, G.; Wen, F.; Wood, E.F. A simulated soil moisture based drought analysis for the United States. *J. Geophys. Res. D Atmos.* **2004**, *109*, D24108. [CrossRef]
49. Sheffield, J.; Wood, E.F. Global trends and variability in soil moisture and drought characteristics, 1950–2000, from observation-driven simulations of the terrestrial hydrologic cycle. *J. Clim.* **2008**, *21*, 432–458. [CrossRef]
50. Kim, E.S. Simulation of daily soil moisture content and reconstruction of drought events from the early 20th century in Seoul, Korea, using a hydrological simulation model, BROOK. *J. Ecol. F. Biol.* **2010**, *33*, 47–57. [CrossRef]
51. Leeper, R.D.; Bell, J.E.; Vines, C.; Palecki, M. An evaluation of the North American Regional Reanalysis simulated soil moisture conditions during the 2011–2013 drought period. *J. Hydrometeorol.* **2017**, *18*, 515–527. [CrossRef]
52. Sánchez, N.; González-Zamora, Á.; Piles, M.; Martínez-Fernández, J. A New Soil Moisture Agricultural Drought Index (SMADI) integrating MODIS and SMOS products: A case of study over the Iberian Peninsula. *Remote Sens.* **2016**, *8*, 287. [CrossRef]
53. Keshavarz, M.R.; Vazifedoust, M.; Alizadeh, A. Drought monitoring using a Soil Wetness Deficit Index (SWDI) derived from MODIS satellite data. *Agric. Water Manag.* **2014**, *132*, 37–45. [CrossRef]
54. Carrão, H.; Russo, S.; Sepulcre-Canto, G.; Barbosa, P. An empirical standardized soil moisture index for agricultural drought assessment from remotely sensed data. *Int. J. Appl. Earth Obs. Geoinf.* **2016**, *48*, 74–84. [CrossRef]
55. Srivastava, P.K.; Pandey, P.C.; Petropoulos, G.P.; Kourgialas, N.N.; Pandey, V.; Singh, U. GIS and Remote Sensing Aided Information for Soil Moisture Estimation: A Comparative Study of Interpolation Techniques. *Resources* **2019**, *8*, 70. [CrossRef]
56. Blyverket, J.; Hamer, P.D.; Schneider, P.; Albergel, C.; Lahoz, W.A. Monitoring Soil Moisture Drought over Northern High Latitudes from Space. *Remote Sens.* **2019**, *11*, 1200. [CrossRef]
57. Suzuki, K.; Matsuo, K.; Yamazaki, D.; Ichii, K.; Iijima, Y.; Papa, F.; Yanagi, Y.; Hiyama, T. Hydrological Variability and Changes in the Arctic Circumpolar Tundra and the Three Largest Pan-Arctic River Basins from 2002 to 2016. *Remote Sens.* **2018**, *10*, 402. [CrossRef]
58. Riordan, B.; Verbyla, D.; McGuire, A.D. Shrinking ponds in subarctic Alaska based on 1950–2002 remotely sensed images. *J. Geophys. Res. Biogeosci.* **2006**, *111*. [CrossRef]
59. Biniak-Pieróg, M. Dynamics of water content in light bare soil in summer half-year in the period of 2003-2012 and its agro-meteorological determinants. *J. Water Land Dev.* **2014**, *22*, 41–50. [CrossRef]
60. Gao, L.; Shi, B.; Tang, C.; Gu, K. Variation of soil moisture under bare soil, grass and concrete covers. *Electron. J. Geotech. Eng.* **2014**, *19*, 3495–3505.
61. Novak, M.D. Dynamics of the near-surface evaporation zone and corresponding effects on the surface energy balance of a drying bare soil. *Agric. For. Meteorol.* **2010**, *150*, 1358–1365. [CrossRef]
62. Wang, T.; Singh, S.K.; Bárdossy, A. On the use of the critical event concept for quantifying soil moisture dynamics. *Geoderma* **2019**, *335*, 27–34. [CrossRef]
63. Brutsaert, W. Daily evaporation from drying soil: Universal parameterization with similarity. *Water Resour. Res.* **2014**, *50*, 3206–3215. [CrossRef]
64. IUSS Working Group WRB. *World Reference Base for Soil Resources 2006*; World Soil Resources Reports No. 103; FAO: Rome, Italy, 2006.
65. Żyromski, A.; Biniak-Pierog, M.; Szulczewski, W.; Kordas, L.; Kabała, C.; Gałka, B. *Mathematical Modelling of Evapotranspiration of Selected Energy Crops*; Wyd. UP we Wrocławiu: Wrocław, Poland, 2016; ISBN 978-83-7717-253-7.
66. World Meteorological Organisation. *Guide to Meteorological Instruments and Methods of Observation*, 7th ed.; World Meteorological Organisation: Geneva, Switzerland, 2008.
67. IMGW. *Monthly Agrometeorological Review, 1975–2000*; IMGW: Warszawa, Poland, 2000.
68. Topp, G.C.; Davis, J.L.; Annan, A.P. Electromagnetic determination of soil water content: Measurements in coaxial transmission lines. *Water Resour. Res.* **1980**, *16*, 574–582. [CrossRef]
69. Skierucha, W.; Sławiński, C.; Wilczek, A.; Żyromski, A.; Biniak-Pierog, M. Telemetric system for the measurement of soil moisture based on the TDR technique. *Water Environ. Rural Areas* **2012**, *12*, 257–267.

70. Susha Lekshmi, S.U.; Singh, D.N.; Shojaei Baghini, M. A critical review of soil moisture measurement. *Measurement* **2014**, *54*, 92–105. [CrossRef]
71. Skierucha, W.; Wilczek, A.; Szypłowska, A.; Sławiński, C.; Lamorski, K. A TDR-based soil moisture monitoring system with simultaneous measurement of soil temperature and electrical conductivity. *Sens. Switz.* **2012**, *12*, 13545–13566. [CrossRef] [PubMed]
72. Schmuck, A. Dry spells and high atmospheric precipitation in the Wrocław voivodship in 1950–1959. *Geogr. J.* **1962**, *33*, 411–440.
73. ADMS—Soil Categories. Available online: http://www.susza.iung.pulawy.pl/en/kategorie/ (accessed on 14 June 2020).
74. Doroszewski, A.; Jadczyszyn, J.; Kozyra, J.; Pudełko, R.; Stuczyński, T.; Mizak, K.; Łopatka, A.; Kozyra, P.; Górski, T.; Wróblewska, E. Fundamentals of the Agricultural Drought Monitoring System. *Water Environ. Rural Areas* **2012**, *12*, 77–91.
75. Aydin, M.; Yang, S.L.; Kurt, N.; Yano, T. Test of a simple model for estimating evaporation from bare soils in different environments. *Ecol. Modell.* **2005**, *182*, 91–105. [CrossRef]
76. Babaeian, E.; Homaee, M.; Montzka, C.; Vereecken, H.; Norouzi, A.A.; van Genuchten, M.T. Soil moisture prediction of bare soil profiles using diffuse spectral reflectance information and vadose zone flow modeling. *Remote Sens. Environ.* **2016**, *187*, 218–229. [CrossRef]
77. Gorrab, A.; Simonneaux, V.; Zribi, M.; Saadi, S.; Baghdadi, N.; Lili Chabaane, Z.; Fanise, P. Bare soil hydrological balance model "MHYSAN": Calibration and validation using SAR moisture products and continuous thetaprobe network measurements over bare agricultural soils (Tunisia). *J. Arid Environ.* **2017**, *139*, 11–25. [CrossRef]
78. Quinn, R.; Parker, A.; Rushton, K. Evaporation from bare soil: Lysimeter experiments in sand dams interpreted using conceptual and numerical models. *J. Hydrol.* **2018**, *564*, 909–915. [CrossRef]
79. Flammini, A.; Corradini, C.; Morbidelli, R.; Saltalippi, C.; Picciafuoco, T.; Giráldez, J.V. Experimental Analyses of the Evaporation Dynamics in Bare Soils under Natural Conditions. *Water Resour. Manag.* **2018**, *32*, 1153–1166. [CrossRef]
80. Alvenäs, G.; Jansson, P.-E. Model for evaporation, moisture and temperature of bare soil: Calibration and sensitivity analysis. *Agric. For. Meteorol.* **1997**, *88*, 47–56. [CrossRef]
81. Wang, Y.; Magliulo, V.; Yan, W.; Shangguan, Z. Assessing land surface drying and wetting trends with a normalized soil water index on the Loess Plateau in 2001–2016. *Sci. Total Environ.* **2019**, *676*, 120–130. [CrossRef]
82. Teng, J.; Zhang, X.; Zhang, S.; Zhao, C.; Sheng, D. An analytical model for evaporation from unsaturated soil. *Comput. Geotech.* **2019**, *108*, 107–116. [CrossRef]
83. Merlin, O.; Olivera-Guerra, L.; Aït Hssaine, B.; Amazirh, A.; Rafi, Z.; Ezzahar, J.; Gentine, P.; Khabba, S.; Gascoin, S.; Er-Raki, S. A phenomenological model of soil evaporative efficiency using surface soil moisture and temperature data. *Agric. For. Meteorol.* **2018**, *256–257*, 501–515. [CrossRef]
84. Miler, A.T.; Urbaniak, M.; Krysztofiak-Kaniewska, A. Changes of soil moisture in the unsaturated zone during rainless periods in the Martew Forest Area. *Infrastruct. Ecol. Rural Areas* **2017**, *2*, 631–644.
85. Gomboš, M.; Kandra, B.; Tall, A.; Pavelková, D. Analysis of non-rainfall periods and their impacts on the soil water regime. In *Hydrology—The Science of Water*; IntechOpen: London, UK, 2019; p. 20.

MDPI
St. Alban-Anlage 66
4052 Basel
Switzerland
Tel. +41 61 683 77 34
Fax +41 61 302 89 18
www.mdpi.com

Resources Editorial Office
E-mail: resources@mdpi.com
www.mdpi.com/journal/resources

MDPI
St. Alban-Anlage 66
4052 Basel
Switzerland

Tel: +41 61 683 77 34

www.mdpi.com

ISBN 978-3-0365-4924-8